Actin Binding Proteins in the Regulation of the Astrocytic Cytoskeleton

Von der Fakultät für Lebenswissenschaften

der Technischen Universität Carolo-Wilhelmina zu Braunschweig

zur Erlangung des Grades einer

Doktorin der Naturwissenschaften

(Dr. rer. nat.)

genehmigte

D i s s e r t a t i o n

von Stefanie Katharina Schweinhuber
aus Hamburg

1. Referent: Prof. Dr. Martin Korte
2. Referent: Prof. Dr. Reinhard Köster
eingereicht am: 16.06.2014
mündliche Prüfung (Disputation) am: 18.08.2014

Druckjahr 2014

Vorveröffentlichungen der Dissertation

Teilergebnisse aus dieser Arbeit wurden mit Genehmigung der Fakultät für Lebenswissenschaften, vertreten durch den Mentor der Arbeit, in folgenden Beiträgen vorab veröffentlicht:

Tagungsbeiträge:

S. Schweinhuber, M. Korte and M. Rothkegel

'Role of profilin 2 in cell motility of chicken fibroblasts'

34th Annual Meeting of the German Society for Cell Biology (DGZ), Bonn, March 2011

S. Schweinhuber, K. Rottner, M. Korte and M. Rothkegel

'The role of Cortactin in Connexin43 mediated signaling in astrocytes'

2nd International Meeting of the German Society for Cell Biology (DGZ) on Actin Dynamics, Regensburg, September 2012

S. Schweinhuber, K. Rottner, M. Korte and M. Rothkegel

'The lack of cortactin leads to reduced intercellular signaling in astrocytes'

10th Meeting of the German Neuroscience Society, Göttingen, March 2013

S. Schweinhuber, M. Korte and M. Rothkegel

'Profilins modulate the morphology and motility of astrocytes'

9th FENS Forum of Neuroscience, Mailand, July 2014

THEY ALWAYS SAY TIME CHANGES THINGS, BUT YOU ACTUALLY HAVE TO CHANGE THEM YOURSELF.

ANDY WARHOL

FÜR MEINE ELTERN

Table of Contents

Zusammenfassung

Neuronen und Gliazellen repräsentieren die beiden Hauptzellpopulationen im Gehirn. Aus historischer Perspektive wurden Neuronen als die einzigen informationsverarbeitenden Zellen betrachtet. Während der letzten 20 Jahre jedoch, veränderte sich die Sichtweise von einer rein unterstützenden Funktion hin zu einer aktiven Rolle der Gliazellen in diversen kognitiven Prozessen. Netzwerke bestehend aus untereinander verbundenen Astrozyten und Neuronen sind während Lern- und Gedächtnisprozessen einem kontinuierlichen Wandel unterworfen. Die Morphologie von Astrozytenfortsätzen bestimmt hierbei die enge räumliche Assoziation mit Neuronen. Kleine periphere Fortsätze der Astrozyten bilden zusammen mit der neuronalen Prä- und Postsynapse eine strukturelle Einheit, die als *Tripartite Synapse* bezeichnet wird. Für die hochdynamischen Veränderungen dieser Fortsätze ist hauptsächlich das Mikrofilamentsystem verantwortlich. In diesem Zusammenhang konnte das Aktin-bindende Protein Profilin 1 (PFN1) als Regulator des Aktivitäts-abhängigen Auswachsens von Astrozytenfortsätzen identifiziert werden. Folglich ist die vorliegende Arbeit auf die Analyse der zugrundeliegenden molekularen Mechanismen fokussiert. Kultivierte Astrozyten exprimieren neben dem ubiquitären PFN1 auch die neuronale Isoform PFN2a. Eine Isoform-spezifische RNA Interferenz induzierte Hemmung der Expression von PFN1 und PFN2a führte zur Identifikation beider Profiline als Modulatoren der Zellgröße und Adhäsion. Zusätzlich sind beide Isoformen essentiell für die Forskolin-induzierte *Stellation* und die Motilität von Astrozytenfortsätzen. Eine alternative Induktion von morphologischer Plastizität durch die Applikation eines ROCK Inhibitors indes war lediglich PFN2a abhängig. Darüber hinaus moduliert ausschließlich PFN2a die Komplexität von Astrozyten. Im Gegensatz dazu, konnte für PFN1 eine exklusive Rolle in der Regulation der Aktin Dynamik in Astrozytenfortsätzen nachgewiesen werden. Somit sind Profilin Isoformen wichtige Modulatoren der Morphologie und Motilität von Astrozyten mit sowohl überlappenden als auch Isoform-spezifischen Funktionen. Da das Aktin-bindende Protein Cortactin in der interzellulären Kommunikation von Astrozyten impliziert wurde, untersuchte ich dessen zelluläre Funktion. Cortactin defiziente kultivierte Astrozyten wiesen Beeinträchtigungen der Proliferation, der Aktin Dynamik und im Migrationsverhalten auf. Zusätzlich wurde das Zusammenspiel des in Astrozyten vorherrschenden Gap junction Proteins Connexin 43 mit Cortactin untersucht. Der Verlust von Cortactin bewirkte eine Reduktion der Interkonnektivität von Astrozytennetzwerken. Dieser Phänotyp konnte eindeutig der direkten interzellulären Kommunikation via Connexin 43 Kanälen zugeordnet werden. Zusammengefasst eröffnet diese Arbeit neue Einsichten in die Regulation der Morphologie, Motilität und Interkonnektivität von Astrozyten durch die Aktin-bindenden Proteine PFN1, PFN2a und Cortactin.

Abstract

Neurons and glial cells represent the two main cell populations in the brain. Historically, neurons have been attributed to be the only information processing unit of the brain. In the last two decades, however, knowledge about the not merely trophic and mechanical supporting functions of astrocytes has exploded. Networks consisting of interconnected neurons and astrocytes undergo a continuous change and adaptation during learning and memory processes. The morphology of astrocytic processes determines the close structural association with neurons. As integral part of the tripartite synapse, peripheral astrocytic processes ensheath the pre- and postsynapse. Their highly dynamic morphology depends to a great extent on the actin cytoskeleton. In this context, the actin binding protein profilin 1 (PFN1) has recently been shown to regulate the activity-dependent outgrowth of PAPs. Consequently, this thesis focusses on the underlying mechanisms of astrocytic morphological plasticity. Here, I demonstrate that cultured murine astrocytes in addition to the ubiquitous PFN1 also express the neuronal isoform PFN2a. To analyze the cellular function of profilins in astrocytes, advantage of a shRNA mediated isoform-specific downregulation was taken. I could show that the knockdown of PFN1 as well as PFN2a led to a significant decrease in cell adhesion and cell size. Both isoforms proved to be as well crucial for forskolin-induced astrocytic stellation and motility of astrocytic processes. However, the ROCK inhibition-induced stellation response solely relied on PFN2a. Moreover, exclusively the downregulation of PFN2a resulted in a significantly reduced complexity of astrocytes in both slice cultures and dissociated cultures. In contrast, FRAP analysis revealed that solely the knockdown of PFN1 impaired actin dynamics in astrocytic processes. Thus, profilin isoforms are suggested as important modulators of astrocytic morphology and motility with overlapping as well as isoform-specific functions. Since also the actin binding protein cortactin was suggested to fulfil a crucial role in the intercellular communication, I investigated the cellular function of cortactin in astrocytes. Primary astrocytic cultures derived from *cttn*$^{-/-}$ animals revealed impaired actin dynamics, a reduced proliferation rate and an altered migration behavior, when compared to wild type astrocytes. Moreover, the interplay of the gap junction protein connexin43 and cortactin was analyzed by calcium imaging. Here, *cttn*$^{-/-}$ cultures exhibit a reduced interconnectivity even in the presence of the purinergic receptor antagonist suramin. Additionally, direct inhibition of connexin43 solely reduced the calcium wave velocity of wild type cultures. Consequently, cortactin is suggested as a modulator of the actin cytoskeleton and the intercellular communication in astrocytes. Taken together, this study provides new insights into the regulation of astrocytic morphology, motility and interconnectivity by the actin binding proteins PFN1, PFN2a and cortactin.

1. Introduction

Generations of philosophes have tried to understand the complexity of their own thoughts, resulting in the reduction to the basic principle ‘I think, therefore I am’ of René Decartes. This multifaceted reflection of the human existence and our mental capability is only possible because the human brain consists of a network containing more than 100 trillion synaptic connections (Eroglu and Barres, 2010). The astonishingly complex network in the vertebrates’ central nervous system is built up of a plethora of different, interconnected cells. They can be roughly divided into two major groups, namely the electrically excitable neurons, also called nerve cells, and the glial cells. Traditionally, glial cells are thought to solely fulfil a supporting role for neurons. Several recent studies, however, provide convincing evidence for an active role of glia subtypes in fundamental physiological processes such as breathing (Gourine et al., 2010) or synaptic plasticity (Pannasch et al., 2011).

1.1. Glial cells

The term ‘neuroglia’ was first used by Virchow in 1846, when he described the connective substance embedding “nervous elements” (p. 890 in Virchow, 1856; cited in (Somjen, 1988)). The concept, what neuroglia are and how they interact with neurons in the central nervous system (CNS) changed drastically over time, but the term lasted. During the following years, neuroglia were found to be multipolar cells existing in close proximity to blood vessels and neurons. Interestingly, already in 1893 Andriezen (Andriezen, 1893) described the differences between fibrous glia from the white matter and protoplasmic glia residing in the grey matter. This concept was adopted and extended by Ramón y Cajal (1913); Figure 1.1), when he added the “third element”, adendritic or apolar cells, to the concept. Subsequently, the modern classification of glia cells was established by del Río-Hortega (1920).

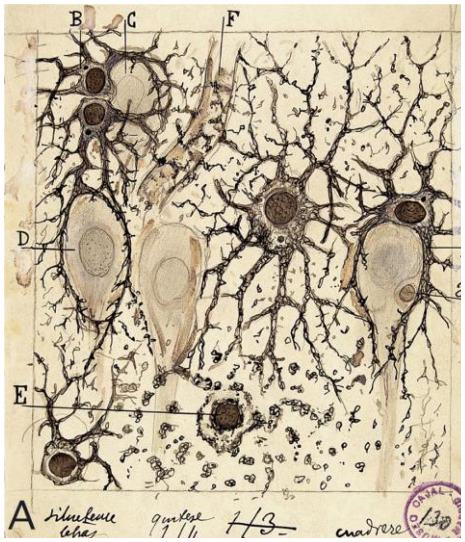

Figure 1.1 | Drawing of Ramón y Cajal after examination of neocortical sections (1913). Astrocytes (dark cells) display a complex morphology characterized by relatively small somata, several thick processes and fine distal structures ensheating the adjacent neurons (e.g. “D”, light grey cells).

1.1.1. Major types of glia

With his description of microglia and oligodendrocytes, del Río-Hortega (del Río-Hortega, 1932; del Río-Hortega, 1920) was the founder of the current classification of glial cells into four groups: Protoplasmic astrocytes of the gray matter (Figure 1.2; A), fibrous astrocytes of the white matter (Figure 1.2; B), microglia (Figure 1.2; C) and oligodendrocytes (Figure 1.2; D).

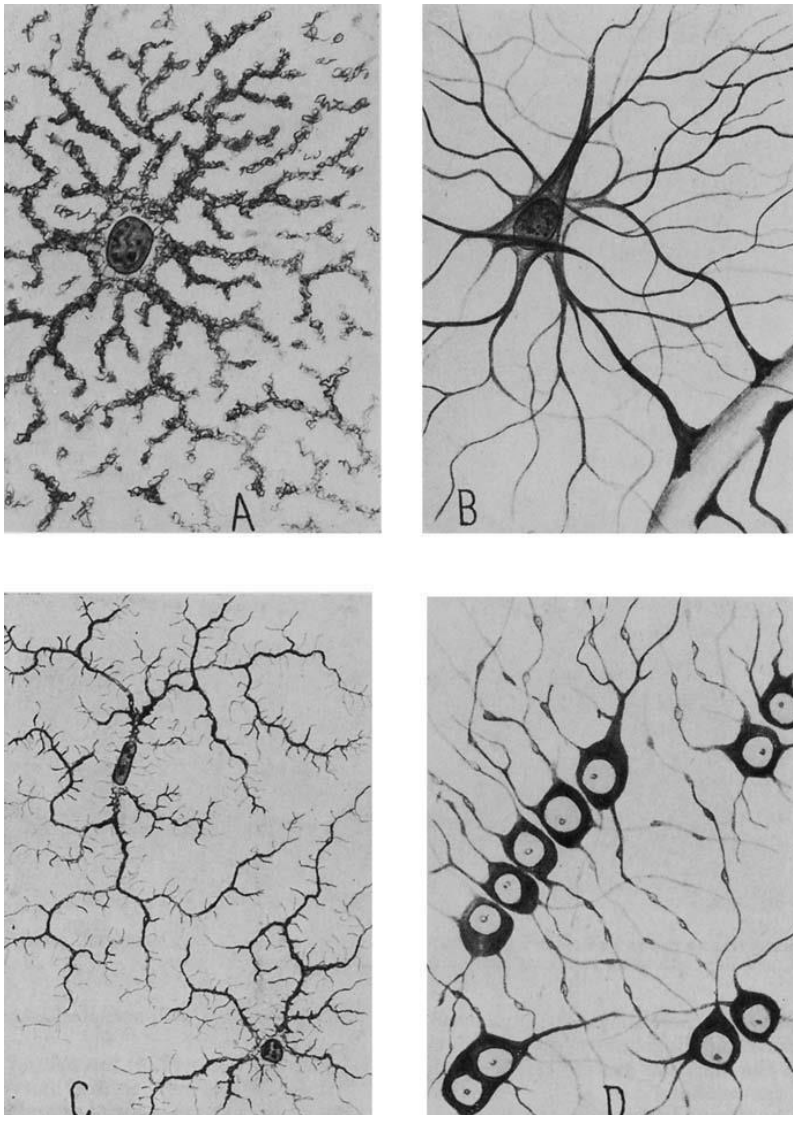

Figure 1.2 | Illustration of the four major types of glia by del Río-Hortega (1920). **(A)** Protoplasmic neuroglia found in the grey matter. **(B**) Fibrous neuroglia found in the white matter. **(C)** Microglia. **(D)** Oligodendrocytes, termed “interfascicular glia” by del Río-Hortega of the white matter.

After this precise characterization of glia cells perfectly differentiating them from neurons was generally accepted, further scientific effort was focused on glial cell function and their interaction with neurons.

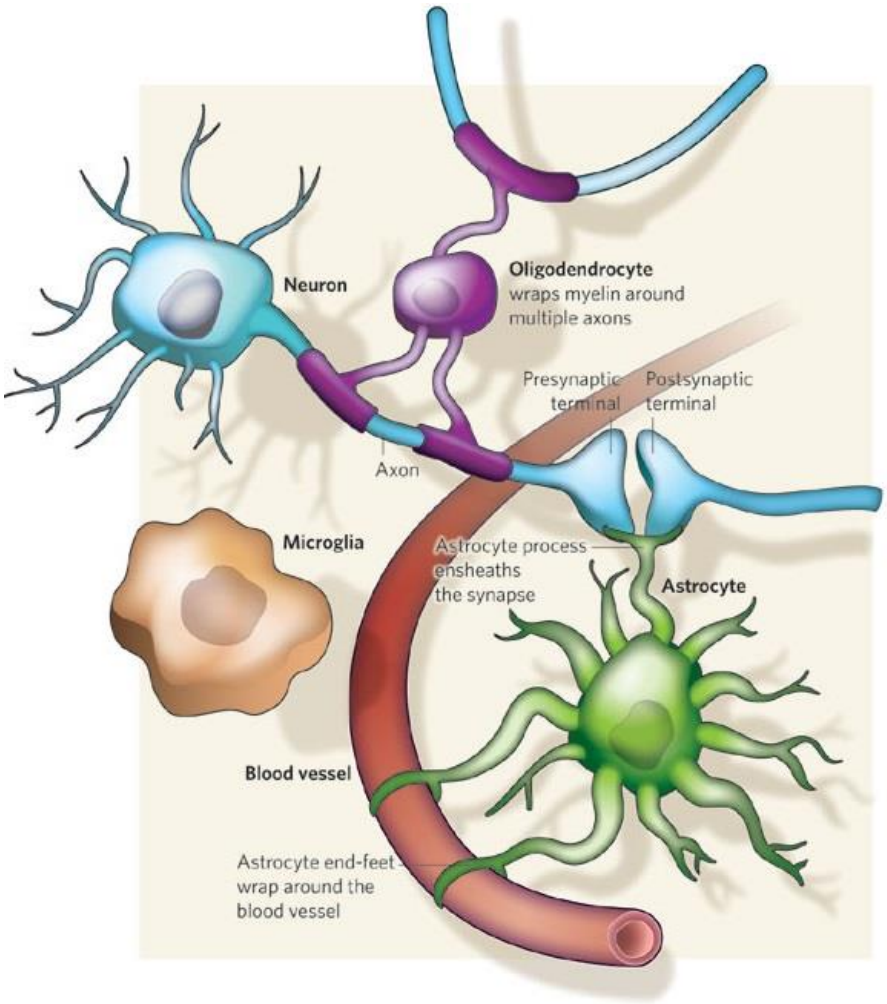

Figure 1.3 | Interactions between glia and neurons. The three major types of glia interact with neurons (blue) and surrounding blood vessels (red). Oligodendrocytes (purple) built up myelin sheath around the axon of neurons, thereby accelerating neuronal transmission. Microglia (brown) are the resident immune cells in the nervous system keeping it under constant surveillance for damage and infection. Astrocytes (green) interact with both blood vessels and neurons contributing to the homeostasis in the brain. Ensheathing the synaptic cleft, astrocytes actively modulate synaptic transmission. (Allen and Barres, 2009)

To our current knowledge, the three major groups oligodendrocytes, microglia and astrocytes have the following characteristics:

Oligodendrocytes (Figure 1.3; purple) are well known for their lipid-rich membrane structure called myelin, which is wrapped around the axons of vertebrates' neurons. Myelin acts as an insulator essential for high conduction velocities of action potentials. Without this insulation, the complex organization of the vertebrates' nervous system would not be possible. Various diseases have been described, most prominent multiple sclerosis, which involve "demyelination" of axons and thereby illustrating the importance of myelin sheaths to the complex nervous system.

Microglia (Figure 1.3; brown) are the resident immune cells in the brain, derived from mesenchymal/mesodermal origin. These cells acquire a specialized phenotype in the CNS, differentiating them drastically from their precursors, the blood-derived monocytes. As immune cells, they constantly survey the brain for any damage or infection and clear up dead cells and cell debris. With their highly plastic processes, they are also proposed to interact with synapses, specifically to remove inappropriate connections by phagocytosis.

Astrocytes (Figure 1.3; green) fulfill different and very complex roles in the mature brain. For instance, they contribute to the homeostasis in the brain by controlling blood flow, but they also remove neurotransmitter molecules from the extrasynaptic space, thereby regulating synaptic transmission. Recently, astrocytes have been implicated also in bidirectional communication with neurons. Therefore, astrocytes became a new determinant of all processes involving neuronal plasticity. For this reason, the next paragraph is dedicated solely to them.

1.1.2. Astrocytes

Astrocytes are the most numerous (Savchenko et al., 2000) and additionally most diverse type of neuroglia in the CNS. They exhibit a vast heterogeneity in virtually every aspect of their biology, for instance in their morphology, glutamate receptor expression, gap junction coupling and Ca^{2+} signaling (Matyash and Kettenmann, 2010). In the mature brain, as earlier mentioned, astrocytes are broadly divided into two groups: protoplasmic astrocytes residing in the grey matter and fibrous astrocytes found in the white matter. Another apparent morphological class are radial astrocytes, like the Bergmann glia in the cerebellum. Protoplasmic astrocytes are characterized by their heavily branched morphology, exhibiting numerous fine processes attaining a length of about 50 µm. With all these processes, they interact with neurons and blood vessels, forming the so called ‘perivascular’ endfeet. Fibrous astrocytes, however, have much less elaborate processes but instead, they are much longer (up to 300 µm). They form so called ‘perinodal’ processes contacting axons at nodes of Ranvier (Kettenmann and Verkhratsky, 2011). To address the role of morphological plasticity of astrocytes and to analyze the underlying mechanisms, dissociated cultures of astrocytes have been used for about 40 years. Here, astrocytes attain a flat, epithelioid morphology. Still, they were shown to be able to reacquire, at least partially, the *in situ* phenotype by co-cultivation with dissociated neurons (Hatten, 1985) or, in an actin dependent manner, after the application of dibutyryl cAMP (db-cAMP, (Goldman and Abramson, 1990)). This process, often referred to as stellation, is characterized by a cytoplasmic retraction, the formation of thin processes and

actin remodeling (Baorto et al., 1992; Racchetti et al., 2012; Ramakers and Moolenaar, 1998).

Neuronal-glial signaling: the concept of the tripartite synapse

In the grey matter, the small processes of protoplasmic astrocytes are closely associated with synaptic structures. These highly motile structures are termed peripheral astrocytic processes (PAPs) and enwrap presynaptic terminals as well as postsynaptic structures. Perisynaptic glia express various receptors for neurotransmitter, enabling them to receive direct input from the synapse. These receptors are characterized by their high affinity and slow desensitization, implying a low concentration of neurotransmitter to be sufficient for astrocytic activation (for details see (Araque et al., 2014). Astrocytes respond with localized or global changes in intracellular calcium ion concentration (Wang et al., 2006). Activated glia in turn release so called 'gliotransmitters' such as ATP (Di Castro et al., 2011; Halassa et al., 2009), D-serine (Henneberger et al., 2010; Takata et al., 2011) and glutamate (Han et al., 2012; Min and Nevian, 2012; Navarrete et al., 2012). This functional and structural association of perisynaptic astrocyte to synaptic structures gave rise to the term 'tripartite synapse' (Figure 1.4).

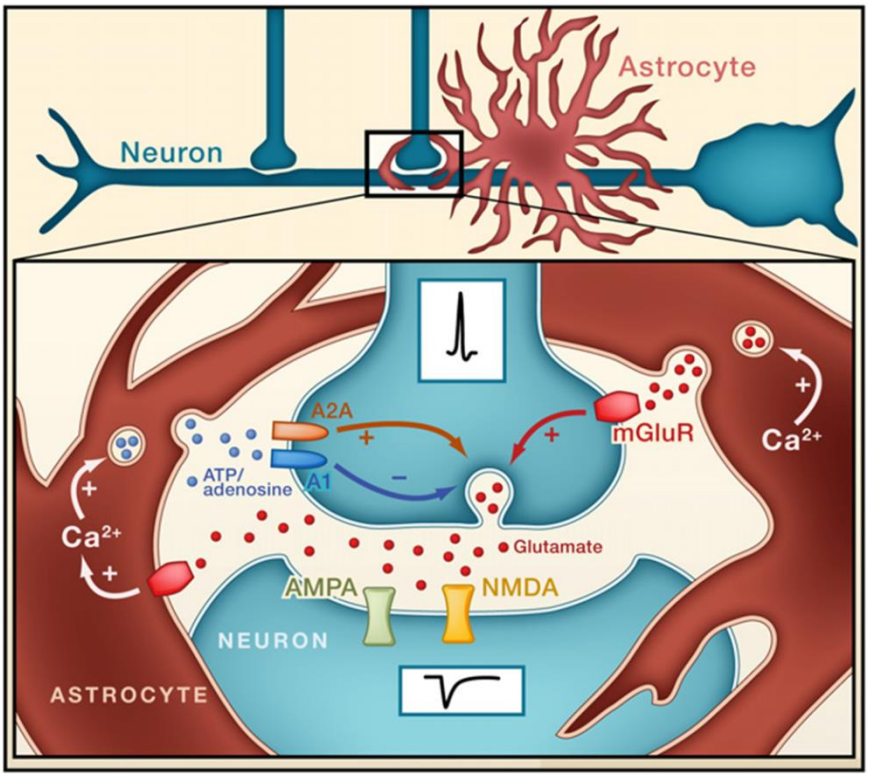

Figure 1.4 | The tripartite synapse. The pre- and postsynapse is ensheathed by an astrocytic process. Astrocytes detect action potentials through their metabotropic glutamate receptors (mGluRs). This in turn leads to calcium elevations, which may trigger the release of 'gliotransmitters' affecting synaptic transmission. Adapted from (Navarrete and Araque, 2011)

Astrocytes react upon neuronal stimuli also with morphological plasticity, for instance, the coverage of the synapse by the corresponding PAP is increased upon whisker stimulation *in vivo* (Genoud et al., 2006). Accordingly, retraction of PAPs from the synapse results in alteration of synaptic transmission (Oliet et al., 2001). This highly dynamic morphology depends to a great extent on the actin cytoskeleton, as application of cytochalasin D drastically impairs the motility of astrocytic processes (Haber et al., 2006).

Intercellular signaling in astrocytes

A single astrocyte can enwrap several thousands of synapse, thereby modulating synaptic transmission. An interconnected network of astrocytes could couple neurons into functional units, implicating astrocyte-astrocyte communication in complex cognitive functions (Navarrete and Araque, 2011). Therefore, the understanding of the underlying mechanisms initiating and regulating glial interconnectivity are matter of investigation. Astrocytes in culture exhibit a pronounced calcium wave following diverse stimuli that propagates up to hundreds of cells (Cornell-Bell et al., 1990; Scemes and Giaume, 2006). The mechanism of intercellular calcium wave (ICW) propagation has been studied intensively in cultured astrocytes. Two distinct mechanisms have been defined: (1) gap junctional channels between neighboring astrocytes allow direct intercellular diffusion of second messengers or (2) calcium-raise induced release of ATP, which diffuses extracellularly to purinergic receptors of neighboring and distant cells (Figure 1.5, (Scemes and Giaume, 2006)).

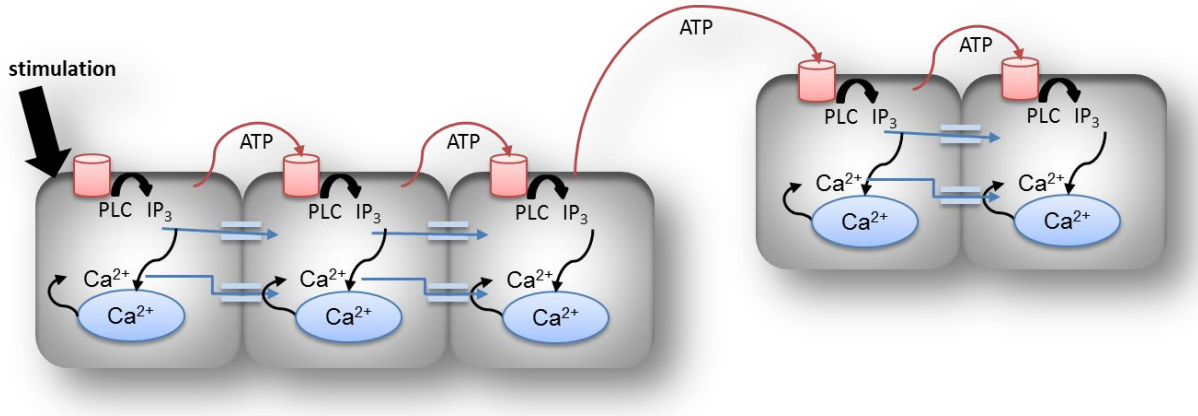

Figure 1.5 | Intercellular calcium wave propagation. Mechanical stimulation of a glia cell evokes a local Ca^{2+} elevation, which is propagated by two distinct mechanisms. Upon stimulation, Ca^{2+} is released from internal stores in response to IP_3. IP_3 or Ca^{2+} can diffuse to adjacent cells through gap junctions (light blue channels) and thereby cause direct short range signaling (blue). Additionally, the local calcium increase causes the release of ATP, which in turn can bind to purinergic receptors (red barrels) on neighboring as well as non-contacting astrocytes (adapted from (Haydon, 2001)).

For several years, long-range glial signaling via calcium waves was thought to be only relevant during development (Parri et al., 2001), in pathological conditions (Peters et al., 2003) or in specialized tissues like the retina (Newman and Zahs, 1998). But recently, large-scale calcium waves ('glissandi') in the hippocampal astrocytes of living rats under physiological conditions were described (Kuga et al., 2011). These large-scale calcium waves were found to emerge upon neuronal activity and influence the flow of red blood cells, indicating a physiological relevance of this phenomenon. Glissandi exhibit dependence on purinergic receptors as well as on gap junctions, in concordance to the intercellular calcium waves in cultured astrocytes. These findings promote further studies to investigate the fundamental properties of large-scale calcium waves in culture and *in situ.*

The gap junctional channels of astrocytes are composed of connexins, a family of highly conserved integral membrane proteins. A single connexin molecule consists of four transmembrane domains, connected by two extracellular loops and one intracellular loop, with intracellular N- and C-terminal tails. An oligomer of six connexins is termed connexon or hemichannel. Two hemichannels on opposing cells form a gap junction. Astrocytes are extensively coupled by gap junctions forming the so called 'glial syncytium' (Rash et al., 2001). Astrocytes express the connexins Cx30, Cx43 and spatially restricted also Cx26 (for review see (Theis and Giaume, 2012). Cx43 is established as a central player in brain development and physiology (Elias et al., 2007; Pannasch and Rouach, 2013). Recently, the predominantly in the gray matter expressed Cx30 was revealed to be a critical regulator of synaptic strength by controlling the localization of PAPs to the synaptic clefts (Pannasch et al., 2014). Mice depleted of both Cx30 and Cx43 were completely lacking astrocytic coupling in the hippocampus (Wallraff et al., 2006). In cultured astrocytes devoid of neuronal cells, Cx43 is the predominant isoform (Giaume et al., 1991). As already mentioned, the second important pathway of intercellular communication in astrocytes is mediated by the extracellular messenger ATP. The intracellular Ca^{2+} elevations are caused here by the activation of P2 purinoreceptors (Butt, 2011). These receptors are subdivided into two families: the metabotropic P2Y receptors and the ionotropic P2X receptors. Glial cells in the CNS express a variety of different purinergic receptors (for review see (Burnstock and Knight, 2004). P2 family receptors are involved in the control of neuron-glia interactions during development and disease (for review see (Del Puerto et al., 2013).

Despite certain progress during the last years in elucidating the molecular mechanisms underlying the glia-neuron and glia-glia interconnection, a variety of questions remains unanswered. The majority of astrocytic functions were shown to rely on their intrinsic high

plasticity. Only very few studies, however, did address the role of astrocytic cytoskeleton, allowing this astonishing amount of cellular plasticity.

The astrocytic cytoskeleton

As in other eukaryotic cells, the astrocytic cytoskeleton consists of three main types of filaments: microfilaments, intermediate filaments and microtubules. A vast majority of research on the cytoskeleton of astrocytes has been performed on their main and very prominent intermediate filament protein glial fibrilliary acidic protein (GFAP). GFAP was not only shown to provide structural stability for astrocytes but also to be involved in essential astrocytic functions (for review: (Middeldorp and Hol, 2011)). Microtubules and their role in astrocytic migration and polarization have been extensively studied by Etienne-Manneville and colleagues (reviewed in: (Dupin and Etienne-Manneville, 2011; Etienne-Manneville, 2013).

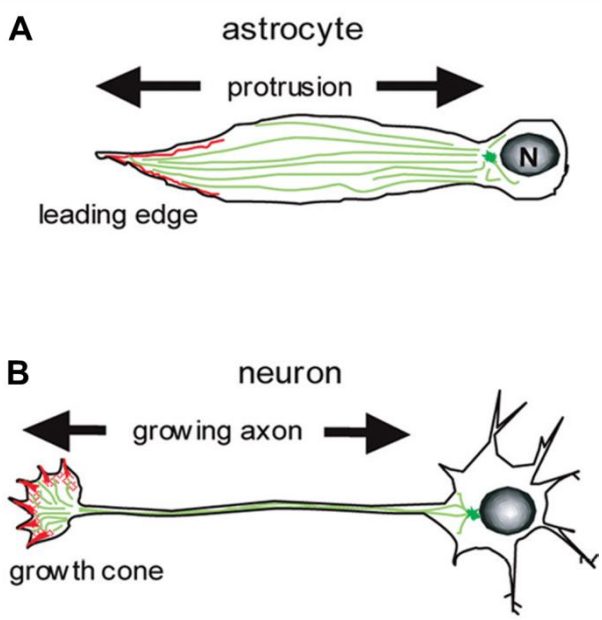

Figure 1.6 | Organization of actin and microtubule cytoskeleton in cellular protrusions of in astrocytes and neurons. (A) Astrocytes display long (up to 100 µm) protrusions markedly enriched of microtubules (green) upon induced migration. Filamentous actin (red) is mainly located at the leading edge of the migrating astrocyte. **(B)** In growing neurons, the actin rich zone (red) is limited to the growth cone, while long microtubules (green) extend from the cell body to the growth cone. Adapted from (Etienne-Manneville, 2004)

1.2. The microfilament system

The highly conserved structural protein actin (42 kDa) was identified in all types of eukaryotes analyzed so far (Schleicher and Jockusch, 2008). In eukaryotic cells actin is present in two forms, the monomeric G-actin and the filamentous F-actin. During the last decades, the mechanism of actin polymerization was precisely analyzed *in vitro*. The initial nucleation is kinetically unfavorable and therefore the speed determining step in the process of actin filament assembly. Under appropriate conditions a nuclei is formed from actin trimer (Cooper et al., 1983), and subsequently, actin monomers are added to form a filament. Due to the polarity of actin monomers, the filament formed has a minus (-) and a plus (+) end exhibiting different kinetics (Pollard, 1986). After incorporation, ATP is

hydrolyzed and a conformational change occurs within the actin molecule which leads to an affinity reduction favoring depolymerization at the minus end of the filament. The subsequent process of constant remodeling (Fujiwara et al., 2002) is known as actin treadmilling (Figure 1.8).

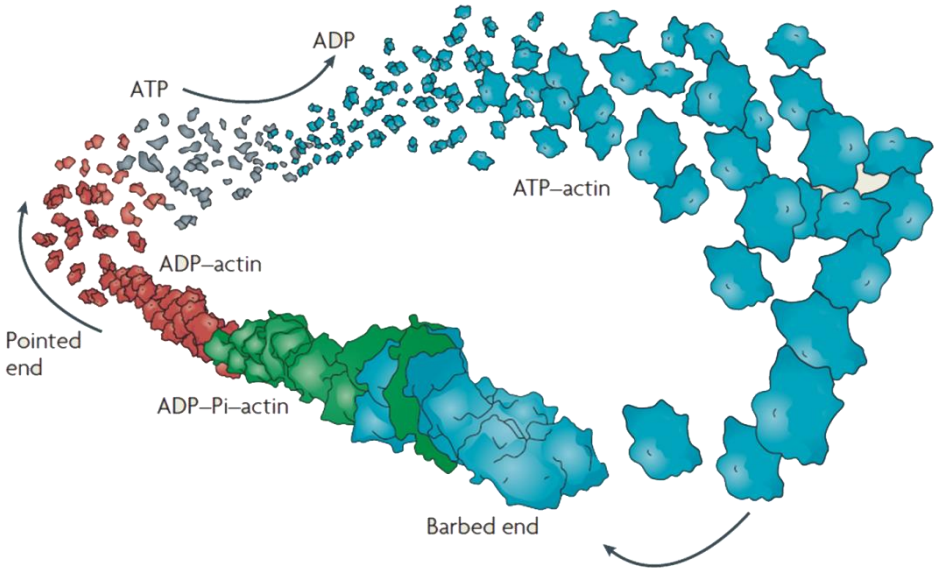

Figure 1.8 | Illustration of actin treadmilling. ATP-bound G-actin preferably bounds to the barbed (+) end of actin filaments. Hydrolyzation of the ATP occurs within the actin filament. Depolymerization of the ADP-bound G-actin takes place at the pointed (-) end of the filament. After depolymerization, the ADP is again exchanged to ATP on free diffusible g-actin. From (Pak et al., 2008)

1.3. Actin binding proteins

In the living cell, actin dynamics are tightly regulated by a plethora of actin binding proteins (ABP). These proteins, for instance sequester actin monomers, promote filament elongation or work as filament caps (Figure 1.9). *De novo* synthesis of actin filaments as a kinetically unfavorable process is facilitated by Arp2/3 complex (Goley and Welch, 2006) and also by formins and WH2-domain containing nucleators (Campellone and Welch, 2010). Activators of the Arp2/3 complex are termed nucleation promoting factors (NPFs), which are divided into class I and II. Class I is composed of the Wiskott-Aldrich syndrome protein (WASP), WASP family Verprolin-homologous protein (WAVE) and several recently discovered proteins (for review (Campellone and Welch, 2010)). Class II consists of cortactin (CTTN) and the haematopoetic-specific protein 1 (HS1), which are characterized by their ability to interact with actin. Constant remodeling of actin filaments is also controlled by numerous proteins, like the small ABPs cofilin and profilin (Figure 1.9).

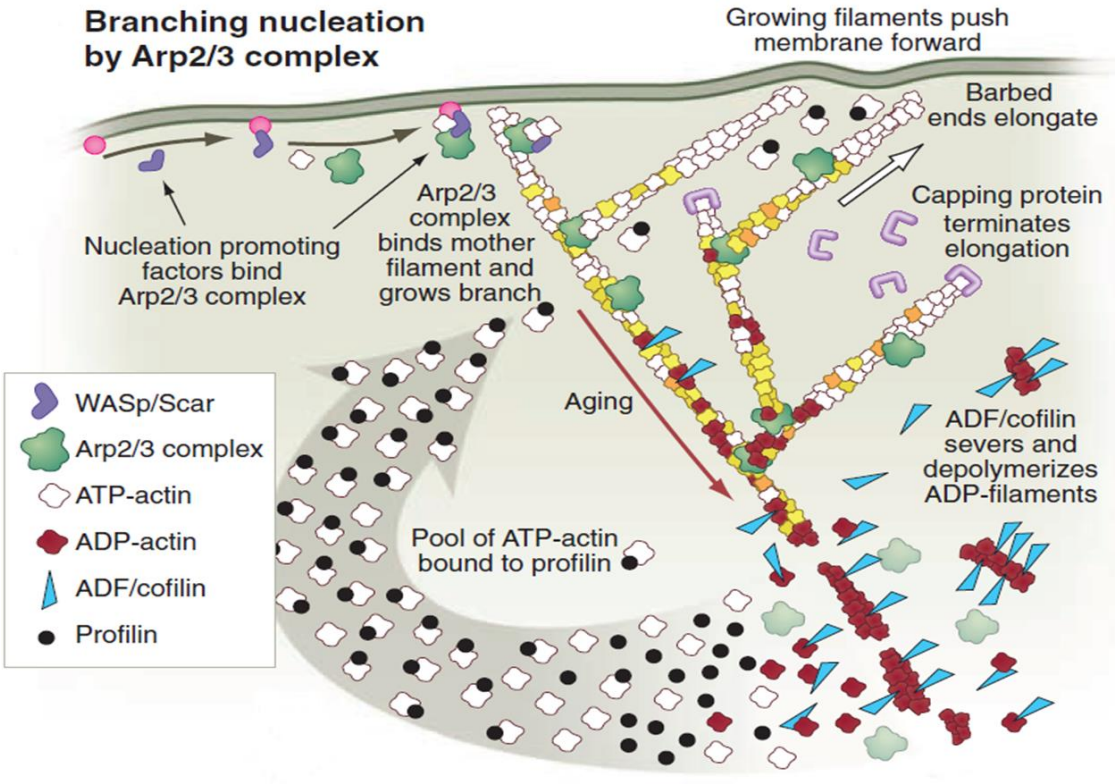

Figure 1.9 | Formation of a branched actin network nucleated by Arp2/3 complex. After initial activation of nucleation promoting factors (NPFs, here WASp/Scar) by external signals, these factors bind to the Arp2/3 complex. This activated complex subsequently binds to a mother filament and initiates the formation of a new daughter filament. The barbed ends of the new filament rapidly elongate by the addition of profilin bound ATP loaded actin monomers. The growth of some filaments is terminated by the binding of a capping protein (light purple). Hydrolization of ATP at actin molecules within the filament indicates filament aging. ADP-actin is subsequently severed or depolymerized by ADF/cofilin. The G-actin pool is thereby replenished. Profilin binds to monomeric actin and recharges it with ATP, reintroducing ATP-actin into the cycle. (Pollard and Cooper, 2009)

Disassembly of actin filaments is especially important to provide barbed ends for the generation of new filaments and to replenish the monomer pool. This process is driven by the family of actin depolymerization factors: ADF, cofilin-1 and cofilin-2. These proteins preferentially bind to ADP-bound actin at the pointed end and promote filament severing or depolymerization. The G-actin binding protein profilin facilitates the exchange of ADP to ATP at the actin molecule and also interacts with various ligands besides actin (Jockusch et al., 2007). Therefore, profilins are interesting players in the regulation of actin dynamics in eukaryotic cells.

1.3.1. Profilins

First described as inhibitor of actin polymerization in 1977 by Carlsson and colleagues (1977), profilins are small (14 – 17 kDa) actin monomer binding proteins. Profilins are proteins common to all so far analyzed eukaryotes. Relatively primitive, single cell organisms like *Saccharomyces cerevisiae* possess one gene coding for profilin (Haarer et al., 1990), whereas some in plants up to ten different genes coding for profilin isoforms were identified (Huang et al., 1996). In mammalia, four different genes coding for profilin isoforms have so far been identified (for review (Jockusch et al., 2007)). Studies comparing primary sequence homology between profilins exhibited a relatively low similarity. Nevertheless, the three dimensional structures of profilins are highly conserved throughout the phyla (Polet et al., 2007). Profilins are characterized by their ability to bind to G-actin, phosphatidylinositol and proteins containing poly-proline stretches (Figure 1.10).

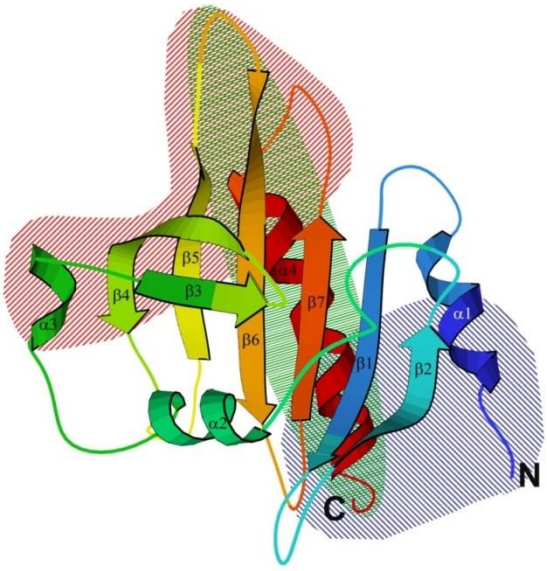

Figure 1.10 | Three dimensional structure of bovine profilin. The three major ligand binding sites are indicated. Red: G-actin; green: phospholipids; blue: poly-proline ligands (Jockusch et al., 2007)

Basing on these properties, profilins interact with numerous ligands, influencing focal contacts, synaptic scaffold, membrane trafficking and Rho GTPase dependent signaling in the cytosol (for review (Jockusch et al., 2007; Witke, 2004)).

Mammalian profilin isoforms

In mammalia, four different profilin genes with different expression patterns have been described. Profilin 1 (PFN1) was shown to be ubiquitously expressed and essential (Witke et al., 1998; Witke et al., 2001). PFN2, however, was shown to be alternatively spliced, resulting in the biochemically distinct isoforms PFN2a and PFN2b (Di Nardo et al., 2000; Lambrechts et al., 2000). PFN2a shows its highest expression in brain (Witke et al., 1998), while PFN2b is especially expressed in kidney (Di Nardo et al., 2000). Additionally, two testis specific profilin isoforms PFN3 and 4 have been identified (Braun et al., 2002; Hu et al., 2001; Obermann et al., 2005). Here, the focus will be on the profilin isoforms PFN1 and PFN2a, which are expressed throughout the mammalian CNS. Mammalian PFN1 and PFN2a display about 65% sequence homology (Witke, 2004). Their biochemical properties are similar but not identical. Specifically, both isoforms have an identical affinity to G-actin but PFN2a has a higher affinity to poly-(L)-proline stretches combined with a lower affinity towards phosphatidylinositol 4,5 bisphosphate (PIP_2) (Lambrechts et al., 2000) compared to PFN1.

Cellular functions of profilins

The importance of PFN1 to fundamental cellular functions in mammalian cells becomes evident by the result of its depletion from mice: they fail to develop beyond the blastocyst stage (Witke et al., 2001). Also, the inhibition of PFN1 function in bovine zygotes or early embryos by antibodies block the development of the respective animal (Rawe et al., 2006). Furthermore, a RNA-interference (RNAi) based approach revealed a central role of PFN1 in endothelial proliferation, migration and early cord morphogenesis (Ding et al., 2006). In neuronal cells, where two profilin isoforms are expressed, the analysis of the specific roles of profilin isoforms is far more complicated. The targeted depletion of PFN1 from principal neurons did not reveal obviously impaired neuronal functions or morphology (Gorlich et al., 2012). These findings promote two alternative hypotheses: (1) PFN1 may be dispensable in neuronal cells and (2) PFN2a may compensate the lack of PFN1 in all essential functions. Mice lacking PFN2a are vital, but exhibit brain specific alterations in controlling vesicle release, neuronal excitability and complex behavior (Pilo Boyl et al., 2007). Consistently, PFN2a was found to be associated with effectors of exocytotic and endocytotic pathways (Witke et al., 1998). Furthermore, the lack of PFN2a was shown to increase endocytosis, while its overexpression inhibited the aforementioned process (Gareus et al., 2006). The postsynaptic role of profilins is currently under debate, as neither the transgenic mouse lacking PFN1 in principal neurons nor the $PFN2a^{-/-}$ transgenic mouse exhibit altered postsynaptic properties. Nevertheless, several studies indicate both profilin isoforms in postsynaptic plasticity. In fact, re-introduction of either

PFN1 or PFN2a was sufficient to rescue structural alterations in the dendritic spine number caused by the RNAi-mediated knockdown of PFN2a (Michaelsen et al., 2010). Furthermore, both PFN1 (Neuhoff et al., 2005) and PFN2a (Ackermann and Matus, 2003) have been shown to be targeted to dendritic spines upon unspecific activity induction. Also a more specific induction of neuronal activity by brain-derived neurotrophic factor (BDNF) was adequate to target both profilin isoforms to dendritic spines (Murk et al., 2012). Taken together, these findings support the hypothesis, that profilin isoforms can compensate for each other in most cellular functions. Still, PFN2a was found to have isoform specific function in the brain: PFN1 was not capable to rescue alterations in the dendritic morphology of PFN2a downregulated pyramidal neurons (Michaelsen et al., 2010) and additionally, PFN2a exhibit a far more pronounced colocalization with gephyrin (Murk et al., 2012). But also PFN1 has isoform specific properties. Specifically, solely PFN1 translocates to the nucleus of neuronal cells upon BDNF stimulation (Murk et al., 2012). Furthermore, for the avian PFN1, protein level and cellular localization was shown to be culture condition dependent (Murk et al., 2009). The current theoretical understanding of the underlying molecular mechanisms was summarized by Jockusch and colleagues (Figure 1.11; (2007)).

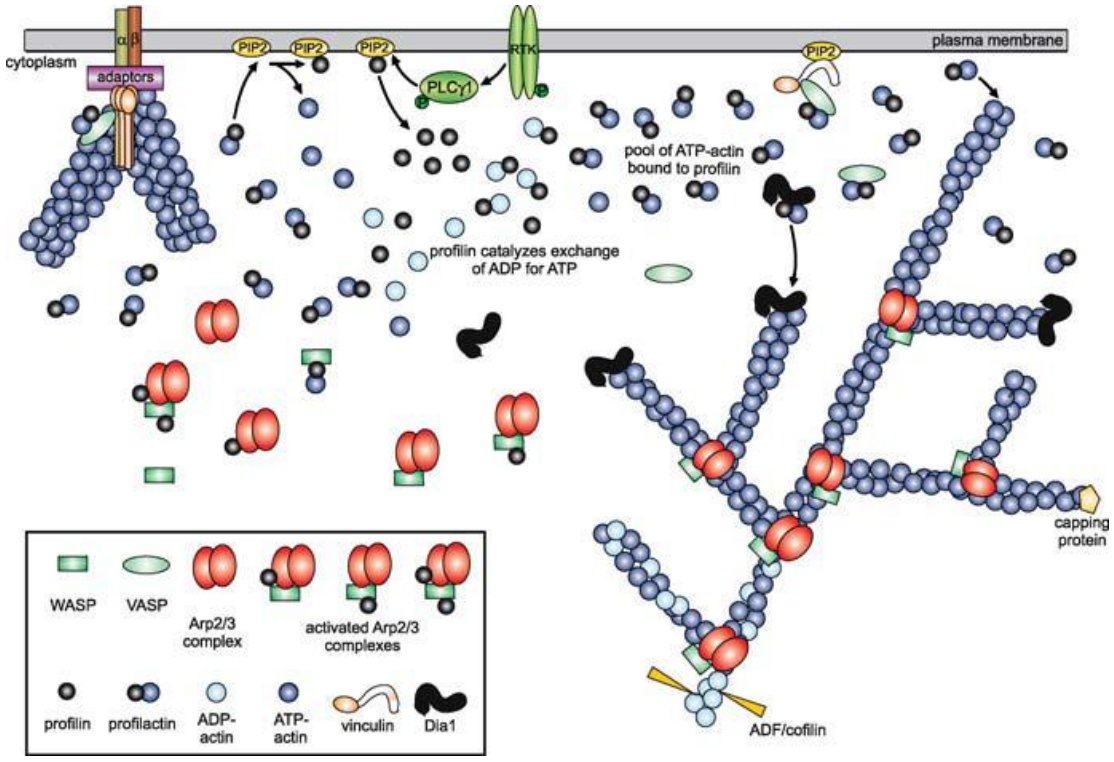

Figure 1.11 | Illustration of the functional involvement of profilins at the plasma membrane. Profilin is bound to the membrane in a PIP_2 dependent manner. Upon release from the membrane, profilin interacts with G-actin and is involved its charging with ATP (center). This profilin-ATP-G-actin complex participates in the generation and elongation of actin filaments for instance needed for adhesion complexes (left) or actin networks (right). Hypothetic model by (Jockusch et al., 2007)

Regulation of profilins by phosphorylation

During the last decades several studies addressed the regulation of profilin isoforms by phosphorylation. Initial *in vitro* studies revealed profilin as a phosphorylation target of protein kinase C (Hansson et al., 1988; Vemuri and Singh, 2001). This phosphorylation was subsequently shown to alter the interaction of profilin with actin and poly-(L)-proline (Sathish et al., 2004). The phosphorylation was found to be dependent upon activation of the PI3-kinase, resulting in an increased affinity towards poly-(L)-proline and monomeric actin. Da Silva and colleagues described an essential role of PFN2a phosphorylation by the RhoA dependent kinase ROCK in neuronal outgrowth (2003). ROCK dependent profilin phosphorylation at serine residue 137 reduces the affinity towards actin and huntingtin (Shao et al., 2008). The same authors recently described profilin desphosphorylation to be performed by the protein phosphatase 1 (Shao and Diamond, 2012). This ROCK dependent pathway is altered in the spinal muscular atrophy disease, where the loss of survival of motor neuron protein leads to a hyper-phosphorylation of PFN2a (Nolle et al., 2011). As a third pathway leading to profilin isoform phosphorylation, protein kinase A (PKA) dependent phosphorylation was found (Figure 1.12; (Lederer, 2002)). However, PKA dependent phosphorylation of profilin isoforms has not been attributed to a specific cellular process so far.

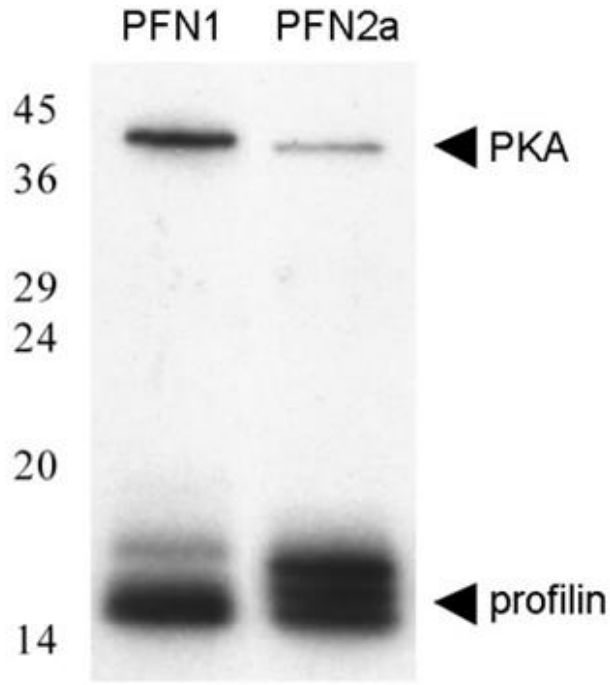

Figure 1.12 | PKA phosphorylates profilins at multiple sites *in vitro*. Catalytic subunit of the cAMP-dependent protein kinase A (PKA) was used to phosphorylate PFN1 or PFN2a. Adapted from (Lederer, 2002)

Taken together, phosphorylation of PFN1 and PFN2a markedly alters the biochemical properties of the profilin isoforms and is therefore indicated in the regulation of numerous cellular processes.

Role of profilin 1 in astrocytes

Analysis of the astrocytic transcriptome in comparison to other cell populations in the brain revealed an expression of both PFN1 and PFN2a in astrocytes (Cahoy et al., 2008; Doyle et al., 2008; Lovatt et al., 2007). Nevertheless, so far only the function of PFN1 has been addressed in studies with astrocytes. Molotkov and colleagues investigated the importance of PFN1 to the formation and motility of peripheral astrocytic processes (2013). The morphological analysis of astrocytes expressing an actin-binding deficient PFN1-mutant revealed a decrease of size for astrocytes expressing the profilin mutant, but no alterations in the overall morphology. Additionally, the response to Ca^{2+} induced protrusion outgrowth was drastically reduced in mutant astrocytes. These findings suggest PFN1 as a regulator of Ca^{2+} induced outgrowth of PAPs. PFN1 was also proposed in the radial migration of cerebellar granule neurons along Bergmann glia in the cerebellum (Kullmann et al., 2012). Their results revealed a slight reduction in the overall length of astrocytic processes in PFN1 knockout animals. Moreover, adhesion between Bergmann glia and cerebellar granule neurons was drastically reduced if either one of both interaction partners was depleted of PFN1, suggesting PFN1 as a regulator of adhesion and process length in Bergmann glia.

In summary, the precise role of profilin isoforms in diverse cellular functions of astrocytes and the question of the overlapping, as well as specific functions of PFN1 and PFN2a remain elusive.

1.3.2. Cortactin

Besides profilins, also the Arp2/3 complex and its class I NPFs were recently identified as regulators of astrocytic morphology and function (Murk et al., 2013). Hence, the class II NPF cortactin is likely to be also involved in this context. In 1991, cortactin was discovered as a major substrate of the v-Src tyrosine kinase and shortly afterwards described as an F-actin binding protein (Wu and Parsons, 1993; Wu et al., 1991). Cortactin is composed of 546 amino acids and attains a size of 80 to 85 kDa. It exhibits a complex domain structure (Figure 1.13).

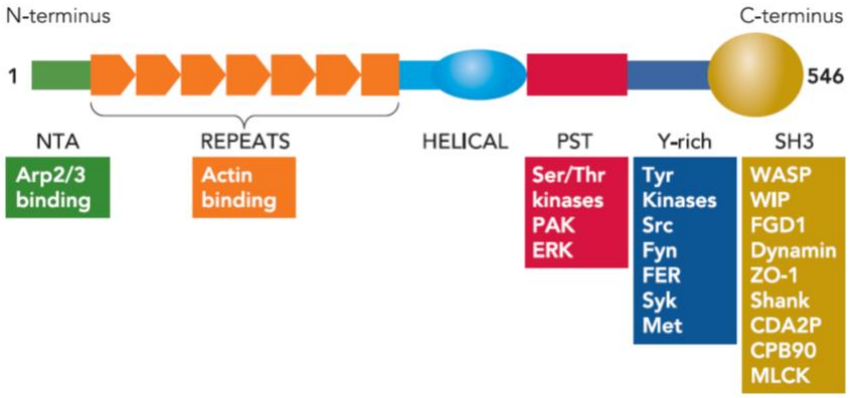

Figure 1.13 | Domain structure of cortactin. Functional domains are indicated on top and interaction partners for the respective domain are indicated below. N-Terminal half interacts with the cytoskeletal elements, whereas the c-terminal half harbors the phosphorylation sides and the SH3 domain regulating interaction with other proteins. (Cosen-Binker and Kapus, 2006)

Specifically, the N-terminal half consist of an 'N-terminal acidic region' (NTA), which harbors the binding site for the Arp3 subunit of the Arp2/3 complex and 6.5 tandem repeats, responsible for the binding to filamentous actin. The C-terminal consists of an α-helical domain with unknown function, followed by a proline-serine-threonine (PST) and tyrosine rich region (Y-rich), harboring several phosphorylation sides and a Src homology 3 domain (SH3). By these characteristics, cortactin is thought to link receptor mediated signal transduction to cytoskeletal organization of the cell.

Cellular functions of cortactin

Cortactin was found to be a key regulator of cytoskeletal dynamics in various cellular processes (Ammer and Weed, 2008; MacGrath and Koleske, 2012). In fact, functions of cortactin were described at a plethora of sites of dynamic changes in cellular structure: entry sites of intracellular pathogens (Selbach and Backert, 2005), invadopodia of tumorous cells (Bowden et al., 2006), lamellipodia of migrating cells (Bryce et al., 2005), the leading edge of growth cones (Kinnunen et al., 1998; Kurklinsky et al., 2011), endocytotic vesicles (Cao et al., 2003; Kaksonen et al., 2000) and intercellular contacts (El Sayegh et al., 2004; Helwani et al., 2004). In neuronal cells cortactin is, besides its role in growth cone motility, notably localized in spines (Hering and Sheng, 2003) and undergoing activity dependent redistribution (Iki et al., 2005; Seese et al., 2012). In 2009, Lai and colleagues suggested a regulatory function of cortactin (Lai et al., 2009). Specifically, cortactin was described to be dispensable for Arp2/3 complex activation during lamellipodia protrusion or clathrin mediated endocytosis. Nevertheless, migration of cortactin depleted cells was impaired, but could be rescued by the introduction of constitutively active Rho GTPases Rac1 and Cdc42. This indicates a role of cortactin in the activation of Rac1 and Cdc42.

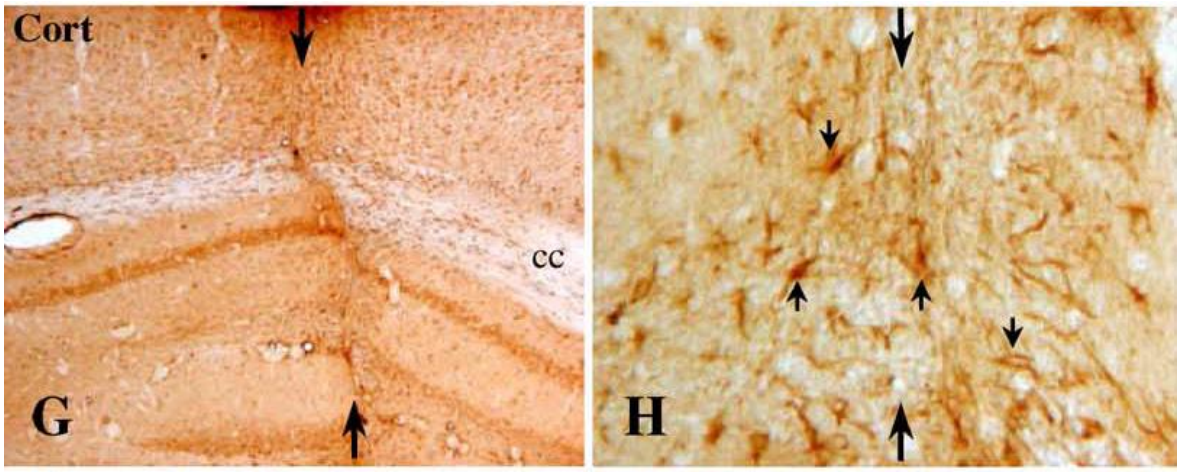

Figure 1.14 | Expression pattern of cortactin after a CNS injury. 2 weeks after induction of a mechanical lesion in the cerebral cortex **(G, arrows)**, protein distribution was analyzed. Intense cortactin immunoreactivity was observed in astrocytes at the lesion site **(H, arrows)**. Adapted from (Decourt et al., 2005)

The cellular function of cortactin in astrocytes has so far not been addressed in detail. Cortactin expression was shown to be upregulated in astrocytes (Figure 1.14; (Decourt et al., 2005), but the underlying mechanisms are still unknown. Nevertheless, Cdc42 fulfils an important function in the migration and polarization of astrocytes in culture (Etienne-Manneville and Hall, 2001; Osmani et al., 2010) and *in vivo* (Robel et al., 2011), and Rac1 was indicated as a key regulator of astrocytic stellation (Racchetti et al., 2012).

Cortactin is also likely to fulfil a role in the intercellular communication of astrocytes. The major astrocytic connexin Cx43 was shown to interact directly with cortactin in seminiferous tubules (Vitale et al., 2009).

All in all, these findings hint to a remarkable cellular function of cortactin in astrocytes.

1.4. Aim of study

Astrocytes are highly plastic cells with a complex and ramified morphology. Changes in cellular morphology and motility are closely related to astrocytic function. Their thin, heavily branched and exceedingly motile processes enwrap pre- and postsynapse, framing an intimate partnership essential for synaptic function. Astrocytic motility and morphology is reliant on the dynamic microfilament system. Actin dynamics are tightly regulated by a plethora of actin binding proteins. The work presented in this thesis focusses on two major regulators of cytoskeletal dynamics; profilins and cortactin.

(1) Until today, the functional diversity of profilin isoforms 1 and 2a has not been addressed in astrocytes. Studies of their properties in neuronal cells revealed isoform specific as well as overlapping cellular functions. Here, the specific physiological functions of PFN1 and PFN2a in astrocytes are to be analyzed taking advantage of a RNA-interference based isoform specific knockdown system. Additionally, the underlying molecular mechanisms liking astrocytic morphology and profilin activity are to be investigated.
(2) Cortactin is highly implicated as a modulator of astrocytic intercellular communication and, additionally, astrocytic response to brain injury. In this approach, cultured astrocytes of conventional cortactin knockout mice were used to address the question of the cellular functions of cortactin.

Finally, both experimental approaches aim to gain new insights into the involvement of the microfilament system and its regulators in fundamental physiological functions of astrocytes.

2. Materials and methods

2.1. Reagents

All chemicals used in this thesis have been distributed by AppliChem, Hoechst, Invitrogen, PAA, Roth or Sigma. Exceptions were described separately. All enzymes have been purchased at New England BioLabs or Fermentas.

2.2. Solutions and media

Dulbeccos's Modified Eagle Medium (DMEM)	
Glucose	1.0 g
L-Glutamine	20 ml
FCS	10%
Na-Pyruvate	3.7 g

Enriched DMEM for Transwell Assay	
Glucose	4.5 g
L-Glutamine	20 ml
FCS	20%
Na-Pyruvate	3.7 g
Chicken embryo extract	2%

Lysogeny Broth (LB)-Medium	
Trypton	10 g/l
NaCl	10 g/l
Yeast Extract	5 g/l
Agar (Plates)	15 g/l
Anitibiotics if necessary	Ampicillin 100 µg/ml Kanamycin 50 µg/ml

Phosphate Buffered Saline (PBS), pH 7.4:	
KCl	2.7 mM
KH_2PO_4	1.5 mM
NaCl	137 mM
Na_2HPO_4	10.4 mM

HBSS for Imaging	
10 x HBSS stock solution	50 ml
CaCl2 · H2O	145 mg
$NaHCO_3$	175 mg
H_2O (MilliQ)	ad. 500 ml

10x TAE buffer	
Tris	96,8 g
Glacial acetic acid	22,8 ml
0,5 M EDTA; pH 8	40 ml
H_2O (MilliQ)	ad. 2 L

4x DNA sample buffer	
Bromophenol blue	250 mg
Xylene Cyanole	250 mg
150 mM Tris	33 ml
Glycerol (87%)	60 ml
H_2O (MilliQ)	7 ml

4x SDS sample buffer	
Tris/HCl (pH 6.8)	375 mM
SDS	2%
Glycerol 87%	12%
Bromophenol Blue	0.05%
β-Mercaptoethanol	10%

10x SDS buffer	
Tris	60.6 g
Glycine	288.2 g
SDS (pH 8.6)	20 g
H_2O	ad. 2 l

Separation gel buffer	
Tris	1.5 M
SDS (pH 8.8)	0.4%

Stacking gel buffer	
Tris	0.6 M
SDS (pH 6.8)	0.4%

1x Semi-dry blot buffer	
Tris/HCl (pH 8.5)	25 mM
Glycine	150 mM
Methanol	10%

10x TBS	
Tris/HCl (pH 7.6)	0.2 M
NaCl	1.37 M

1x TBS-T	
10x TBS	100 ml
Tween 20	0.1%

1x TBS-T	
10x TBS	100 ml
Triton X-100	0.1%

1:250 Trypsin/EDTA
Stocking Solution 1:10 in PBS

AM-Calcium dye solution
Dilute 50 µg AM-Calcium dye (Oregon Green® 488 BAPTA-1, Invitrogen) in 50 µl DMSO. Add 10 µl 2.5% Pluronic Acid in DMSO to 5 ml HBSS for imaging and pool both solutions.

Protease Inhibitor Mix	
Pepstatin A	1:500
AEBSF	1:500
Trasylol	1:100

Gey's Balanced Salt Solution pH 7.4 (GBSS)	
$CaCl_2$ * 2 H_2O	1.5 mM
KCl	5 mM
KH_2PO_4	0.22 mM
$MgCl_2$ * 6 H_2O	1 mM
$MgSO_4$ * 7 H_2O	0.28 mM
NaCl	137 mM
Na_2HCO_3	2.7 mM
Na_2HPO_4	0.86 mM
D-Glucose	5.5 mM

Kynurenic acid
Dissolve 946 mg Kynurenic acid in 5 ml 1 M NaOH, stir 2-3 h, add 45 ml H_2O, store sterile in 1 ml aliquots.

Preparation solution for organotypic cultures pH 7.2	
GBSS	98 ml
Glucose	1 ml
Kynurenic acid	1 ml

Cell culture medium for organotypic cultures	
BME	100 ml
HBSS	50 ml
Equine donor serum	50 ml
GlutaMAX (200 mM)	1 ml
Glucose (50%)	2 ml

2.3. Plasmids

For the analysis of profilin isoforms in astrocytes, several existing plasmids were used. To achieve a brighter fluorescence signal the coral GFP reporter gene was exchanged for an enhanced GFP fused to the 20-amino-acid farnesylation signal from c-Ha-Ras. Additionally, GFP gene expression was increased by the insertion of the Woodchack posttranscriptional regulatory element (WPRE).

As the co-expression of GFP-ß-actin and the respective shRNA construct was necessary for the analysis of the fluorescence recovery after photobleaching, profilin isoform targeting shRNA constructs were modified by the substitution of the GFP against mApple cDNA derived from pMApple-N1. All used plasmids are listed in table 2.1.

Table 2.1 | Plasmids used in this thesis.

Plasmid	Description	Reference
pEGFP-ß-actin	ß-actin fused to enhanced green fluorescent protein	C.A. Schönenberger
pRNAT-U6.3/Hygro-siFluc	siRNA Expression Vector targeting firefly luciferase	GenScript
pRNAT 1.3	siRNA Expression Vector based on pRNATU6.3/Hygro by GenScript, targeting PFN1	Kai Murk
pRNAT 2.13	siRNA Expression Vector based on pRNATU6.3/Hygro by GenScript, targeting PFN2a	Kai Murk
pEGFP-f	farnesylated enhanced green fluorescent protein (CMV promoter)	Clontech
pMCherry-f	farnesylated fluorescent protein mcherry (CMV promoter)	Bachelor Thesis Melissa O'Brien
pMApple-N1	Fluorescent protein mApple (CMV promoter)	Michael W. Davidson
pRNAT U6.2 lenti	lentiviral expression vector with U2 promoter	GenScript
pRNATin-H1.4/Lenti-EGFP-F(W)	Lentiviral shRNA expression vector based on pRNATin-H1.4/Lenti by GenScript, targeting PFN1	Jannike Köhle
pZNL-U6-sh1.3-dCMV-cGFP	Lentiviral shRNA expression vector based on pRNAT U6.2 lenti by GenScript, targeting PFN1	Jannike Köhle
pZNL-U6-sh2.13-dCMV-cGFP	Lentiviral shRNA expression vector based on pRNAT U6.2 lenti by GenScript, targeting PFN2a	Jannike Köhle
pZNL-U6.2-sifluc-f(W)	Lentiviral shRNA expression vector with a farnesylated eGFP and a WPRE site, targeting firefly luciferase	This Thesis
pZNL-U6-sh1.3-EGFP-F(W)	Lentiviral shRNA expression vector with a farnesylated eGFP and a WPRE site, targeting firefly luciferase	This Thesis
pZNL-U6-sh2.13-EGFP-F(W)	Lentiviral shRNA expression vector with a farnesylated eGFP and a WPRE site, targeting firefly luciferase	This Thesis
pRNAT-U6-siFluc-mApple	siRNA Expression Vector based on pRNATU6.3/Hygro by GenScript, targeting firefly luciferase	Eva Saxinger
pRNAT1.3-delta-mApple	siRNA Expression Vector based on pRNATU6.3/Hygro by GenScript, targeting PFN1	This Thesis
pRNAT2.13-delta-mApple	siRNA Expression Vector based on pRNATU6.3/Hygro by GenScript, targeting PFN2a	Michael Hano
pZNL-dCMV-EYFP-cttn	Lentiviral expression vector for a YFP-cortactin fusion protein (delta CMV promotor)	Julia Niederstraßer
pZNL-BiproCttn-IRES-EGFP-F(W)	Lentiviral expression vector for bipro tagged cortactin	Franziska Schreiner

2.4. Antibodies

Table 2.2 | Primary antibodies

primary antibody	Target	species	concentration	reference
PFN1 C (P7624)	Profilin 1	rabbit	1:400 (IF) 1:10000 (WB)	Sigma
PFN1 N (P7749)	Profilin 1	rabbit	1:200 (IF) 1:6000 (WB)	Sigma
4H5 anti PFN2a	Profilin 2a	mouse	1:100 (IF)	Murk et al. 2012
#361	Profilin 2a	rabbit	1:20000 (WB)	Murk et al. 2009
mcCortactin	Cortactin	mouse	1:1700 (IF) 1:17000 (WB)	Lai et al., 2009
4F11 anti cortactin	Cortactin	rabbit		
Synapsin 1&2	Synapsin 1&2	rabbit	1:5000 (WB)	Synaptic Systems
mcTubulin (DM 1A)	Tubulin	mouse	1/10000 (WB)	Sigma
rGFAP (AB5804)	Glial Fibrillary Acidic Protein	rabbit	1:1000 (IF) 1:10000 (WB)	Chemicon
mcGFAP (G-A-5)	Glial Fibrillary Acidic Protein	mouse	1:500 (IF)	Sigma

Table 2.3 | Secondary antibodies and reagents

secondary antibody	conjugate	reference
Anti mouse IgG (115-225-166)	Cy2	Dianova
Anti mouse IgG (115-165-166)	Cy3	Dianova
Anti mouse IgG (115-175-068)	Cy5	Dianova
Anti mouse IgG (A 9044)	peroxidase	Sigma
Anti rabbit IgG (111-165-144)	Cy3	Dianova
Anti rabbit IgG (111-025-144)	TRITC	Dianova
Anti rabbit IgG (A 0545)	peroxidase	Sigma
Anti rabbit IgG	Cy2	Dianova
Anti rabbit IgG	Cy5	Dianova
Phalloidin-TRITC	TRITC	Sigma
Phalloidin-FITC	TRITC	Sigma
DAPI		AppliChem
IB4 (I21412)	TRITC	Invitrogen

2.5. Mouse strains

Wild type cultures were always prepared from Bl6/C57 animals.

Conventional Cortactin knockout mice (*cttn*$^{-/-}$) were generated in the group of Prof. Dr. Klemens Rottner (Institute of Genetics, University of Bonn) as described earlier (Schnoor et al., 2011). These animals were backcrossed into a Bl6/C57 background.

2.5.1. Genotyping of *cttn*$^{-/-}$ mice

Genotypes of transgenic mice were determined by PCR using material gained from a tail biopsy.

Table 2.4 | Primer for genotyping

Target	Name	Primer sequence (5'→ 3')
CTTN	Cttn exon7 del fw	CCTGGAATAAGTCAGCCAAGC
	Cttn exon7 del rv	ATGGCCCTAGAGGTCAAAGC
	Cttn-allele-loxPfw	AGGGTCTGACCATCATGTCC
	Frt-detRv	GTGCTGTTCATCCACAATGC

Table 2.5 | standard PCR mix for 25µl reaction volume

Component	Concentration
PCR buffer	10 µM
dNTP's	10 nM
Forward primer	100 nM
Reverse primer	100 nM
Taq polymerase	1 u
DNA	ND (1µl)

Table 2.6 | PCR program for genotyping

Temperature	Time
95°C	2 min
95°C	20 sec
58°C	30 sec
72°C	45 sec
Repeat step 2 – 4	34 times
72°C	3 min

Subsequently, amplified DNA was loaded onto a 1.5% agarose gel and an electric field was applied for around 40 min. PCR products indicate genotypes as follows:

PCR 1: WT 650 bp

PCR 2: WT 1000 bp
del-allele 300 bp

2.6. Molecular biology

2.6.1. Preparation of competent *E. coli*

For effective DNA uptake *E. coli* cells have to be prepared as follows. The competence was induced by the calcium chloride method, by which the cell's membrane was passively made permeable to DNA.

Therefore, a single colony of *E. coli* XL1 blue was cultivated at 37°C in 3 ml LB-medium overnight. *E. coli* were diluted in 100 ml fresh media up to a weak clouding. Bacteria were grown at 37°C until they reach an OD_{600} of 0.4-0.5, which correspondents to the early logarithmic growth phase. All subsequent steps take place at 4°C. The culture was centrifuged for 10 min and 1800 x g. Then, the pellet was resuspended with 15 ml pre-chilled 50mM $CaCl_2$ and incubated on ice for 30 min. After the next centrifugation step (10 min, 1800 x g), cells were resuspended in 4 ml of pre-chilled $CaCl_2$ and incubated on ice for one hour. For storage at -70°C, glycerol to a final concentration of 15% was added to the suspension. Finally, the competent cells were partitioned into 200 µl aliquots.

2.6.2. Transformation of competent *E. coli*

By transformation the plasmid DNA of interest was yielded to the bacterial cell. The plasmid usually contained an antibiotic resistance, which allows for selection of the bacteria containing the designated plasmid by adding the antibiotic to the growth medium.

After thawing of *E. coli*, 1 µl of plasmid DNA was added to 30 µl bacterial suspension and incubated for 30 min on ice. Due to the lower transformation efficiency of recently ligated plasmids, 5 µl of ligation mixtures were used to transform 100 µl of *E. coli* suspension. Subsequently, suspensions were heat shocked by 42°C for 90 sec and then chilled on ice for 5 min. There upon 500 µl of LB-medium without antibiotics was added and the samples were incubated at 37°C for 30 min (ampicillin resistance) or 60 min (kanamycin resistance). The ligation samples were centrifuged shortly at 1000xg, decanted and resuspended in about 100 µl before plating on an agar plate containing antibiotics. Other transformations were plated directly with a volume of 100 µl.

2.6.3. Preparation of plasmid DNA

In order to prepare small amounts of plasmid DNA for the purpose of clone testing, the buffers P1, P2 and P3 of Qiagen (Hilden, Germany) were used as described below.

An overnight culture of the clone of interest was transferred into an Eppendorf tube and centrifuged for 5 min at 6000 rpm. The pellet was resuspended in 0.3 ml of buffer P1

containing 1:1000 RNase A. Then, 0.3 ml of buffer P2 was added, the tube was inverted 5 times and incubated at room temperature for 5 min. After adding 0.3 ml of buffer P3 and inverting another 5 times, the sample was centrifuged for 10 min at 13000 rpm. The supernatant was transferred into a new Eppendorf tube, and then mixed with 0.6 ml of isopropanol by vortexing. After 30 min of centrifugation at 13000 rpm, the supernatant was removed carefully. The pellet was washed with 70% ethanol and then dried at 70°C. Subsequently the dry pellet was redissolved in 30 µl 20 mM Tris-HCl buffer (pH 7.4).

For preparation of plasmid DNA from *E. coli* in order to transfect eukaryotic cells, the Plasmid Midi Kit of Qiagen was used according to manufacturers' instructions.

2.6.4. Restriction digest

This enzymatic technique was used for cleaving DNA molecules at specific sites in order to generate fitting endings. At these restriction sites, the respective enzyme cleaves the DNA resulting in blunt ends or sticky ends.

A typical restriction protocol:

- 2 µl recommended 10x NEB Buffer
- 2 µl 10x BSA if recommended
- 3 u of every restriction enzyme
- 0.5-1 µg DNA depending on its concentration
- Ad 20 µl (MilliQ H_2O)

2.6.5. Agarose gel electrophoresis

DNA or RNA can be separated by moving the negatively charged molecules through the agarose matrix with an electric field. Due to the non-denaturizing conditions, their movement speed depends on molecules' size, secondary structure and charge.

Depending on the size of the desired fragment, agarose gels of different concentrations from 0.8% to 1.5% diluted in 1xTAE were used. For visualization of DNA fragments Roti® safe gel stain (Roth) was added to the gel.

The electrophoresis takes place at a voltage of 200V and a current of 50 mA for at least 30 min. The size of the fragments was determined by comparison with GeneRuler (Fermentas) as standard.

2.6.6. Elution of DNA fragments from agarose gels

For isolation of specific DNA fragments from agarose gels the „QIA® EXII Gel Extraction Kit“(Qiagen) was used according to the manufacturers' descriptions after cutting out the desired fragment from the gel.

2.6.7. Ligation

For the recombination of DNA fragments (vector and insert) T4 DNA ligase was used. All ligations took place overnight at 16°C with an insert to vector ratio of 3:1. Additionally, the reaction mixture contained 1 µl 10x T4 DNA ligase buffer and 2 u T4 DNA ligase. The reaction volume was 10 µl. As control for uncleaved vector DNA, the insert was replaced by H_2O.

2.7. Cell culture techniques

2.7.1. Preparation of poly-L-ornithine (PLO)-coated cover slips

Coating of cover slips was performed with a ready-to-use PLO solution supplied by Sigma (P4957). A sterile cover slip was placed into each well of a 24 well plate and covered with roughly 0.5 ml of the PLO solution. The plate was incubated at 37°C for 30 min. After subsequent washing of the wells with sterile MilliQ H_2O, plates were air-dried under the clean bench and used directly.

2.7.2. Preparation of mixed glia cell cultures

Generally glia cell cultures were prepared from p4 – p7 mice pups. Alternatively, cortices of p4 - p5 mice were used directly after hippocampus preparation. In that case, the procedure starts at removing of the meninges.

Initially, pups were decapitated. Afterwards the skull has to be removed using a small scissor and forceps. The sharp edge of a spatula was used to cut the brain horizontally, parallel to the skull base, starting posterior. Then, the brain was put upside-down into pre-chilled 1xHBSS (Gibco, 14185-045) and placed under a binocular. The colliculi, cerebellum and hippocampus were then removed using a rounded spatula. Subsequently, all meninges were removed. Cleaned cortices were collected in a new petri-dish containing pre-chilled HBSS on ice. Collected cortices were then transferred into a 50 ml falcon containing about 10 ml of pre-chilled HBSS. Cortices were shred by 3 times pipetting the solution with a 10 ml glass pipette. After centrifugation (2 min, 200xg), supernatant was discarded, replaced by pre-warmed Trypsin-EDTA (Gibco, R-001-100, 1 ml per cortex) and incubated in the water-bath for 8 – 10 min. In the meantime, 2 – 3 fire-

polished Pasteur pipettes with diminishing tip sizes were prepared. Trypsin-EDTA was discarded and 2 time the volume of TE DMEM + 10% FCS was added. Subsequently, the suspension was homogenized through the flame-narrowed glass pipettes until a single cell suspension was obtained and again centrifuged at 200xg for 5 min. The resulting pellet was resuspended in fresh DMEM +FCS and P/S and then seeded onto 75 cm² tissue culture flasks (about 2 – 3 cortices per flask) and incubated at 37°C and 10% CO_2.

2.7.3. Purification and handling of glia cell cultures

Two to three days after preparation the culture was carefully washed with PBS and the medium was replaced against DMEM+FCS without antibiotics. At DIV 7, cultures were placed on a shaker and incubated at 37°C and 220 rpm for 18 – 24 h. Afterwards, cultures were washed vigorously with PBS and fresh culture medium was added. At around 80% confluence, 10 µM cytosine β-D-arabinofuranoside (Sigma) was added for 48 h hours to avoid proliferation of microglia. Between DIV10 and DIV14, cells were passaged. Either they were used for experiments directly (Spreading assay, Transwell assay) or seeded on PLO-coated cover slips at a density of about $4*10^4$ cells per well of a 24-well plate. Extensive growth of microglia was engaged with the application of 75 µM L-leucine-methylester (Sigma) in DMEM + 10% FCS for 90 min (Hamby et al., 2006), if necessary. Cells have been used for experiments until DIV28.

2.7.4. Preparation of organotypic cortical cultures

Organotypic cortical slice cultures were prepared similar to organotypic hippocampal slice cultures (Stoppini et al., 1991). Briefly, p4-5 mice were decapitated, the skull was removed and the dorsal half of the brain was transferred to ice cold GBSS. Cortex was cut into 400 µm transversal slices with a McIllwain tissue chopper and kept at 4°C for 30 min in GBSS. Cultivation was subsequently performed on tissue culture inserts (Millicell, 0.4 µm pore diameter, hydrophilic PTFE membrane). On each insert, 3 slices were placed and incubated at 37°C, 5% CO_2 and 99% humidity. 50% of the medium was exchanged twice a week.

2.7.5. Production of lentivirus

For the production of the lentivirus, HEK293T cells were used. The cells were kept in DMEM supplemented with 10% FCS and 500 µg/ml G418. 0.2x TE was used to detach cells. 24 h before transfection, cells were plated onto three 10 cm culture dishes at a density of $3x10^6$ without G418. Transfection was performed with PEI. Three plasmids were transfected at the following amounts:

- 7.5 µg Δ8.9
- 5 µg VSVG
- 10 µg expression vector

Therefore DNA was diluted in 1 ml of serum free DMEM. 67.5 µl of PEI were added and the transfection mixture was given to the cells drop-wise. After 4 – 6 h, the medium was exchanged.

72 h after transfection, cell culture supernatant was transferred into 50 ml Falcon tubes and centrifugated at 3000 x g for 10 min. Supernatant was filtered through a 0.45 µm filter into a new falcon tube, subsequently 1.5 ml aliquots were stored at -70°C until usage.

2.7.6. Transduction of eukaryotic cells

For transduction of primary glia cell cultures, cells were washed with PBS and subsequently, new medium together with the lentiviral particles in a 1:2 dilution was added. Virus containing medium was exchanged 2-3 days after transduction. Cells were transduced with lentivirus Usifluc-GfW and U2.13-GfW, respectively, 9 days or with U1.3-GfW 5 days before the experiments. Expression visualized by GFP-fluorescence started 2 days after transduction. For the lentivirus inducing the expression of cortactin, the transduction took place 7 to 8 d before the experiments.

2.7.7. Transfection of eukaryotic cells

Dissociated astrocytes were transfected using Lipofectamine2000 (Invitrogen) either on DIV14 or DIV18, depending on the construct used. Briefly, 1 µg DNA was diluted in 50 µl DMEM without FCS per well of a 24 well plate. Also, 2 µl Lipofectamine were mixed with 50 µl DMEM for each well. Both solutions were united after 5 min, vortexed and incubated for additional 20 min at RT. In the meantime, culture medium was exchanged to fresh, pre-warmed DMEM without FCS. The incubated transfection mix was subsequently added dropwise to the well. After an incubation time of 4 h, the transfection mix was replaced with pre-warmed DMEM with FCS and the cultures were kept at 37°C, 10% CO_2, and 99% humidity until being used for experiments at DIV 21.

2.7.8. Biolistic transfection using the Helios Gene Gun

Organotypic cortical slice cultures were transfected at DIV 7 using the Helios Gene Gun system of Bio-Rad. Gold microcarriers 600 nm in diameter were shot onto the slice with helium at pressure of 90 psi. To avoid damage of the tissue due to gold clumps, culture inserts with a pore size of 3 µm were used as filters. Bullets for the Gene Gun were prepared using the tubing preparation station provided by Bio-Rad. Here, 12.5 µg of gold

and 25 µg of pEGFP-F was used for controls. Bullets for the knockdown plasmids contained 15 µg of gold and 15 µg of pEGFP-F and 15 µg of pRNAT1.3 or pRNAT2.13.

For the coating of the DNA to the gold microcarriers, Ca_2Cl precipitation was performed (O'Brien and Lummis, 2006; Wellmann et al., 1999). Briefly, the gold microcarriers were mixed with 100 µl of 0.05 M spermidine (Sigma) and clumps were destroyed by 10 s of sonification. 100 µl of 1 M Ca_2Cl were added drop-wise followed by 10 min incubation at room temperature. To clean the gold microcarriers of residual spermidine, four washing steps in 99% ethanol were performed using a bench-top centrifuge at 100xg. Finally, the god microcarriers were dissolved in 1 ml of 99% ethanol containing 0.05 mg/ml polyvinylpyrrolidone (PVP) 75 cm of Tefzel tubing (Biorad) were cleaned by 10 min flow on nitrogen in the tubing preparation station (Biorad) and subsequently the gold suspension was added. To ensure homogenous distribution of DNA coated gold particles the tubing was rotated for 30 s and then dried was nitrogen for 5 min.

After biolistic transfection, organotypic cortical slice cultures were incubated at 37°C and 5% CO_2 until fixation and subsequent morphological analysis at DIV 14.

2.7.9. Immunocytochemistry

Primary astrocytic cultures (DIV 21) were fixed with 4% formaldehyde in PBS for 15 min, permeabilized with 0.2% Triton X-100 for 10 min and subsequently incubated with the respective primary antibodies for 1 h at 37°C or overnight. Secondary anti-rabbit or anti-mouse antibodies conjugated with Cy2, Cy3, or Cy5 were diluted 1:400 in PBS and incubated for 30 min at 37°C. Finally, cultures were counterstained with DAPI (4',6-diamidino-2-phenylindole) diluted 1:1000 in PBS for 10 minutes at 37°C, washed and mounted using Fluoro-Gel (Emsdiasum, USA).

2.7.10. Profilin localization

DIV 21 primary astrocytic cultures were fixed and immunostained. For the analysis of the localization, anti-PFN1 antibody P1C and monoclonal anti-PFN2a antibody 4H5 were used. To visualize astrocytes, a staining with anti-GFAP antibody was performed. Cellular nuclei were stained with DAPI. Six images per experiment were taken with the Olympus SystemBX61WI FluoView 1000 equipped with a 40x oil immersion objective (NA 1.3). Fluorescence intensity of the profilin staining was measured with FIJI software (Schindelin et al., 2012). The ratio between one area colocalized with DAPI staining and one area of the same size beneath the DAPI staining was used for analysis.

2.7.11. Morphological analysis of dissociated astrocytes

Transfected, vital and GFAP positive cells (Figure 2.1: A) were selected and imaged with an Axioplan 2 (Zeiss) equipped with a 63 x objective (1.32 NA). Cell perimeter and cell area were measured with FIJI software. First, cells were stitched together if necessary (pairwise stitching tool of FIJI) and a threshold, conserving the cellular outline as precise as possible, was set. Afterwards the image was made binary and the “wand”-tool was selected for automatic detection of the cellular outline (Figure 2.1: B). Finally, the outline as well as the area inside of the outline was measured by FIJI measuring tool and exported to Microsoft Excel.

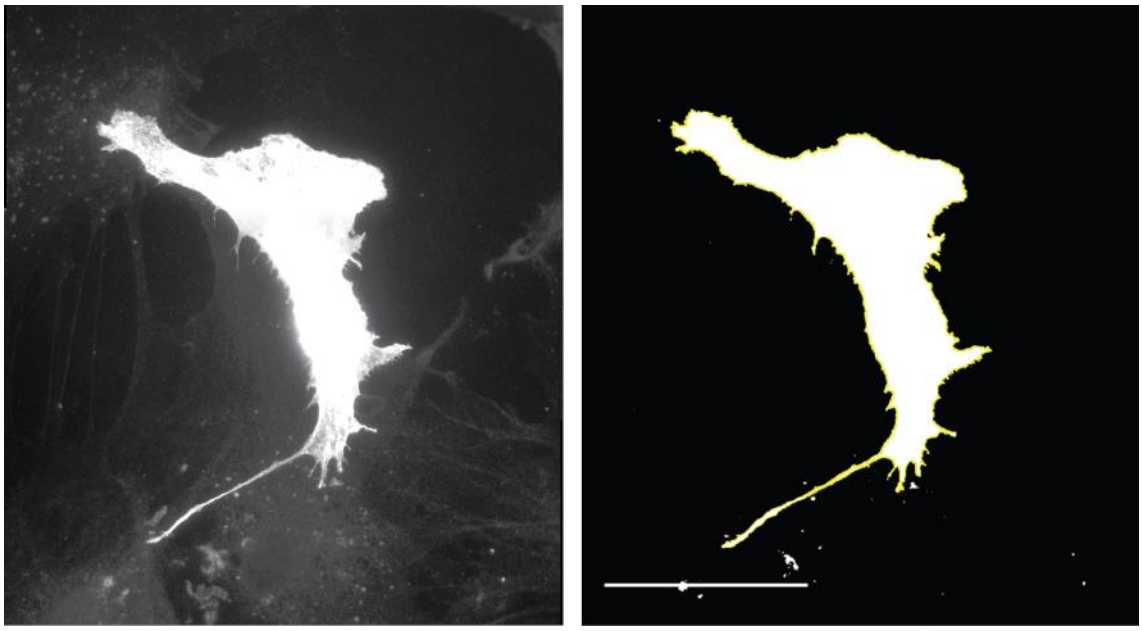

Figure 2.1 | Visualization of the morphological analysis with FIJI. (A) Original image of a mApple expressing astrocyte **(B)** Processed image of the astrocyte from A. Yellow outline indicates the cellular perimeter used for subsequent analysis. White are included into the yellow outline was taken as cellular surface. scale bar: 50 µm

For categorization into polygonal and stellate astrocytes, the ratio of cell perimeter to cell area was used. Astrocytes with a ratio > 0.25 were totaled as stellate.

2.7.12. Morphological analysis of astrocytes in organotypic cortical slices

To analyze the morphology of astrocytes in organotypic cortical slice cultures, the transfected cells were imaged with an Axioplan 2 (Zeiss) equipped with a 63 x objective (1.32 NA). Z-stacks had a size of 0.5 µm. Length and width of individual astrocytes were determined using the measuring tool of FIJI. The higher value was defined as length and the smaller as width independent of the orientation of the respective cell. Astrocytes extended over more than one image were stitched together by the use of the respective

stitching tools provided by FIJI. Volume analysis was performed using Bitplane Imaris 7.0. Here, a virtual surface was created with the respective wizard setting surface area detail level at 0.2 µm and the background subtraction at 0.8 µm. The resulting volume data were exported to Microsoft excel and used for analysis.

2.7.13. Migration assay

To analyze the migration behavior of cultivated astrocytes, two types of migration assays were performed. On the one hand, a classical *in vitro* scratch induced wound healing assay (Etienne-Manneville, 2006) was performed. For this assay, $2*10^5$ astrocytes were plated in a 6 well plate at DIV 10 - 13. At DIV 21, a scratch wound of about 300 – 400 µm was induced with a micropipette tip. By painting a cross on the bottom of the cell culture dish, retrieving of the specific, imaged section of the wound was achieved. This section was imaged at 24 h and 48 h after scratch induction.

On the other hand, migration was analyzed by the usage of cell culture inserts of Ibidi (80209, Martinsried, Germany). These inserts (Figure 2.2.) offer the initiation of reproducible gap between the cells without producing cell debris, which could probably influence the assay.

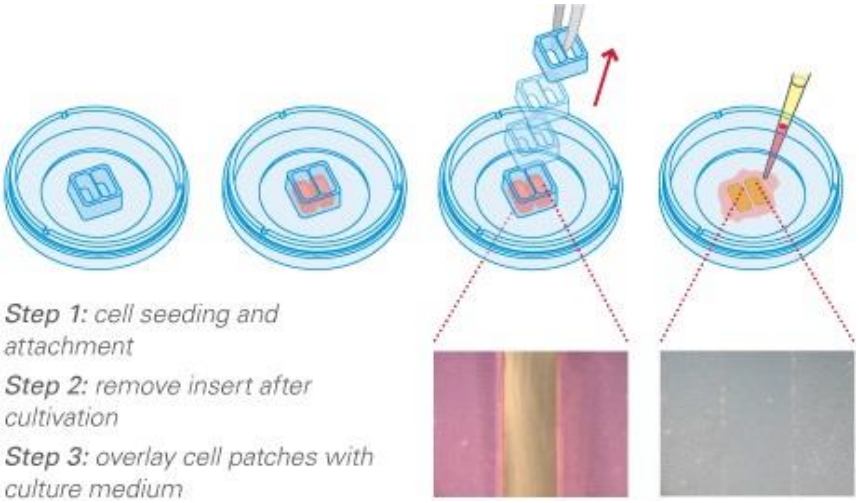

Figure 2.2 | Illustration of *in vitro* wound healing assay with the ibidi cell culture insert. First, the inserts are attached to the bottom of the cell culture dish. Afterwards, a defined amount of cells is seeded into the two distinct chambers. After allowing the cells to attach properly, the insert is removed and the migration of the cells monitored. Taken from www.ibidi.com

For these experiments, the insert was placed into an uncoated 12 well plate. 70 µl of a DIV 14 cell suspension with a concentration of $3*10^5$ astrocytes per ml were pipetted into each chamber. 2 days later, the insert was removed and subsequently, the initial image

was taken. The insert was cleaned with sterile MilliQ directly after removal and reused. Again, the imaged section was marked by a cross on the bottom of the cell culture plate. The same section was subsequently imaged 24 h and 48 h after initiation of the assay.

Both types of wound healing assay were analyzed with the imaging software NIS-elements (Nikon). The size of the gap between both cell fronts was measured. For the analysis of the migration, the difference between the gap size at the starting time point and the later time point was calculated. Thereby, the area newly covered with cells in the depicted period of time was determined. This value was normalized to the mean of the control and defined as “normalized wound closure in %”.

2.7.14. Spreading assay

Adhesion and spreading of transduced DIV14 primary astrocytes were analyzed by plating $1*10^5$ cells on PLO-coated cover slips. After 6 h of incubation, cells were washed two times with 1xPBS and fixed with 4% formaldehyde in PBS. Subsequently, they were stained with mcGFAP and Phalloidin. Using the 20x (1.25 NA) objective of an Axioplan 2 (Zeiss), astrocytes were classified into two groups: well-spread flat cells (group 1) and compact, round cells (group 2).

2.7.15. Transwell assay

To analyze the motility of astrocytic processes, chemotactic attraction to FCS was used. Astrocytes were serum starved overnight and subsequently, $1*10^5$ cells were plated into the upper chamber of transwell devices (3 µm pores, Greiner bio-one, Frickenhausen, Germany). Cells were allowed to spread their processes into the bottom chamber containing serum-supplemented DMEM for 24 h before being fixed and stained with phalloidin, mcGFAP antibody and DAPI. Focal planes above and below the insert were taken with a confocal laser scanning microscope (LSM 510 Meta, Zeiss, Göttingen, Germany) using a multitrack technique to monitor the individual channels separately.

For analysis, again FIJI was used. First GFP and GFAP channel was separated from all others (2.2: A) and a threshold was set (2.2: B) prior to making the pictures binary. Afterwards, a merged picture of the binarized GFP and the GFAP channel of one focal plane was made.

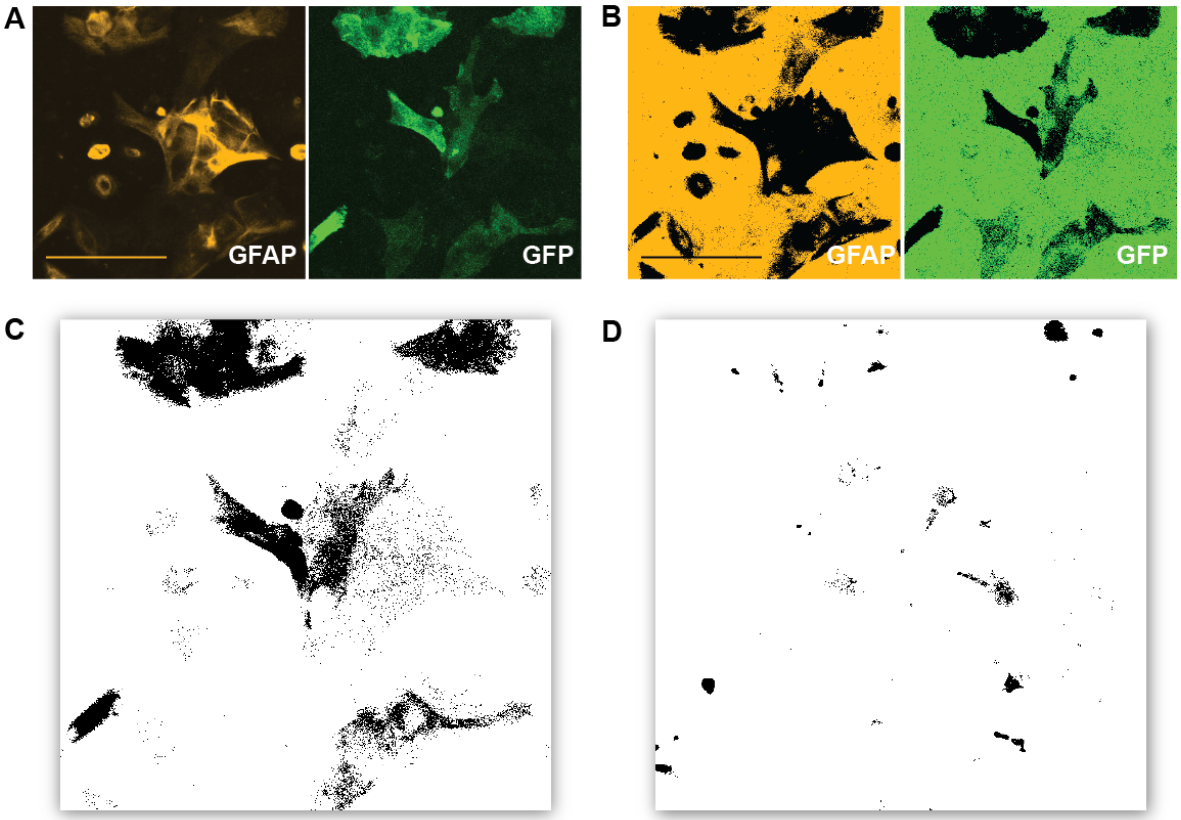

Figure 2.3 | Visualization of the analysis of the transwell assay. (A) Original images representing one focal plane above the transwell membrane. GFAP channel indicates astrocytes; GFP channel indicates transduced cells. **(B)** Images from A underwent the setting of a threshold and subsequent binarization. **(C)** Merged, binarized image of B. (**D**) Merged and binarized image of the focal plane below the transwell membrane at the same position as C. scale bar: 100 µM.

The merged area (Figure 2.2: C upside, D bottom side) was again made binary and subsequently, its area was automatically determined by the usage of the particle analyzer tool. The threshold for the smallest possible structure was set at 5 µm (area of a 3 µm pore: π*radius = 4.71 µm). Afterwards, the area covered area below the insert was divided by the total covered area to get a ratio which determines the percentage of cell area extended through the pores.

2.7.16. Whole cell extract preparation

To analyze the proteins of interest in the glial cell culture, cells were washed with PBS and subsequently harvested with a cell scraper. For 10 cm TC dish, cells were scraped in a total amount of 1 ml PBS containing protease inhibitor cocktail and, for 2-D electrophoresis, also a phosphatase inhibitor cocktail (1:100, Serva). Suspension was collected in an Eppendorf reaction tube and centrifuged at 2000 rpm for 5 min. Supernatant was discarded and the pellet shock frozen in liquid nitrogen oxide. Further preparation for 2D gel electrophoresis will be described separately (2.7.17). Dry pellet was

subsequently resuspended in an appropriate volume of PBS with protease inhibitor mix (ca. 50 µl per 10 cm TC) and cell lysis was achieved by repeated freeze and thaw cycles. After 4 cycles, the sample was centrifuged at maximum speed in a benchtop centrifuge for 5 min. Supernatant subsequently underwent a Bradford assay to determine the protein amount.

2.7.17. Sample preparation for 2D gel electrophoresis

Starting point is a shock frozen cell pellet, prepared like mentioned earlier (2.7.16). First, the solubilizing buffer HC was prepared as follows:

- 900 µl HC
- 2.5 µl Pepstatin A
- 2.5 µl AEBSF
- 10 µl Trasylol
- 10 µl Phosphatase inhibitor cocktail
- 20 µl 1 M DTT
- 3 µl 2 M TRIS (to adjust pH between 8.4 and 9.0)

For 50 mg dry pellet, 150 µl solubilizing buffer was added. The solution was vortexed and underwent 2 freeze and thaw cylces and incubated for 15 min in a rotator. 5 µl di-methyl-acrylamide was added, incubated 30 min in a rotator and subsequently, the reaction was stopped by adding 10 µl 1 M DTT. Afterwards, the samples were centrifuged 20 min at 16000xg, 4°C. The supernatant was kept and underwent a protein determination by Bradford assay. Aliquots were made and stored at -70°C until usage. Frequent freezing and thawing was avoided.

2.8. Biochemical methods

2.8.1. Bradford assay

For the determination of protein concentrations Bradford assay was performed. As standard, a serial dilution of 1 mg/ml BSA in PBS was used. For the average sample in this thesis, protein dilutions between 1:10 and 1:200 were useful. 20 µl of the respective protein dilution was pipetted into a well of a 96 well plate (Nunc, Maxisorb). Subsequently, 100 µl of Bradford reagent was added and the plate was measured by an ELISA-reader at 595 nm after 5 min of incubation. Sample protein concentrations were calculated from the BSA standard curve using linear regression analysis.

2.8.2. SDS-PAGE (sodium dodecyl sulfate polyacrylamide gel electrophoresis

In this thesis, separating gels with varying pore sizes were used due to the variance in size of proteins probed. Most SDS-Pages were performed with gradient gels containing a gradient from 10 – 20% polyacrylamide. These gels were prepared in a gel casting chamber (Sigma Chemical Co., St. Louis, USA, Model C 4072) with the aid of a gradient mixer. The reagents used are depicted in table 2.7.

Table 2.7 | Reagents used for the preparation of gradient gels.

	Separation gel		**Stacking gel**
	10%	**20%**	**4%**
Milli-Q H_2O	32 ml	6 ml	31 ml
Separation gel buffer	19 ml	19 ml	-
Stacking gel buffer	-	-	12.5 ml
Acrylamide solution	25 ml	51 ml	6.5 ml
10% APS	400 µl	400 µl	800 µl
TEMED	20 µl	20 µl	40 µl

Samples were diluted in a defined volume of 4x SDS sample buffer and boiled for 5 min at 95°C. After adding the denatured protein samples to the wells, an electric field was applied across the gel. Until the proteins reach the separating gel, it was 225V and 10 mA per gel. After that, the current was increased to 25 mA per gel. The current was kept until the stained band reached the lower boarder of the separating gel.

As protein weight standard Page Ruler Plus Protein Ladder (Thermo Fischer Scientific) was used.

2.8.3. 2-D gel electrophoresis

Protein samples were prepared for rehydration of the strip for isoelectric focusing (Bluestrip, Serva) as follows. 155 µl solution containing 1.4 µl 1 M DTT, 2 µl ampholytes, 1.4 µl bromophenolblue and 50 µg of total protein extract were mixed by vortexing and used for rehydration overnight. The next day, the isoelectric focusing was performed using the following program:

- 200 V for 20 min
- 450 V for 15 min
- 750 V for 15 min
- 2000 V for 30 min

Afterwards, the strips were prepared for the SDS-PAGE by first equilibrating them in 10 ml 1x NuPAGE sample buffer (Invitrogen) supplemented with 0.5 ml 1 M DTT on a shaker. After 15 min, solution was exchanged to an alkylation buffer containing 232 mg iodacetamide in 10 ml 1x NuPAGE sample buffer and incubated for additional 15 min. The strips were subsequently transferred onto a SDS-PAGE gel (10 – 20% gradient or 13.5% PAA-gel). Air bubbles were excluded by the embedding of the strip in 0.5% agarose in 1x SDS running buffer. 10 µl Page Ruler Plus was used as molecular mass standard. Finally, electric field was applied for 90 min at 125V and 10 mA per gel.

2.8.4. Western Blot

In this thesis, the semi-dry blotting technique was used. The electrodes were placed directly in contact with the sandwich containing of 3 layers of blot filter paper, a piece of polyvinylidene fluoride (PVDF) membrane, the gel and 3 additional layers of blot filter paper. For Western Blotting of 2-D gels, the membrane consisted of nitrocellulose. All parts of this sandwich were equilibrated in 1x blot buffer with 10% methanol for at least 5 min, with the PVDF membrane being pre-incubated in 100% methanol.

The proteins were transferred at a current of 100 mA per gel and a voltage of 100 V for one hour. The membrane was incubated in 5% milk diluted in TBS-T for one hour to block free binding sites and afterwards washed several times with 1 x TBS-T. Then, the membrane was incubated with diluted primary antibody over night at 4°C, and subsequently washed with 1 x TBS-T for removing unbound antibodies. Incubation with the secondary antibody (goat anti mouse/rabbit IgG HRP conjugated) took place for at

least 1 h at room temperature. After subsequent washing of the membrane with 1 x TBS-T and 1 x TBS-X, the blot was incubated with an appropriate substrate (Pierce ECL Western Blotting Substrate, Thermo Fisher Scientific or Luminata Crescendo, Millipore) for the HRP enzyme. The emitted light was detected by X-ray films (Pierce).

2.9. Imaging techniques

2.9.1. Calcium imaging

To analyze the intercellular connectivity in the primary astrocytic culture, calcium imaging was performed. DIV 20 – 28 astrocytes were bulk loaded with Oregon Green® 488 BAPTA-1 AM. Specifically, cover slips were transferred into a 35 mm TC dish and incubated with the dye diluted in HBSS for 30 min at 37°C. Subsequently, cover slips were washed and allowed to recover in HBSS for additional 30 min. The cells were kept at room temperature in an open imaging chamber with a continuous perfusion (0.5 ml/min) of HBSS to a maximum of 2 h. To induce an intercellular calcium wave, specific astrocytes were stimulated mechanically with a patch pipette. To gain a patch pipette, the standard settings for electrodes for single cell electroporation were used: GC150F-10, O.D. 1.5mm x I.D. 0.86mm, Harvard Apparatus (Kent): tip diameter 1-2 µm. Intercellular calcium waves were imaged using an upright Olympus BX61W1 (Olympus) controlled by the Cell^{M} software and equipped with a 10x0.3-N.A. objective (Olympus). 300 pictures with an interval of 200 ms were taken at a binning of 344 x 258 with a lamp intensity of 23% and an illumination period of 120 ms.

Suramin treatment was performed with a 100 µM solution of suramin (Sigma) in HBSS in a continuous perfusion. 15 min after initiation of the treatment, the first experiments were performed. Treatment with the Cx43 specific peptide gap27 (SRPTEKTIFII) and the scrambled control peptide ‘scr’ (TFEPIRISITK) was performed without continuous perfusion. The cover classes were pre-incubated for 30 min in an open petri dish containing 300 µM of the respective peptide diluted in HBSS. Subsequently, experiments were performed directly in the petri dish.

Images were analyzed using ImageJ (NIH). To determine the amount of cells involved into a single calcium waves, the cell counter tool of ImageJ was used. Afterwards, the percentage of cells involved was calculated from the total amount of cells in a field of view vs the responding cells. The area of the induced ICW was measured by the use of the freehand selection tool. Area was measured at the latest time point the wave still appeared to be compact. For the cw velocity, the distance between the point of initiation

and two points at the border of the primary calcium wave was determined and divided through the amount of time elapsed since the initiation.

2.9.2. Fluorescence recovery after photobleaching (FRAP)

For FRAP experiments, a co-transfection of either the control plasmid, or sh-RNA expressing plasmid specific for PFN1 or PFN2a, respectively, with eGFP-ß-actin was performed. Controls and PFN2a knockdown plasmids were transfected 7 d (DIV 14) before the experiment, whereas PFN1 specific knockdown plasmid was transfected 3 d before the experiment. All experiments were performed at DIV21 on small astrocytic processes. Only healthy cells with many processes and a moderate expression of both constructs were used. The cells were kept at 32°C in an open imaging chamber with a continuous perfusion (0.5 ml/min) of HBSS. The Olympus system BX61WI FluoView 1000 (FV1000) was used to excite eGFP-ß-actin with an excitation wavelength of 488 nm. The power of the excitation laser was adjusted to a low level (1-2%; 5-8 µW) to reduce photobleaching as much as possible still achieving a good signal-to-noise ratio. Scan speed was set to 8 µs per pixel and a line averaging of two (Kalman filtering) were used for an image size of 640 × 128 pixels (final pixel size of 76nm) with a 60x water immersion objective (NA1.0). To increase the z-section's depth the pinhole was opened to 500 µm and the gain and the offset were set to zero. The photobleaching of a 4 x 4 µm area was performed using the SIM scanner unit Olympus FV5-LDPSU at an excitation wavelength of 405 nm and a power of 100% (8 mW) for 500 ms. Baseline was determined by taking 5 images at two second intervals before bleaching. The fluorescence recovery was monitored for 3 min after bleaching.

Analysis was performed using FluoView1000 Software. Three regions of interest were defined: The first (Figure 2.4; A; 2) was localized at the bleached area. The second was used as bleaching correction (Figure 2.4; A; 3) and placed at an adjacent astrocytic process. The last ROI was defined as background (Figure 2.4; A; 4). The resulting data were exported to Microsoft Excel, where intensity values of square 3 and 4 were used for correction. These corrected recovery curves were then used for comparison between different groups.

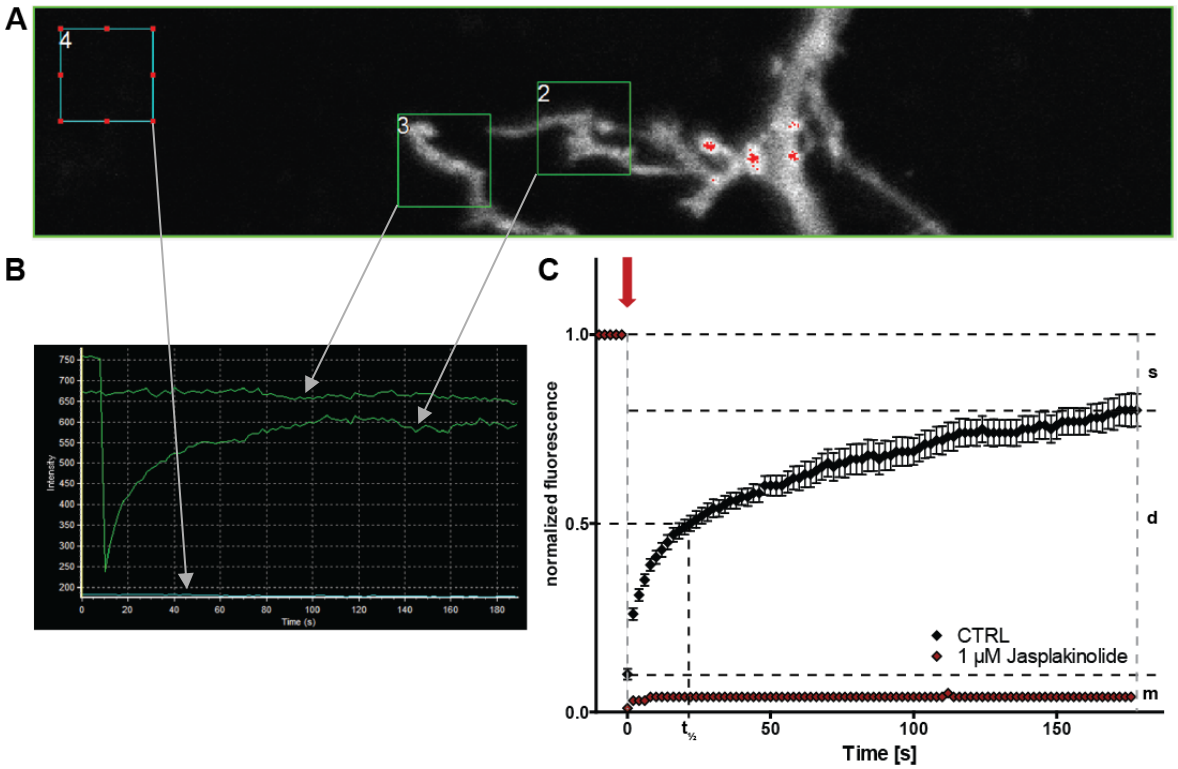

Figure 2.4 | Illustration of the analysis and establishment of FRAP in astrocytic processes. (A) Original image from a time lapse series. The three ROIs are marked with squares. Square (2) corresponds to the region which was bleached, whereas square (3) was used for bleaching correction and square (4) used for background correction. The ROIs are connected to their respective traces over time B with red arrows. **(B)** Fluorescence intensity traces of the indicated areas in A. **(C)** Recovery curve corrected for bleaching and background of untreated PAPs (black) compared to a correspondingly corrected recovery curve of Jasplakinolide treated PAPs (red). Red arrow indicates bleaching. $t_{½}$: x-axis position to determine turnover time. s: stable pool d: dynamic pool m: monomeric pool.

To verify the specificity of this technique for actin dynamics in small astrocytic processes, actin dynamics were inhibited by the application of 1 µM Jasplakinolide (Figure 2.4; C). As there was no recovery for PAPs treated with Jasplakinolide, the use of this FRAP technique is generally applicable to analyze actin dynamics in this system.

2.10. Statistical analysis

The statistical analysis was performed using Microsoft Excel and GraphPad Prism. The data obtained were compared between two different experimental conditions using an unpaired two-tailed Student's t-test. Data including more than 2 different groups were analyzed using a one-way ANOVA followed by a *post-hoc* Tukey's Multiple Comparison Test. In some cases, a two-way ANOVA followed by a *post-hoc* Tukey's Multiple Comparison Test was necessary. Values of $p<0.05$ were considered as being significant and plotted as follows *$p<0.05$; **$p<0.01$; ***$p<0.001$. Data shown are indicated as mean ± SEM.

3. Results

3.1. Profilins modulate astrocytic morphology and function

Profilins have been described to be essential regulators of the actin cytoskeleton in eukaryotic cells (Jockusch et al., 2007; Witke, 2004). Recent studies on their role in the CNS have revealed isoform specific functions of PFN1 and PFN2a in neuronal cells (Michaelsen et al., 2010; Murk et al., 2012; Pilo Boyl et al., 2007). In astrocytes, so far only the role of PFN1 in two very specific processes was addressed: Namely, the outgrowth of PAPs upon stimulation with caged calcium (Molotkov et al., 2013) and the radial migration and glial cell adhesion of granule neurons in the cerebellum (Kullmann et al., 2012). Consequently, the precise role of profilin isoforms in a variety of astrocytic functions remains elusive. The results presented in this section provide insights into the overlapping as well as the isoform specific cellular functions of PFN1 and PFN2a in astrocytes.

3.1.1. Cultured astrocytes express PFN1 and PFN2a

Cultured dissociated hippocampal neurons are accompanied by astrocytes. These cells positive for the astrocytic marker glial fibrilliary acidic protein (GFAP) were, besides the ubiquitous PFN1 also immunoreactive for PFN2a (Figure 3.1).

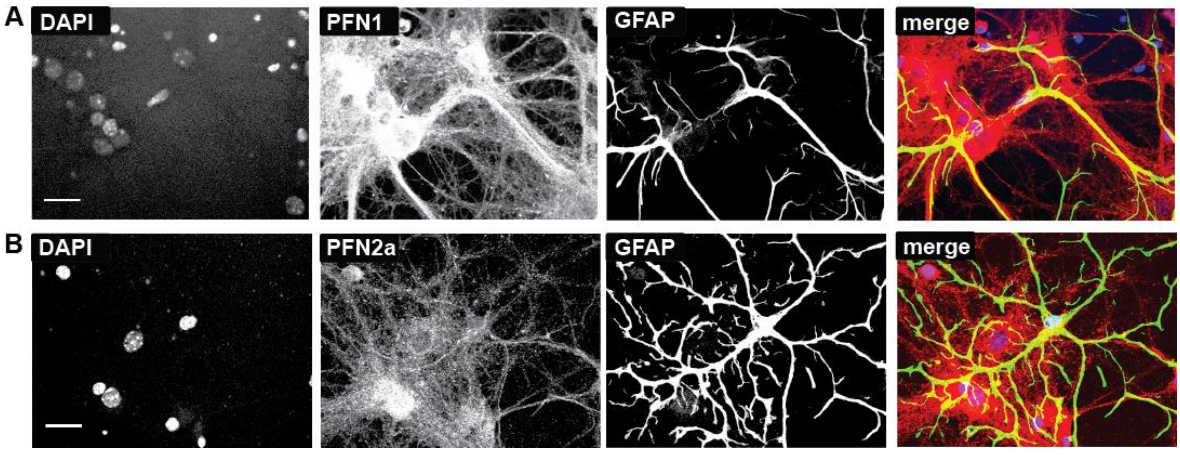

Figure 3.1 | Astrocytes express two profilin isoforms. Dissociated hippocampal co-cultures of astrocytes and neurons. Both astrocytes and neurons express **(A)** PFN1 and **(B)** PFN2a. Scale bar: 20 µM

Up to this finding, the expression of PFN1 and PFN2a was generally accepted as a unique characteristic of neurons. Nevertheless, transcriptome studies also give evidence for the expression of the aforementioned profilin isoforms in astrocytes (Cahoy et al., 2008; Doyle et al., 2008; Lovatt et al., 2007). To analyze the role of these two isoforms in this context, dissociated astrocytic cultures devoid of neurons were used. In contrast to

astrocytes co-cultivated with hippocampal neurons, attaining a stellate morphology, astrocytes cultured in the absence of neurons attain a flat, epithelial morphology. However, these astrocytes still express both isoforms, which was verified by immunoblotting (Figure 3.2).

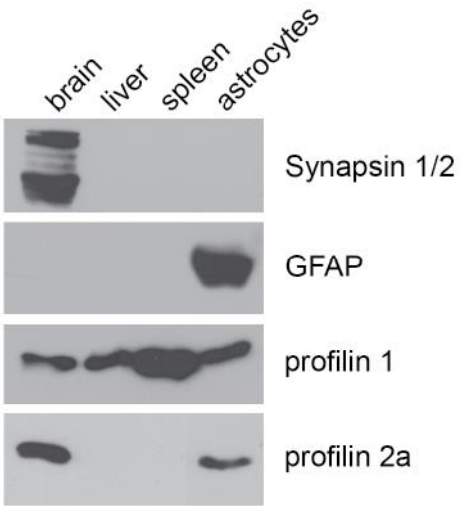

Figure 3.2 | Western blot analysis of cultured astrocytes compared to mouse brain, liver, and spleen. Astrocytic cultures as well as brain lysate show clear immunoreactivity to a PFN2a specific antibody, whereas liver and spleen lysates are negative. Immunoreactivity to the ubiquitous profilin isoform PFN1 is obvious in all probed cells and tissues.

Extracts of glia cell cultures were compared to whole brain lysates and, as negative control, mouse liver and spleen. Whole brain extracts as well as glia culture extracts were immunoreactive to both PFN1 and PFN2a specific antibodies, whereas the liver and spleen lysates were only positive for PFN1. Despite displaying a highly conserved three dimensional structure (Polet et al., 2007), profilins have been shown to interact with a differing set of ligands in the mammalian brain (Witke et al., 1998). Therefore, PFN1 and PFN2a are assumed to be involved in different cellular functions (Gorlich et al., 2012; Michaelsen et al., 2010; Murk et al., 2012; Pilo Boyl et al., 2007). Consequently, the isoform specific cellular role of PFN1 and PFN2a was addressed in astrocytes.

3.1.2. Protein levels of PFN1 and PFN2a can be reduced separately

For the analysis of the two profilin isoforms in astrocytes, it was taken advantage of the shRNA mediated, isoform-specific knockdown. The deployed lentiviral vector construct consists of a shRNA driven by an U6-promoter and its expression is reported by a farnesylated enhanced GFP (Figure 3.3; A). In this study, lentivirusses encoding for an siRNA targeted to the firefly luciferase (UsiFluc) as control or shRNAs specific for PFN1 (Ush1.3) or PFN2a (Ush2.13), respectively, were used. The aforementioned viruses were subsequently applied to dissociated astrocytes for an isoform specific modulation of the

cellular profilin level. These cultures were harvested for western blot analysis and subsequently probed for PFN1 and PFN2a immunoreactivity (Figure 3.3; B).

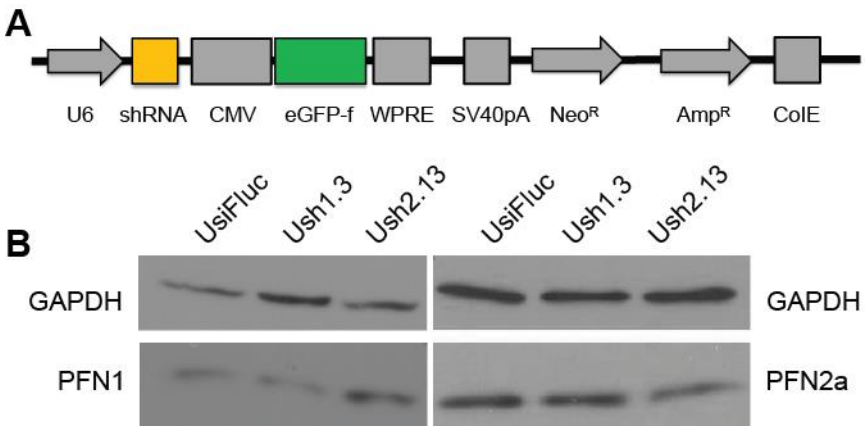

Figure 3.3 | Isoform specific downregulation of cellular profilin levels by lentvirusses. (A) Schematic representation of the vector construct used for the production of lentivirus. The respective shRNA is driven by an U6-promotor and a full length CMV promoter drives the expression of a farnesylated enhanced GFP. **(B)** Western Blot analysis of dissociated astrocytic cultures. Astrocytes were transduced with the indicated lentivirus and harvested 9 days later. PFN1 immunoreactivity is reduced for astrocytes transduced with Ush1.3 but not for astrocytes transduced with Ush2.13. PFN2a immunoreactivity is reduced for astrocytes transduced with Ush2.13 but not for astrocytes transduced with Ush1.3. This demonstrates an isoform specific knockdown. GAPDH was used as a loading control.

To compare the respective profilin levels, GAPDH was used to normalize. The amount of PFN1 was reduced in the cultures transduced with Ush1.3, but not in the cultures transduced with Ush2.13. This underlines an isoform specific knockdown of PFN1 in astrocytes. A potential compensatory up-regulation of PFN1 in Ush2.13 cultures could not been excluded. The protein level of PFN2a was obviously reduced in cultures transduced with Ush2.13, but not in cultures transduced with Ush1.3. Therefore, also the shRNA targeted to PFN2a was verified to be specific in astrocytic cultures. Due to the transduction efficiency of less than 50% (data not shown), residual immunoreactivity is caused by non-transduced astrocytes in the culture. Lentiviral transduced astrocytic cultures were used for motility analysis in the spreading- and the transwell-assay.

For the analysis of single, mature astrocytes, transfection of the respective plasmid was used to deliver the respective shRNA. In these constructs, the expression of the shRNA is driven by an U6 promoter and mApple served as reporter (Figure 3.4; A). The efficacy of the profilin knockdown constructs was determined measuring the relative fluorescence of MOCK transfected astrocytes to astrocytes either expressing the PFN1 or the PFN2a specific shRNA (Figure 3.4; B).

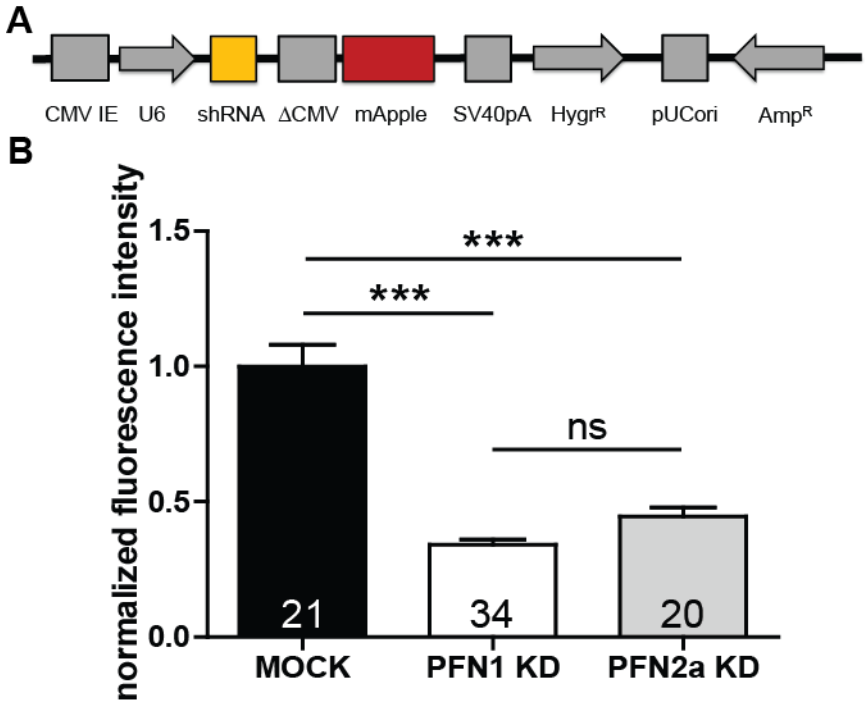

Figure 3.4 | Downregulation of profilin isoforms in single astrocytes. (A) Schematic representation of the construct used for transfection of astrocytes. The respective shRNA is driven by a CMV enhanced U6-promotor, while a truncated CMV promotor drives the expression of mApple. **(B)** Statistical analysis of fluorescence intensities of transfected astrocytes. Ratios between transfected and non-transfected cells were used to correct for the intensity of the immunofluorescence. The mean fluorescence intensity ratio of astrocytes transfected with the control plasmid pRNAT-siFluc was set to 1. Analysis of astrocytes transfected with either pRNAT-1.3 or pRNAT-2.13 exhibits a highly significant reduction to 0.34±0.02 or 0.45±0.03, respectively.

Astrocytes transfected with pRNAT-1.3 exhibit a residual anti PFN1 fluorescence intensity of 34%, which corresponds to a highly significant reduction. Also astrocytes transfected with pRNAT-2.13 exhibit a highly significant reduction in anti PFN2a fluorescence intensity to about 45%. These results indicate an efficient interference of the delivered shRNAs with PFN1 and PFN2a mRNAs in mature astrocytes, respectively. Transfected single astrocytes were subsequently used for morphological analysis or imaged in the fluorescence recovery after photobleaching (FRAP) experiments.

3.1.3. Profilins are essential for spreading and adhesion of astrocytes

Spreading and adhesion are processes reliant on actin dynamics as well as on both profilin isoforms (Murk et al., 2009). Consequently, the effect of profilin loss on adhesion and spreading of astrocytes was investigated (Figure 3.5).

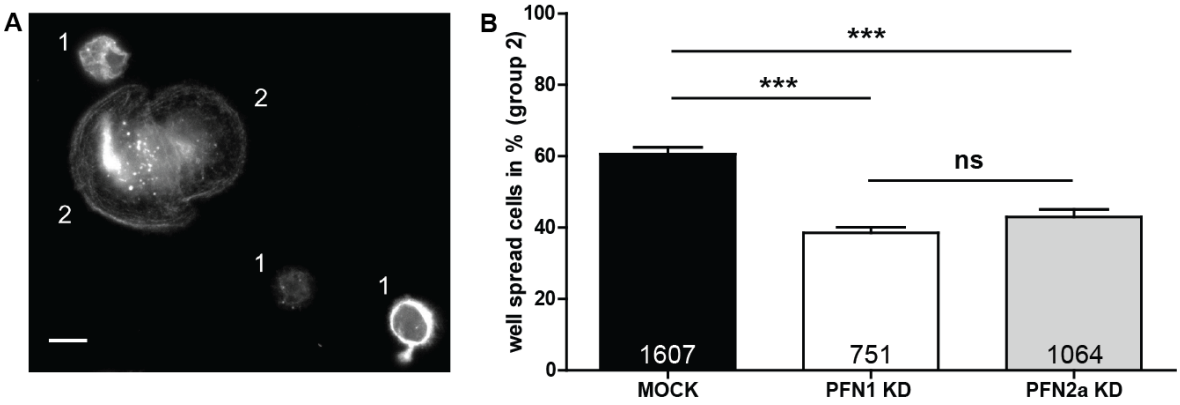

Figure 3.5 | Both profilins have a drastic effect on spreading and adhesion of astrocytes. (A) Spreading-adhesion assay. Astrocytes were allowed to adhere to PLO-coated coverslips for 6 h, were subsequently fixed and stained with Phalloidin as well as anti-GFAP. According to their morphology and the appearance of their actin cytoskeleton, cells were classified into two groups: round cells lacking obvious spreading (group 1) and well spread cells (group 2). Scale bar: 10 µm **(B)** Statistical analysis of astrocytes transduced with either Usifluc (MOCK, black), Ush1.3 (PFN1 KD, white) or Ush2.13 (PFN2a KD, light grey) subjected to the spreading assay in A and subsequently classified into groups 1 and 2. 60.60±1.9% of control cells were classified into group 2, whereas only 38.55±1.5% of PFN1 knockdown cells and 42.96±2.1% of PFN2a knockdown cells were well spread according to criteria. Quantitative data was tested for significance by one-way ANOVA followed by a *post-hoc* Tukey's Multiple Comparison Test. Significance is indicated as follows *p<0.05; **p<0.01; ***p<0.001. Data are shown as mean ± SEM.

Indeed, statistical analysis of the percentage of well-spread astrocytes 6 h after plating (Figure 3.22; B) reveals a highly significant decrease for cells with a reduced profilin level compared to control (black, 60.60±1.9%). There is no statistical relevant difference between astrocytes expressing PFN1 (white, 38.55±1.5%) or PFN2a (light grey, 42.96±2.1%) specific shRNA. The percentage of transduced astrocytes was found to be evidently reduced, especially for the PFN1 knockdown group, but also slightly for the PFN2a knockdown group. In accordance with these findings, transduced astrocytes subjected to a scratch wound assays revealed similar alterations in the respective transduction rates. As a result, the scratch wound assay was not appropriable to investigate the migration behavior of profilin knockdown astrocytes. The mentioned reduction may indicate a reduced viability or proliferation rate of profilin knockdown astrocytes, but this question was not addressed further. Overall, these findings suggest both profilins to be regulators of astrocytic spreading and adhesion.

3.1.4. PFN2a modulates morphology of astrocytes in organotypic slices

Recent studies revealed PFN2a as a modulator of the morphology in pyramidal hippocampal neurons (Michaelsen et al., 2010). To ensure a functional role of PFN2a in astrocytes in an *in vivo*-like situation, a morphological analysis of astrocytes in organotypic slice cultures was performed.

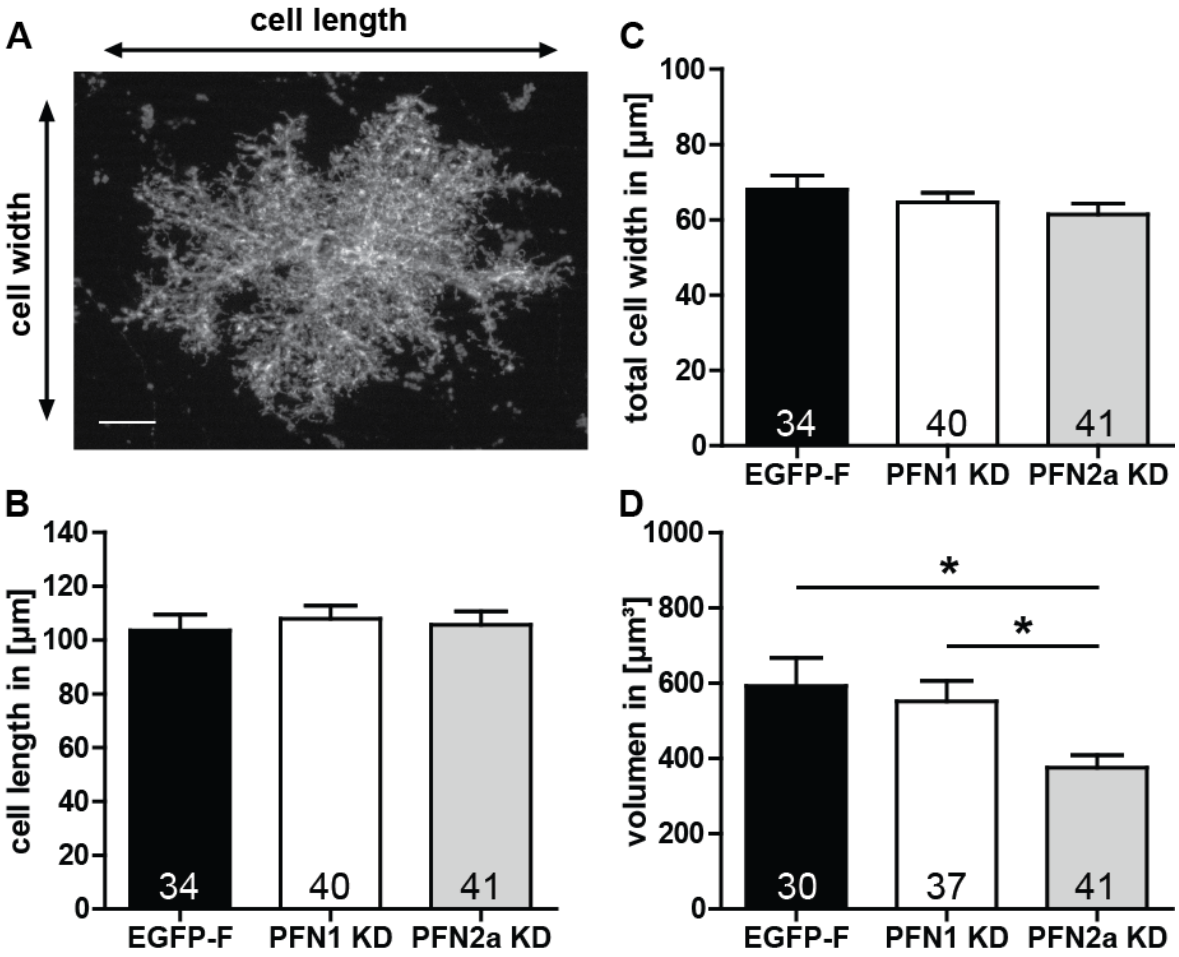

Figure 3.6 | Volume of astrocytes is modulated by PFN2a. (A) Morphology of astrocytes in organotypic slice cultures is similar to the *in vivo* situation. Scale bar: 10 µm. Cell length and width of transfected astrocytes were measured. The higher value was defined as length and the smaller as width of the respective astrocyte independent of its orientation. **(B)** Statistical analysis of the total cell length of astrocytes either expressing GFP as control or the shRNA specific for PFN1 or PFN2a, respectively. Length of the measured cells was unaltered. (EGFP-F: 103.6±6.0 µm; PFN1 KD: 107.9±4.9 µm; PFN2a KD: 105.7±5.0 µm) **(C)** Statistical analysis of the total cell width of astrocytes from B. Astrocytes expressing the shRNA specific for PFN2a showed a slight tendency towards a reduced cell width. (EGFP-F: 68.1±3.7 µm; PFN1 KD: 64.7±2.5 µm; PFN2a KD: 61.4±2.9 µm) **(D)** Statistical analysis of the volume of astrocytes from B. Astrocytes expressing the shRNA specific for PFN2a (375.6±33.2 µm²) displayed a significant reduction of their volume compared to control (592.6±74.3 µm²) or PFN1 knockdown (551.8±54.4 µm²) astrocytes. Quantitative data was tested for significance by one-way ANOVA followed by a *post-hoc* Tukey's Multiple Comparison Test. Significance is indicated as follows *p<0.05; **p<0.01; ***p<0.001. Data are shown as mean ± SEM.

Here, the astrocytes are adjacent to neurons and other types of glial cells, resembling the situation in a functional brain. Astrocytes occupy a discrete area in brain tissue (Bushong et al., 2002; Halassa et al., 2007), which indicates the importance of a tight regulation of their size and volume to guarantee an optimal support for the adjacent neurons. Astrocytes attain a star-like morphology (Figure 3.6; A) in these slice cultures gained from the murine cortex. In contrast to acutely prepared tissue, the benefit of this system is the possibility to manipulate the desired cells by transfection. Taking advantage of the shRNA mediated knockdown, the morphology of astrocytes with a reduced PFN1 or PFN2a protein level was examined in this culture system (Figure 3.6). Neither the length nor the width of astrocytes expressing the shRNAs specific for PFN1 or PFN2a was significantly altered (Figure 3.6; B and C). This finding suggests a mechanism regulating the length of the large processes independent of profilins, or alternatively compensation by the other profilin isoform. Interestingly, the down regulation of PFN2a leads to a drastic reduction in the volume of astrocytes (Figure 3.6; D). The volume of an astrocyte defines the area covered by its processes in the tissue and thereby its interconnection with other cells. This obvious and statistically relevant reduction to about 60% of the volume of control astrocytes for PFN2a knockdown cells is therefore a clear evidence for the importance of PFN2a in astrocytes. The knockdown of PFN1, however, revealed no significant alteration in the volume of the transfected astrocytes.

3.1.5. Profilins modulate the morphology of dissociated astrocytes

Not only PFN2a, but also PFN1 is suggested as a modulator of astrocytic morphology by a recent study of Molotkov and colleagues demonstrating a cell size reduction for dissociated astrocytes expressing an actin-binding-deficient PFN1 mutant (2013). This is in line with the recent observation of reduced process length in Bergmann glia of conditional PFN1 knockout mice (Kullmann et al., 2012). Consequently, the morphology of dissociated astrocytes was investigated, addressing the question of an isoform specific role of profilins (Figure 3.7). Therefore, the cell perimeter (Figure 3.7; A) and cell surface area (Figure 3.7; B) of transfected astrocytes were determined. Both, cell perimeter and cell surface area of cells expressing the shRNA specific for PFN1 or PFN2a are significantly reduced compared to control cells. This size reduction in line with the recently described cell perimeter reduction caused by an actin-binding-deficient PFN1 (Molotkov et al., 2013) and suggests both profilins as regulators of astrocytic cells size. Interestingly, the ratio of cell perimeter to cell area (Figure 3.7; C) is apparently not altered. This was also found by Molotkov and colleagues analyzing the actin-binding-deficient PFN1.

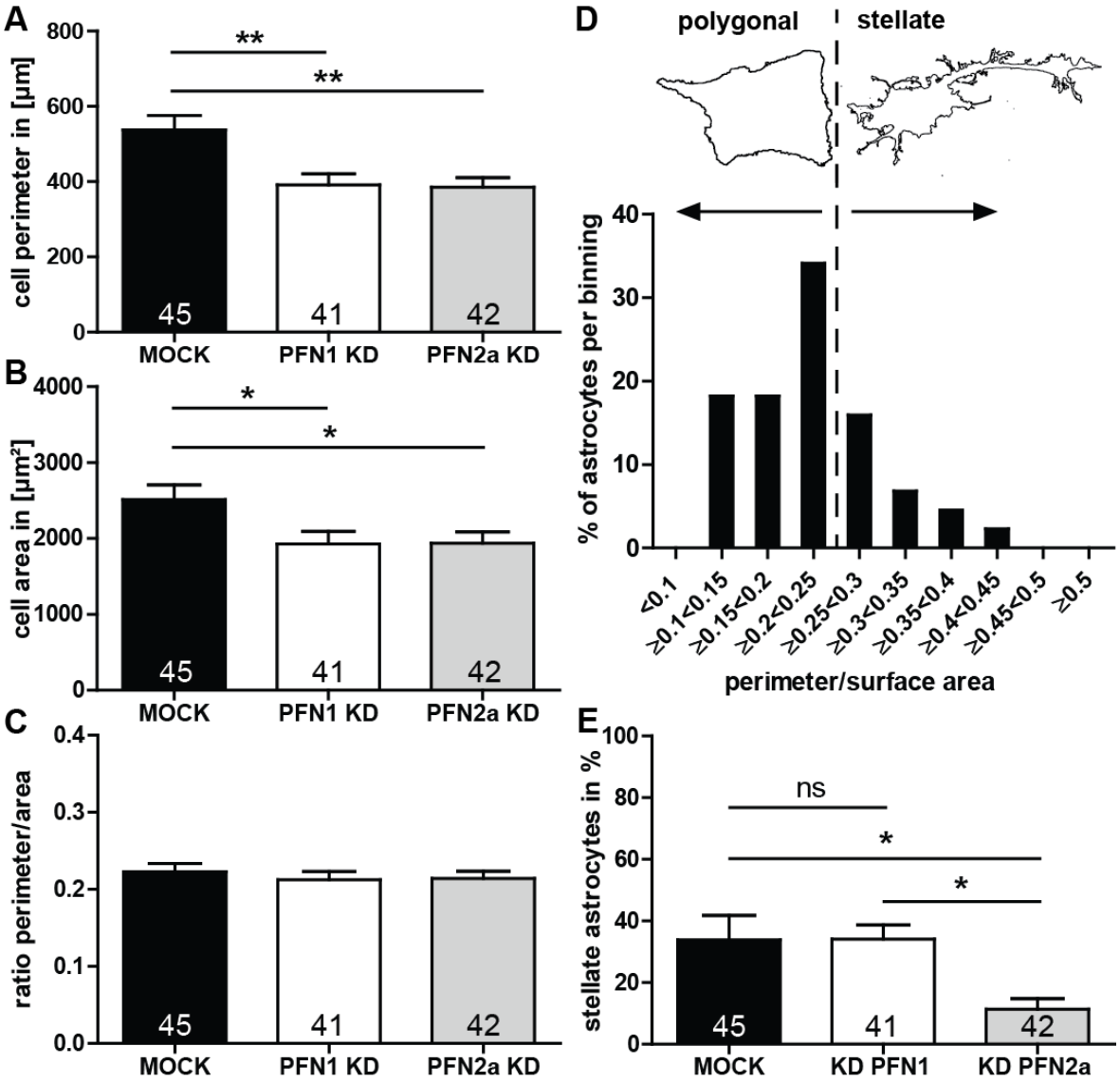

Figure 3.7 | Downregulation of profilin isoforms alters the morphology of astrocytes. (A) Cell perimeter of both PFN1 and PFN2a knockdown cells are significantly reduced, whereas the **(B)** cell area is only significantly decreased for PFN1 knockdown astrocytes. **(C)** Ratio between cell perimeter and cell surface area is not altered. **(D)** Categorization of astrocytes into two groups: stellate and polygonal. Astrocytes were subdivided into different classes according to their ratio between cell perimeter and cell area. Subsequently, cells with a ratio above 0.25 were added up to achieve the percentage of stellate astrocytes, the remaining were totaled to the group of polygonal astrocytes. The border between these two groups is indicated as dashed line. **(E)** The amount of stellate cells is significantly reduced in the group of PFN2a reduced cells. Quantitative data was tested for significance either by Student's t-test (A, B, C) or by one-way ANOVA followed by a *post-hoc* Tukey's Multiple Comparison Test. Significance is indicated as follows *p<0.05; **p<0.01; ***p<0.001. Data are shown as mean ± SEM.

To further investigate the morphology of the dissociated astrocytes, a frequency analysis according to the ratio between cell perimeter and cell surface area was performed (Figure 3.7; D). The resulting frequency distribution was used to subdivide the astrocytes into two groups. One group, termed "polygonal" includes astrocytes with a perimeter to area ratio

below 0.25. The majority of cells at basal conditions in serum containing media is included into this group. Astrocytes with a ratio of perimeter to area above 0.25 were classified as stellate. Applying this classification to the transfected astrocytes from Figures 3.7 A and B, reveals that the group of cells expressing the PFN2a specific shRNA contains significantly less stellate astrocytes (11.37±3.4%) compared to both other groups (MOCK: 33.87±7.9%; PFN1 KD: 34.17±4.6%). These results indicate PFN2a as a regulator of astrocytic stellation and additionally, both profilin isoforms as modulators of cell size in cultured astrocytes.

3.1.6. Profilins modulate morphological changes induced by serum starvation

Since a variety of stimulation protocols in the literature are performed on serum starved astrocytes (Murk et al., 2013; Racchetti et al., 2012; Ramakers and Moolenaar, 1998), first the potential influence of serum starvation on dissociated astrocytes was investigated. The starvation period was set as short as possible to avoid potential damage to the cells. Astonishingly, already a 4 hour period of serum depletion induces a non-significant ($p=0.1760$) increase in MOCK transfected astrocytes classified as stellate from 34% to 49% (Figure 3.8; A and E). As depicted in Figure 3.8 graphs B and F, astrocytes expressing the PFN1 specific shRNA display a stronger response to serum starvation. The percentage of stellate cells is significantly ($p=0.0187$) raised from 34% to 54%. This was exceeded by astrocytes transfected with pRNAT-U2.13 (Figure 3.8; C and G), where the increase in the percentage of stellate cells upon serum starvation from 13% to 51% was highly significant ($p=0.0005$).

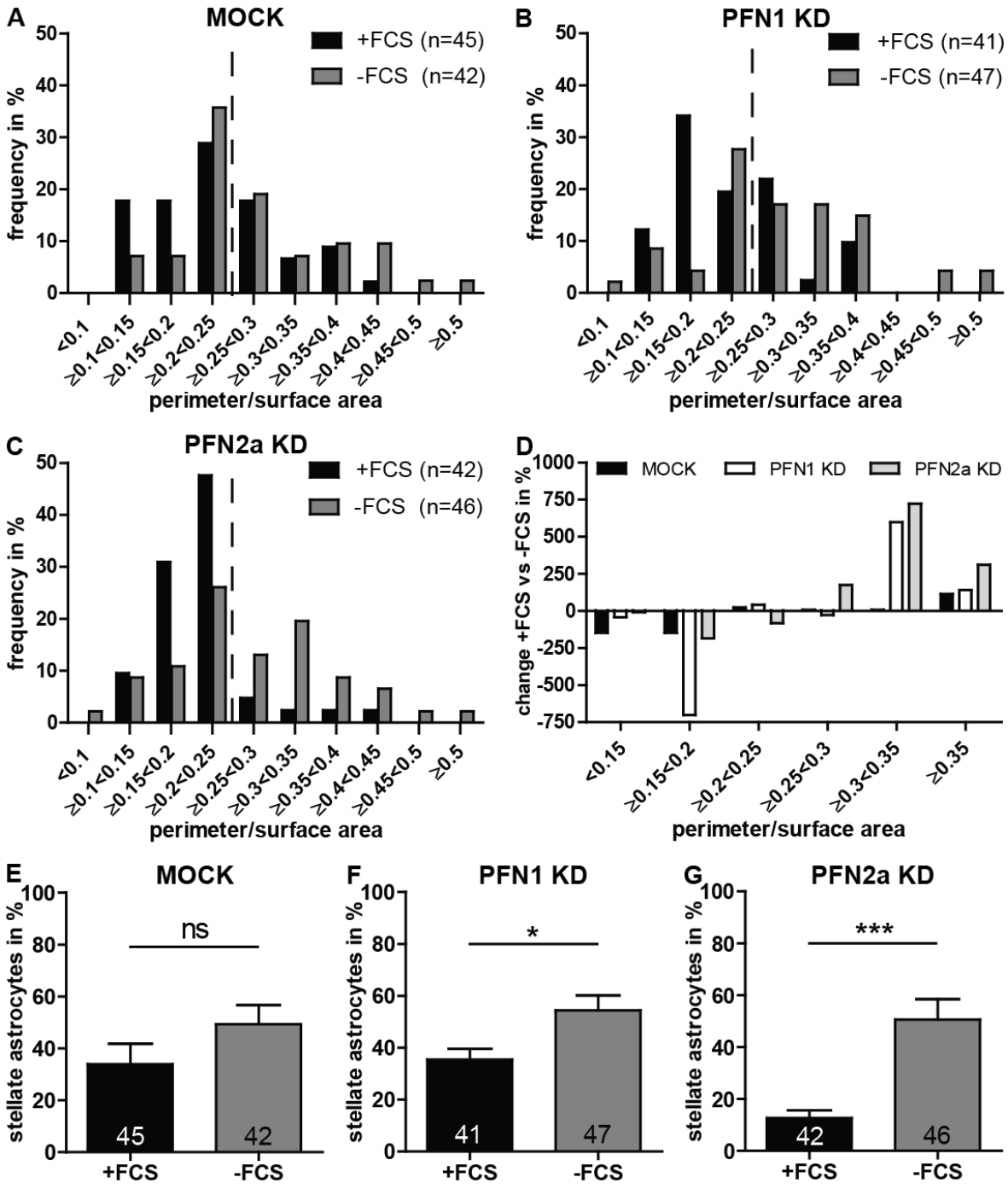

Figure 3.8 | Profilins modulate serum starvation induced morphology changes. **(A)** Frequency analysis of MOCK transfected astrocytes incubated in DMEM +FCS (black, +FCS) or DMEM –FCS for 4 h (grey, -FCS). A slight shift towards a higher perimeter to area ratio is visible. **(B)** Frequency analysis of astrocytes transfected with pRNAT-1.3 subjected to the same treatment as A. The shift to a higher perimeter to area ratio is evident. **(C)** Frequency analysis of pRNAT-2.13 transfected astrocytes treated as cells in A. Quantification reveals a drastic shift towards a higher perimeter to area ratio. Dashed line indicates border between polygonal (left) and stellate cells (right). **(D)** Diagram illustrating the change per subclass between serum containing and serum depleted conditions. MOCK (black) transfected cells display only a slight change totaled up to 450%, whereas the change in the group of PFN1 (white) as well as PFN2a (light grey) knockdown astrocytes exhibit a drastic net change summed to 1554% and 1483%, respectively. - *Continued on the following page* -

- *Continued from the previous page* - **(E)** MOCK transfected starved astrocytes display a non-significant tendency towards a higher percentage of stellate cells (+FCS: 33.87±7.9%; -FCS: 49.32±7.4%). **(F)** Starvation induced a significant increase in the percentage of stellate cells in astrocytes expressing the shRNA specific for PFN1 (+FCS: 35.42±4.2%; -FCS: 54.38±5.8%). **(G)** Statistical analysis of PFN2a knockdown astrocytes revealed a highly significant increase in stellate astrocytes induced by starvation (+FCS: 12.62±3.0%; -FCS: 50.62±7.8%). Quantitative data was tested for significance by Student's t-test. Significance is indicated as follows *p<0.05; **p<0.01; ***p<0.001. Data are shown as mean ± SEM.

To illustrate these changes induced by serum starvation, the fluctuations per subclass were calculated and presented in Figure 3.8 graph D. Subclasses, which did not contain cells subjected to both treatments were fused to the adjacent subclass. The net change was determined by totaling the change per subclass. The group of MOCK (black) transfected cells exhibits a net change of 450%, whereas the groups of PFN1 (white) and PFN2a (light grey) knockdown cells displayed a far more drastic net change of 1554% and 1483%, respectively. This indicates an important role of profilin isoforms in the cellular response to serum deprivation.

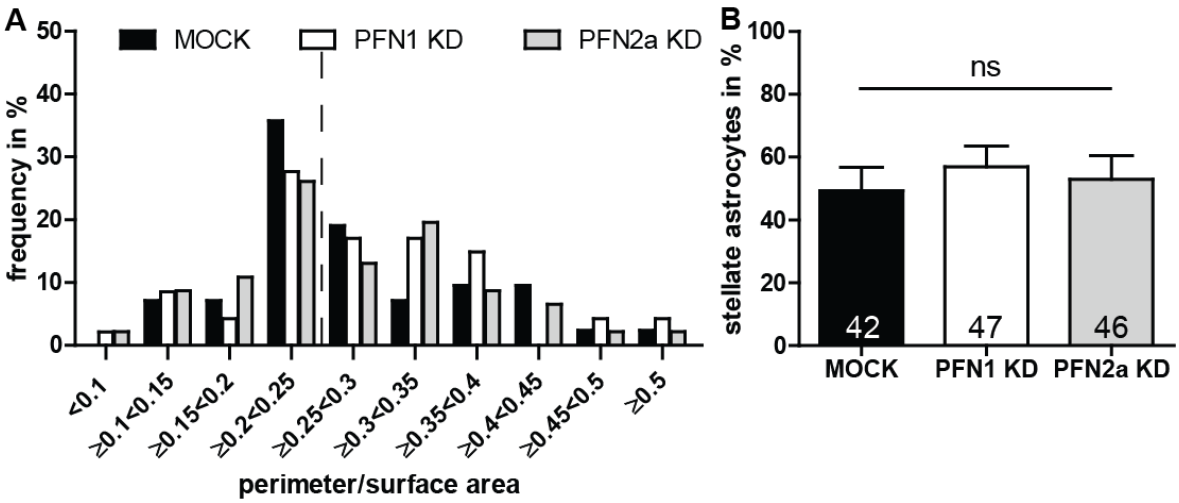

Figure 3.9 | 4 h serum starvation leads to a disappearance in differences between controls and profilin knockdown groups. **(A)** Frequency analysis of astrocytes transfected either with pRNAT-siFluc, pRNAT-1.3 or pRNAT-2.13, respectively. Frequency distribution appears to be largely unaltered. Dashed line indicates border between polygonal (left) and stellate (right) cells. **(B)** Comparison of the percentage of stellate astrocytes from A. No significant changes are displayed. Quantitative data was tested for significance by one-way ANOVA followed by a *post-hoc* Tukey's Multiple Comparison Test. Significance is indicated as follows *p<0.05; **p<0.01; ***p<0.001. Data are shown as mean ± SEM.

As the comparison of astrocytes transfected either with pRNAT-siFluc, pRNAT-1.3 or pRNAT-2.13, respectively, kept under serum deprivation for 4 h, revealed no differences between these three groups (Figure 3.9), this treatment was suitable as control condition to all further experiments. To further investigate the profilin dependent reaction to serum deprivation, also morphological data of astrocytes starved for 24 h was taken into account.

Interestingly, as illustrated with Figure 3.10, the change in the percentage of stellation varies depending on the respective profilin knockdown.

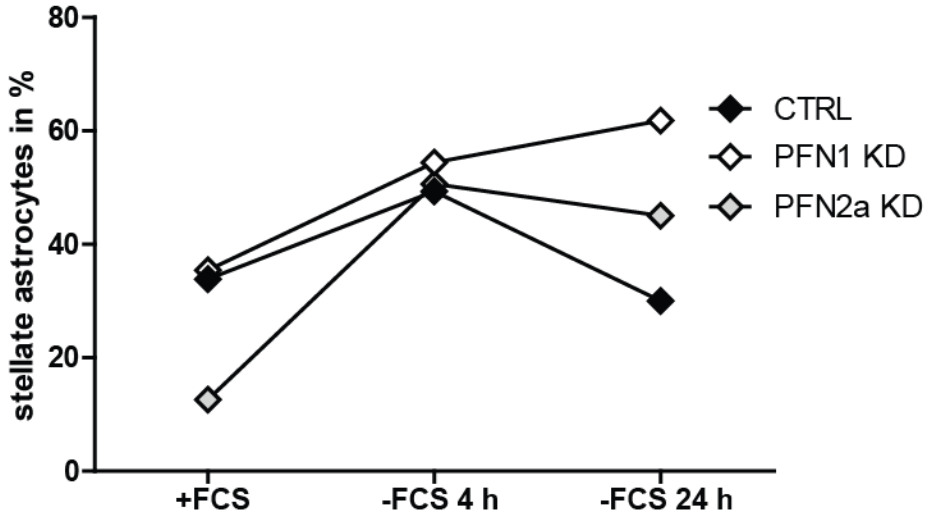

Figure 3.10 | Starvation induces temporally distinct profilin isoform dependent morphological changes. Astrocytes were depleted of FCS for 4 or 24 h and subsequently, they were categorized into stellate and polygonal cells by their morphology. Control astrocytes (black) display an increase of the amount of stellate cells upon serum deprivation for 4 h. This change is rescinded upon 24 h of serum depletion, where the amount of stellate astrocytes is indistinguishable from +FCS condition (+FCS: 34% vs –FCS 24 h: 30%). Astrocytes expressing the PFN1 specific shRNA show an obvious increase in the percentage of stellate cells upon 4 h of serum deprivation (+FCS: 35%; -FCS 4 h: 54%). This increase even rises further to 62% for 24 h of serum deprivation. Down regulation of PFN2a resulted in a very low percentage of stellate astrocytes in serum containing conditions (13%). This percentage increased drastically by serum deprivation for 4 h (51%). Serum deprivation for 24 h (45%) however did not lead to a further rise, but to a slight decrease of the percentage of stellate astrocytes.

Control astrocytes (black) display a non-significant increase in the amount of stellated astrocytes upon 4 h of serum deprivation, which disappeared after 24 h. The serum deprivation induced stellation can therefore be described as transitory. Examination of astrocytes expressing the shRNA specific for PFN1 (white) revealed an altered progression. Despite a similar response to serum deprivation for 4 h, the percentage of stellated astrocytes did not decrease to +FCS-like percentages after 24 h of serum deprivation, but showed an additional increase. This further rise from 54% to 62% indicates an important role of PFN1 in the adaptation of astrocytes to serum deprived conditions. Astrocytes expressing the shRNA specific for PFN2a displayed yet another progression of their morphological response to serum deprivation. Astrocytes of this group showed a very drastic and highly significant response to 4 h of serum deprivation. This increase in the percentage of stellate astrocytes from 13% to 51% simply resulted in an equal percentage compared to the other two groups. After 24 h of serum deprivation,

PFN2a knockdown astrocytes displayed a slight decrease to 45% stellate cells. This can be described as a stagnation of the progression, as the percentage of stellate astrocytes is not reversed to +FCS-like amounts, but also no further rise can be found. Altogether, these finding indicate profilins as substantial proteins in the regulation of the starvation response in astrocytes.

These interesting findings on the profilin dependent reaction of astrocytes to serum starvation promoted a further examination of profilins under serum deprived conditions. Already in 1974, serum deprivation was shown to increase cellular cyclic AMP levels in mouse fibroblasts (Oey et al.). This in turn activates the cAMP dependent protein kinase A. Thus, subsequent proteins in the PKA dependent pathways are phosphorylated. Here, 2D gel electrophoresis was used to analyze potential alteration in the phosphorylation change of profilins under serum deprived conditions. At first, samples for 2D gel electrophoresis were incubated with alkaline phosphatase (AP). Then they were compared to controls to confirm the presence of phosphorylated PFN2a (p-PFN2a) in the astrocytic cultures (Figure 3.11).

Figure 3.11 | Cultured astrocytes subjected to serum starvation for 4 h contain phosphorylated PFN2a. Astrocytes were harvested after 4 h of serum starvation and directly used (-FCS 4 h) or subsequently incubated with alkaline phosphatase (-FCS 4 h + AP). The left spot (lower pI) corresponds to a phosphorylated form of PFN2a as its disappearing after treatment with AP.

Application of alkaline phosphatase resulted in the disappearance of the spot with the lower isoelectric point (pI), thereby demonstrating the presence of a phosphorylated form of PFN2a in dissociated astrocytic cultures.

Also, PFN1 phosphorylation state was examined in astrocytic cultures (Figure 3.12). Either an anti PFN1 antibody raised against the N-terminal region of PFN1 or against the C-terminal region of PFN1 was used. While the N-terminal anti-PFN1 antibody recognizes two distinct spots, the C-terminal anti PFN1 antibody only recognizes the spot localized to a higher pI. The signal obtained with the N-terminal anti-PFN1 antibody was unfortunately very weak.

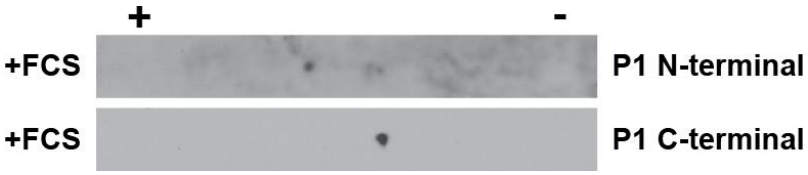

Figure 3.12 | C-terminal phosphorylation of PFN1 in astrocytic cultures. Astrocytic cultures kept under basal conditions were harvested and subjected to 2D gel electrophoresis. Western blot analysis was performed with either an anti-PFN1 antibody raised against the N-terminal region of PFN1 (P1 N-terminal) or an anti-PFN1 antibody raised against the C-terminal region of PFN1 (P1 C-terminal). Antibody directed against the C-terminus of PFN1 was not capable of detecting the phosphorylated PFN1 form detected as the left (lower pI) dot by the other antibody.

However, PFN1 is phosphorylated in its C-terminal region in dissociated astrocytic cultures. These findings are in line with a phosphorylation at the Serine 137, which was shown in HEK293T cells (Shao et al., 2008).

To correlate morphological changes upon serum deprivation dependent on the PFN2a knockdown, 4 h serum starved cultures were analyzed for the phosphorylation status of PFN2a (Figure 3.13).

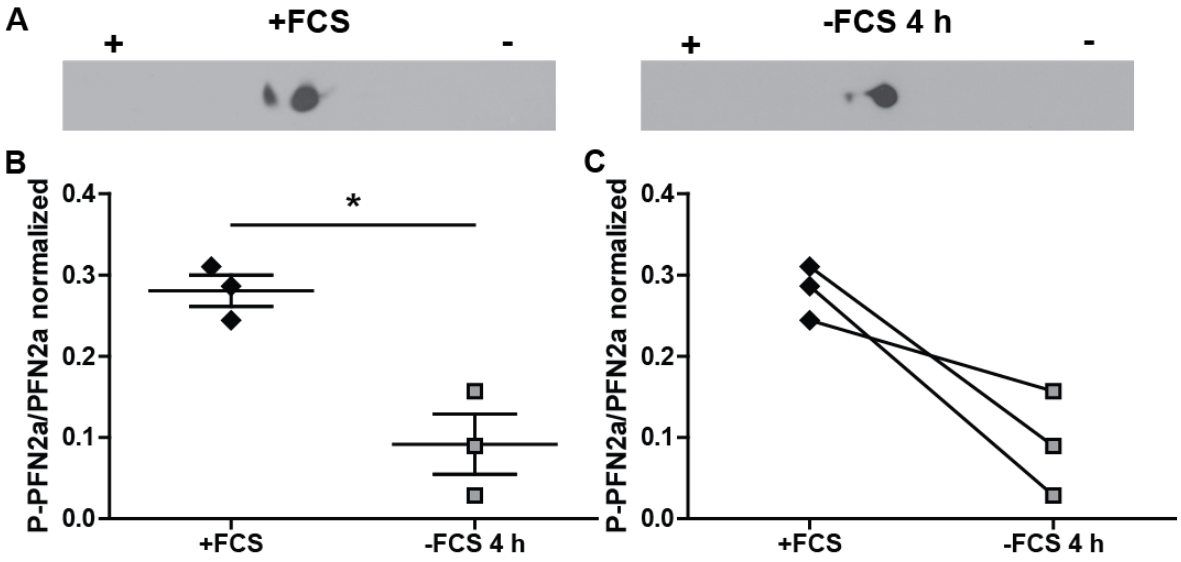

Figure 3.13 | 4 h of serum deprivation decreases amount of phosphorylated PFN2a. (A) 2D-geleletrophoresis with subsequent Western Blot analysis. Astrocytic cultures were either kept in DMEM supplement with FCS (+FCS) or were serum starved for 4 h (-FCS 4 h). **(B)** Quantification of the phosphorylation status of PFN2a from three independent experiments. Dot intensities were measured with Image J. Subsequently, intensity values of all dots were totaled and the intensity of the left dot was divided through the total intensity. The mean relative amount of phosphorylated PFN2a was significantly decreased in serum deprived cultures (0.09±0.04) compared to control cultures (0.28±0.02). **(C)** Visualization of the three independent experiments. All three experiments show a decrease of p-PFN2a for serum depleted conditions in comparison to control. Quantitative data was tested for significance by Student's t-test. Significance is indicated as follows *p<0.05; **p<0.01; ***p<0.001. Data are shown as mean ± SEM.

Interestingly, the amount of p-PFN2a was significantly reduced in 4 h serum deprived astrocytes compared to control astrocytes. Considering the phosphorylated form of PFN2a as the inactive one (Da Silva et al., 2003), this finding supports a role of PFN2a in the structural remodeling of the astrocytic cytoskeleton upon serum deprivation. Since the serum depletion dependent morphological changes were reversed after 24 h (Figure 3.10), also astrocytic cultures subjected to a pronounced (48 h) serum deprivation were analyzed in the 2D gel electrophoresis. Remarkably, serum deprivation was found to induce a non-significant 60% increase in the fraction of p-PFN2a (Figure 3.14).

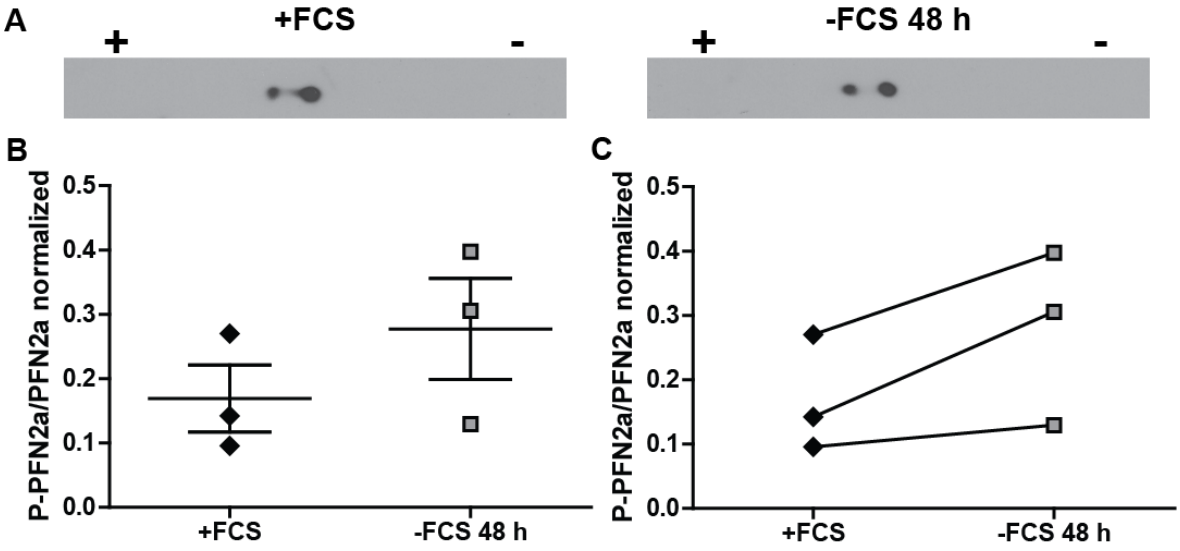

Figure 3.14 | 48 h of serum deprivation slightly increases amount of phosphorylated PFN2a. (A) 2D-geleletrophoresis with subsequent Western Blot analysis. Astrocytic cultures were either kept in DMEM supplement with FCS (+FCS 48 h) or were serum starved for 48 h (-FCS 48 h). **(B)** Quantification of the phosphorylation status of PFN2a from three independent experiments. Dot intensities were measured with Image J. Subsequently, intensity values of all dots were totaled and the intensity of the left dot was divided through the total intensity. The mean relative amount of phosphorylated PFN2a was slightly increased in serum deprived cultures (0.28±0.08) compared to control cultures (0.17±0.05). **(C)** Visualization of the three independent experiments. All three experiments show an increase of p-PFN2a for serum depleted conditions in comparison to control. Quantitative data was tested for significance by Student's t-test. Significance is indicated as follows *p<0.05; **p<0.01; ***p<0.001. Data are shown as mean ± SEM.

All three performed experiments mutually display a trend of a varying strength to an increase of the fraction of p-PFN2a after 48 h of serum deprivation (Figure 3.14; C). Comparing the phosphorylation state of PFN2a between 4 h and 48 h serum deprived astrocytes, the results hint at a temporally distinct regulation of the activity of PFN2a by phosphorylation. Collectively, consideration of the serum dependent phosphorylation state of profilins and the impact on morphology is crucial for the interpretation of further results on astrocytic morphology.

3.1.7. Forskolin induces PKA dependent stellation in astrocytes

To determine whether profilin isoforms play a role in other dynamic changes in the actin cytoskeleton of astrocytes, remodeling of the astrocytic microfilament system was induced by forskolin, a stimulation agent raising intracellular cAMP levels. The elevated cAMP level leads to actin and Arp2/3 complex dependent dynamic changes of the actin cytoskeleton (Goldman and Abramson, 1990; Murk et al., 2013).

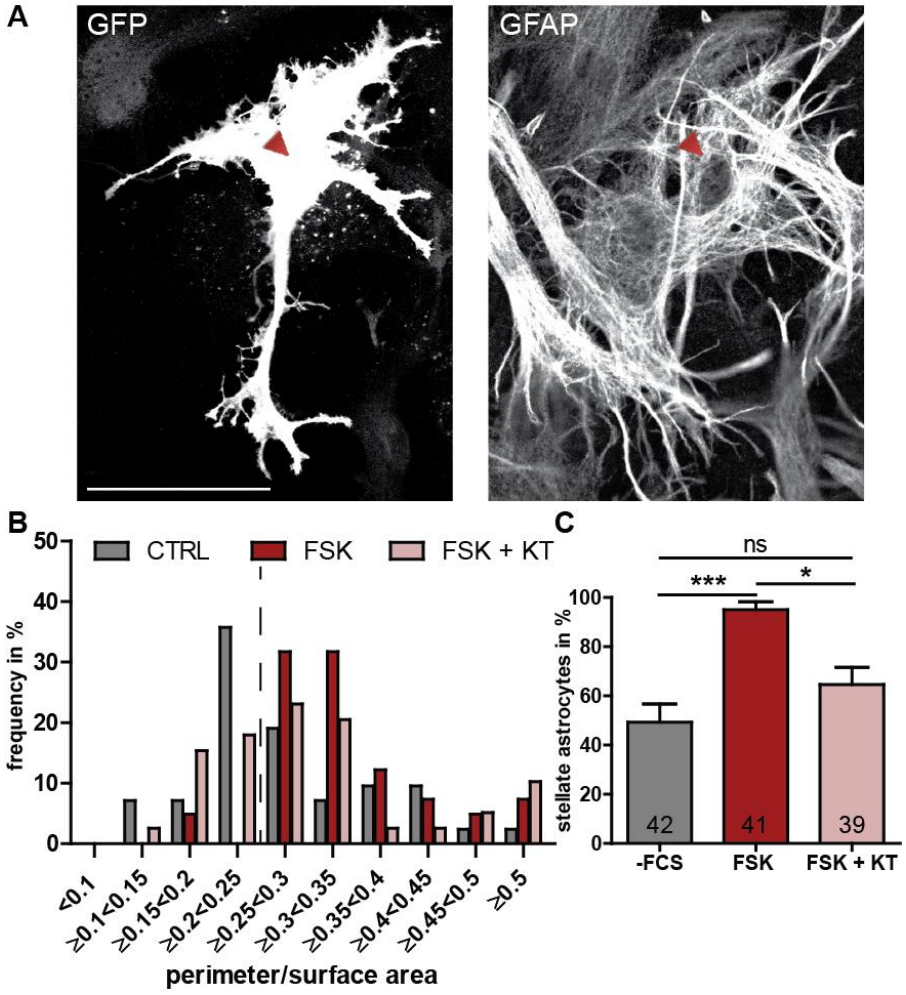

Figure 3.15 | Astrocytes undergo PKA dependent stellation upon treatment with forskolin. (A) MOCK transfected cell treated with 10 µM forskolin for 2h. Astrocytes attained a process bearing morphology, also characterized by condensed GFAP positive structures. Red arrow indicates position of transfected astrocyte. **(B)** Frequency analysis of control astrocytes (-FCS, grey), astrocytes treated with forskolin (FSK, red) and astrocytes treated with forskolin and 100 nM KT5720 (FSK + KT, rose). FSK treatment induces a shift towards a higher perimeter to surface area ratio, which is largely inhibited by co-application of KT5720. Dashed line indicates border between polygonal (left) and stellate (right) cells. **(C)** Statistical analysis reveals a highly significant increase in the percentage of stellate astrocytes, whereas the co-application of FSK + KT results in no significant changes. Quantitative data was tested for significance by one-way ANOVA followed by a *post-hoc* Tukey's Multiple Comparison Test. Significance is indicated as follows *p<0.05; **p<0.01; ***p<0.001. Data are shown as mean ± SEM.

Initially, the effect of 10 µM forskolin in serum depleted medium was determined on MOCK transfected astrocytes. These astrocytes underwent a strong contraction and thereby reduction of their cell area (Figure 3.15; A). This drastic change in cellular morphology becomes evident considering the frequency analysis (Figure 3.15; B), where the application of forskolin causes an obvious shift to higher perimeter to area ratios. Accordingly, the percentage of stellate cells increased drastically in the group of MOCK transfected cells upon forskolin treatment (Figure 3.15; C). As the increase of cAMP levels directly activates the cAMP-dependent protein kinase A (PKA), experiments were performed experiments with co-application of the specific PKA inhibitor KT5720 in order to abolish morphological changes produced by forskolin treatment (Kase et al., 1987). Indeed, MOCK transfected cells treated with both FSK and KT5720 (Figure 3.15; rose) exhibit a significantly reduced percentage of stellate cells (64.58±7.0%) compared to forskolin treatment alone (95.00±3.3%). Still, a non-significant tendency to a higher percentage of stellate cells in comparison to control (49.32±7.4%) was evident.

As a next step, it was analyzed if these morphological changes rely on profilins undergoing a PKA dependent phosphorylation change upon forskolin treatment in astrocytic cultures. The phosphorylation status of PFN2a was again analyzed by 2D gel electrophoresis. In fact, the fraction of phosphorylated PFN2a was significantly increased in forskolin treated cultures in comparison to controls (Figure 3.16). This increase was at least to some extent directly dependent on PKA, as the simultaneous application of the PKA inhibitor KT5720 reduced the effect of forskolin. Treatment with both substances did not significantly raise the amount of phosphorylated PFN2a compared to control. Figure 3.16 C illustrates the progression of the p-PFN2a fraction in two independent experiments. Besides the significant increase upon forskolin treatment, also the decrease in p-PFN2a amount by the co-application of forskolin and KT5720 becomes evident. These results demonstrate the phosphorylation of PFN2a by PKA in the living cell. With these new insights, a morphological analysis of astrocytes expressing either the PFN1 or the PFN2a specific shRNA subjected to forskolin treatment was highly promoted.

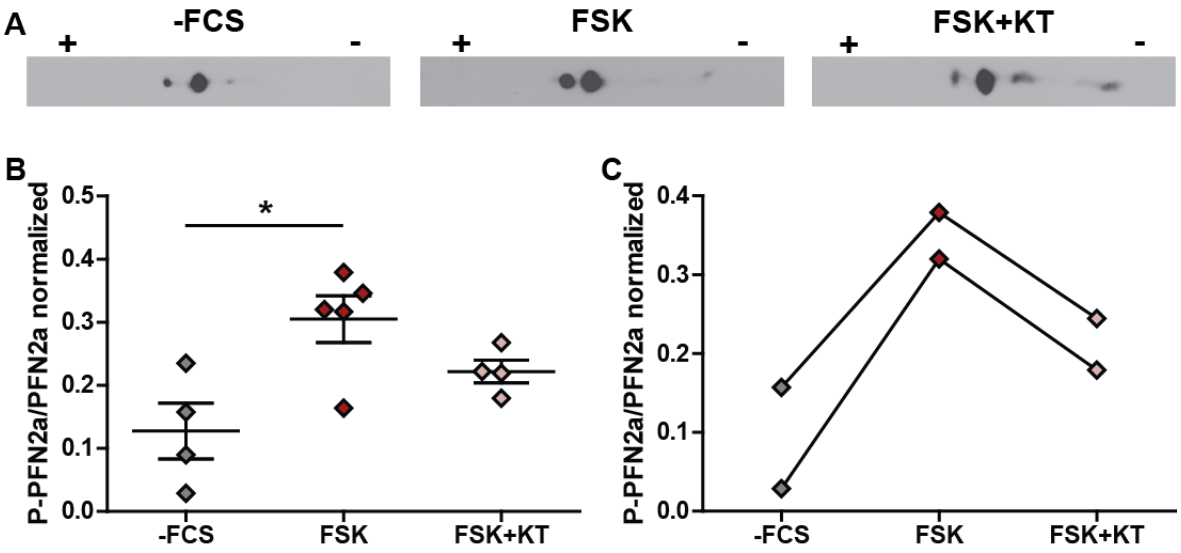

Figure 3.16 | Forskolin treatment increases the amount of phosphorylated PFN2a. (A) 2D gel electrophoresis with subsequent Western Blot analysis. Astrocytic cultures were kept in DMEM without supplement (-FCS), treated with 10 µM forskolin for 2 h (FSK) or treated with 10 µM Forskolin for 2 h in the presence of 100 nM KT5720 (FSK+KT) **(B)** Quantification of the phosphorylation status of PFN2a. Dot intensities were measured with Image J. Subsequently, intensity values of all dots were totaled and the intensity of the left dot was divided through the total intensity. The mean relative amount of phosphorylated PFN2a was significantly increased in forskolin treated cultures (0.31±0.04) compared to control cultures (0.13±0.04). Cultures treated with both FSK and KT attained a fraction of 0.22±0.02, which is a non-significant decrease (p=0.1063) compared to forskolin treated cultures. **(C)** Visualization of two independent experiments, where all three treatments were available. Both experiments show an increase of p-PFN2a upon forskolin treatment and a decrease comparing forskolin treated vs. forskolin and KT5720 treated cultures. Quantitative data was tested for significance by one-way ANOVA followed by a *post-hoc* Tukey's Multiple Comparison Test. Significance is indicated as follows *p<0.05; **p<0.01; ***p<0.001. Data are shown as mean ± SEM.

Interestingly, cells expressing either the PFN1 specific or the PFN2a specific shRNA show no significant response to forskolin (Figure 3.17). These astrocytes failed to contract upon forskolin treatment (Figure 3.17; A, red arrowhead), whereas adjacent non-transfected cells successfully underwent stellation (Figure 3.17; A, blue arrowhead). Nevertheless, PFN1 knockdown as well as PFN2a knockdown astrocytes frequently show more small processes compared to non-stimulated controls (non-quantified observation). Frequency analysis of astrocytes with a reduced protein level of PFN1 (Figure 3.17; B) treated with forskolin show a slight increase in astrocytes with a cell perimeter to cell area ratio above 0.4. Additionally, PFN1 KD transfected cells treated with FSK + KT (rose) display a peak of cells with a ratio between 0.35 and 0.4., which leads to an increase in the percentage of stellate astrocytes (54.38±5.8% to 66.25±10.0%). However, the percentage of stellate cells in this group was not significantly altered upon the respective treatments.

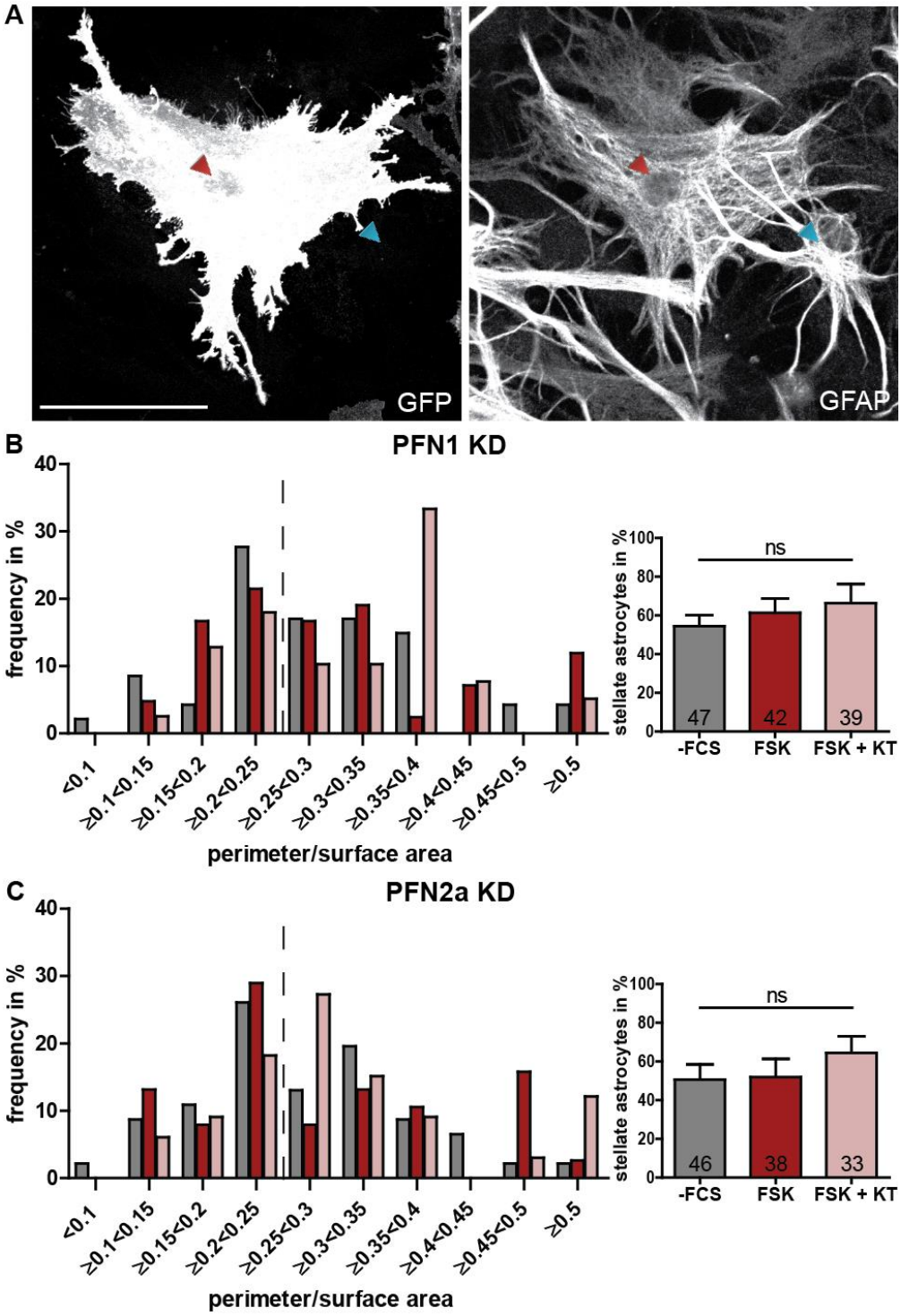

Figure 3.17 | Profilins are essential for forskolin induced morphological changes. (A) Astrocyte expressing a shRNA specific for PFN1 treated with forskolin. The GFP expressing cell (red arrowhead) does not contract properly whereas the adjacent, untransfected astrocyte (blue arrowhead) underwent stellation. **(B, C)** Statistical analysis of astrocytes transfected with pRNAT-1.3 or pRNAT-2.13, respectively. PFN1 KD transfected cells treated with FSK + KT (rose) display a peak of cells with a ratio between 0.35 and 0.4. PFN1 KD (B) or PFN2a KD (C) cells reveal no further significant effect of both treatments. Dashed line indicates border between polygonal (left) and stellate (right) cells. Quantitative data was tested for significance by one-way ANOVA followed by a *post-hoc* Tukey's Multiple Comparison Test. Significance is indicated as follows *p<0.05; **p<0.01; ***p<0.001. Data are shown as mean ± SEM.

Moreover, also the frequency analysis of cells expressing the PFN2a specific shRNA (Figure 3.17; C) reveals several minor alterations resulting from forskolin or forskolin and KT5720 application. Specifically, a higher percentage of astrocytes treated with forskolin attain a perimeter to area ratio above 0.45. Co-application of forskolin and KT5720 leads to an increased amount of cells with a perimeter to area ratio between 0.25 and 0.3 as well as above 0.45. These changes result in an increased percentage of stellate astrocytes for the group of FSK + KT treated cells (50.62±7.8% to 64.49±8.6%). Still, none of these alterations results in a significant change in the total percentage of stellate astrocytes.

The quantification of the relative change per subclass caused by forskolin treatment (Figure 3.18) illustrates the reduced response of astrocytes expressing either the PFN1 or the PFN2a specific shRNA upon stimulation.

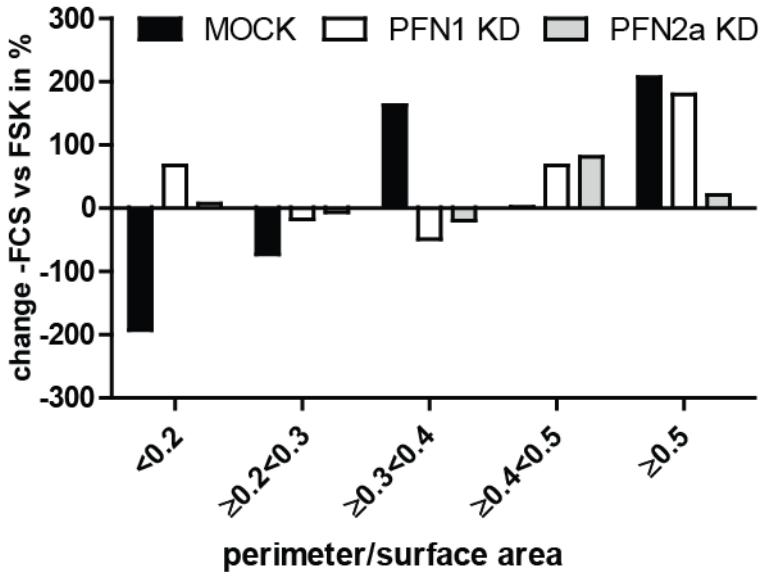

Figure 3.18 | Illustration of the total changes per subclass comparing control cells (-FCS 4h) with forskolin treated cells (10 µM 4h). MOCK transfected cells (black) display obvious changes. Furthermore, cells expressing the PFN1 specific shRNA (white) also show some evident changes, especially in the subclass of ≥0.5.

Mock transfected cells display a net change of 639%, while PFN1 and PFN2a knockdown cells only exhibit a net change of 382% and 136%, respectively. The difference between PFN1 and PFN2a knockdown astrocytes becomes evident in the subclass of markedly stellated astrocytes (≥0.5), where PFN1 knockdown cells show an increase comparable to control astrocytes. This difference additionally supports a more pronounced role of PFN2a in the stellation process.

Direct comparison of astrocytes transfected with either pRNAT-siFluc, pRNAT-1.3 or pRNAT-2.13 and treated with forskolin (Figure 3.19) confirmed the differences between

the control group and both knockdown groups. MOCK transfected cells (black) display an evident shift in the frequency distribution of cells upon forskolin treatment compared to the other two groups (Figure 3.19; A). Statistical analysis of the percentage of stellate astrocytes (Figure 3.19; B) revealed a significantly reduced response to forskolin treatment for cells expressing a PFN1 and PFN2a specific shRNA, compared to control cells. The percentage of stellate astrocytes decreases from 95% for control astrocytes to 58% and 49% for PFN1 and PFN2a knockdown cells, respectively.

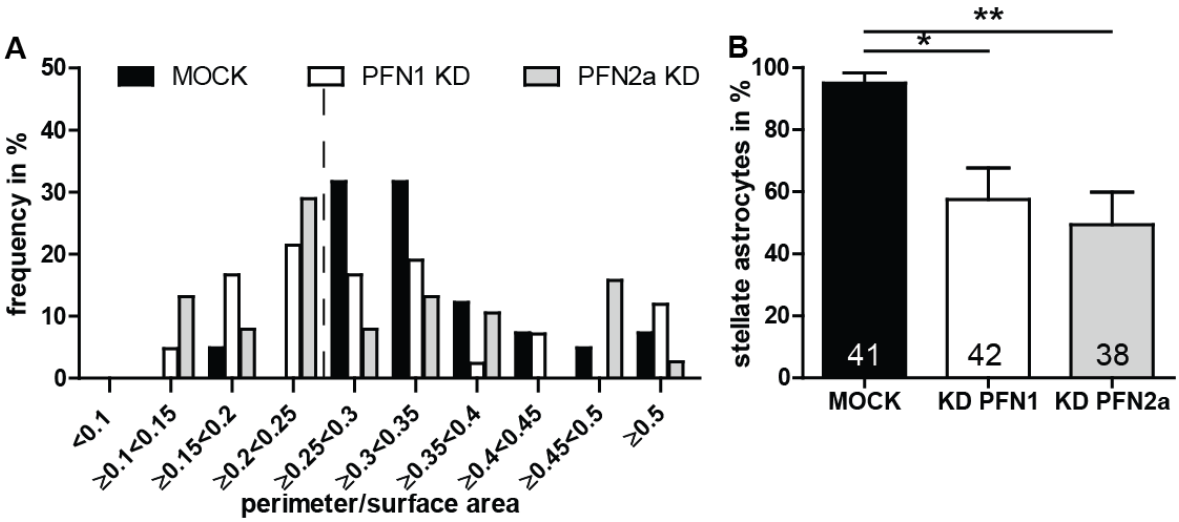

Figure 3.19 | Forskolin induced stellation depends on profilins. (A) Frequency analysis of astrocytes treated with 10 µM forskolin for 4 h. Cells were transfected with either pRNAT-siFluc (MOCK, black), pRNAT-1.3 (KD PFN1, white) or pRNAT-2.13 (KD PFN2a, light grey). Frequency distribution is obviously altered between the groups. Dashed line indicates border between polygonal (left) and stellate (right) cells. **(B)** Statistical analysis of the percentage of stellate astrocytes reveals a significantly reduced percentage for astrocytes with reduced amount of PFN1 (57.50±10.1%) as well as astrocytes with a reduced PFN2a level (49.38±10.5%) compared to control (95.00±3.3%). Quantitative data was tested for significance by one-way ANOVA followed by a *post-hoc* Tukey's Multiple Comparison Test. Significance is indicated as follows *p<0.05; **p<0.01; ***p<0.001. Data are shown as mean ± SEM.

These results reveal a major role of both profilin isoforms in actin remodeling during forskolin induced stellation process. It is also quite evident that the application of PKA inhibitor KT5720 shows, an additional effect (Figure 3.17; B), at least on cells with a reduced amount of PFN1. These findings led to further examination of the interplay between PKA activation or inactivation and profilins.

3.1.8. PKA inhibition has a PFN2a-specific effect on astrocytic morphology

Consequently, morphological analysis of astrocytes transfected with either pRNAT-siFluc, pRNAT-1.3 or pRNAT-2.13 and treated with specific PKA inhibitor KT5720 for 4 hours was performed.

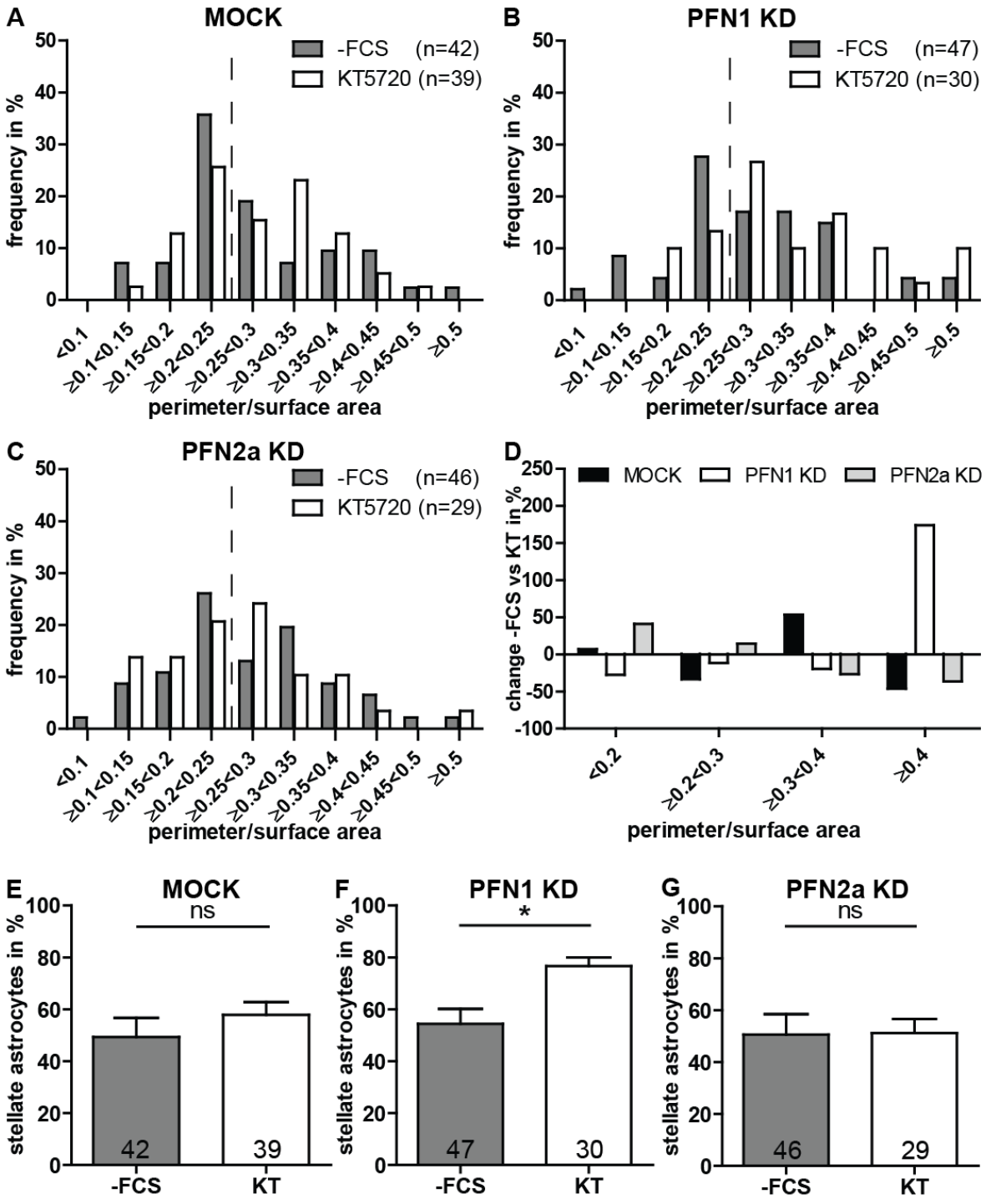

Figure 3.20 | Morphological analysis of astrocytes treated with KT5720. (A) Frequency analysis of MOCK transfected astrocytes, treated either with 100 nM KT5720 for 4 h in DMEM without FCS (KT, white) or untreated in DMEM without FCS (-FCS, grey) as control. **(B, C)** Frequency analysis of astrocytes transfected with pRNAT-1.3 (PFN1 KD, B) or pRNAT-2.13 (PFN2a KD, C), respectively, subjected to the same treatment as A. Dashed line indicates border between polygonal (left) and stellate (right) cells. **(D)** Diagram illustrating the change per subclass between control conditions and KT5720 treatment. MOCK (black) transfected cells as well as PFN2a (light grey) knockdown astrocytes display only a slight change totaled up to 140% and 119%, respectively. PFN1 (white) knockdown astrocytes exhibit an evidently increased net change summed up to 233%. - *Continued on the following page* -

- *Continued from the previous page* - **(E)** MOCK transfected KT5720 astrocytes display a slight, non-significant tendency towards a higher percentage of stellate cells (-FCS: 49.32±7.4%; KT: 57.92±4.8%). **(F)** PKA inactivation induced a significant increase in the percentage of stellate cells in astrocytes expressing the shRNA specific for PFN1 (-FCS: 54.38±5.8%; KT: 76.67±3.3%). **(G)** The percentage of stellate PFN2a knockdown astrocytes was unaltered by KT5720 treatment (-FCS: 50.62±7.8%; KT: 51.17±5.4%). Quantitative data was tested for significance by Student's t-test. Significance is indicated as follows *p<0.05; **p<0.01; ***p<0.001. Data are shown as mean ± SEM.

Control astrocytes (Figure 3.20; A and E) subjected to KT5720 treatment reveal a slight shift towards a higher cell perimeter to cell area ratio, which has no significant consequences for the percentage of stellate cells compared to control conditions. Still, a slight tendency towards an increased amount of stellate astrocytes is detectable (-FCS: 49.32±7.4%; KT: 57.92±4.8%). Interestingly, PFN1 downregulated astrocytes (Figure 3.20; B and F) exhibit an evident shift in the frequency analysis as well as a significant increase of the portion of stellate astrocytes by 22% upon KT5720 treatment (p=0.0102). This result hints to a gain-of-function of PFN2a in the absence of PFN1 or a regulatory function of PFN1, inhibiting the stellation response upon PKA inhibition. Astrocytes expressing the PFN2a specific shRNA (Figure 3.20; C and G), however, exhibit no detectable response to KT5720 treatment. The percentage of stellate astrocyte was found to reach 51% for both control and KT5720 treated astrocytes, thereby hinting towards a role of PFN2a in the response to PKA inhibition. Comparison of the changes per subclass induced by KT5720 treatment (Figure 3.20; D) promotes a modulatory role of PFN1 in the response to PKA inhibition. Especially in the subclass of '≥0.4', an obvious increase of PFN1 knockdown astrocytes was exhibited, in contrast to both other groups. The monitored changes sum up to 140% for control astrocytes, 233% for PFN1 knockdown astrocytes and 119% for PFN2a knockdown astrocytes. These net changes underline the importance of PFN1 in the proper response to PKA signaling. Direct comparison of astrocytes transfected with either pRNAT-siFluc (MOCK, black), pRNAT-1.3 (PFN1 KD, white) or pRNAT-2.13 (PFN2a KD, light grey) treated with KT5720 (Figure 3.21) emphasizes the importance of PFN1 in this context. Here, the frequency analysis (Figure 3.21; A) only displays subtle alterations in the frequency distribution between the different analyzed groups. Nevertheless, the evident shift in PFN1 knockdown astrocytes towards a higher perimeter to area ratio persists in the comparison to the other two groups. Accordingly, significantly more PFN1 downregulated astrocytes attained a stellate morphology (76.67±3.3%), compared to MOCK transfected (57.92±3.3%) or PFN2a knockdown (51.17±5.4%) astrocytes (Figure 3.21; B).

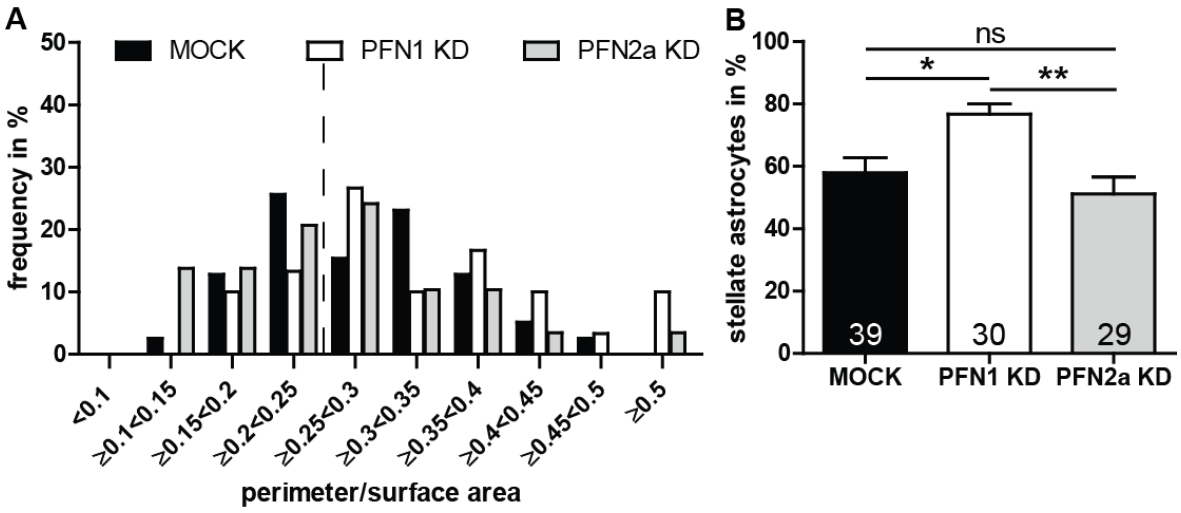

Figure 3.21 | Comparison of the percentage of stellate astrocytes in KT5720 treated cells. (A) Frequency analysis of astrocytes transfected with either pRNAT-siFluc (MOCK, black), pRNAT-1.3 (PFN1 KD, white) or pRNAT-2.13 (PFN2a KD, light grey). Dashed line indicates border between polygonal (left) and stellate (right) cells. (B) The percentage of stellate astrocytes is significantly increased for PFN1 down regulated astrocytes (76.67±3.3%) compared to both other groups (MOCK: 57.92±3.3%; PFN2a KD: 51.17±5.4%). Quantitative data was tested for significance by one-way ANOVA followed by a *post-hoc* Tukey's Multiple Comparison Test. Significance is indicated as follows *p<0.05; **p<0.01; ***p<0.001. Data are shown as mean ± SEM.

Collectively, keeping the balance between both profilin isoforms was found to be essential for regulating astrocytic morphology during PKA inhibition.

3.1.9. Modification of PKA activity changes the localization of profilin isoforms

PFN1 has been shown to localize both in the cytosol and in the nuclei of different mammalian cell types (Mayboroda et al., 1997; Rawe et al., 2006; Skare et al., 2003; Stuven et al., 2003). Also PFN2a has been described to localize not only in the cytosol but also in the nuclei of chicken fibroblasts (Murk et al., 2009) and rodent neurons (Murk et al., 2012). Therefore, dissociated astrocytic cultures were stained with isoform specific antibodies and analyzed the subcellular distribution of both PFN1 (Figure 3.22) and PFN2a (Figure 3.23) in these cells.

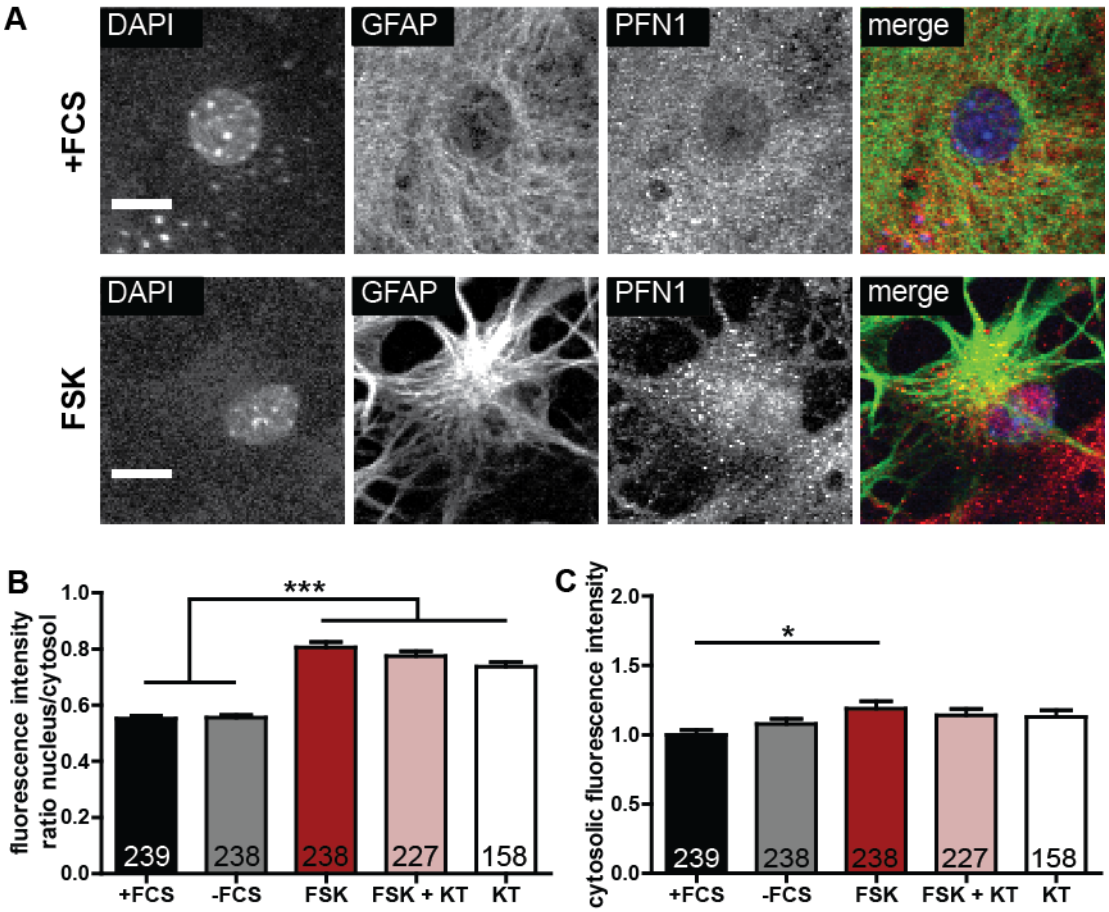

Figure 3.22 | PKA activity influences the localization of PFN1. (A) Control cell (+FCS) and a forskolin treated cell (FSK) stained for PFN1. In addition to the morphological change, the amount of PFN1 in the nucleus of the cell treated with forskolin increases. **(B)** Statistical analysis of the fluorescence intensity ratio between cytosol and nucleus for anti-PFN1. The amount of PFN1 in the astrocytic nucleus is increased by treatment with either forskolin (0.81±0.02) or KT5720 (0.74±0.02) or both (0.771±0.02) compared to controls (+FCS: 0.55±0.01; -FCS: 0.55±0.01). **(C)** Quantification of cytosolic PFN1 intensities dependent on the indicated treatment normalized to serum containing conditions (+FCS: 1.00±0.03). Forskolin treatment (1.19±0.05) leads to a slight but significant increase in cytosolic fluorescence intensity compared to serum containing control. Quantitative data was tested for significance by one-way ANOVA followed by a *post-hoc* Tukey's Multiple Comparison Test. Significance is indicated as follows *p<0.05; **p<0.01; ***p<0.001. Data are shown as mean ± SEM.

At control conditions (Figure 3.22; A; +FCS) PFN1 is predominantly localized to the cytosol, while the nucleus appears to be almost devoid of a fluorescence signal. This apparently changed with the application of forskolin (Figure 3.22; A; FSK), when the PFN1 fluorescence intensity in the nucleus increased. To quantify these observations, the fluorescence intensities in the nucleus as well as in a cytosolic part beneath the nucleus were measured. Subsequently, the ratio between these two intensities was compared between the treatments (Figure 3.22; B). No changes were found comparing the fluorescence intensity ratio of controls with or without FCS. The treatment with either forskolin or KT5720 or the combination of both led to

a highly significant increase of the anti-PFN1 fluorescence intensity in the nuclei. This demonstrates an influence of the steady-state PKA activity on the subcellular localization of PFN1. In addition, a statistical analysis of the cytosolic anti-PFN1 fluorescence intensity was performed to examine a potential influence on the total cellular amount of PFN1 (Figure 3.22; C). Solely the forskolin treated cells exhibit significant increase of cytosolic anti-PFN1 fluorescence intensity by roughly 20% in comparison to control condition. These results hint to a forskolin induced increase in the PFN1 level in astrocytes.

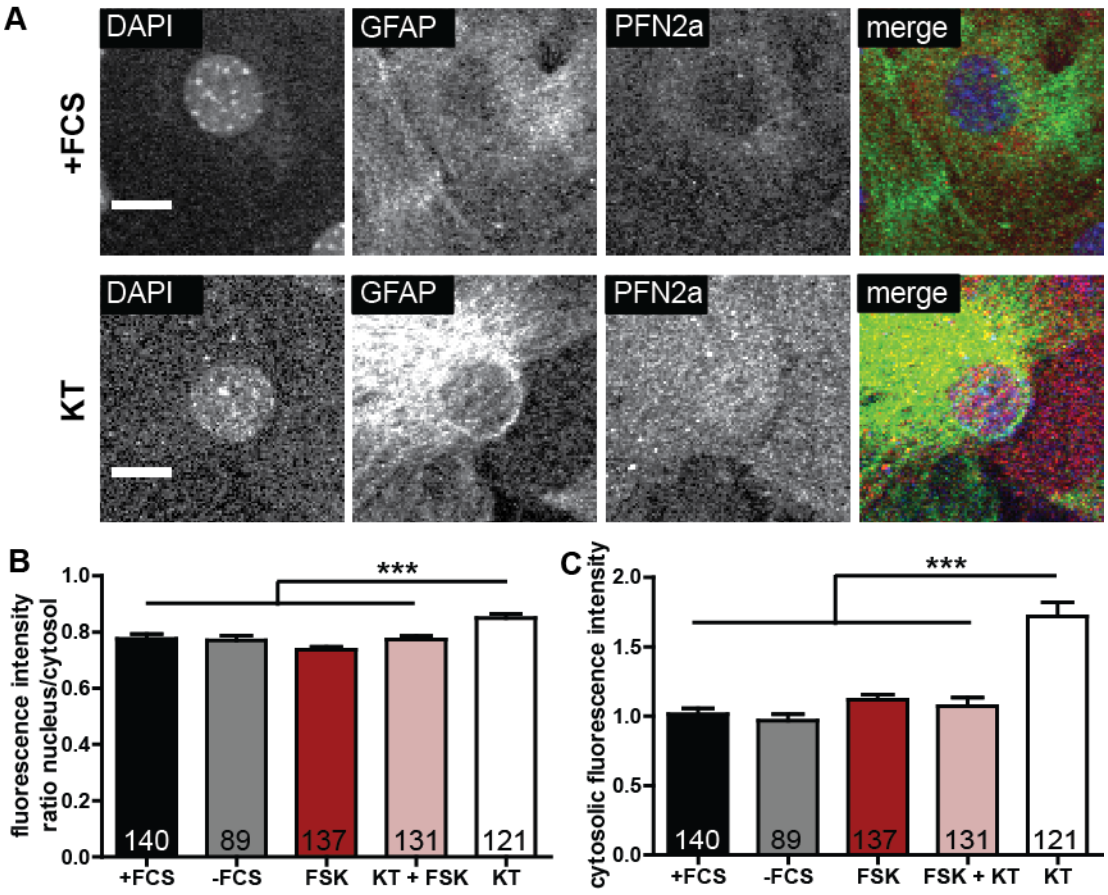

Figure 3.23 | KT5720 treatment influences the localization of PFN2a. (A) Control cell (+FCS) and a KT5720 treated cell (KT) stained for PFN2a. The amount of PFN2a in the nucleus of the astrocyte increased in comparison to control upon KT5720 treatment. **(B)** Quantification of the anti-PFN2a fluorescence intensity ratio between cytosol and nucleus. The ratio of PFN2a in the nucleus compared to cytosol is increased by specific inhibition of PKA (KT: 0.85±0.01; +FCS: 0.78±0.02). **(C)** Statistical analysis of the anti-PFN2a cytosolic fluorescence intensity upon the respective treatment normalized to serum containing conditions (+FCS: 1.00±0.04). PFN2a intensities dramatically increase upon treatment with KT5720 (KT: 1.72±0.10) compared to all other treatments. Quantitative data was tested for significance by one-way ANOVA followed by a *post-hoc* Tukey's Multiple Comparison Test. Significance is indicated as follows *p<0.05; **p<0.01; ***p<0.001. Data are shown as mean ± SEM.

Analogous to PFN1, the localization of PFN2a was investigated in this context. At control conditions (Figure 3.23; A; +FCS), also PFN2a is rather localized in the astrocytic cytosol,

but did not respond accordingly to forskolin treatment in contrast to PFN1. Strikingly, PFN2a specifically translocates to the nucleus upon KT5720 treatment (Figure 3.23; A; +KT). The quantification of the fluorescence intensity ratios exhibits no alterations for serum containing, serum starved, forskolin treated or forskolin and KT5720 treated cells (Figure 3.23; B). Solely treatment with KT5720 led to a highly significant increase in PFN2a fluorescence intensity by roughly 10% in the nuclei compared to all other groups. The analysis of the cytosolic anti-PFN2a fluorescence revealed a drastic increase in intensity by 70% also solely for KT5720 (Figure 3.23; C). These alterations in PFN2a protein level and localization point to an isoform specific effect of PKA inactivation. Consequently, the morphology of KT5720 treated cells was analyzed.

3.1.10. Motility of astrocytic processes depends on profilins

The plasticity of astrocytic processes is essential for an effective neuronal-glial partnership. These highly dynamic processes enwrap the synapse, thereby regulating synaptic function and plasticity (Araque et al., 2014). Basis for this structural plasticity is the dynamic actin cytoskeleton (Haber et al., 2006). Additionally, a functional PFN1 was demonstrated to be important for calcium stimulation induced outgrowth of astrocytic processes (Molotkov et al., 2013). Consequently, the involvement of both profilin isoforms into the motility of astrocytic processes was investigated. To fulfil this task, advantage of a Boyden-chamber based, modified pseudopodia isolation assay (Cho and Klemke, 2002; Thomsen and Lade Nielsen, 2011) was taken (Figure 3.24). After 24 h of incubation, the majority of the cell surface is still localized to the upper side of the Boyden chamber membrane (Figure 3.24; A), but in addition, cell processes are also detectable at the bottom side (Figure 3.24; B). The extension of cellular processes was independent of cell body translocation, as there were no nuclei visible at the bottom side of the membrane (Figure 3.24; B; DAPI). Processes extended throughout the pores of the membrane contained filamentous actin (Figure 3.24; B; Actin), which indicates a motility based on actin dynamics. Quantification of this transwell assay (Figure 3.24; C) reveals a translocation of about 20% of the total cell surface area to the bottom side for controls (MOCK, black). Down regulation of profilin isoforms drastically decreases the percentage of cell area at the bottom side to about 8% for PFN1 (white) and 12% for PFN2a (light grey), respectively.

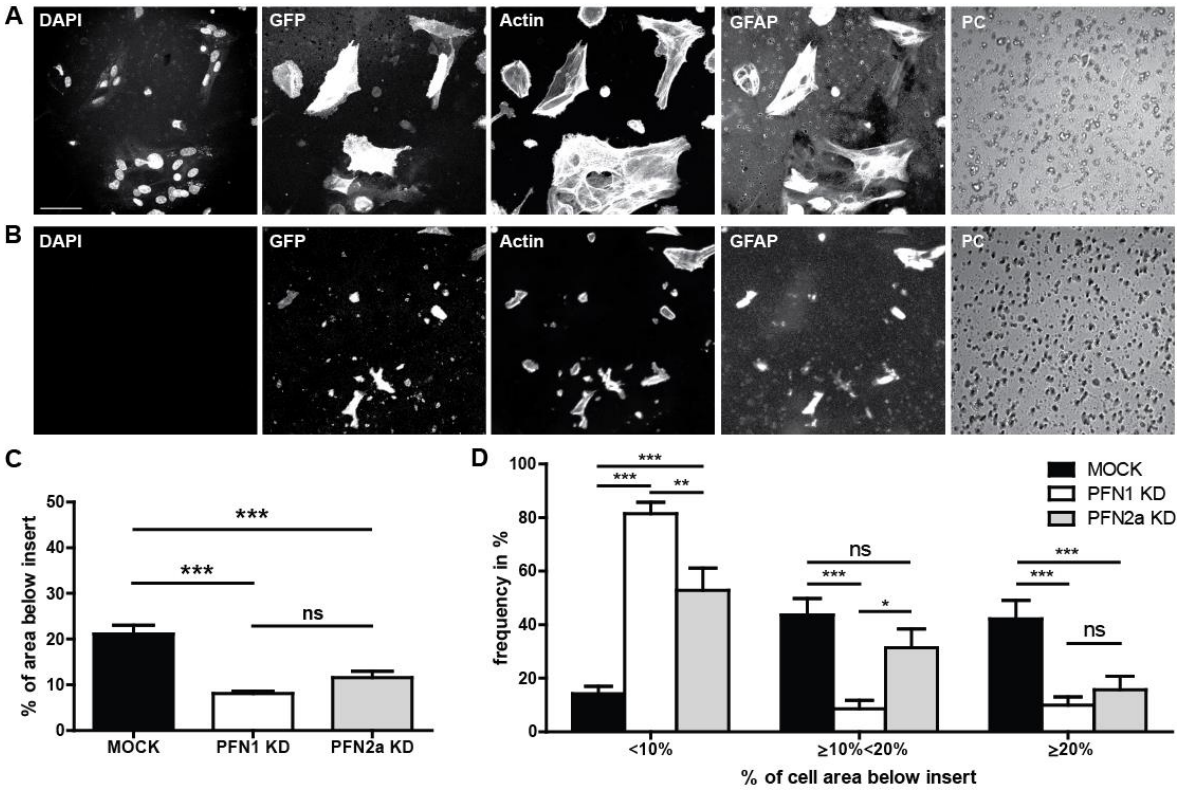

Figure 3.24 | Profilins control the motility of astrocytic processes. The **(A)** upside and **(B)** bottom side of a transwell insert after 24 h of incubation is displayed. Cells were stained for GFAP to identify astrocytes. DAPI positive nuclei are solely visible on the upside of the membrane. Scale bar: 50 µm **(C)** Quantification of GFP and GFAP positive membrane on the bottom side in relation to the upper side. Reduction of either profilin isoform resulted in a significant decrease of GFP positive membrane on the lower surface of the insert. At least, 300 cells were analyzed for each group. **(D)** For a more detailed analysis, results were subdivided into three classes depending on the percentage of the membrane ratio from upper surface to lower surface of the inserts. Samples grouped into the <10% class displayed only a sparse pattern of processes on the bottom side. Significantly more samples with a reduced amount of PFN1 compared to controls and PFN2a knockdown were classified into this group. Quantitative data was tested for significance by either one-way ANOVA or two-way ANOVA (D) followed by a *post-hoc* Tukey's Multiple Comparison Test. Significance is indicated as follows *p<0.05; **p<0.01; ***p<0.001. Data are shown as mean ± SEM.

To illustrate the differences between the effects of the reduction of PFN1 or PFN2a protein levels, the fields of view were classified into groups depending on their portion of membrane at the bottom side (Figure 3.24; D). In about 80% of analyzed fields of view, the knockdown of PFN1 led to an evident reduction (bin “<10%”) of cell area at the bottom side in comparison to PFN2a KD (52.86±8.3%) and MOCK transfected cultures (14.24±2.8%). Contrarily, in about 31% percent of analyzed fields of view, the knockdown of PFN2a only led to a moderate declined cell area on the bottom side (bin “≥10% <20%”), which is significant to PFN1 knockdown cultures (8.57±3.2%) but not significantly altered compared to controls (43.57±6.1%). These findings support a major role of PFN1 in the serum induced motility of astrocytic processes.

3.1.11. Solely PFN1 knockdown impairs actin dynamics in astrocytic processes

To further examine the importance of profilin isoforms to actin cytoskeleton based motility in astrocytic processes, fluorescence recovery after photobleaching (FRAP) experiments were performed. Therefore, dissociated astrocytes were co-transfected with a GFP-ß-actin encoding plasmid and additionally, pRNAT-siFluc, pRNAT-1.3 or pRNAT-2.13, respectively. Time lapse images of GFP-ß-actin expressing astrocytic processes (Figure 3.25; A) bleached at time point zero were taken and subsequently, fluorescence recovery was monitored for a total of 3 min.

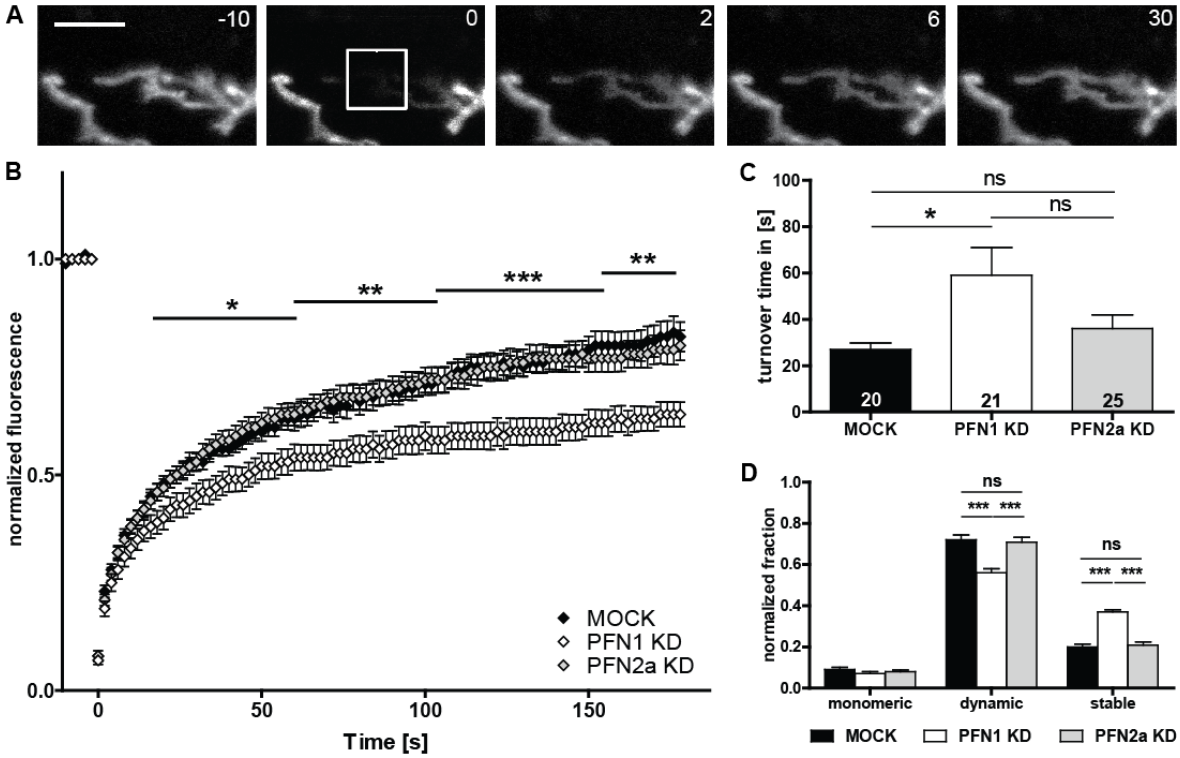

Figure 3.25 | PFN1 knockdown specific impairment of actin dynamics in astrocytic processes. (A) Astrocytes co-expressing GFP-actin and siFluc, shPFN1 or shPFN2a, respectively, were used for FRAP analysis to determine the effect of profilins on actin dynamics in PAPs. GFP-actin fluorescence was bleached from a square of 4x4 µm (rectangular area) containing one or two small astrocytic processes and fluorescence recovery was monitored for 180 s. Scale bar: 5 µm. **(B)** Recovery curve for control, as well as PFN1 and PFN2a knockdown astrocytes. Solely intensity values of cells with a reduced level of PFN1 are significantly lower compared to control. **(C)** Turnover time was accordingly increased in shPFN1 expressing cells compared to controls. **(D)** Analysis of the actin pools reveals, solely for PFN1 knockdown cells, a reduction of the dynamic pool and a corresponding increase of the stable pool. Quantitative data was tested for significance by either one-way ANOVA (C) or two-way ANOVA (A, B) followed by a *post-hoc* Tukey's Multiple Comparison Test. Significance is indicated as follows *p<0.05; **p<0.01; ***p<0.001. Data are shown as mean ± SEM.

Quantification of the fluorescence recovery of control, PFN1 knockdown and PFN2a knockdown astrocytes (Figure 3.25; B) displayed no alterations in the recovery curve of astrocytes with a reduced amount of PFN2a, compared to controls. In contrast, the knockdown of PFN1 resulted in significantly declined values of the fluorescence recovery curve. Furthermore, the actin turnover of PFN1 knockdown astrocytes was significantly decelerated compared to control (Figure 3.25; C). Downregulation of PFN2a, however, did not lead to a significant alteration of the actin turnover rate. These findings suggest PFN1 as a regulator of actin dynamics and thus of structural plasticity of astrocytic processes, whereas PFN2a only plays a subsidiary role in this context. Accordingly, a statistical analysis of respective proportional distribution of actin pool was carried out (Figure 3.25; D). The three pools are defined as (1) the monomeric, which represents the amount of freely diffusible G-actin, (2) the dynamic pool as the one which recovers during observation period and (3) the stable pool which is not replaced during the experiment. Quantification of the actin pools displays a significant reduction of the dynamic pool for PFN1 knockdown astrocytes as well as a corresponding significant increase of the stable pool. Once more, astrocytes lacking PFN2a are indistinguishable from control astrocytes in this analysis. Further characterization of the recovery curves obtained from these FRAP experiments was performed by the classification of recovery curves by their extent of recovery (Figure 3.26).

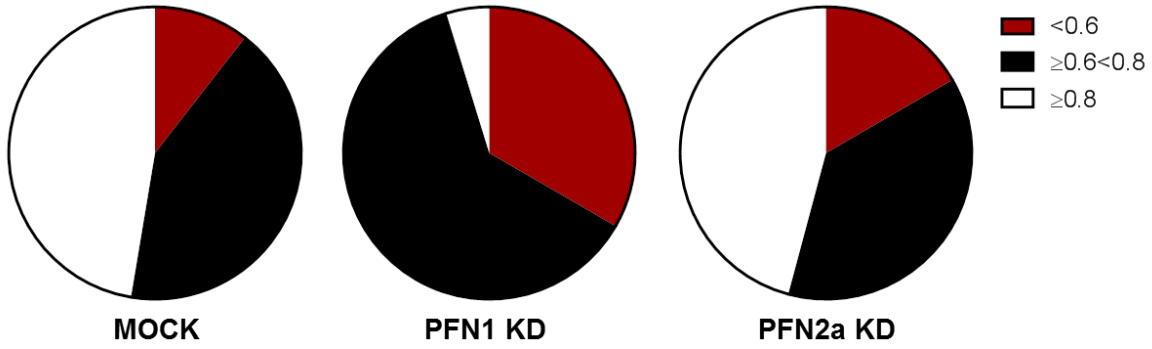

Figure 3.26 | Astrocytic processes binned by their normalized extend of recovery. 47% of MOCK transfected cells, 5% of PFN1 knockdown and 46% of PFN2a knockdown astrocytes regain intensity values equal or higher (unimpaired, white) compared to the mean of control (0.80±0.04). 42%, 62% and 38% of control, PFN1 knockdown and PFN2a knockdown astrocytes exhibit a mildly impaired fluorescence recovery (black), respectively. Evidently impaired recovery extents were found for 11% of control astrocytes, 33% of PFN1 knockdown astrocytes and 17% of PFN2a knockdown astrocytes.

The mean recovery of control astrocytes (0.80±0.04) was used as reference. Processes achieving a recovery extent to about 80% were categorized as unimpaired (‘≥0.8’, white), while a recovery to at least 60% was classified as mildly impaired (‘≥0.6<0.8’, black). Astrocytic processes regaining less than 60% of their initial fluorescence intensity were

categorized as processes with drastically impaired actin dynamics ('<0.6', red). These pie charts illustrate clearly the affected actin dynamic of astrocytes expressing the PFN1 specific shRNA by the heavily impaired fluorescence recovery in astrocytic processes. While 47% of MOCK transfected astrocytes and 46% of PFN2a knockdown astrocytes regain intensity values equal or higher compared to the mean recovery of the control, only 5% of PFN1 knockdown astrocytes display a fluorescence recovery to that amount. Taken together, these findings point to an isoform specific role of PFN1 in regulating actin dynamics in astrocytic processes.

3.1.12. Astrocytic stellation induced by ROCK inactivation relies on PFN2a

In addition to the induction of astrocytic stellation by cAMP rising reagents, the morphology of astrocytes can be modulated via the RhoA dependent pathway (Abe and Misawa, 2003; Koyama et al., 1996; Racchetti et al., 2012; Suidan et al., 1997). Inhibition of RhoA or its kinase ROCK induces stellation in astrocytic cultures, which indicates a constant stimulation of RhoA in cultured astrocytes. In dissociated neurons, ROCK was described to phosphorylate PFN2a and thereby regulate the outgrowth of neurites (Da Silva et al., 2003). Therefore, the functional role of profilins in this context was addressed.

At first, the morphology of astrocytes subjected to a 24 hour treatment with the ROCK inhibitor Y27632 was investigated. Astrocytes underwent an evident stellation, characterized by cytoplasmatic retraction and an increased optical density of the cell body and the main processes (Figure 3.27; A). According to the procedure described above, astrocytic perimeter and surface area were measured and the ratio between both parameters was used to classify the astrocytes as polygonal or stellate (Figure 3.27; B). In contrast to the other morphological studies, all analyzed cells were obtained from one experiment. Consequently, no statistical tests are performed on these data. Nevertheless, ROCK inhibition resulted in an obvious 50% increase in the percentage of stellate cells in the group of control astrocytes. As described earlier, 24 h serum depletion already led to an evident stellation of astrocytes expressing the shRNA specific for PFN1. As a result, the 18% increase in the percentage of stellate astrocytes upon Y27632 treatment is far less apparent in comparison to controls. Astrocytes expressing the shRNA specific for PFN2a, however, display almost no response to the application of Y27632. The percentage of stellate astrocytes was only increased by 5%, which corresponds to no change considering the single experiment contributing to this data. These findings hint at a major role of PFN2a regulating the stellation process upon ROCK inhibition, further supporting the hypothesis of PFN2a as a key target of ROCK mediated phosphorylation (Da Silva et al., 2003).

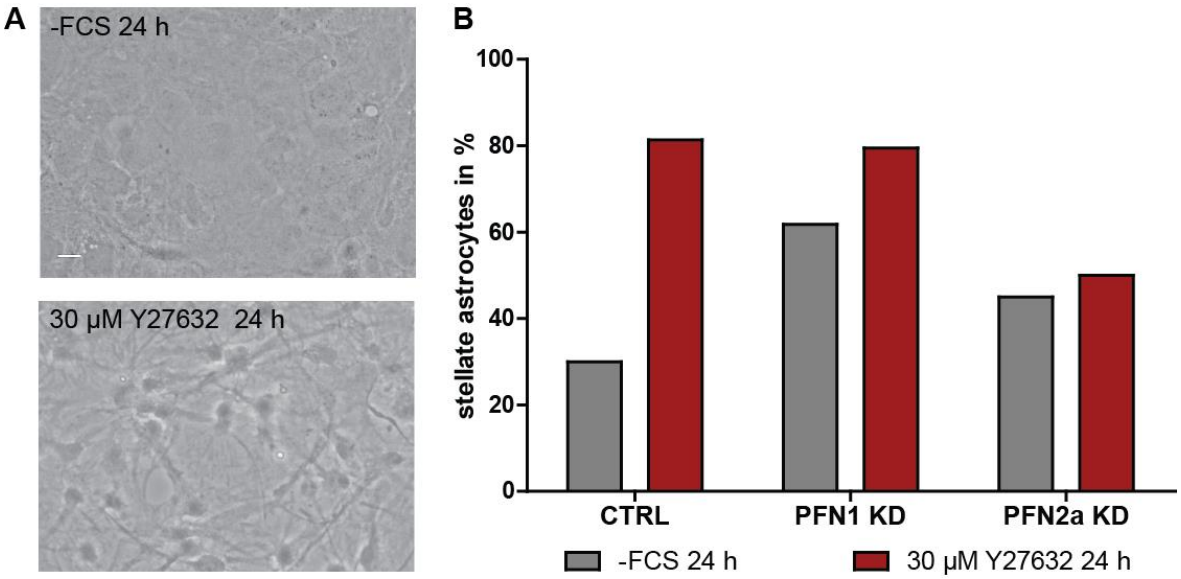

Figure 3.27 | ROCK inhibition induced stellation is modulated by profilin isoforms. (A) Astrocytes either serum starved for 24 h (-FCS 24 h) or treated with 30 µM of the ROCK inhibitor Y27632 (30 µM Y27632 24 h) in serum free medium. Treatment with Y27632 leads to an evident change in astrocytic morphology towards a condensation of processes. Scale bar: 10 µm **(B)** Statistical analysis of one experiment. Astrocytes transfected with pEGFP-f responded to the treatment with a drastic increase in the percentage of stellate astrocytes (30% to 81.4%). Down regulation of PFN1 resulted in an already increased percentage of stellate cells (61.8%) under control conditions. Treatment of PFN1 KD astrocytes with Y27632 slightly increased the percentage of stellate cells by 17.6% (79.44%). Knockdown of PFN2a resulted in a 15% increase of stellate astrocytes under control conditions (45%), but the treatment with Y27632 only lead to additional 5% of stellate cells (50%). Approximately 20 cells were analyzed per group.

As a next step, the expression levels of profilins in astrocytic cultures subjected to Y27632 for 24 hours were analyzed by Western blotting. Cultures kept in serum containing medium served as controls. Protein levels were determined from two independent cultures per experiment (Figure 3.27; A). Statistical analysis of the profilin isoform amounts normalized to the respective GAPDH bands revealed several alterations (Figure 3.28; B). The comparison of PFN1 protein levels in serum starved astrocytic cultures to controls exhibits a significant decrease in PFN1 amount. This result suggests, in line with the morphological data earlier described, a role of PFN1 in the astrocytic response to starvation. ROCK inhibition in turn led to no significant changes of the amount of PFN1. PFN2a protein level displays different results. Here, the amount of PFN2a is not altered upon serum depletion for 24 h, while the cellular protein level is significantly increased by ROCK inhibitor treatment. This evident increase supports an isoform specific cellular function of PFN2a in the ROCK pathway.

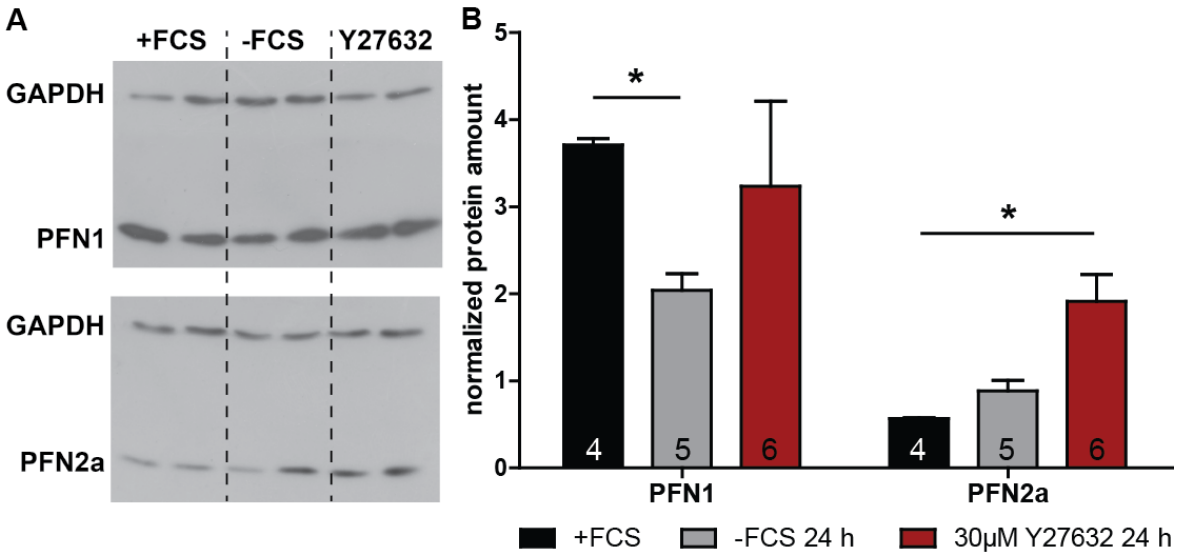

Figure 3.28 | Western Blot analysis of astrocytic cultures revealed changes in profilin levels upon ROCK inhibitor treatment. (A) Example western blots of one experiment. For each experiment, two independent cultures were either kept in DMEM with serum (+FCS), serum deprived for 24 h (-FCS) or treated with 30 µM Y27632 in DMEM (Y27632). Lysates were probed for PFN1 and PFN2a with GAPDH serving as loading control. **(B)** Statistical analysis of PFN1 and PFN2a protein level in astrocytic cultures. The normalized amount of PFN1 was significantly decreased for serum deprived cultures in comparison to controls. While ROCK inhibitor treated cells display a non-significant increase of PFN1. Serum deprivation had no significant effect on the PFN2a level in the cultures, whereas the treatment with Y27632 led to a significant increase in PFN2a level compared to controls. Quantitative data was tested for significance by Student's t-test. Significance is indicated as follows *p<0.05; **p<0.01; ***p<0.001. Data are shown as mean ± SEM.

To elucidate the underlying molecular mechanism, PFN2a phosphorylation status in astrocytes subjected to Y27632 treatment was analyzed. Phosphorylation dependent regulation is generally thought to be a fast process. Consequently, astrocytic cultures were treated for 60 minutes, subsequently harvested, total protein extracts were prepared and analyzed by 2D-gelelctrophoresis and Western blotting (Figure 3.29). Apparently, serum depletion for 60 minutes resulted in a highly variable fraction of phosphorylated PFN2a in astrocytes (Figure 3.29; B), while serum containing control and cultures treated with Y27632 displayed a relatively low variance. Considering experiments carried out on astrocytes starved for 48 hours (Figure 3.12) the slight increase in the fraction of phosphorylated PFN2a is comparable. No changes in the phosphorylation status of PFN2a comparing serum depleted and ROCK inhibitor treated cultures have been found. Interestingly, the comparison of the three individual experiments (3.29; C) reveals two experiments displaying an increase in p-PFN2a upon serum depletion together with a decrease comparing serum starved with Y27632 treated astrocytic cultures. The third experiment displays no alterations between serum containing and serum depleted cultures, but an increase of phosphorylated PFN2a upon Y27632 treatment.

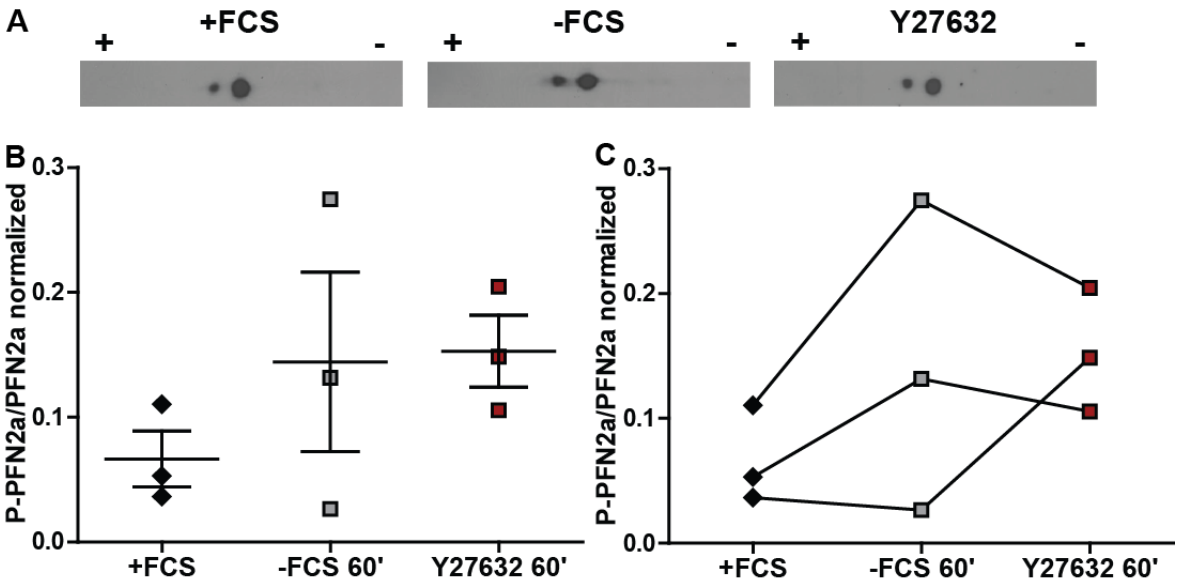

Figure 3.29 | Analysis of ROCK inhibition dependent PFN2a phosphorylation status. (A) Western blot analysis of astrocytic cultures either kept in serum (+FCS), were serum starved for 60' (-FCS) or treated with 30µM ROCK inhibitor Y27632 in serum free media (Y27632) harvested at DIV21. **(B)** Quantification of the phosphorylation status of PFN2a from (A). Dot intensities were measured with Image J. Subsequently, intensity values of all dots were totaled and the intensity of the left dot was divided through the total intensity. +FCS cultures appeared to contain the smallest amount of phosphorylated PFN2a (0.07±0.02). Astrocytic cultures depleted of serum for 60' showed a highly divers ratio (0.14±0.07). Cultures treated with Y27632 for 60' display a slight increase in the amount of phosphorylated PFN2a (0.15±0.03) compared to +FCS cultures. **(C)** Visualization of the three independent experiments. Two experiments show an increase of p-PFN2a by serum depletion. These two experiments also display a decrease comparing the relative p-PFN2a amounts of –FCS and Y27632 treated cultures. The third experiment displays almost no difference between serum containing and serum depleted conditions. Additionally, ROCK inhibition leads to an increase in the relative amount of p-PFN2a. Quantitative data was tested for significance by one-way ANOVA followed by a *post-hoc* Tukey's Multiple Comparison Test. Significance is indicated as follows *p<0.05; **p<0.01; ***p<0.001. Data are shown as mean ± SEM.

Assuming an increase of the p-PFN2a fraction upon serum depletion to be the general response, this third experiment would be an outlier. Overall, serum depletion was emphasized to cause an increase in the p-PFN2a fraction of dissociated astrocytes. Additionally, ROCK inhibitions may cause a reduction in the amount of p-PFN2a.

Since 60 minutes of serum deprivation was shown to be unreliable as a control, again a 24 hour treatment with Y27632 was used to analyze ROCK dependent PFN2a phosphorylation status in dissociated astrocytes (Figure 3.30).

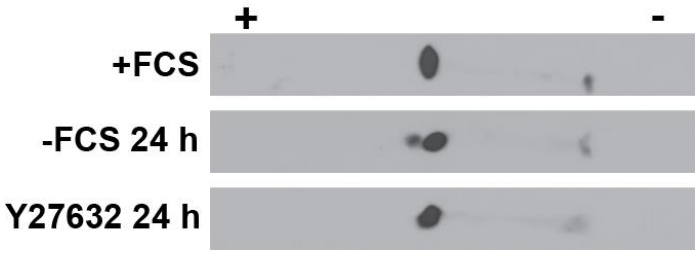

Figure 3.30 | Analysis of ROCK dependent PFN2a phosphorylation status after 24 h of treatment. Serum containing cultures (+FCS) display no phosphorylated PFN2a, while cultures starved for 24 h exhibit a evident fraction of p-PFN2a (-FCS 24 h). ROCK inhibition in serum starved cultures (Y27632 24 h) resulted in a complete disappearance of the p-PFN2a spot.

In this experiment control cultures kept in serum containing medium did not display phosphorylated PFN2a. Serum starvation for 24 hours induced an evident increase in the fraction of phosphorylated PFN2a. Interestingly, the application of Y27632 to serum starved cultures completely abolished PFN2a phosphorylation, inducing a state comparable to normal conditions. These results indicated that the RhoA-ROCK pathway also regulated phosphorylation state of PFN2a.

Conclusively, these data provide new insights into the cellular role of profilin isoforms in astrocytes. Importantly, solely PFN1 was shown to directly alter actin dynamics in astrocytic processes analyzed by FRAP. The induced morphological changes by both serum depletion and forskolin stimulation as well as the induced motility of astrocytic processes and adhesion of astrocytes were heavily reliant on PFN1. In addition, due to the PKA-activity dependent translocation into the nucleus PFN1 may be involved in nuclear functions. While PFN2a modulates astrocytic morphology in both slice cultures and dissociated astrocytes in an isoform specific manner. Furthermore, the cellular fraction of phosphorylated PFN2a increases upon induced changes like application of forskolin and serum starvation. Inhibition of both PKA and ROCK reverses the phosphorylation of PFN2a, indicating PFN2a as part of these two distinct pathways. Cellular motility and adhesion was also found to be reliant on PFN2a, while FRAP analysis revealed that PFN2a does not directly influence actin dynamics in astrocytes. Thus, PFN2a appears to fulfil an isoform specific function in the integration of signals in astrocytes and thereby, indirectly influencing actin dynamics. Alternatively, PFN1 can fully compensate for PFN2a in actin dynamics but not in signaling.

Taken together, these studies demonstrate that PFN1 and PFN2a act as major regulators of astrocytic morphology and function with both overlapping and isoform specific roles.

3.2. The role of cortactin in astrocytes

The protein cortactin was entitled “The grey eminence of the cytoskeleton” (Cosen-Binker and Kapus, 2006) due to the overwhelming amount of cellular processes and functions in which it has been implicated. Great progress has been made in the last years elucidating the role of cortactin in cell migration and cancer (MacGrath and Koleske, 2012) and also, several studies investigate its function in the CNS (Chen and Hsueh, 2012; Decourt et al., 2005; Hering and Sheng, 2003; Iki et al., 2005; Kurklinsky et al., 2011; Racz and Weinberg, 2004). Furthermore, Cortactin is implicated to play an important role in astrocytes, because the direct interaction with Cx43 (Vitale et al., 2009) and the upregulation in astrocytes in response to induced cortical lesion (Decourt et al., 2005) has been demonstrated. Therefore, the following section is dedicated to the analysis of the cellular function of cortactin in astrocytes.

3.2.1. Cortactin deficient astrocytes display a reduced proliferation

To analyze the function of cortactin in astrocytes, dissociated astrocytic cultures of conventional cortactin knockout (*cttn*$^{-/-}$)-mice and their wild type littermates were prepared. As a first step, astrocytic cultures of *cttn*$^{-/-}$ and *cttn*$^{+/+}$ animals were analyzed for basic parameters. Depletion of cortactin had no obvious effect on viability of astrocytes. Also cell adhesion and spreading after replating was unobtrusive. Nevertheless, the density of *cttn*$^{-/-}$ astrocytes appeared to be diminished compared to the respective controls. Therefore, the proliferation of *cttn*$^{-/-}$ astrocytes was analyzed in relation to wild type astrocytes (Figure 3.31).

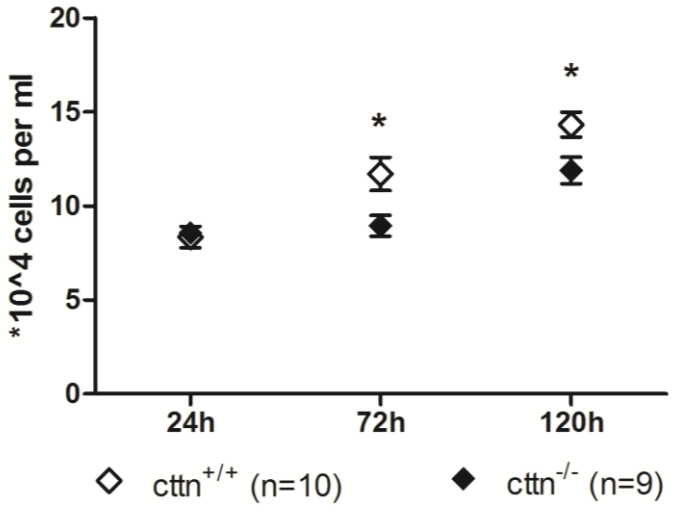

Figure 3.31 | *cttn*$^{-/-}$ astrocytes display a reduced proliferation rate. DIV 10 - 12 astrocytes were counted and replated onto 6 well plates at a density of $1*10^5$ cells per well. Astrocytes were harvested and counted after indicated time points. After 72 h and 120 h the amount of c*ttn*$^{-/-}$ astrocytes was significantly reduced. Quantitative data was tested for significance by an unpaired two-tailed Student’s t-test. Significance is indicated as follows *p<0.05; **p<0.01; ***p<0.001. Data are shown as mean ± SEM.

Statistical analysis of cell proliferation of both genotypes revealed a significantly reduced rate for *cttn*$^{-/-}$ cultures. This reduced proliferation rate indicates an influence of cortactin on

the mitosis of astrocytes. However, astrocytes depleted of cortactin are still proliferating, displayed by the highly significant increase in cell numbers comparing the 24 h time point to the 120 h time point ($8.57\pm0.4*10^4$ cells to $11.89\pm0.7*10^4$ cells). Taking these differences in astrocytes of both genotypes into account, an analysis of the role of cortactin in astrocytic morphology, motility and function was performed.

3.2.2. *Cttn*$^{-/-}$ astrocytes show no significant changes in morphology

Astrocytic cultures of cortactin knock out animals are indistinguishable from wild type cultures. Nonetheless, a quantitative analysis was performed to describe the morphology of *cttn*$^{-/-}$ astrocytes in detail. For these studies cultures of wild type and *cttn*$^{-/-}$ astrocytes were transfected with pmCherry-F. Statistical analysis of transfected astrocytes (Figure 3.32) revealed a slight increase in the percentage of stellate astrocytes in cortactin deficient cultures. In *wild type* cultures, the percentage of stellate cells was found to be 59% and elevated by roughly 10% in *cttn*$^{-/-}$ cultures. These alterations were not significant, but the shift in the frequency distribution was evident (Figure 3.32; A).

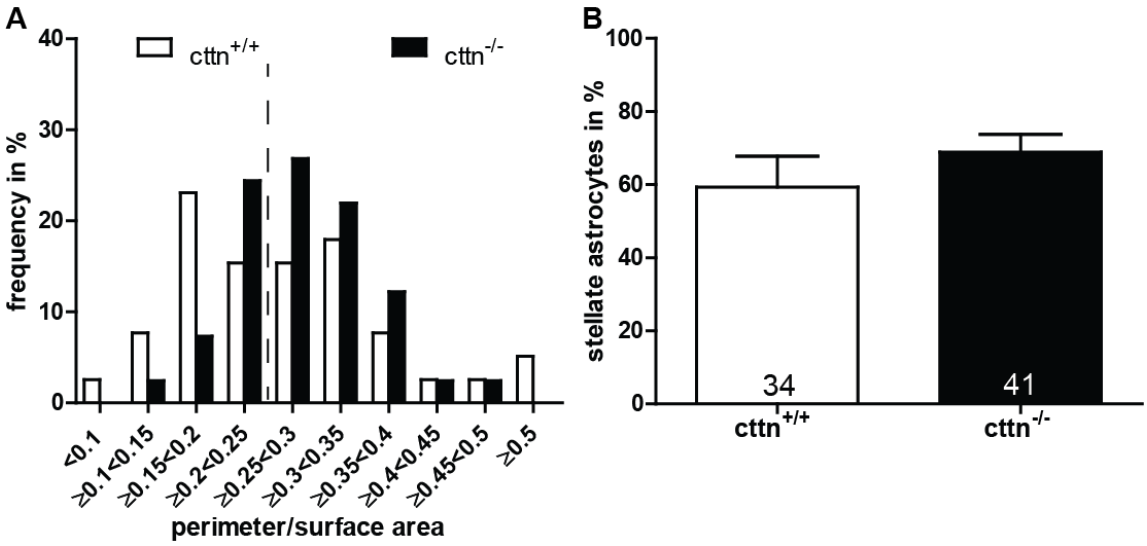

Figure 3.32 | Morphological analysis of *cttn*$^{+/+}$ and *cttn*$^{-/-}$ astrocytes. (A) Frequency analysis of *cttn*$^{+/+}$ and *cttn*$^{-/-}$ astrocytes transfected with pmCherry-F. The frequency distribution displays a slight shift to an elevated perimeter to area ratio for cortactin depleted astrocytes. **(B)** Classification into stellate and polygonal cells reveals a slight increase in the percentage of stellate astrocytes in *cttn*$^{-/-}$ cultures (68.9±4.8%) compared to wild type astrocytes (59.29±8.5%). The dashed line in A indicates the border between polygonal and stellate cells. Quantitative data was tested for significance by an unpaired two-tailed Student's t-test. Significance is indicated as follows *p<0.05; **p<0.01; ***p<0.001. Data are shown as mean ± SEM.

This analysis revealed only a subtle change in astrocytic morphology in *cttn*$^{-/-}$ cultures compared to wild type. Therefore, cortactin plays no essential role in astrocytic stellation under basal conditions. One could suspect a role of cortactin in the modulation of an

induced stellation process, for instance upon CNS damage. But this question has was not addressed in this thesis.

3.2.3. Cortactin influences migration behavior of *cttn*$^{-/-}$ astrocytes

In the mature, healthy CNS, migration of astrocytes most likely only plays a subsidiary role. Nevertheless, CNS lesions induce a massive alteration in astrocytic morphology, the reactive astrogliosis (Sofroniew, 2009) as well as the migration to the site of injury (Buffo et al., 2010; Okada et al., 2006). *In vivo* studies suggested cortactin as a player in the astrocytic reaction to induced brain lesion due to its highly increased expression in astrocytes 2 weeks after mechanical trauma (Decourt et al., 2005). Astrocytic migration is a complex process, which is only partially understood so far. Fibroblasts depleted of cortactin, however, exhibit a decreased directional migration (Lai et al., 2009). Consequently, the potential role of cortactin in the migration of astrocytes was investigated by the use of an *in vitro* scratch induced wound healing assay (Etienne-Manneville, 2006). The typical wound width was about 300 to 400 µm and its closure took from 36 to 48 hours. Astrocytes moved in a unidirectional manner, initially protruding a pronounced, elongated pseudopodium-like structure. Migration of astrocytes was accompanied by remodeling of both microtubules and microfilaments. (Figure 3.33; A). Since the classic *in vitro* scratch induced wound healing assay (Figure 3.33; B) only resulted in an statistically relevant increase in the variance of the *cttn*$^{-/-}$ group (F-Test to compare variances; p=0.0311), it was decided to proof these results by the use of the IBIDI wound healing assay based on cell culture inserts. Here, a standardized gap of 500 µm width between the cells is generated by a cell culture insert. Thereby, astrocytes were not wounded by the initiation of the scratch and no cell debris could influence cell migration. This method resulted in a markedly prolonged time frame for wound closure. Frequently, gaps were still exposed after 48 h. Several gaps took up to 72 h for complete closure. In case of *cttn*$^{-/-}$ astrocytes, 2 gaps did not exhibit any observable closure within 24 h. Statistical analysis (Figure 3.33; C) revealed a non-significant reduction of wound closure rate of about 30% for cortactin depleted astrocytes in comparison to controls. Significance was not achieved due to the high but equal (F-Test to compare variances; p=0.3731) variances within each group.

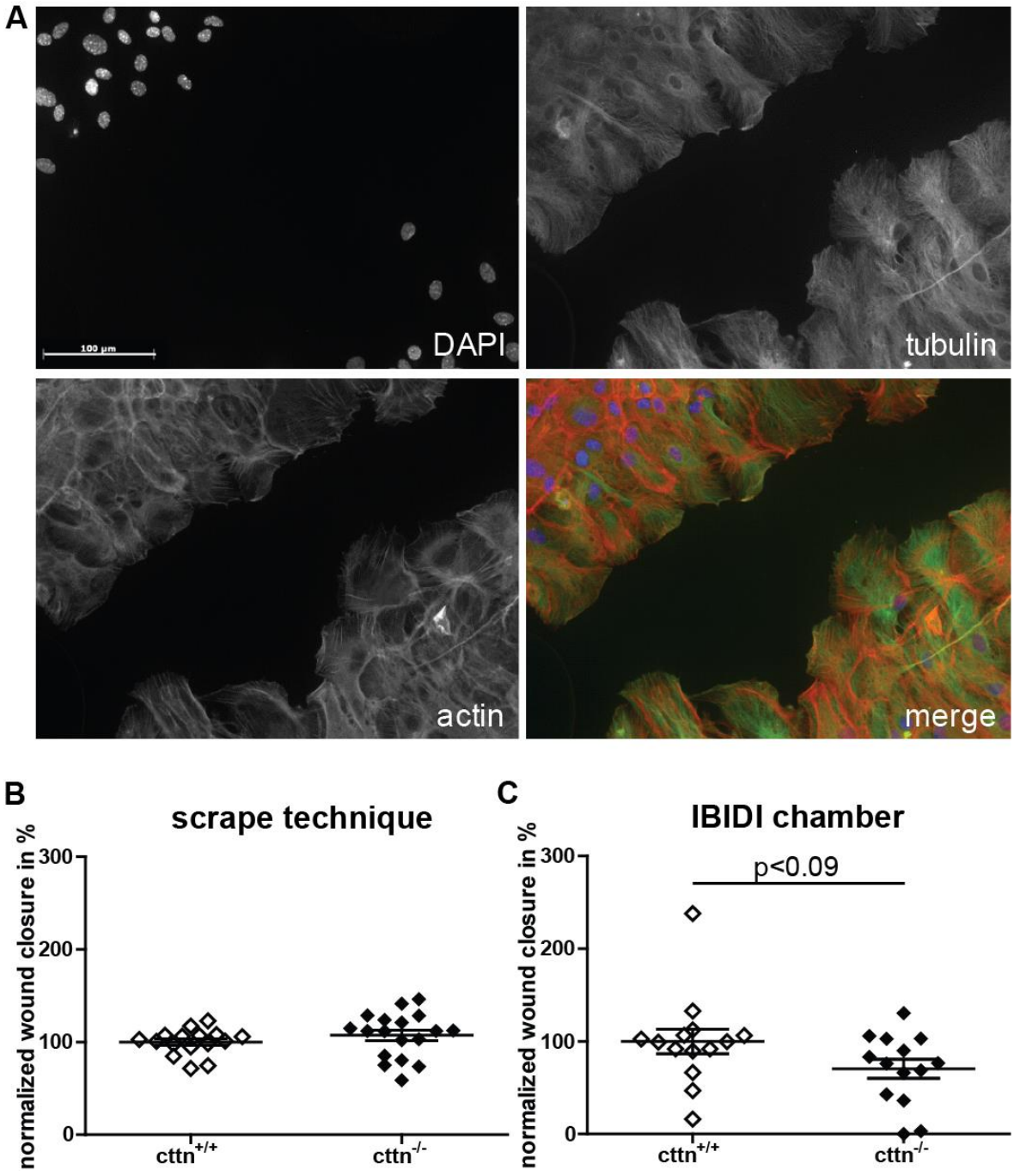

Figure 3.33 | Migration assay of *cttn*$^{-/-}$ and *cttn*$^{+/+}$ astrocytes. (A) Scratch induced migration assay of astrocytes 24 h post scratch wound initiation. Astrocytes underwent polarization accompanied by the reorganization of both microtubules (tubulin) and microfilaments (actin). **(B)** Statistical analysis of scratch induced wound closure 24 h post scraping. The wound was initiated by a scrape with a micropipette tip. Comparison of normalized wound closure rate showed no alterations. **(C)** Statistical analysis of wound closure 24 h post removal of IBIDI inserts. Here, a defined gap between astrocytes was achieved by seeding $2.1*10^4$ cells into each chamber of an IBIDI insert. *cttn*$^{-/-}$ astrocytes displayed a non-significant tendency (70.36±10.2%) of a slower gap closure compared to *cttn*$^{+/+}$ cells. Quantitative data was tested for significance by an unpaired two-tailed Student's t-test. Significance is indicated as follows *p<0.05; **p<0.01; ***p<0.001. Data are shown as mean ± SEM.

These results are in line with the migration phenotype described by Lai and colleagues (2009), and might indicate a role for cortactin in the migration of astrocytes, but leave no hint for either the involvement of the microfilament system or microtubules in this context. Therefore, a further investigation of the role of cortactin in actin dynamics of astrocytes was performed by FRAP.

3.2.4. Actin dynamics are altered in *cttn*$^{-/-}$ astrocytes

The analysis of actin dynamics by the use of fluorescence recovery after photobleaching (FRAP) allows insights into the ability and speed of the microfilament system to exchange actin monomers at sites of interest. Here, the aim was to achieve insights into the relevance of cortactin to actin dynamics in astrocytes. Despite cortactin is not enriched in astrocytic processes (Thomsen and Lade Nielsen, 2011), an initial set of FRAP experiments targeting the PAPs of cortactin knock out and wild type controls was performed. In fact, compared to wild type cells, only a subtle reduction of fluorescence values in cortactin knock out cells was detectable within 3 minutes (Figure 3.34).

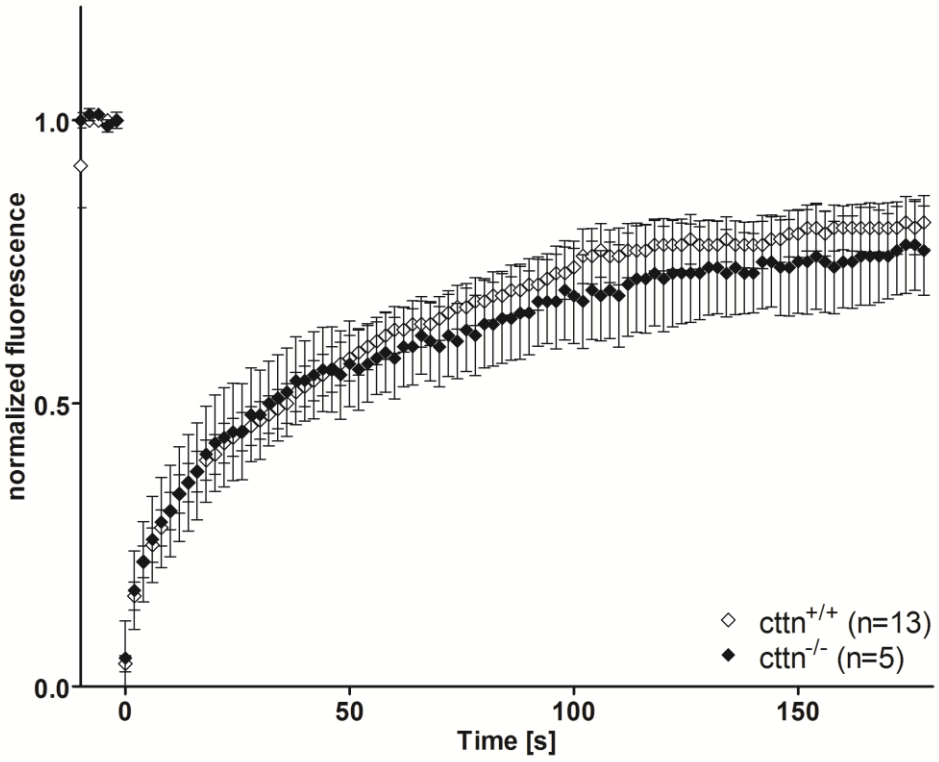

Figure 3.34 | FRAP analysis of small processes of *cttn*$^{-/-}$ and *cttn*$^{+/+}$ astrocytes. Recovery curves of both genotypes display subtle differences. Specifically, *cttn*$^{+/+}$ astrocytes attained an intensity value of 0.82±0.05 while *cttn*$^{-/-}$ astrocytes reached 0.77±0.08.

These findings promote a prolonged monitoring of fluorescence recovery in larger structures, where the localization of cortactin is unquestionable. Consequently, subsequent FRAP experiments were performed on a larger cell surface area localized to the cell cortex for a prolonged time period (Figure 3.35).

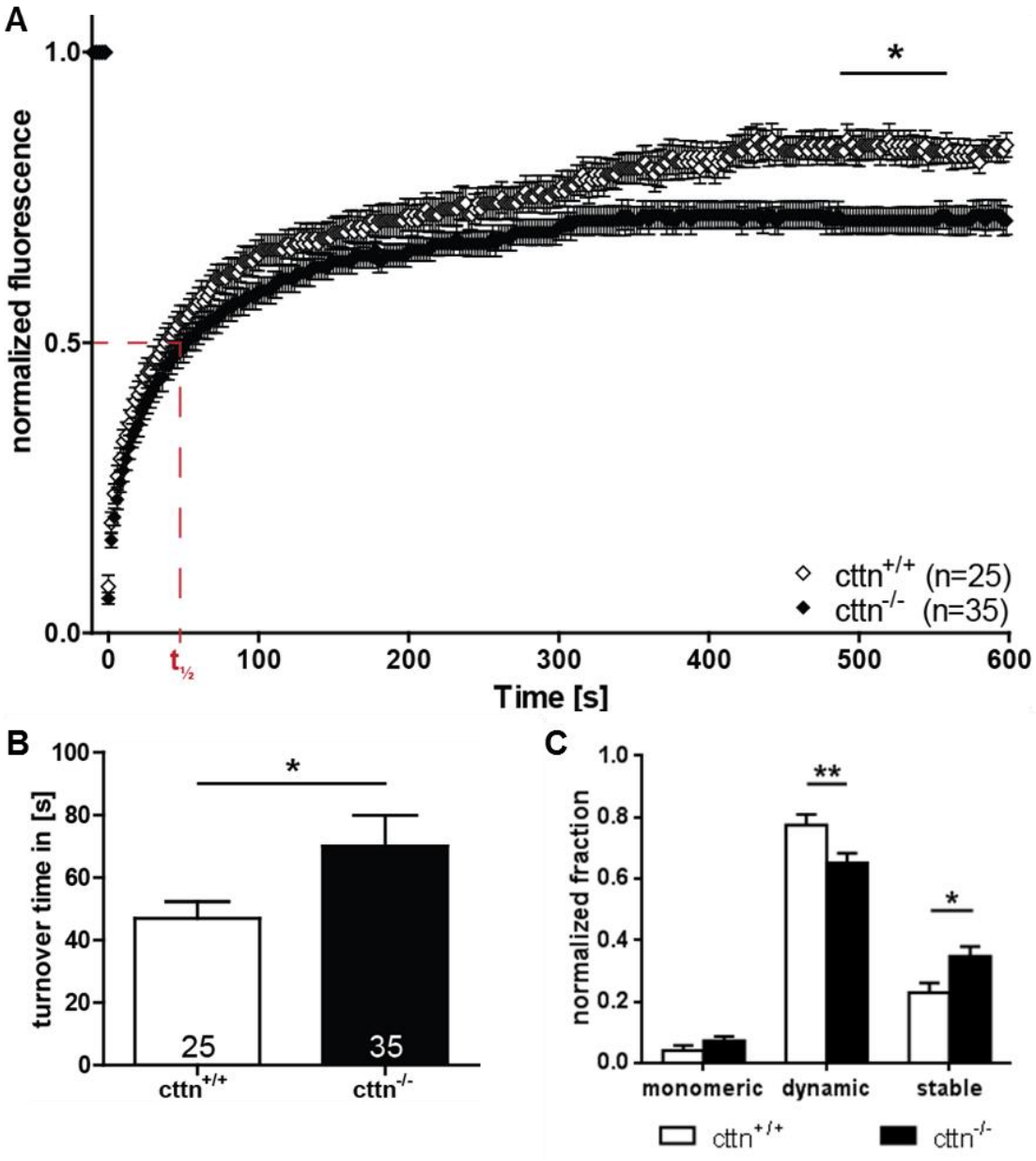

Figure 3.35 | Fluorescence recovery after photobleaching is reduced upon cttn deletion. (A) Recovery curve for a large (12 µm x 12 µm) area located at the cell cortex. Intensity values are decreased for cortactin deficient astrocytes. **(B)** Turnover time of cttn-/- astrocytes is increased (70.06±9.8 s) compared to cttn+/+ (46.96±5.3 s) **(C)** Analysis of actin pools reveals a decrease in the dynamic and a corresponding increase in the stable pool for cortactin depleted cells compared to control. Quantitative data was tested for significance by an unpaired two-tailed Student's t-test. Significance is indicated as follows *p<0.05; **p<0.01; ***p<0.001. Data are shown as mean ± SEM.

Here, fluorescence recovery was monitored for 10 minutes. The fluorescence recovery curve (Figure 3.35; A) shows reduced values for cortactin knockout cells for its whole progression, but the difference is only significant in the range from 488 s to 560 s. This indicates a minor role of cortactin for actin dynamics in astrocytes. Nevertheless, the determination of the turnover time reveals significant changes between wild type and cortactin astrocytes (Figure 3.35; B). Specifically, the turnover time was increased from 46.96±5.3 s for *cttn*$^{+/+}$ to 70.06±9.8 s for *cttn*$^{-/-}$ astrocytes. Also, the variances in both groups differed significantly (F test to compare variances: p=0.0001), which indicates an inhomogeneous population of cortactin knockout astrocytes. These unequal populations consistently force the usage of a Welch's correction in the t-test (p=0.0442). Calculation of the actin pools at the last time point (Figure 3.35; C) exhibits no significant changes for the monomeric pool (*cttn*$^{+/+}$: 0.040±0.017; *cttn*$^{-/-}$: 0.073±0.014). However, a significant decrease in the dynamic pool (*cttn*$^{+/+}$: 0.775±0.035; *cttn*$^{-/-}$: 0.652±0.031) and a corresponding increase in the stable pool (*cttn*$^{+/+}$: 0.229±0.032; *cttn*$^{-/-}$: 0.348±0.031) for cortactin knockout astrocytes in comparison to wild type astrocytes were found. These results suggest cortactin as promoter of actin dynamics in astrocytes. To illustrate the alterations in distribution of the recovery extent between wild type and cortactin knockout astrocytes, cells were binned by their maximum recovery after 10 min (Figure 3.36).

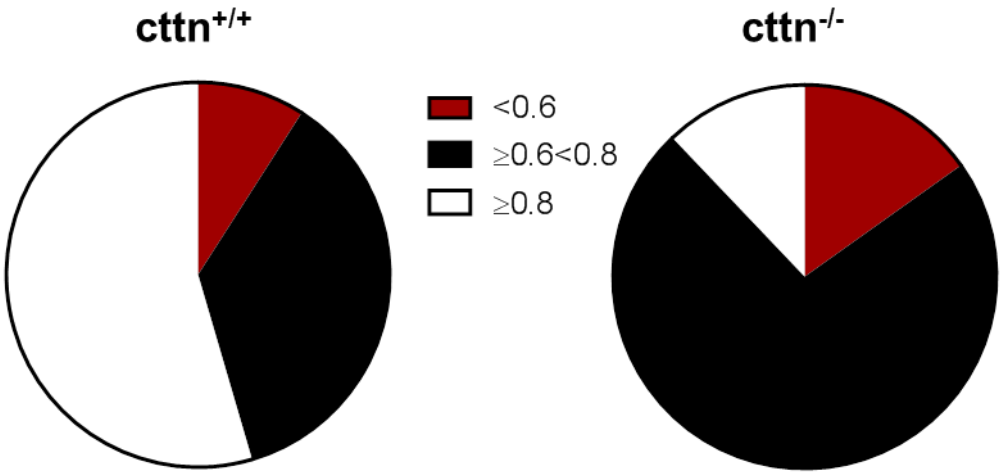

Figure 3.36 | Average fraction of cells binned by normalized extent of recovery from <0.60 to >0.80. 88% of cttn-/- cells show a reduced recovery compared to the mean of cttn+/+ cells (0.80 ± 0.03). Analysis of the actin pools reveals, solely for PFN1 knockdown cells, a decrease in the dynamic and a corresponding increase in the stable pool.

The resulting pie charts display about 67% of recovery curves of the wild type to attain a total recovery of 0.8 or more, whereas only about 21% of cortactin knockout astrocytes were classified into this group. Most recovery curves (63%) of *cttn*$^{-/-}$ astrocytes were classified as marginally impaired (bin '≥0.6<0.8'), but only 27% of wild type recovery curves match this category. Additionally, the amount of curves which were clearly reduced in their extent of recovery (bin '<0.6') are increased for *cttn*$^{-/-}$ astrocytes (16%) in comparison to *cttn*$^{+/+}$ astrocytes (7%). In total, 88% of *cttn*$^{-/-}$ astrocytes show a fluorescence recovery to a diminished extent, while only 33% of *cttn*$^{+/+}$ astrocytes do. These findings underline the importance of cortactin in actin dynamics.

3.2.5. Cortactin in connexin43 mediated signaling

Cortactin is not only described as actin binding protein, but it also interacts with a plethora of proteins in different cell compartments and thereby is involved in various processes (Ammer and Weed, 2008; Cosen-Binker and Kapus, 2006). Recently, cortactin was found to interact directly with connexin43 (Cx43; (Vitale et al., 2009)), the major connexin isoform in mature astrocytes (Orthmann-Murphy et al., 2008). Furthermore, in cultures the glial interconnectivity depends on the presence of filamentous actin (Cotrina et al., 1998). Consequently, it was of interest, if and how cortactin interacts with Cx43 to regulate actin dependent astrocytic interconnectivity.

Both *cttn*$^{-/-}$ and *cttn*$^{+/+}$ astrocytes express connexin43

To analyze the interplay between cortactin and Cx43 in the context of astrocytic interconnectivity, at first the expression of the connexin in dissociated glial cultures was examined. The protein level of connexin43 increased during cultivation period (Figure 3.37, A). While DIV14 dissociated astrocytes only show two slight bands for Cx43 with a more intense staining of the lower band, DIV21 astrocytes depict two much stronger and equally distributed bands in the Western blot. This, together with an increased cell density during this cultivation period, suggests an enhanced interconnectivity between astrocytes of a later cultivation stage. The increased amount of Cx43 could be the consequence arising from a higher cell density.

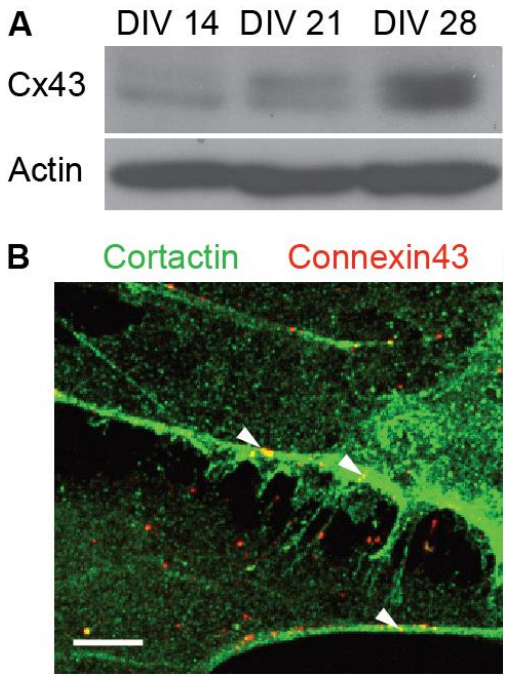

Figure 3.37 | In cultured astrocytes, Cx43 puncta are colocalized with cortactin. (A) Western Blot analysis of the expression of connexin43. Cells were harvested after 14, 21 or 28 days in culture. The amount of Cx43 increases during the cultivation period. Actin served as gel loading control. **(B)** Confocal analysis of the localization of cortactin (green) and Cx43 (red) in astrocytes revealed a partial colocalization of Cx43 puncta with intensive cortactin staining (yellow; arrowheads) in dissociated astrocytes. Scale bar: 10 µm

As a next step, analysis of the subcellular localization of cortactin and Cx43 in relation to each other was performed. Immunostaining of both proteins revealed a partial colocalization mainly at the cell cortex of astrocytes. This partial colocalization hints towards a temporally limited interaction of cortactin and Cx43 at the astrocytic cortex. Consequently, potential consequences for the amount or the distribution of Cx43 in cortactin knock out astrocytic cultures were examined. The loss of cortactin may cause alterations in the stability of Cx43, resulting in a reduced overall amount. Alterations in the subcellular localization could hint to an involvement of cortactin in the transport or the anchoring of Cx43. Western Blot analysis of cell lysates of *cttn*$^{-/-}$ primary astrocytic cultures exhibited highly diverse amounts of Cx43. Consequently, an analysis of Cx43 positive puncta in both *cttn*$^{+/+}$ and *cttn*$^{-/-}$ cultures was performed. The total number of Cx43 puncta was slightly reduced in *cttn*$^{-/-}$ astrocytes compared to wild type controls (Figure 3.38). Additionally, *cttn*$^{-/-}$ cultures were transduced with a lentivirus re-introducing cortactin cDNA into the cells. Also for these cultures, the amount and the size of Cx43 puncta was determined. Cx43 positive plaque size was unaltered between both genotypes (data not shown). The statistical analysis revealed an almost significant increase in Cx43 puncta in comparison to untreated *cttn*$^{-/-}$ astrocytes. Comparison between transduced *cttn*$^{-/-}$ and wild type astrocytes revealed no statistical relevant alterations, but a slight increase of the amount of Cx43 puncta for the former. These results may suggest a cortactin level dependence of Cx43 puncta or at least a positive correlation between cortactin and Cx43 level.

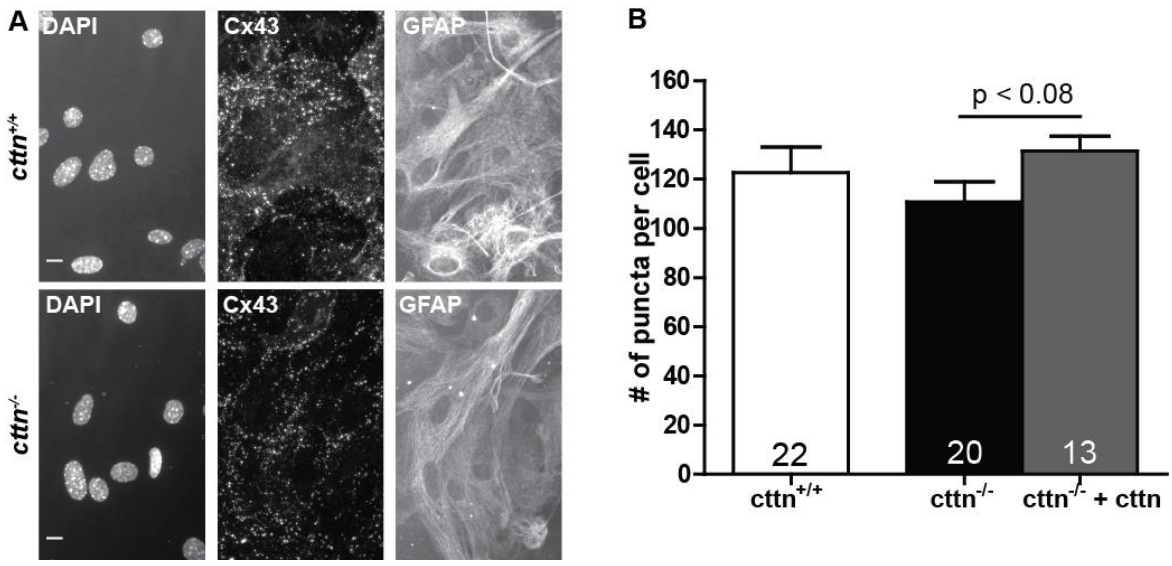

Figure 3.38 | Statistical analysis of Cx43 puncta in dissociated astrocytes. (A) *cttn*$^{+/+}$ and *cttn*$^{-/-}$ astrocytic cultures immunostained for Cx43 and GFAP. Scale bar: 10 µm **(B)** Quantification of (A). Cortactin knockout cells show a tendency towards a reduced amount of Cx43 puncta (110.7±8.1) compared to wild type (122.7±10.4) and *cttn*$^{-/-}$ astrocytes transduced with a cortactin encoding lentivirus (131.3±6.1). Quantitative data was tested for significance by one-way ANOVA followed by a *post-hoc* Tukey's Multiple Comparison Test. Significance is indicated as follows *p<0.05; **p<0.01; ***p<0.001. Data are shown as mean ± SEM.

Nevertheless, as the potential temporally restricted colocalization suggests, the influence of cortactin on Cx43 mediated intercellular signaling could mainly be of a functional nature. Therefore, an analysis of the functional properties of intercellular gap junctions by calcium imaging was performed.

Intercellular calcium waves are impaired upon depletion of cortactin

Intercellular calcium waves have been shown to rely on the microfilament system (Cotrina et al., 1998). The same study also describes Cx43 positive puncta in the plasma membranes to remain unaffected by the treatment with cytochalasin D. These findings hint towards an indirect interaction between Cx43 and actin filaments. Consequently, the question arises, if cortactin may be involved in the interplay of actin and Cx43 in the formation of intercellular calcium waves. To address this question, the properties of mechanically induced intercellular calcium waves in *cttn*$^{+/+}$ and *cttn*$^{-/-}$ astrocytic cultures were compared. Calcium waves always spread from the point of initiation (Figure 3.39). In the first 15 to 20 s after mechanical stimulation, the wave appeared to be very compact (“primary calcium wave”). Afterwards the waves decay, but the unidirectional movement of the residual partial waves persists. This very reliable phenomenon was used to analyze the influence of cortactin on intercellular communication in astrocytes.

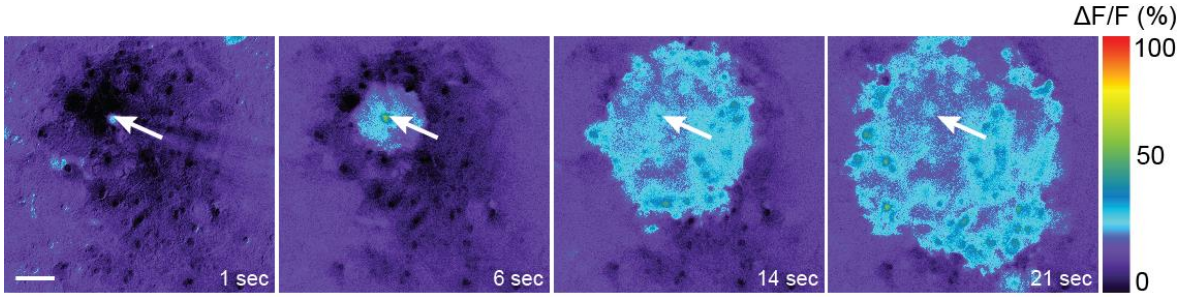

Figure 3.39 | Example of a mechanically induced calcium wave. After mechanical stimulation with a patch pipette tip (white arrow), the calcium signal increase is slowly protruding from cell to cell. Scale bar: 100 µm.

Initially, the size of the respective calcium waves was determined (Figure 3.40). Calcium waves induced in wild type cultures included roughly 60% of the cells in the field of view, whereas in cortactin knockout cultures, the amount of cells involved was found to be significantly reduced to about 49% (Figure 3.40; A). Additionally, the area covered by the calcium wave was significantly decreased for *cttn*$^{-/-}$ cultures (Figure 3.40; B). In detail, calcium waves induced in wild type cultures covered a mean area of 0.216±0.010 mm², which was reduced to 0.164±0.012 mm² in knock out cultures. Generally, a high variation in the sizes of the respective calcium waves was observed. As a further readout, the velocity of the respective calcium waves was investigated.

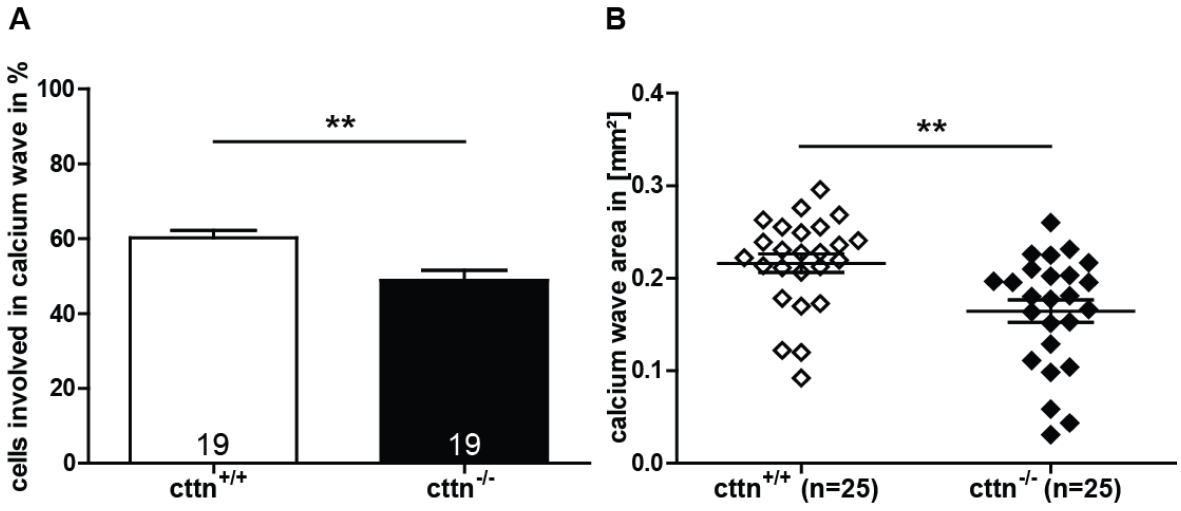

Figure 3.40 | Mechanically induced intercellular calcium waves are smaller in *cttn*$^{-/-}$ astrocytic cultures. (A) The percentage of cells in the field of view included into the respective calcium wave was counted and compared to the total amount of cells. This calculation resulted with 60.24±1.9% for *cttn*$^{+/+}$ and 48.87±2.7 for *cttn*$^{-/-}$ astrocytic cultures in a significant alteration. **(B)** Quantification of the area covered by the primary calcium wave. Cortactin depletion leads to a significant reduction of the covered area from 0.216±0.010 mm² for wild type to 0.164±0.012 mm² for cortactin knockout. Quantitative data was tested for significance by an unpaired two-tailed Student's t-test. Significance is indicated as follows *p<0.05; **p<0.01; ***p<0.001. Data are shown as mean ± SEM.

The velocities were compared between calcium waves induced in *cttn*$^{-/-}$ and *cttn*$^{+/+}$ astrocytic cultures (Figure 3.41). In these experiments, a rescue as well as a gain-of-function approach taking advantage of lentiviral gene delivery was additionally used.

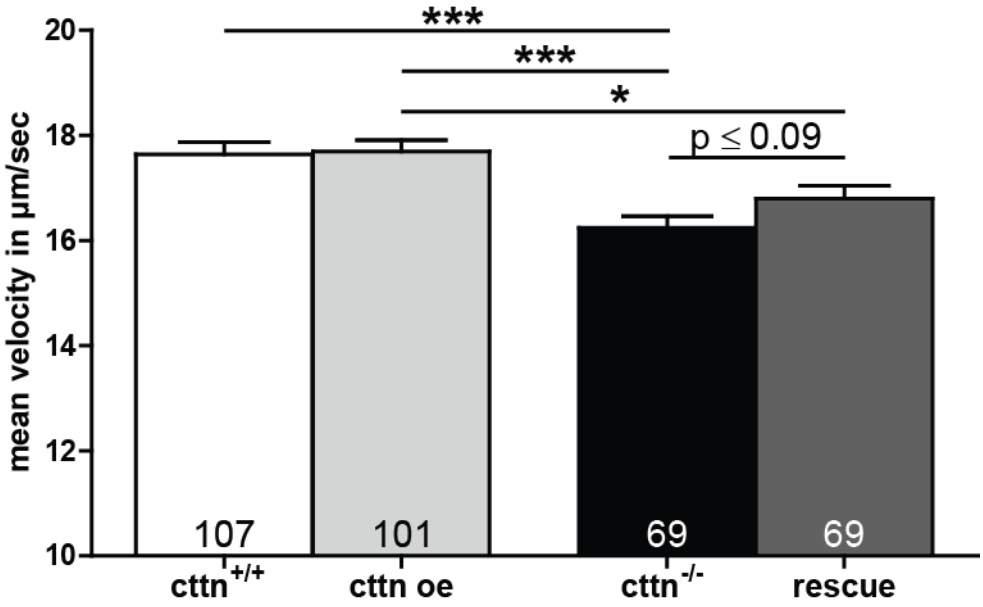

Figure 3.41 | Calcium wave velocity. Astrocytic cultures of both *cttn*$^{+/+}$ and *cttn*$^{-/-}$ animals were analyzed for the velocity of their calcium waves. Additionally, a recombinant cortactin was introduced into the cultures by a lentivirus (cttn oe and rescue). The velocity of calcium waves in *cttn*$^{-/-}$ cultures (16.24±0.22 µm/sec) was highly significantly reduced compared to *cttn*$^{+/+}$ cultures (17.64±0.23 µm/sec). Cortactin over expression in wild type cultures (17.70±0.21 µm/sec) lead to no changes compared to untreated wild type cultures. But in contrast to non-transduced *cttn*$^{+/+}$ cultures, cortactin over expressing cultures showed a significantly higher velocity than virus transduced *cttn*$^{-/-}$ cultures ("rescue": 16.80±0.24 µm/sec). A slight, non-significant increase of velocity from non-transduced to cortactin expressing *cttn*$^{-/-}$ cultures was observed. Quantitative data was tested for significance by one-way ANOVA followed by a *post-hoc* Tukey's Multiple Comparison Test. Significance is indicated as follows *p<0.05; **p<0.01; ***p<0.001. Data are shown as mean ± SEM.

Wild type cultures exhibit a calcium wave velocity of 17.64±0.23 µm/sec, which is indistinguishable from wild type cultures with an over expression of cortactin (17.70±0.21 µm/sec). This uniformity indicates that the overexpression of cortactin has no effect on calcium wave propagation, which is therefore not directly dependent on the protein level of cortactin. Nevertheless, knock out cultures (16.24±0.22 µm/sec) exhibit a significantly decreased velocity of induced calcium waves compared to wild type cultures. Expression of exogenous cortactin in knock out cultures reduces the difference in calcium wave velocity between wild type and knock out cultures to a non-significant tendency. Nevertheless, the increase of calcium wave velocity caused by the re-introduction of cortactin (16.80±0.24 µm/sec) was not sufficient for a significant rescue compared to untreated knock out cultures (p=0.09). These findings rather suggest a role of cortactin in

the development of intercellular communication in cultured astrocytes than a direct effect on the calcium wave propagation. Still, the partial rescue achieved by re-introduction of cortactin into knock out cultures hints towards a direct dependency of the monitored calcium waves on cortactin. Potentially, the time point of the administration of the lentivirus was too late during the cultivation period or the transduction rate was too low to achieve a significant effect.

Suramin treatment drastically inhibits calcium waves

Two distinct pathways, on the one hand the gap junctional one and on the other hand the paracrine one were described to act in parallel to spread intercellular calcium waves (Scemes and Giaume, 2006). Therefore, it was necessary to exclude a potential connection of the cortactin dependent phenotype to non-contacting, Cx43 independent calcium signaling. The P2-receptor antagonist suramin was used to abolish paracrine spreading of the induced calcium wave during these experiments. In wild type cultures the application of the drug leads to a very obvious effect in the calcium wave propagation. Specifically, the size and the velocity of the resulting calcium waves were reduced. For these experiments, first calcium waves were induced under control conditions and afterwards in the same culture in the presence of suramin, thereby excluding any effects by culture diversity. To ensure the stability of the calcium wave response over the whole experimental time frame, a wash out of suramin was performed. Removal of suramin restored the size and speed of the induced calcium wave (data not shown).

The reduction in calcium wave size is both evident in the percentage of cells involved in the respective calcium waves (Figure 3.42; A; control: 40.41±2.5%; 100 µM suramin: 14.64±1.5%) as well as in the area (Figure 3.42; B), which is covered by the wave. In these experiments, the area covered by the primary calcium wave was determined as 0.193±0.010 mm^2, while in the presence of suramin, the area was reduced to 0.075±0.054 mm^2. The strong effect of suramin treatment in wild type cultures indicates a striking dependency of the calcium wave propagation on purinergic signaling.

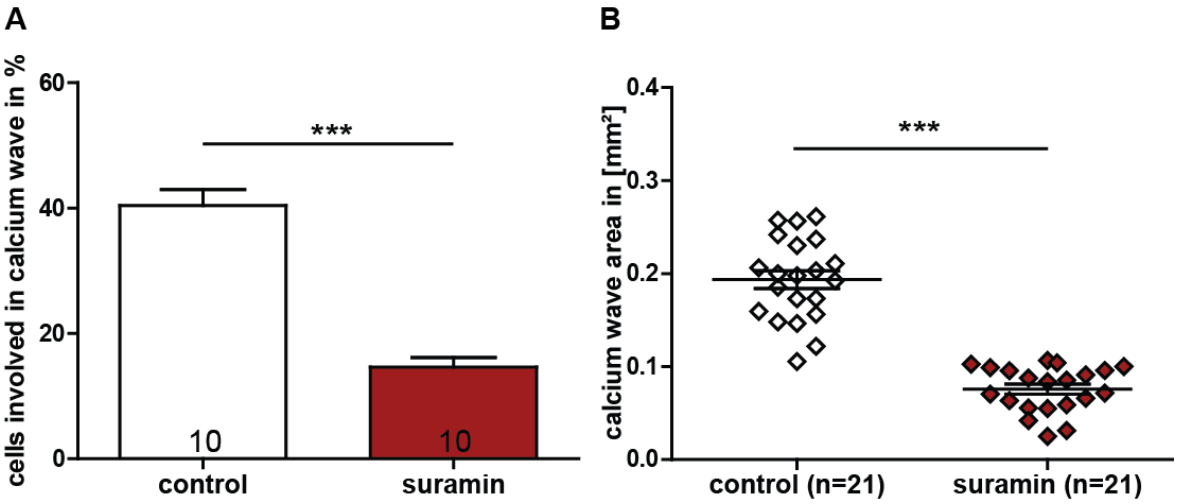

Figure 3.42 | Calcium wave size is reduced by the application of suramin. (A) The percentage of cells in the field of view included into the respective calcium wave was counted and compared to the total amount of cells. This calculation resulted with 40.41±2.5% for control and 14.64±1.5 for suramin treated astrocytic cultures in a significant alteration. **(B)** Quantification of the area covered by the primary calcium wave. Suramin treatment leads to a significant reduction of the covered area from 0.193±0.010 mm² for control to 0.075±0.054 mm² suramin treated cultures. Quantitative data was tested for significance by one-way ANOVA followed by a *post-hoc* Tukey's Multiple Comparison Test. Significance is indicated as follows *p<0.05; **p<0.01; ***p<0.001. Data are shown as mean ± SEM.

After the characterization of the effect of suramin application on the size of calcium waves under these experimental conditions, the velocity of waves induced in *cttn*$^{+/+}$ and *cttn*$^{-/-}$ astrocytic cultures was compared.

Cortactin influences gap junctional communication of astrocytes

To investigate, if cortactin influences the spreading of induced calcium waves via the gap junctions, velocity was determined in the presence of suramin (Figure 3.43). Mechanically induced calcium waves recorded under control conditions (Figure 3.43; A; white) revealed a mean velocity of 19.2±0.7 µm/sec for wild type cultures and 16.9±0.8 µm/sec for cortactin knock out cultures. This reduction was significant and even more drastic compared to the data shown in Figure 3.41. The administration of suramin to wild type cultures resulted in a decrease of calcium wave velocity by about 25% compared to control velocity (14.9±0.6 µm/sec). In suramin treated knock out cultures the mean calcium wave velocity was also reduced by about 25% compared to control levels (12.9±0.5 µm/sec). In the presence of suramin, the statistically relevant reduction of calcium wave velocity for *cttn*$^{-/-}$ cultures in comparison to *cttn*$^{+/+}$ cultures was persistent (red line and asterisk). Comparison of the relative reduction in calcium wave velocity by the application of suramin to cultures of both genotypes illustrates this almost identical reduction to 75% (figure 3.43; B).

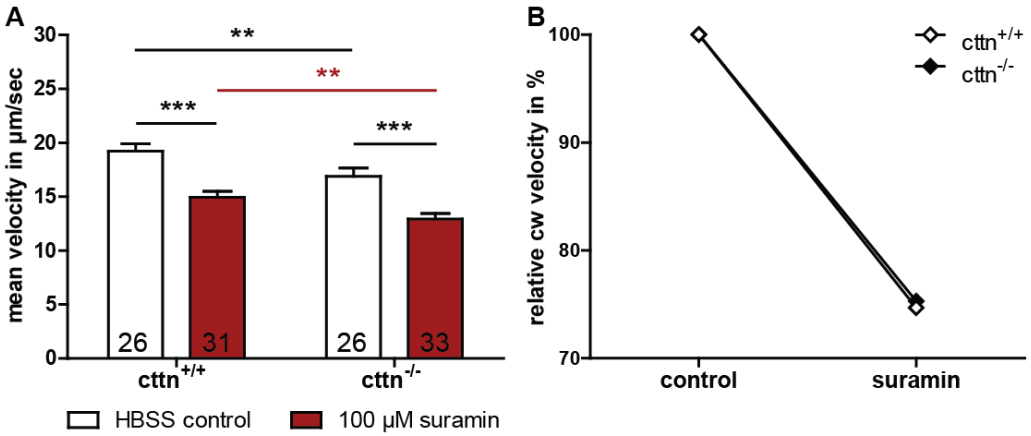

Figure 3.43 | Reduction of calcium wave velocity is persistent in the presence of suramin. (A) Statistical analysis of the mean velocity of calcium waves induced in *cttn*$^{+/+}$ and *cttn*$^{-/-}$ cultures treated with 100 µM suramin or HBSS as control. In *cttn*$^{+/+}$ cultures, control waves displayed a mean velocity of 19.2±0.7 µm/sec, whereas the application of suramin led to a highly significant decrease in velocity to 14.9±0.6 µm/sec. In *cttn*$^{-/-}$ cultures, control waves showed a mean velocity of 16.9±0.8 µm/sec. Also here, the application of suramin led to a highly significant decrease in velocity to 12.9±0.5 µm/sec. Reduction of calcium wave velocity for *cttn*$^{-/-}$ in comparison to *cttn*$^{+/+}$ culture was persistent in the presence of suramin (red line and asterisk). **(B)** Comparison of the reduction in calcium wave propagation velocity of *cttn*$^{+/+}$ and *cttn*$^{-/-}$ astrocytic cultures by 100 µM suramin. The decrease of calcium wave velocity to 75.3% and 74.7%, respectively, was almost identical in both genotypes. Quantitative data was tested for significance by one-way ANOVA followed by a *post-hoc* Tukey's Multiple Comparison Test. Significance is indicated as follows *p<0.05; **p<0.01; ***p<0.001. Data are shown as mean ± SEM.

This similar effect of suramin on calcium waves induced in cultures of both genotypes indicates no alterations concerning the non-contacting calcium signaling. Purinergic signaling was therefore found to be independent of cortactin. Taken together, these data suggest an effect of cortactin on gap junctional calcium wave propagation. Since the involvement of cortactin in the purinergic pathway was hereby excluded, subsequently, the role of the interaction between cortactin and Cx43 had to be confirmed in this context. Already in the last century, the knockout of Cx43 was shown to decrease the percentage of cells involved in a mechanically induced calcium wave from 63% to 29% (Naus et al., 1997). The residual coupling was explained by the presence of other connexin isoforms like Cx30 and Cx26 in dissociated astrocytic cultures, although these isoforms were expressed to a lesser extent (Giaume et al., 1991; Giaume and Liu, 2012). The residual coupling of 49% found in the cortactin knockout combined with the unobtrusive localization of Cx43 in the knock out cultures point to a certain amount of functional Cx43 containing gap junctions. Consequently, a very specific inhibition of Cx43 was necessary to achieve convincing results. In this approach, the Cx43 mimetic peptide gap27 was used and a scrambled peptide (scr) served as control (Wang et al., 2012). The mimetic peptide gap27 corresponds to the second extracellular loop of connexin43. Therefore,

extracellular application of gap27 is supposed to specifically inhibit Cx43 mediated gap junctional coupling. In these experiments, calcium waves were induced in a petri dish containing the respective peptide dissolved in HBSS without a perfusion. The lack of the continuous perfusion resulted in an overall decrease of the calcium wave velocity under basic conditions (HBSS, data not shown). After a pre-incubation with the respective peptide for 30 minutes, calcium waves were either induced in wild type or in cortactin knock out cultures. The velocity of mechanically induced calcium waves in wild type cultures was slightly, but significantly reduced in the presence of gap27 (Figure 3.44; A). Cultures incubated in HBSS containing the scrambled peptide (white, *cttn*$^{+/+}$ scr) displayed a mean velocity of 15.3±0.3 µm/sec, which is more than 2 µm/sec decreased in comparison to experiments under continuous perfusion (17.6±0.2 µm/sec). Calcium waves induced in wild type astrocytic cultures incubated with the gap27 peptide (red, *cttn*$^{+/+}$ gap27) exhibit a mean velocity of 14.5±0.2 µm/sec. This speed is significantly reduced in comparison to the velocity of calcium waves induced in the presence of the scrambled peptide (p=0.0089). Investigation of astrocytic cultures from *cttn*$^{-/-}$ animals did not reveal a significant alteration of the calcium wave velocity upon incubation with the Cx43 specific peptide (p=0.24; Figure 3.44; B). Calcium waves induced in cortactin knock out cultures incubated with the scrambled peptide attained a speed of 15.6±0.2 µm/sec (black, *cttn*$^{-/-}$ scr), while incubation with the gap27 peptide led to a velocity of 15.3±0.2 µm/sec (rose, *cttn*$^{-/-}$ gap27).

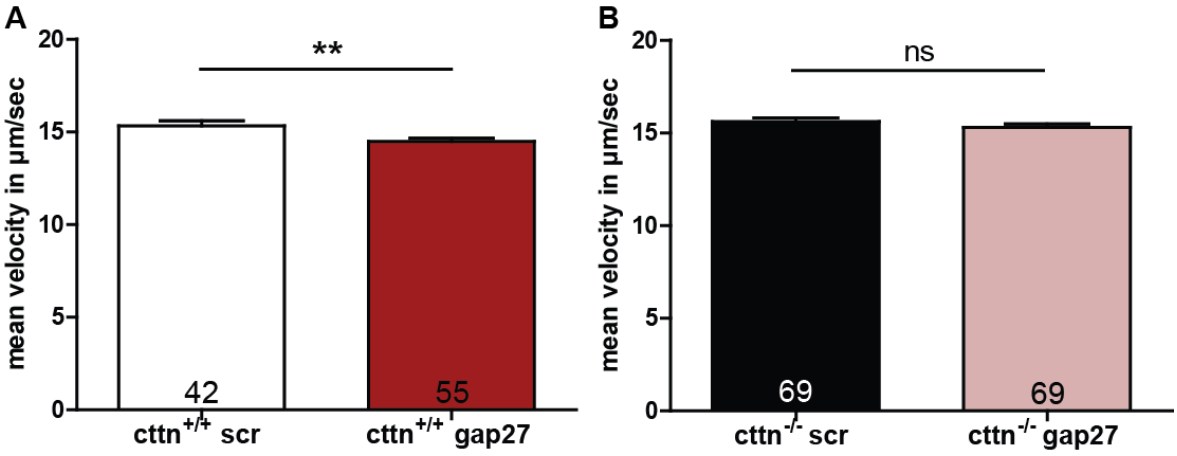

Figure 3.44 | Application of connexin mimetic peptide solely affects calcium wave velocity in wild type cultures. (A) Statistical analysis of calcium wave velocity in wild type astrocytic cultures. Treatment with 300 µM of the Cx43 specific mimetic peptide gap27 resulted in a significantly reduced calcium wave velocity (scr: 15.3±0.3 µm/sec vs. gap27: 14.5±0.2 µm/sec). **(B)** Statistical analysis of calcium wave velocity in cortactin knock out astrocytic cultures. Treatment with the Cx43 specific mimetic peptide gap27 resulted in no significant alterations in calcium wave velocity (scr: 15.6±0.2 µm/sec vs. gap27: 15.3±0.2 µm/sec). Quantitative data was tested for significance by an unpaired two-tailed Student's t-test. Significance is indicated as follows *p<0.05; **p<0.01; ***p<0.001. Data are shown as mean ± SEM.

Under these experimental conditions, comparison of the velocity of induced calcium waves did not exhibit an alteration between wild type and knock out cultures ($p=0.38$). The velocity values for the knock out cultures were even found to be slightly increased compared to wild type. Nevertheless, the application of the Cx43 specific peptide solely had a significant effect on the wild type cultures, were cortactin as an interaction partner is present. Collectively, these data suggest cortactin as a modulator of Cx43 based astrocytic coupling.

Summed up, cortactin was revealed to be important for processes involving the microfilament system like proliferation and migration. The dynamic of the actin cytoskeleton was demonstrated to be impaired by the depletion of cortactin. Also, analysis of the interdependence of cortactin and Cx43 in the context of intercellular communication in astrocytes supports the idea of gap junctional communication modulated by cortactin. The presented data suggests cortactin as a modulator of actin dynamics as well as a functionally relevant interaction partner of the major gap junction protein Cx43 in astrocytes.

4. Discussion

The integrity and plasticity of the intercellular communication is of tremendous importance for the glia-neuronal network in the mammalian brain. During the last two decades, knowledge about the not merely trophic and mechanical supporting functions of astrocytes has dramatically grown (Rodnight and Gottfried, 2013). In the mature brain, astrocytes reside in close proximity to neurons. Their peripheral processes envelope the synapse forming an intimate partnership entitled ‘tripartite synapse’. Moreover, the formation of glial networks enables astrocytes to assemble information processing units consisting of interconnected astrocytes and neurons. Since plasticity of astrocytes may play a relevant role in this context, the present study aims to give insights into the regulation of the astrocytic cytoskeleton by actin binding proteins.

The presented data provide new understandings of the astrocytic function of profilins, which are either isoform specific or overlapping. I found redundant as well as isoform-specific functions of both PFN1 and PFN2a in modulating astrocytic morphology and motility. Specifically, the knockdown of PFN1 as well as PFN2a led to a significant decrease in cell adhesion and cell size. Both isoforms proved to be as well crucial for forskolin-induced astrocytic stellation and the motility of astrocytic processes. However, FRAP analysis revealed that solely the knockdown of PFN1 affected actin dynamics in small astrocytic protrusions. In contrast, the downregulation of PFN2a exclusively resulted in a significantly reduced amount of stellate astrocytes both in dissociated and slice culture.

Furthermore, I could demonstrate that cortactin modulates actin dynamics and intercellular communication in astrocytes. Cortactin deficient astrocytes only show minor alterations in morphology and motility, but exhibit a defect in proliferation and actin dynamics. Additionally, the knockout of cortactin led to impaired calcium wave propagation in dissociated astrocytes. This phenotype was independent of purinergic signaling, since it was preserved in the presence of the P2X and P2Y antagonist suramin. The subsequent inhibition of Cx43 mediated intercellular communication by connexin mimetic peptides revealed interdependence between cortactin and Cx43.

4.1. Profilin isoforms as regulators of astrocytic morphology and function

The two isoforms PFN1 and PFN2a have been demonstrated to be differentially involved in various important cellular processes of neuronal cells (Gorlich et al., 2012; Michaelsen et al., 2010; Murk et al., 2012; Pilo Boyl et al., 2007). Since the expression of these two isoforms was revealed not to be a unique characteristic of neurons, the functional relevance of PFN1 and PFN2a was addressed in astrocytes.

4.1.1. Expression of PFN Isoforms

Ever since the human PFN2 was identified as novel profilin isoform in 1993 (Honore et al., 1993), most research on its cellular function was performed in neurons. Nonetheless, the expression pattern was defined as much broader. An additional strong presence of PFN2 transcripts in skeletal muscle and kidney as well as a moderate expression in heart, placenta, lung, and liver were described (Honore et al., 1993). Upon discovery of the alternative splicing of PFN2, expression of PFN2a and PFN2b transcripts in mouse tissue was investigated by RT-PCR (Di Nardo et al., 2000; Lambrechts et al., 2000). Here, expression of PFN2a was detected in brain, skeletal muscle, heart, kidney, liver, and skin. However, there was no PFN2a protein expression detectable in the murine liver in this thesis. Examination of PFN2 protein levels (Witke et al., 1998) revealed the highest expression in brain tissues, with minor protein expression in skeletal muscle, kidney, and uterus. Consistent with Witke and colleagues (1998), PFN2a was not expressed in spleen, while PFN1 was expressed to high amounts. Considering specific cell types, expression of PFN2a was also reported for non-CNS cells like aortic endothelial cells (Fan et al., 2012). Also within the CNS, PFN2a was found in various cell types like astrocytes (Cahoy et al., 2008; Doyle et al., 2008; Lovatt et al., 2007), oligodendrocytes (Cahoy et al., 2008), ependymal cells (Murk, 2008) and microglia (Schweinhuber, data not shown). Consequently, the focus of PFN2a in neurons may have led to a bias concerning the variety of cellular functions this profilin isoform potentially fulfils in different cell types. The presented work steps out of this line by investigating the cellular functions of both profilin isoforms in parallel in astrocytes.

4.1.2. Isoform specific knockdown of profilins

The isoform specific RNA interference mediated knockdown of either PFN1 or PFN2a used in this thesis was established in HeLa cells (Murk, 2008). Also studies addressing the isoform specific function of PFN1 or PFN2a in neurons took advantage of the respective constructs (Zessin, unpublished data (Michaelsen et al., 2010; Zessin, 2010)).

While HeLa cells were completely devoid of the respective profilin isoform (Murk, 2008), in neurons residual expression of about 31% for PFN1 (Zessin, personal communication) and 27% for PFN2a (Michaelsen et al., 2010) was detected. The knockdown of PFN1 achieved in neurons is therefore comparable to the knockdown levels in astrocytes. The reduction of PFN2a levels was less successful in astrocytes than in neurons. Still, the achieved protein level reduction was sufficient to induce various structural and functional consequences. Interestingly, the acute downregulation of PFN2a used here lead to an increase of PFN1 levels in two independent experiments performed during my thesis. Transgenic mice lacking PFN2, however, reveal no obvious increase in PFN1 levels (Pilo Boyl et al., 2007). Potentially, due to the long term downregulation in PFN2$^{-/-}$ animals the balance of the regulatory machinery for the cytoskeleton is restored by a compensatory mechanism. Pilo Boyl and colleagues (2007) for instance did not address possible alterations in the cellular level of components of the RhoA-ROCK pathway, which was shown to regulate PFN2a activity (Da Silva et al., 2003). Moreover, alterations in profilin levels could be compensated by changes in cofilin expression or activity, since a concurrent regulation event occurs (Yun et al., 2012). In accordance with another study (Gorlich et al., 2012), here no alterations in PFN2a expression were observed upon PFN1 knockdown. It is possible that a change in the activation of PFN2a is sufficient to take over the non-isoform specific cellular functions of PFN1. In summary, the shRNA approach utilized in this thesis is valid to investigate the consequences of acute profilin downregulation in astrocytes.

4.1.3. Profilin isoforms in adhesion and migration of astrocytes

Several studies address the role of profilins in migration and adhesion in a plethora of different cell types. However, the majority solely examines the function of PFN1 in these processes. In human vascular endothelial cells, siRNA mediated PFN1 knockdown caused defects in focal adhesion assembly, spreading, proliferation and migration (Ding et al., 2006). The same group revealed the interaction of PFN1 with both actin and proline-rich ligands to be essential for the aforementioned cellular functions (Ding et al., 2009). Also in breast epithelial cells, siRNA mediated knockdown of PFN1 resulted in a reduced vitality and migration (Simpson et al., 2008). Since the genetic PFN1 knockout is lethal during early development, the tissue specific CRE-expression was used in recent approaches demonstrating a negative impact of PFN1 depletion on migration and cytokinesis in chondrocytes (Bottcher et al., 2009) as well as on migration and adhesion in Bergmann glia (Kullmann et al., 2012). In summary, these findings are in line with the evident defect in adhesion upon PFN1 downregulation in astrocytes. A possible explanation for this result is the interaction of PFN1 with the vasodilator-stimulated

phosphoprotein VASP (Reinhard et al., 1995), which is important for focal adhesions. Moreover, also in non-cancerous endothelial aortic cells overexpression of PFN1 was described to increase the number of focal contacts thereby increasing cellular adhesion (Moldovan et al., 1997). Conflicting results have been reported for invasive carcinomas. PFN1 knockdown was shown to enhance the motility of breast cancer cells (Bae et al., 2009; Zou et al., 2007). This was accompanied by an impaired cellular adhesion (Zou et al., 2007) and an enhancement of VASP at the leading edge (Bae et al., 2009). Also in hepatocarcinoma cells, PFN1 downregulation led to an increase in proliferation and migration (Wu et al., 2006). Accordingly, PFN1 overexpression resulted in a decreased proliferation and migration (Wu et al., 2006), while focal adhesions were increased (Zou et al., 2007). These context specific consequences of PFN1 depletion promote two alternative hypothesizes. On the one hand, Ding and colleagues (2012) suggest an actin-independent function of PFN1 in cell motility. In that model, PFN1 negatively regulates the recruitment of lamellipodin and Ena/VASP, thereby inhibiting membrane protrusion. In the absence of PFN1, lamellipodin easily binds to PIP_2, promoting Ena/VASP recruitment and consequently cellular motility. On the other hand, these cancerous cells are capable of compensatory PFN2 expression. Consequently, PFN2 could rescue the migration defect, but PFN1 would fulfil an isoform specific function at focal adhesions. Additionally, the aforementioned studies provide an explanation for the reduced percentage of transduced cells in PFN1 downregulated astrocytes. First, Simpson and colleagues found a reduced vitality in PFN1 knockdown cells (2008). Second, both human vascular endothelial cells and chondrocytes display an evident reduction in cellular proliferation upon profilin depletion, which was explained by a reduced ability of these cells to create sufficient force for abscission during late cytokinesis (Bottcher et al., 2009; Ding et al., 2006). Again, analysis of cancerous cells revealed contradictory results concerning the effects of PFN1 on proliferation (Wu et al., 2006). Since a dysregulation in proliferation is a common characteristic of carcinomas (Croce, 2008), this result is likely to be rather a consequence of general alterations in cancer cells than reflecting the physiological situation. Early experiments in Dictyostelium amoebae revealed an impaired migration upon depletion of both profilin isoforms, while the PFN1 knockout was not sufficient to cause a phenotype (Haugwitz et al., 1994). This study provides evidence for a potential compensatory function of PFN2 in the absence of PFN1 and additional demonstrates both profilins to be involved in cellular migration. Also in avian fibroblasts, the knockdown of PFN1 was not sufficient to cause an impaired migration or adhesion, while the knockdown of PFN2 significantly impaired focal adhesion formation, adhesion and migration (Murk et al., 2009). The described defects increased in severity upon simultaneous downregulation of both profilin isoforms, indicating also a role for PFN1 and a compensatory mechanism

involving PFN2. The siRNA mediated downregulation of PFN2 in breast epithelial cells, however, exhibit an increased migration speed in a wound heal assay (Simpson et al., 2008). PFN2 knockdown cells revealed a fast, erratic, poorly polarized mode of migration characterized by a reduction in adhesion to the substrate. This phenotype was not caused by alterations in the vitality of the cells. These findings support a role of PFN2a in the adhesion of astrocytes. Additionally, in accordance with my results, knockdown of PFN2a exhibits far less severe consequences for the vitality of cells. In the scratch wound assays, PFN2a knockdown astrocytes showed a highly varying migration behavior (Schweinhuber, data not shown). Astrocytes migrate, like epithelial cells, as a group of cells unidirectional to the wound. Nevertheless, the migration velocity is around five times slower (Etienne-Manneville and Hall, 2001). Consequently, a defect in adhesion would not cause a comparably severe increase in cellular motility. Therefore coverage of the migration phenotype by the adhesion phenotype could result in an unobtrusive migration behavior of PFN2a knockdown astrocytes.

4.1.4. Predominantly PFN2a modulates the morphology of astrocytes

In this thesis, RNAi mediated downregulation of the cellular amount of both PFN1 and PFN2a, respectively, resulted in a significant decrease in the overall size of cultured astrocytes. This finding is consistent with the cell size reduction caused by the expression of an actin-binding deficient PFN1 (Molotkov et al., 2013) and the 15% reduction in process length of $PFN1^{-/-}$ Bergmann glia (Kullmann et al., 2012). In contrast, profilin deficient Dictyostelium mutants are 10 times larger compared to controls (Haugwitz et al., 1994). But since these cells are also multinucleated, the increase in size is likely to be a consequence of a cytokinesis defect. The morphological data presented in this thesis are independent of potential cytokinesis phenotypes, because the transfection with the respective plasmids was performed when the astrocytes are at a mature, barely dividing state. However, the two studies performed on astrocytes solely focus on PFN1, while the morphological consequences of a PFN2a loss are only quantified in neurons. Already the first step in the development of neurons, the initial neurite outgrowth relies on PFN2a (Da Silva et al., 2003; Pilo Boyl et al., 2007). In the absence of PFN2a, process outgrowth was drastically increased within the first 24 hours. However, this phenotype disappeared already after 48 hours (Pilo Boyl et al., 2007). Dissociated astrocytes expressing the shRNA specific for PFN2a exhibit a higher percentage of polygonal cells, indicating a positive influence of PFN2a on process outgrowth. Since the analysis was performed on mature, DIV 21 astrocytes, an initial outgrowth of astrocytic processes negatively regulated by PFN2a cannot be excluded. Morphological analysis of PFN2a downregulated mature dissociated hippocampal neurons, however, revealed a reduction in dendritic

complexity (Zessin, 2010). Therefore, PFN2a is suggested as positive regulator of the complexity of major cellular processes in both dissociated neurons and astrocytes.

Yet, the aforementioned morphological studies were performed in dissociated cultures, where the interaction between neurons and astrocytes as well as the neuronal circuits are not preserved. Nevertheless, also solely PFN2a downregulated astrocytes in slice cultures of mouse cortices exhibit a volume reduction. This finding suggests a decline in the amount of astrocytic processes and therefore complexity. Consistently, Michaelsen and colleagues (2010) described PFN2a as an important modulator of dendritic architecture of CA1 pyramidal neurons. The expression of recombinant PFN1 was not sufficient to rescue the observed phenotype (Michaelsen et al., 2010). PFN1 knockdown revealed only subtle, non-significant alterations in the volume of astrocytes. This result is consistent with the mild dendritic phenotype of PFN1 knockdown in pyramidal neurons (Zessin, personal communication). In summary, these findings suggest isoform specific functions in the maintenance of the structural integrity of major processes, which appears to be similar for *in vivo*-like astrocytes. Consequently, future experiments should clarify the potential rescue of the PFN2a knockdown phenotype in astrocytes with the expression of recombinant PFN1 and PFN2a.

4.1.5. Profilins regulate the starvation response of astrocytes

Throughout the literature, serum starvation is frequently performed as a standard procedure to prepare cells for an experiment in serum free conditions (Benziane et al., 2009; Bouzakri et al., 2006; Lindahl et al., 2007; Murk et al., 2013; Racchetti et al., 2012; Ramakers and Moolenaar, 1998; Tsuji et al., 2002). This practice neglects influences of serum starvation on the physiology of the examined cells. Generally, total protein amounts per culture dish tended to be lower in serum-starved cells compared to non-starved controls (Schweinhuber, data not shown), which was also described in the literature (Pirkmajer and Chibalin, 2011). This tendency is in line with the described decrease in protein synthesis and the associated increased proteolysis in serum starved cells (Epstein et al., 1975; Hershko and Tomkins, 1971; Zetterberg and Larsson, 1985). The existence of several studies using serum starvation as a tool to investigate the cellular response to stress (Arrington and Schnellmann, 2008; Levin et al., 2010) or to induce autophagy and apoptosis (Bhutia et al., 2010; Terra et al., 2011; Zhao et al., 2010), underlines the major impact of serum depletion on eukaryotic cells. Also in immortalized primary human fetal astrocytes apoptosis was induced by serum starvation (Bhutia et al., 2010; Lee et al., 2008). Here, an activation of the phosphatidylinositol 3-kinase (PI 3K)/AKT pathway was shown to promote survival of the astrocytes. Additionally, several glioma cell lines exhibit an increased activation of PI 3K and AKT upon serum depletion induced stress (Levin et

al., 2010). Interestingly, PFN1 protein expression and AKT activation by phosphorylation were shown to be interconnected (Caglayan et al., 2010; Jin et al., 2012). The overexpression of recombinant PFN1 in vascular smooth muscle cells results in an increased activation of the PI3K/AKT pathway (Caglayan et al., 2010). The latter study demonstrates the augmentation of PFN1 protein level parallel to an increase of activated AKT upon angiotensin treatment in aortic tissue (Jin et al., 2012). Interestingly, the increase in phosphorylation level of AKT and thereby its activation revealed a temporally restricted pattern in HEK293 cells (Pirkmajer and Chibalin, 2011). Specifically, one to six hours after serum depletion, a significant increase in the amount of p-AKT was monitored, while after 24 hours, the phosphorylation level was again reduced to baseline. These results bear a striking resemblance to the temporal morphological changes in astrocytes upon serum starvation. Since the simultaneous rise in both p-AKT and PFN1 (Caglayan et al., 2010; Jin et al., 2012), an increase in PFN1 or PFN2a level or activation would be consequent for 4 hours serum starved astrocytes. Indeed, PFN2a phosphorylation level was significantly reduced upon 4 hours of serum depletion, suggesting an activation of PFN2a. Since neither PFN1 nor PFN2a protein level was examined after 4 hours, a putative upregulation has to be investigated in the future. Astonishingly, the initial morphological change in response to serum depletion may be profilin independent, since in comparison to wild type PFN1 and PFN2a knockdown astrocytes display an indistinguishable phenotype. A possible explanation for a largely unimpaired initial response to serum starvation would be a primarily cofilin driven remodulation of the actin cytoskeleton. Otherwise, the profilin isoforms may compensate each other in this context. Consequently, the complete independence of these morphological changes from profilins has to be investigated by the knockdown of both isoforms simultaneously. Nevertheless, especially PFN1 downregulated astrocytes reveal a defect in adaptation to serum depleted conditions. This is particularly puzzling, since PFN1 protein levels were found to be reduced upon 24 hours of serum depletion in this thesis. However, the knockdown may cause a fall below the critical protein concentration for PFN1, while the reduction of about 45% during serum starvation may be in the physiological range. Moreover, these two events may not be directly interconnected. On the one hand, knockdown of PFN1 may cause compensatory alterations in the regulation of cytoskeletal dynamics, resulting in an imbalance of the morphological changes. On the other hand, reduction of the cellular amount of PFN1 upon serum depletion may be interconnected with other, non-morphological responses to serum starvation of astrocytes.

Starvation was shown to increase cellular cAMP levels (Oey et al., 1974), thereby activating PKA. Since the increase of astrocytic cAMP levels is generally accompanied by an augmented amount of stellated cells (Lim et al., 1973; Shapiro, 1973), this pathway

represents a potential candidate for the observed morphological changes upon serum starvation. But as neither PFN1 nor PFN2a knockdown impaired the stellation response to serum starvation, this cAMP dependent pathway is unlikely to play a role in this context. Also the small GTPases Rac1 and RhoA together with the Rho-associated coiled coil-containing protein kinase (ROCK) are suggested in the cellular response to starvation and stress. A comprehensive analysis of the response of glioma cells to serum starvation-induced stress revealed an activation of Rac1 (Levin et al., 2010). Since Rac1 is important to the process of stellation (Racchetti et al., 2012), an involvement of Rac1 into the stellation response of astrocytes to serum deprivation is likely. An activation of Rac1 could cause an inactivation of RhoA (Lawson and Burridge, 2014). Thus, a subsequent ROCK inhibition as well as cofilin and profilin dephosphorylation would result in a stellation response.

As a matter of course, changes in the cellular morphology are not the only response of eukaryotic cells to serum starvation. Additionally, a process entitled macroautophagy characterized by a degradation of cytoplasmatic material into a double membrane compartment, takes places (Mizushima et al., 2008). Actin was suggested to fulfil a role at the early stages of autophagosome formation (Aguilera et al., 2012). Moreover, the same study revealed RhoA as an activator of starvation-induced autophagy, while Rac1 was described as an inhibitor (Aguilera et al., 2012). Consequently, ROCK inhibition impaired the autophagic response to serum deprivation. RhoA activation is assumed to cause PFN phosphorylation at Serine 137 and thereby inhibiting its activity (Shao et al., 2008). Autophagy is thought to promote cell survival at unfavorable conditions, which is beneficial for short time ranges but may promote to cancerous transformations (Bhutia et al., 2010; Gozuacik and Kimchi, 2004; Mathew et al., 2007; White and DiPaola, 2009). In combination with the significant downregulation of PFN1 in several carcinomas (Gronborg et al., 2006; Janke et al., 2000; Wu et al., 2006; Zoidakis et al., 2012), these findings promote RhoA-ROCK-PFN dependent regulation of serum starvation-induced autophagy. Moreover, also the cell detachment is a starvation stress-induced process dependent on ROCK1 (Shi et al., 2013). Shi and colleagues found ROCK1 deficient mouse embryonic fibroblasts to reveal a weakened response to serum starvation by reduced cell detachment and caspase-3 activation. Since ROCK1 was shown to phosphorylate PFN at Serine 137 (Shao et al., 2008), the subsequent PFN inactivation is prevented by the ROCK1 knockout. Consequently, active PFN might be a positive regulator of cell survival under stress conditions. This conceptual idea would match the defect in adaptation to serum starvation of PFN1 knockdown astrocytes.

Taken together, the response of eukaryotic cells to serum deprivation is a complex, temporally well-defined process. Since some of the cell types used in the aforementioned studies are quickly dying upon starvation and other, like astrocytes, survive serum deprivation up to one week, the time scales may also depend on the model system. To fully understand the role of profilin isoforms in this context, a systematic investigation of their phosphorylation states as well as the concomitant, profilin dependent morphological alterations including time points from 1 hour to 48 hours are mandatory.

4.1.6. Profilins regulate stimulus dependent morphological changes in astrocytes

The induction of morphological plasticity in astrocytes by the application of cAMP elevating agents is a standard procedure used for about 40 years (Lim et al., 1973; Pinto et al., 2000; Shapiro, 1973). In the present study, an essential function of both profilin isoforms for the induced stellation in the response to forskolin treatment was demonstrated. Forskolin treatment is assumed to activate both PKA via the cAMP elevation and PI3K (Perez et al., 2005). Consequently, several different signaling pathways are involved in the regulation of profilin activity upon forskolin induced stellation. Phosphorylation of profilins through various signaling cascades has been assigned to differential alterations of biochemical properties. An overview is presented in Figure 4.1.

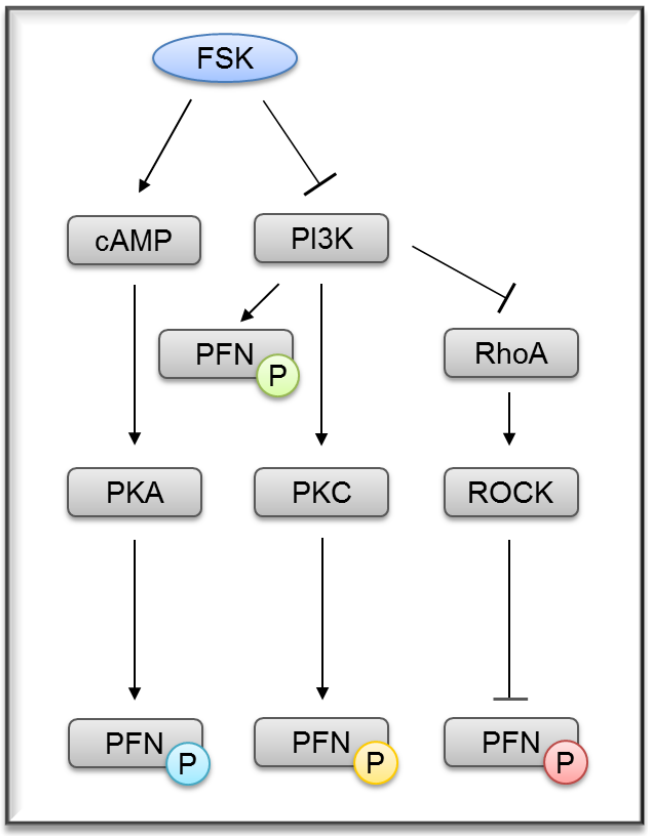

Figure 4.1 | Forskolin modulates profilin phosphorylation. Forskolin treatment both increases cAMP levels and inactivates PI3K, thereby inactivating the RhoA pathway. PKA dependent phosphorylation of PFN results in a reduced affinity towards actin, while persistently interacting with PLP-stretches (light blue). PI3K inactivation may result in less phosphorylated PFN with a higher affinity towards both actin and PLP (green) and less phosphorylated PFN with a reduced affinity towards PLP (yellow). Simultaneously, the inactivation of RhoA leads to a decrease in phosphorylated PFN with reduced affinity to both actin and proline-rich proteins (red).

Upon forskolin stimulation, cAMP levels increase which leads to an activation of the cAMP dependent protein kinase PKA and stellation of astrocytes reliant on the actin cytoskeleton (Goldman and Abramson, 1990; Pinto et al., 2000). Direct phosphorylation of PFN1 and PFN2a by PKA has been demonstrated by Lederer (Lederer, 2002). Subsequent analysis of putative PKA phosphorylation sites revealed the serine-residues S58 and S92 for PFN1 as well as S72 and S77 for PFN2a (Murk, 2004). Additional PKA dependent phosphorylation sites, however, cannot be excluded. Furthermore, the PLP binding capability of PKA phosphorylated PFN was unaltered, while the interaction with G-Actin was impaired (Lederer, 2002; Murk, 2004). Consequently, PKA phosphorylated PFN (Figure 4.1; blue P) is released from the PFN:actin complex and available for interaction with PLP binding partners, which are spatially separated from the actin cytoskeleton. Forskolin stimulation also induces cytoskeletal remodeling by inactivating PI3K (Perez et al., 2005). The inactivation of PI3K has various consequences on profilin phosphorylation states. First, this leads to a reduced amount of PFN directly phosphorylated by PI3K

(Sathish et al., 2004). PI3K phosphorylated PFN was described to have and increase affinity to both PLP and G-actin together with no alterations in the binding to PIP_2 (Figure 4.1; green). Secondly, PKC downstream of PI3K is not activated, which in turn results in a reduced PFN phosphorylation (Vemuri and Singh, 2001). PKC phosphorylated PFN (Figure 4.1; yellow) is not capable of binding to PLP-stretches (Lederer, 2002), while exhibiting an unimpaired binding to G-actin. Lastly, PI3K inactivation was shown to result in an inactivation of RhoA (Perez et al., 2005). Its downstream effector ROCK thus releases PFN, which leads to a dephosphorylation of PFN (Da Silva et al., 2003). ROCK dependent phosphorylation of PFN at Serine 137 (Figure 4.1; red) was shown to abolish both the interaction with PLP and reduces the affinity to G-Actin (Shao et al., 2008). Accordingly, the alterations in profilin phosphorylation upon forskolin treatment may result in an increased binding to PLP and thus interacting proteins together with a diminished binding to actin. Taken together, forskolin treatment has complex consequences for the phosphorylation state of profilins. In the present study, the net phosphorylation of PFN2a was increased upon forskolin treatment. Yet, only two phosphorylation states – presumably unphosphorylated and PFN phosphorylated at one side – were detected. Thus, discrimination between different pathways leading to PFN phosphorylation in this context is not possible. The downstream effects of PI3K inactivation concordantly hint at a reduced phosphorylation of PFN succeeding forskolin treatment. Thus, the PKA dependent pathway is likely to be responsible for the observed increase in phosphorylation. Furthermore, co-application of the PKA inhibitor KT5720 lead to an obvious decrease in PFN2a phosphorylation compared to the forskolin treated astrocytic cultures. Due to technical difficulties, PFN1 phosphorylation could not be addressed in this thesis. Nevertheless, PFN1 is phosphorylated at its c-terminus under control conditions, promoting a regulation of PFN1 by phosphorylation in astrocytes. Since both PFN1 and PFN2a knockdown abolished the stellation response to forskolin, a similar activity regulation is likely in this context. The putative alterations of the biochemical properties of profilins by phosphorylation upon forskolin treatment support a role of the interaction between profilins and PLP binding partners in the stellation response of astrocytes. Consequently, future experiments should address the question if actin-binding or PLP-binding deficient profilin mutants are able to rescue the stellation phenotype.

Besides the morphological alterations and the changes in phosphorylation status upon forskolin treatment, also the subcellular localization of profilin isoforms was altered. Specifically, solely PFN1 was found to be enriched in the nucleus in astrocytes subjected to forskolin. Unspecific stimulation of dissociated neurons by KCl treatment also resulted in an elevated amount of both profilin isoforms in the nuclei (Murk et al., 2012). Interestingly, the more specific stimulation via BDNF and thereby activation of the TrkB

receptor pathway (for review (Minichiello, 2009)) solely led to a redistribution of PFN1 to the neuronal nucleus. Since TrkB signaling includes the activation of both PI3K-AKT and PLCγ, PFN1 may undergo an isoform-specific regulation downstream in one of these pathways. In contrast, the more general activity induction by KCl may stimulate additional signaling cascades also affecting PFN2a. In astrocytes, PFN2a localization was unaltered upon unspecific stimulation with forskolin. This finding either hints at a cell type specific cellular function of PFN2a in the nucleus or suggests an alternative stimulus to induce PFN2a translocation in astrocytes. The significance of the translocation of PFN1 to the cellular nucleus is not well understood. Profilins are suggested to be involved in the regulation of nuclear processes. PFN1 also interacts with nuclear actin (Stuven et al., 2003) and colocalizes with several ligands known from the cytoplasm like VASP or mDia1 (Rawe et al., 2006). Furthermore, PFN1 specific antibodies were shown to interfere with pre-mRNA splicing (Skare et al., 2003), which hints to a role of profilin in mRNA processing. Remarkably, in contrast to avian fibroblasts (Murk et al., 2009), PFN1 localization in astrocytes was not altered by serum deprivation. Nonetheless, PFN1 was involved in the astrocytic adaptation to serum starvation. Thus, the molecular mechanisms underlying the response to starvation may be cell type specific. Since cAMP elevations result in altered transcription mediated by PKA activation (Sands and Palmer, 2008), PFN1 translocation may present a novel molecular mechanism modifying transcription in this context. Consequently, also PKA inhibition may result in alterations in process of transcription mediated by profilins as also epidermal growth factor (EGF) induced proliferation of neural stem cells is inhibited by KT5720 (Iguchi et al., 2011). The drastic increase of PFN2a in the nucleus of astrocytes specifically upon KT5720 treatment, however, may also rely on non-PKA specific effects of the used inhibitor.

4.1.7. Inhibition of PKA activity by KT5720

In contrast to the PKA inhibitor H89, which inhibits PKA activity by a similar mechanism (Engh et al., 1996), KT5720 was described to have no effect on astrocytic morphology (Abe and Misawa, 2003). Nevertheless, KT5720 acts on various other kinases (Davies et al., 2000). Thus, the obtained results are interpreted with respect to putative side effects of KT5720 treatment. In the present thesis, KT5720 not only reversed the stellation caused by forskolin treatment, but also added a distinct alteration in the morphological phenotype. One study exhibits KT5720 to inhibit mitogen-activated protein kinase (MAPK), thereby causing morphological alterations in Chinese Hamster Ovary (CHO)-cells (Olsen et al., 1998). Thus, the additive effect on astrocytic morphology may rely on MAPK inactivation. Since the aforementioned study examined the alterations in microtubules in this context, no evidence about the involvement of either actin or profilin is

included. Nevertheless, the effect of KT5720 in astrocytes undoubtedly relies on profilin isoforms, which are not directly involved in microtubule dynamics. Yet, phosphoinositide-dependent kinase 1 (PDK1) is very efficiently inhibited by KT5720 (Davies et al., 2000). PDK1 is crucial for AKT activation (Barry and Gibbins, 2002; Persad et al., 2001) and interacts with PKMζ (Balendran et al., 2000; Hodgkinson and Sale, 2002; Le Good et al., 1998). As already mentioned earlier, a functional interdependence of AKT phosphorylation and the increase of PFN1 levels has been demonstrated (Caglayan et al., 2010; Jin et al., 2012). Applying this hypothesis to PDK1 inactivation by KT5720, subsequent inactivation of AKT accompanying PFN1 protein level reduction could result in a decreased stellation response. Consequently, PFN1 downregulated astrocytes may not respond with a further reduction of the percentage of stellate cells. Indeed, astrocytes expressing the PFN1 specific shRNA rather exhibit an increase in stellation upon KT5720 treatment, while control and PFN2a knockdown astrocytes revealed no alterations. This conclusion, however, does not explain the evident increase in the percentage of stellate astrocytes in PFN1 knockdown astrocytes. Since PKMζ as a downstream target of PDK1 is also inactivated by KT5720, the subsequent and isoform-specific phosphorylation of PFN2a (Böning, 2012; Weller, 2012) is abolished. Expression of recombinant PKMζ was also found to decrease neurite outgrowth in PC12 cells (Weller, 2012). Consequently, non-phosphorylated, active PFN2a (Da Silva et al., 2003) may promote morphological plasticity and thus a stellation response in KT5720 treated astrocytes. In control cells, this response may be counteracted by the AKT mediated reduction of PFN1 protein level.

Furthermore, KT5720 was shown to abolish transcription in CHO-cells (Keezer and Gilbert, 2002). Although another report contradicts their findings (Dimitrova, 2006), a PKA independent effect of KT5720 on transcription cannot be excluded. Interestingly, KT5720 increases the affinity of acetylcholine to M1 muscarinic receptors by 40% (Lazareno et al., 2000). Since astrocytes express muscarinic receptors (Andre et al., 1994) and M1 transactivates the EGF-receptor (Tsai et al., 1997), a EGF stimulation may be mimicked. EGF stimulation is frequently used to stimulate eukaryotic cells including astrocytes. Activation of the EGF-receptor positively regulates proliferation and alters the morphology as well as the cytoskeleton of astrocytes (Puschmann et al., 2014). Moreover, a plethora of subsequent signaling cascades including the PI3K-dependent pathway is altered (Oda et al., 2005). These findings hint at a role of PFN2a in the EGF-stimulation dependent nuclear activities rather than in the PKA modulated transcription.

In summary, further experiments investigating the specificity of the PKA inhibitor KT5720 in this context are necessary to exclude PKA independent effects on cellular morphology and subcelluar profilin localization. As alternative inhibitors of PKA activity R_p-cAMPs,

protein kinase inhibitory peptides or RNAi approaches have been suggested (Murray, 2008).

4.1.8. ROCK inhibition induced morphological changes depend von PFN2a

Modification of RhoA activity is a well-established tool to induce morphological changes in cultivated astrocytes (Abe and Misawa, 2003; Koyama et al., 1996; Racchetti et al., 2012; Suidan et al., 1997). The RhoA downstream kinase ROCK2 is an exclusive interaction partner of PFN2a (Witke et al., 1998). In this thesis, the ROCK inhibitor Y27632 was applied to investigate the underlying, potentially profilin dependent molecular mechanism (Da Silva et al., 2003; Shao et al., 2008). Of course, direct pharmacological inhibition of ROCK has to be considered as a less physiological stimulus than forskolin induced cAMP elevation (Rodnight and Gottfried, 2013). Morphological as well as biochemical evidence presented in the current work suggest a PFN2a dependent molecular mechanism illustrated in Figure 4.2.

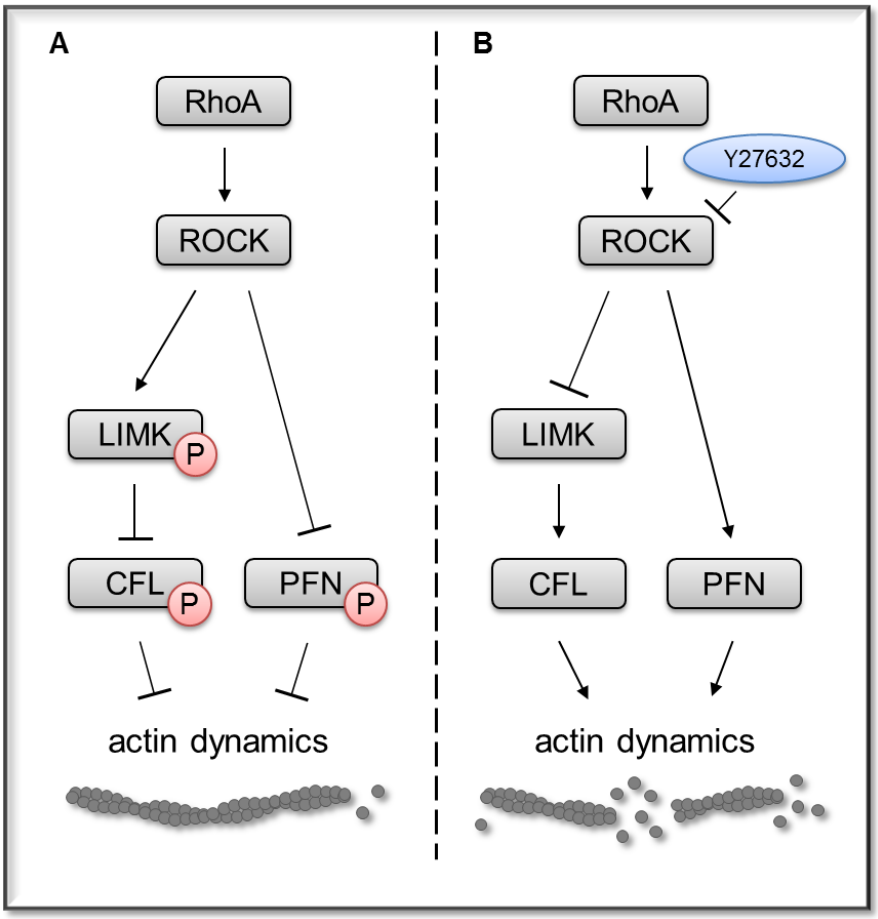

Figure 4.2 | RhoA-ROCK-PFN modulated actin cytoskeleton dynamics. (A) Active RhoA activates ROCK, thus inactivating both cofilin (CFL) and profilin (PFN) via phosphorylation. As a result, actin dynamic is reduced. **(B)** Independent of potential RhoA activity, ROCK is inhibited by Y27632. Accordingly, both cofilin and profilin are dephosphorylated and promote actin dynamics.

The epitheloid morphology of astrocytes in dissociated cultures is caused by a tonic activation of RhoA (Ramakers and Moolenaar, 1998). Consequently, actin dynamics are inhibited through a phosphorylation and thereby inactivation of cofilin and profilin (Bravo-Cordero et al., 2013; Shao et al., 2008). This conceptual idea is in line with the decreased percentage of process bearing astrocytes for the PFN2a knockdown. Consequently, non-phosphorylated PFN2a is crucial to process outgrowth and pharmacologically induced morphological plasticity in astrocytes. The regulation of cofilin and profilin by ROCK results in a concomitant activation of both small actin binding proteins by of ROCK inhibition. This synergistic cooperation of profilin and cofilin may be an efficient molecular mechanism to induce fast dynamics of the actin cytoskeleton (Didry et al., 1998). Both the simultaneous increase in profilin and cofilin protein level or rather activity (Dai et al., 2006), as well as the increase of profilin level by concurrent decrease in cofilin activity (Yun et al., 2012) upon stimulation are reported. Since morphological changes caused by Y27632 appear at a very fast timescale (Racchetti et al., 2012), a simultaneous activation of profilin and cofilin would provide the required quick actin dynamics. Interestingly, ROCK inhibition by Y27632 was shown to activate Rac1 in astrocytoma cells (Salhia et al., 2005). Additionally, Rac1 was revealed as critical determinant of Y27632 induced astrocytic stellation in another study (Racchetti et al., 2012). Since Rac1 is an upstream activator of Arp2/3 complex and also this complex was essential for stellation (Murk et al., 2013), these data reveal a complex and fast remodeling of the astrocytic cytoskeleton by activation of various pathways.

Yet, Y27632 was inhibits PRK2 at a concentration similar to ROCK (Davies et al., 2000). PRK2 was described as an effector of both Rho and Rac GTPases (Vincent and Settleman, 1997) and is regulated by PDK1 (Dettori et al., 2009). Consequently, an influence on the astrocytic morphology by the non-specific inhibition of PRK2 cannot be excluded.

Overall, these data suggest PFN2a as the profilin isoform regulating the response of astrocytes to ROCK inhibition. A direct involvement of PFN1 seems unlikely in this context.

4.1.9. Isoform specific impairment of actin dynamics in astrocytic processes

The motility of astrocytic processes was found to be reliant on both PFN1 and PFN2a. Nevertheless, solely downregulation of PFN1 impaired actin dynamics in the astrocytic peripheral processes. These findings indicate differential, isoform-specific functions of profilin isoforms in astrocytic protrusions. The reduction in dendritic spine numbers in CA1 pyramidal neurons caused by the RNAi mediated downregulation of PFN2a, however,

was rescued by the expression of recombinant PFN1 (Michaelsen et al., 2010). Yet, also the downregulation of PFN1 resulted in a reduction of dendritic spine numbers of pyramidal neurons (Zessin, personal information). In dissociated astrocytes, however, there is no evidence for an altered number of small protrusions neither in PFN1 knockdown nor in PFN2a knockdown cells (Schweinhuber, data not shown). Also the expression of an actin-binding deficient PFN1 had no consequences for the amount of astrocytic protrusions at basal conditions (Molotkov et al., 2013). However, these dissociated astrocytes are cultivated in the absence of neurons, thus not forming tripartite synapses, different results are likely for star-like astrocytes *in situ*. Nevertheless, the activity induced motility of PAPs was drastically impaired by the expression an actin-binding deficient PFN1 mutant (Molotkov et al., 2013). These results are in line with the crucial function of PFN1 in the actin dynamics and directed motility of astrocytic processes demonstrated in the present study. Accordingly, the knockdown of PFN1 in pyramidal neurons dramatically impairs FRAP measured actin dynamics in spines (Michaelsen-Preusse, personal communication). Remarkably, FRAP analysis of PFN1 overexpressing cancer cells also revealed impaired actin dynamics characterized by an elevated percentage of stable F-actin (Lorente et al., 2014). Since also the role of PFN1 in the migration of cancer cells frequently contradicts the results from non-tumorous cells (Ding et al., 2012), this phenotype may be specific for cancer cells. Alternatively, the high intracellular amount of PFN1 inhibits actin assembly, just like in pollen (Hussey et al., 2006). The motility of dendritic spines, however, was not altered for PFN1 knockdown cells (Zessin, personal communication). Contrary findings for PFN2a knockdown neurons suggest isoform-specific roles of profilins in spines. Here, the motility of dendritic protrusions was dramatically elevated, which could not be rescued by the expression of recombinant PFN1 (Remus, 2012). Expression of recombinant PFN2a led to a partial rescue of the phenotype, because overexpression of PFN2a increase the stability of dendritic spines (Ackermann and Matus, 2003). This persistent decrease in stability may be the consequence of alterations in cell-cell adhesion by cadherins, as solely PFN2 knockdown alters the balance of cadherin isoforms in epithelial cells (Simpson et al., 2008). Additionally, FRAP analysis revealed an increase in actin-turnover for PFN2a knockdown spines, indicating an enhanced percentage of highly dynamic actin filaments (Michaelsen-Preusse, personal communication). Astrocytes expressing the shRNA specific for PFN2a, however, exhibited no FRAP phenotype. These results support a cell type specific function of PFN2a in small protrusions. Nevertheless, just like in PFN1 knockdown astrocytes, the directed motility of their processes was impaired. As this cannot be attributed to changes in actin dynamics, an additional cellular function of PFN2a has to play a role in this context. PFN2a interacts with a different subset of PLP-ligands in

the brain compared to PFN1 (Witke et al., 1998). Among them, membrane associated HEM2/NAP1 represents a prominent PFN2a specific interaction partner. NAP1 directly interacts with Rac1 (Kitamura et al., 1997) and forms a complex with Sra-1, Abi-1 and WAVE2 (Steffen et al., 2004). This complex is essential to membrane ruffling and lamellipodia formation, linking Rac1 to site-directed actin assembly. Accordingly, knockdown of PFN2a could alter Rac1 dependent Arp2/3 activation and therefore coordinated actin assembly without affecting general actin turnover. Furthermore, the *Drosophila* homologue of Nap1, KETTE, regulates axonal pathfinding and has been implicated in glia cell migration (Hummel et al., 2000). Thus, PFN1 and PFN2a are suggested to have isoform-specific functions in the specialized small protrusions of both astrocytes and neurons. Additionally, these cellular functions appear to be cell type specific, underlining the importance of the individual molecular identity of spines and PAPs as cellular compartments.

Taken together, profilin isoforms fulfil isoform-specific as well as overlapping cellular functions in astrocytes. PFN1 and PFN2a are suggested as regulators of cell size, adhesion, induced morphological changes and motility of astrocytes. PFN1 is indicated to fulfil isoform-specific cellular functions in the regulation of actin dynamics and nuclear activities. In contrast, solely PFN2a is proposed to modulate the morphological complexity of astrocytes *in situ* and to regulate actin dynamics subsequent to ROCK inhibition.

4.2. Cortactin influences actin dynamics and intercellular communication

Besides profilins, also the actin binding protein cortactin was described to be a critical determinant of cell motility and plasticity in various cell types and tissues. Cortactin is indicated to fulfil an important role in astrocytes due to upregulation in astrocytes located in lesioned brain tissue (Decourt et al., 2005) and its direct interaction with the major gap junction protein Cx43 (Vitale et al., 2009). Thus, cortactin participates in key astrocytic functions and the consequences of cortactin deficiency have been examined in this thesis.

4.2.1. Cortactin modulates the microfilament system of astrocytes

The general unobtrusive phenotype of cortactin knock out astrocytes in culture was on the one hand unexpected due to the potential severe impact of cortactin on diverse cellular processes. However, on the other hand, already Lai and colleagues (2009) described cortactin knockout fibroblasts to have no obvious alterations in basal parameters. Additionally, cortactin knockout has no effect on static adhesion of leucocytes on murine lung endothelial cells (Schnoor et al., 2011). This is also in line with findings from our laboratory, examining the cellular function of cortactin in pyramidal neurons (O'Brien, unpublished data; (Rostosky, 2014; Scharkowski, 2013). These three studies showed that the overall morphology of pyramidal neurons is only mildly altered by the loss of cortactin, matching the subtle alterations in astrocytic morphology. The unobtrusive shift to a slightly increased percentage of stellate astrocytes can be attributed to a couple of different cellular pathways where cortactin is involved. The activity of the Arp2/3 complex was demonstrated to be essential to the process of stellation and its pharmacologic inactivation resulted in a flattening of astrocytes (Murk et al., 2013). Consequently, the knockout of cortactin should have resulted in a reduction of Arp2/3 activity and therefore a flattening of astrocytes. These findings hint at a non-essential function of cortactin as Arp2/3 activator in the context of stellation. Other recent studies in fibroblasts demonstrate altered, filopodia-rich morphologies for both Rac1 knockout (Steffen et al., 2013) and Arp2/3 complex depletion (Suraneni et al., 2012; Wu et al., 2012). The opposing morphological alterations upon Arp2/3 complex inactivation may indicate a differentially modulated morphology in fibroblasts compared to astrocytes. Nevertheless, Rac1 has been established to influence astrocytic morphology in culture (Racchetti et al., 2012). Additionally, Hou and coworkers demonstrated a direct interaction of cortactin with the Cdc42 guanine nucleotide exchange factor (GEF) Fgd1, influencing cell shape (Hou et al., 2003). Disruption of the domain responsible for the Fgd1 binding to cortactin led to an evident increase in filopodia in COS-7 cells. In the absence of cortactin, Fgd1 may not be properly targeted to the cell cortex, causing an increased amount of astrocytic filopodia,

which in turn leads to a larger perimeter of astrocytes. These findings may explain the slight shift towards an enlarged perimeter to area ratio of *cttn*$^{-/-}$ astrocytes, therefore suggesting cortactin as an upstream modulator of Cdc42 and Rac1 activitiy under basal conditions in astrocytes.

As a first striking result concerning the cellular role of cortactin in astrocytes, I showed an impaired proliferation rate in cultures of cortactin knockout astrocytes. Specifically, the onset of cell growth was delayed. These properties of reduced proliferation were also shown for Cx43 knockout astrocytes (Naus et al., 1997; Theis et al., 2004). Actin cytoskeleton dynamics are essential for the last step of the mitosis: the cytokinesis (for review (Fededa and Gerlich, 2012)). During cytokinesis, localized RhoA activity coordinates the formation of a contractile ring consisting of actin filaments with mixed polarities interacting with Myosin II. The formation of actin filaments is thought to rely on the formin mDia2 (Watanabe et al., 2008), while the activity of the Arp2/3 complex is repressed by the Rac1 GAP CYK-4 (Canman et al., 2008). However, in fibroblasts the loss of Arp3, disrupting the Arp2/3 complex, severely reduces the proliferation rate (Lahmann, personal communication). Furthermore, ARPC3 knockout fibroblast also exhibit a conspicuous accumulation of nuclei per cell (Suraneni et al., 2012), indicating a drastic defect in cytokinesis. Since the loss of cortactin did not lead to multinucleated cells, compensation by other NPFs is likely. Alternatively, cortactin may not serve as an NPF in this context. A recent publication, however, demonstrated cortactin as an interaction partner of the Rac1 GEF RCC2/TD60 (Grigera et al., 2012) in mitotic cells. This GEF is, as well as cortactin (Grigera et al., 2012), localized to the equatorial plate of dividing cells and involved in mitosis and cytokinesis (Mollinari et al., 2003). These data, along with the impairment of proliferation shown in this thesis, suggest cortactin as an upstream regulator of Rac1 activity during cytokinesis in astrocytes.

The analysis of the migration behavior of *cttn*$^{-/-}$ astrocytes revealed alterations in both velocity and consistency, which hint at a complex, cortactin dependent regulation of this process in astrocytes. Here, the results varied dependent on the applied technique for wound scratching into the cell monolayer. Inducing the migration by the classic *in vitro* scratch wound healing assay is assumed to set an additional stimulus by the generated cell debris which doesn't occur when using ibidi chambers. Different results in both assays therefore indicate that the induced migration of astrocytes is stimulus dependent and that the intracellular pathways used for the transduction of the respective stimulus rely on cortactin. Studies on the migration of *cttn*$^{-/-}$ fibroblasts, however, revealed a significant decrease of the wound healing rate to about 67,7% of the control cell population (Lai et al., 2009). This value is equivalent to the maximal wound closure rate obtained for *cttn*$^{-/-}$

astrocytes using the ibidi assay (70%). Due to the low number of independent experiments no significant reduction of the migration rate was achieved. However, the effect size is comparable to the results in fibroblasts. In contrast, the migration induced by scratching revealed opposing results. This leads to the assumption, that the stimulus set by the cell debris could compensate for the loss of cortactin in the signal transduction. Additionally, the expression of constitutively active Rac1 as well as Cdc42 restores the wound-healing rate of *cttn*$^{-/-}$ fibroblasts (Lai et al., 2009), indicating a function of cortactin in the activation of GTPases upon wounding. While Rac1 was demonstrated to be essential for migration of fibroblasts in the wound closure assay (Steffen et al., 2013), Cdc42 was important for astrocytic migration and polarity (Etienne-Manneville and Hall, 2001). More recently, Cdc42 depleted astrocytes were found to exhibit a migration phenotype characterized by a severe impairment of directed migration and orientation towards the wound, but only slightly impaired velocity and total migration distance (Robel et al., 2011). This phenotype hints at an additional influence of Rac. Rac1 signaling is essential for the response of astrocytes to hyaluronan, one of the major glycosaminoglycans important for tissue repair and astrocytic activation after CNS injury (Bourguignon et al., 2007; Struve et al., 2005). In the study of Bourguignon and colleagues, treatment with hyaluronan markedly increased the wound closure rate of astrocytes, which was mediated by the phosphorylation of cortactin. This phosphorylation reduced the binding of cortactin to F-Actin, potentially resulting in a destabilization of the actin cytoskeleton necessary for cytoskeletal remodeling. Alternatively, the release of cortactin from the actin cytoskeleton makes it available to activate Rac1 and Cdc42. This mechanism could serve as a positive feedback loop, resulting in the directed migration towards the wound *in vitro* and *in vivo*. A mechanism relying on cortactin is further supported by the evident upregulation of cortactin in astrocytes close to induced brain lesions in mice (Decourt et al., 2005). Interestingly, also ARPC3 deficient fibroblasts were, though lacking lamellipodia, still capable of performing directional migration towards an induced scratch wound (Suraneni et al., 2012). The migration behavior was largely characterized by a severely impaired directionality together with a minor effect on the velocity of the cells, which resembles the phenotype of Cdc42 depleted astrocytes (Robel et al., 2011). Cortactin knock out astrocytes, in contrast to ARPC3 deficient fibroblast, exhibit a largely normal morphology of the leading edge. The validity of this comparison is of course restricted by differential leading edge structures in both cell types (Etienne-Manneville, 2004). A reduced Arp2/3 complex activation upon cortactin depletion could also not explain the differences in the results of the two migration assay techniques. Consequently, the role of cortactin as activator for the Arp2/3 in astrocytic migration remains elusive. Interestingly, various studies demonstrate a decreased motility for Cx43

loss-of-function approaches in different eukaryotic cells (Bates et al., 2007; Cina et al., 2009; Elias et al., 2007; Francis et al., 2011; Fushiki et al., 2003; Wei et al., 2005). These findings promote an interdependence of cortactin and Cx43 also in the context of migration. Conversely, several publications reveal the loss of Cx43 to enhance over all migration (Olk et al., 2010; Qiu et al., 2003; Simpson et al., 2008). Among them, Simpson and colleagues (2008) describe a disorganized, non-polarized mode of migration. This finding is indicative for an interdependence of the Cdc42-Arp2/3 pathway and Cx43. In the same study a loss-of-function approach directed against cortactin did not reveal a phenotype. Yet, since they used the mammary epithelial cell line MCF-10A, the results may vary due to cell type differences. In summary, cortactin is indicated as an upstream activator of the small GTPases Cdc42 and Rac1 in the context of induced astrocytic migration *in vitro* and *in vivo*.

Nevertheless, the depletion of cortactin was also found to impair actin network turnover, thereby indicating an additional role of cortactin as activator of the Arp2/3 complex in astrocytes. Arp2/3 dependent actin turnover in spines of pyramidal neurons was addressed in a recent study (Kim et al., 2013), demonstrating drastically impaired actin dynamics upon Cre mediated Arp2/3 depletion. Consequently, genetic deletion of cortactin is indicated to have similar effects on actin dynamics if the activation of Arp2/3 in this cellular context is reliant on cortactin. The severity of the impairment is consistent with cortactin being an activator of Arp2/3 among others, modulating the actin dynamics in resting astrocytes. Interestingly, analysis of actin fluorescence recovery in cortactin deficient fibroblasts revealed an increased network turnover (Lai et al., 2009). This finding suggests cortactin as a stabilizer of the branched actin network in lamellipodia. Accordingly, cortactin displays an equal distribution throughout the lamellipodial actin network in fibroblasts (Lai et al., 2008). Cortactin was also postulated as inhibitor of cofilin activity in both lamellipodia and invadopodia of cancer cell lines (Oser and Condeelis, 2009). Consequently, the loss of cortactin should result in a higher percentage of active cofilin and therefore, in an increased actin network turnover, as the knockdown of cofilin leads to reduced actin dynamics both in fibroblasts and dendritic spines (Hotulainen et al., 2009; Hotulainen et al., 2005). Alternatively, an enlarged pool of active cofilin could also decrease the actin turnover rate, since a high amount of cofilin was shown to stabilize actin filaments (Andrianantoandro and Pollard, 2006). Taken together, cortactin regulates the actin dynamics of astrocytes, most likely as Arp2/3 activator. Additionally, it fulfils an evident cellular function in the regulation of small GTPases in astrocytes.

4.2.2. Loss of cortactin impairs intercellular calcium signaling

Several lines of evidence reveal astrocytic gap junctional coupling to be reliant on the integrity of the microfilament system (Cotrina et al., 1998; Wang and Rose, 1995; Yamane et al., 2002). However, the persistence of Cx43 positive puncta upon pharmacological destruction of actin filaments indicates an indirect interaction between actin filaments and connexin43 (Cotrina et al., 1998). Since cortactin physically interacts with both actin filaments and Cx43 (Vitale et al., 2009), the attenuated calcium wave properties of *cttn*$^{-/-}$ astrocytes demonstrated in this thesis are consequential.

Initial analysis of the subcellular distribution of both cortactin and Cx43 revealed a partial colocalization in astrocytes. This finding supports a physical interaction of these two proteins in our model system and is in line with the results of Vitale and colleagues (2009). Nevertheless, the colocalization was only observable for a relatively low percentage of Cx43 positive puncta at the cell cortex, hinting at a temporally and locally restricted interaction. These results contradict a role of cortactin in the transport of connexons to the cell cortex. Some noticeable progress has been made in the elucidation of the molecular mechanisms accomplishing the transport of connexons to the cell periphery. This process was demonstrated to be reliant on kinesins and microtubules (Fort et al., 2011; Shaw et al., 2007), but also on actin (Smyth et al., 2012; Theiss, 2002). Smyth and coworkers postulated a 'pausing en route'-concept, where Cx43 vesicles rest in colocalization with F-Actin (Smyth et al., 2012). These rests could either be an actin coordinated transition between different microtubules or some kind of a storage pool for connexins at the cell periphery, comparable to the reserve pool at presynaptic structures (Rizzoli and Betz, 2005). The transition of vesicles from the microfilament system to microtubules relies on the microtubule plus end binding protein EB1 (Wu et al., 2005). Additionally, siRNA mediated knockdown of Cx43 in astrocytes revealed an increase in the protein amounts of tubulin and EB1, hinting at a compensatory enhancement of Cx43 transport (Olk et al., 2010). Since cortactin also interacts with EB1 (Biosse Duplan et al., 2014) in addition to F-actin and Cx43, a disturbed transition of the Cx43 containing vesicles at these resting points would be a potential consequence, in turn altering the transport properties to the cell periphery. Yet, an accumulation of Cx43 plaques in the cytoplasma arrested in a transition position was not observed in *cttn*$^{-/-}$ astrocytes. The assumption of a connexin vesicle storage pool, anchored at the cortical actin cytoskeleton could implicate cortactin as the respective anchoring molecule. Consequently, this storage pool would be dislocated, less stable or less accessible in case of stimuli in *cttn*$^{-/-}$ astrocytes. No obvious alteration in the location of Cx43 puncta was observed, requiring a further analysis of Cx43 puncta localization at a higher resolution in both wild type and cortactin knockout astrocytes. A reduced stability is in line with the slight reduction of Cx43 plaques in *cttn*$^{-/-}$

astrocytes, restored by the expression of recombinant cortactin. A more drastic phenotype was potentially prevented by the anchoring of Cx43 via zonula occludens 1 (ZO-1), which was reported for cardiac myocytes (Zemljic-Harpf et al., 2014). The accessibility of Cx43 upon stimuli was not investigated in this thesis; therefore a role of cortactin in the release on demand remains elusive. The localized interaction at the cell cortex could also hint at either a role of cortactin in the regulation of the correct positioning or a role in the organization of connexons to gap junctional plaques. The process of Cx43 clustering was shown to be dependent on microfilaments but not on microtubules, while already existent cluster were persistent upon pharmacological interference with actin dynamics (Cotrina et al., 1998; Derangeon et al., 2008; Wang and Rose, 1995). Nonetheless, the Cx43 puncta size was not altered in *cttn*$^{-/-}$ astrocytes. In summary, the results on the localization of Cx43 in dependence of cortactin do not suggest a specific function of cortactin in the structural organization of Cx43.

Undeniably, however, the lack of cortactin has functional consequences on the intercellular communication of astrocytes. Gap junctional coupling in interdependence with F-actin was also analyzed in cardiac myocytes, where the connectivity was increased by the pharmacological stabilization of actin filaments (Derangeon et al., 2008). Taking the generally impaired calcium wave properties and the increase in the stable F-actin fraction of *cttn*$^{-/-}$ astrocytes into account, these results appear contradictory. The decrease in actin network turnover should consequently result in an increased gap junctional coupling. These results suggest a function of cortactin in gap junctional coupling independent of its role as modulator of actin dynamics in astrocytes. Of course, the findings in cardiac myocytes cannot rule out the possibility of different molecular mechanisms applying for astrocytes. The functional inhibition of gap junctional communication was demonstrated to alter actin organization in astrocytes (Yamane et al., 2002). However, one of the applied chemical inhibitors was even suggested to alter cellular calcium signaling (Venance et al., 1998), which was used as functional readout (Yamane et al., 2002). Nevertheless, these studies support the general hypothesis of a very close relationship between actin dynamics and gap junctional communication in astrocytes. In this context, the increase of both the number of Cx43 puncta and the ICW velocity upon expression of recombinant cortactin in knock out cultures suggests a direct link between these two events and the presence of cortactin. Yet, in case of the calcium wave velocity, the expression of recombinant cortactin does not completely restore the wild type values. This finding hints at a cellular function of cortactin in the assembly of cell-cell-contacts. The duration of the expression of recombinant cortactin may be sufficient to increase the amount of Cx43 puncta, but the clustering and therefore the establishment of functional gap junctions

might take longer. This would be in line with a microfilament dependent transport (Theiss, 2002) and clustering process of Cx43 (Wang and Rose, 1995).

In contrast to non-physiological dye coupling experiments, the measurement of intercellular calcium waves has the advantage of having physiological relevance (Frisch et al., 2003; Kuga et al., 2011). Beside gap junctions the signal transduction pathway downstream of purinoreceptors is also responsible for the spreading of calcium waves and acts in parallel (Scemes and Giaume, 2006). To exclude cortactin in the signal transduction downstream of purinoreceptors, suramin was used as broad spectrum antagonist. Along with several other studies (Bowser and Khakh, 2007; Cotrina et al., 1998; Kuga et al., 2011; Yamane et al., 2002), application of suramin reduced ICWs. As the impairment of ICWs in *cttn*$^{-/-}$ astrocytes was found to be persistent in the presence of suramin, an involvement of cortactin in the downstream signaling of P2 receptors can be ruled out.

Since astrocytes express various amounts of different connexins (Giaume and Liu, 2012; Theis and Giaume, 2012), despite the loss of their major connexin Cx43 they still exhibit residual calcium wave spreading (Naus et al., 1997) and dye coupling (Theis et al., 2004). To exclude a participation of connexin 30 in the function of cortactin in astrocytic communication the Cx43 specific mimetic peptide Gap27 (Berthoud et al., 2000; Warner et al., 1995), described as inhibitor gap junctional dye transfer (Chaytor et al., 1999) and ICWs (Boitano and Evans, 2000; Isakson et al., 2001), was used to inhibit Cx43 dependent ICWs. Interestingly, the application of gap27 solely reduced the calcium wave velocity in wild type cultures, thereby revealing a functional interaction of cortactin and Cx43 in astrocytes. Gap27 was shown to also inhibit the function of connexin hemichannels (CxHc) already after 10 - 30 min after application (Leybaert et al., 2003). However, inhibition of functional gap junctions was shown to be much slower >1 h (Evans et al., 2006). In this study, the calcium wave velocity was determined for the time frame of 30 min to 90 min of gap27 application. Conclusively, the observed decrease is rather due to the inhibition of Cx43 hemichannels than to the inhibition of fully functional gap junctional channels. This time period was chosen to exclude the possibility of harming the cells by the lacking flow and the consequently reduced supply of fresh buffer. To ensure cortactin to interact functionally with gap junctions, the peptide should be applied for a prolonged period of time. For instance, 72 h treatment with gap27 inhibits the expression of GLT-1, the major glutamate transporter in adult cortical astrocytes (Figiel et al., 2007). However, also an interaction of cortactin with CxHcs is of interest for astrocytic communication and physiology. CxHcs are delivered to the plasma membrane, as earlier mentioned, in a microfilament and microtubules dependent manner (Fort et al., 2011;

Smyth et al., 2012). Arrived at the membrane, they diffuse laterally and subsequently establish a gap junction with another CxHc located on an adjacent cell. These channels provide a pathway for cellular release of for instance ATP and glutamate, regulated by cytosolic Ca^{2+} changes (details in (Evans et al., 2006)). These findings hint at a molecular mechanism involving cortactin mediated modulation of Cx43 in both glia-glia as well as neuron-glia intercellular communication.

In summary, cortactin is indicated to be a major modulator of essential astrocytic functions by regulating actin dynamics, activity of small GTPases and connexin mediated intercellular communication.

4.3. Conclusions for the neuron-glia partnership

Astrocytes are emerging as essential elements of neural circuits in the mammalian brain. Recent publications reveal astrocytes to contribute to virtually every aspect of neuronal structure and function (for review (Clarke and Barres, 2013; Eroglu and Barres, 2010; Orellana et al., 2012). Thus, the following section will be dedicated to illuminate the consequences of the presented results for the interaction between astrocytes and neurons.

4.3.1. Astrocytes in the development and maturation of synapses

The importance of astrocytes to the development of synapses was first proven by the use of astrocyte-free cultures of retinal ganglion cells (Pfrieger and Barres, 1997). Here, the synaptic efficacy was dramatically increased in the presence of astrocytes *in vitro*. Moreover, astrocytes refine their processes concurrently to the period of synaptogenesis (Ullian et al., 2001), using both secreted and contact-mediated signals to influence the newly borne synapse. Recent studies confirmed the crucial role of astrocytes for the synaptogenesis of hippocampal (Hughes et al., 2010; Xu et al., 2010) and cortical neurons (Diniz et al., 2012). Thus, profilin isoforms are implicated to modulate synaptogenesis by regulating the structural association between both cell types during development. Furthermore, astrocytes occupy distinct anatomical domains, only overlapping each other by around 5% (Bushong et al., 2002; Ogata and Kosaka, 2002). Since PFN2a modulates the volume of astrocytes in tissue, it influences the size of the occupied anatomical domains. Therefore, also the amount of synapses reached by a single astrocyte is regulated by PFN2a. Moreover, local astrocytic contact elevates synaptic activity and increased the overall amount of excitatory synapses (Hama et al., 2004). Astrocytes furthermore express a variety of genes implicated in phagocytosis (Cahoy et al., 2008; Doyle et al., 2008; Lovatt et al., 2007), suggesting a phagocytic, synapse pruning function in the brain (Clarke and Barres, 2013). Among these genes, Rac1 is important to rearrange the actin cytoskeleton upon surrounding of cell debris (Ziegenfuss et al., 2012). Since Rac1-dependent regulation of actin dynamics likely involves profilins and PFN2a was shown to interact with the endocytotic machinery in neurons (Gareus et al., 2006), a role of profilins in the putative synaptic pruning function of astrocytes is indicated. Moreover, cortactin influences Rac1 activity levels and may consequently alter the synaptic pruning activity of astrocytes. The lack of astrocytic PFN2a may also contribute to the documented hyperexcitability and increased synapse size in PFN2a$^{-/-}$ mice (Pilo Boyl et al., 2007). Since PFN2a knock out astrocytes will exhibit a reduced motility of processes and a reduced size, glutamate clearance may be reduced, resulting in elevated synaptic excitability. In summary, astrocytic profilins are indicated as pivotal modulators of

synapse development and maturation. Nevertheless, also cortactin may influence synaptogenesis by altering actin dynamics in astrocytic processes or modulation of astrocytic signaling cascades.

4.3.2. Astrocytes in learning and memory

Astrocytes have been reported to affect both the encoding as well as the consolidation of memory. Recent studies revealed astrocytes to actively participate in several forms of synaptic plasticity, for instance cholinergic induced long-term potentiation (Navarrete et al., 2012) in cortex and hippocampus or hippocampal long-term depression and working memory (Han et al., 2012). Furthermore, astrocyte-neuron lactate transport is required for long-term memory formation, illustrating the role of astrocytic metabolic support for memory processes (Suzuki et al., 2011). The interaction of PAPs and spines is almost exclusive to those having an opposed presynapse (Lehre and Rusakov, 2002). Moreover, around 60% of spines are contacted by dynamic astrocytic protusions (Ventura and Harris, 1999). They protrude and retract in response to stimuli (Genoud et al., 2006), thereby altering synaptic transmission (Oliet et al., 2001). Changes in synaptic coverage by PAPs performed by involving profilins would consequently alter synaptic plasticity. As both profilin isoforms are linked to stimulus dependent motility of astrocytic processes, a transduction of neuronal signals to the astrocytic cytoskeleton mediated by profilins is indicated. Moreover, astrocytic gap junctional coupling by Cx43 and Cx30 is established as crucial determinant in the regulation of neuronal circuits and behavior (Pannasch et al., 2014; Pannasch and Rouach, 2013). Modulation of astrocytic interconnectivity by the interaction between cortactin and Cx43 thus may alter neuronal networks and animal behavior. Also Cx43 hemichannels fulfil a role under both physiological and pathological conditions. At basal conditions, hemichannels have a low open probability (Bennett et al., 2003), yet being able to release glutamate (Parpura et al., 2004) and ATP (Stout et al., 2002) into the intercellular space. Interestingly, treatment with amyloid-beta peptide dramatically increases hemichannel opening resulting in increased neuronal death, which is rescued by Cx43 deletion (Orellana et al., 2011; Orellana et al., 2012). Consequently, modification of connexin hemichannel physiology by the interaction with cortactin may have consequences for synaptic plasticity in both the healthy and the Alzheimer's brain.

These new insights into the cellular functions of profilins in astrocytes are summarized in the hypothetical model presented in Figure 4.3. Here, astrocytes expressing both profilin isoforms attain a complex morphology (Figure 4.3; A). Their small peripheral processes are highly dynamic, quickly responding to synaptic activity by profilin mediated actin cytoskeleton remodeling. Profilin depleted astrocytes, in contrast, occupy a reduced area and are less complex (Figure 4.3; B). Moreover, their PAPs exhibit a drastically reduced

motility, resulting in a slow interaction with the respective synapse. This may lead to altered synaptic properties.

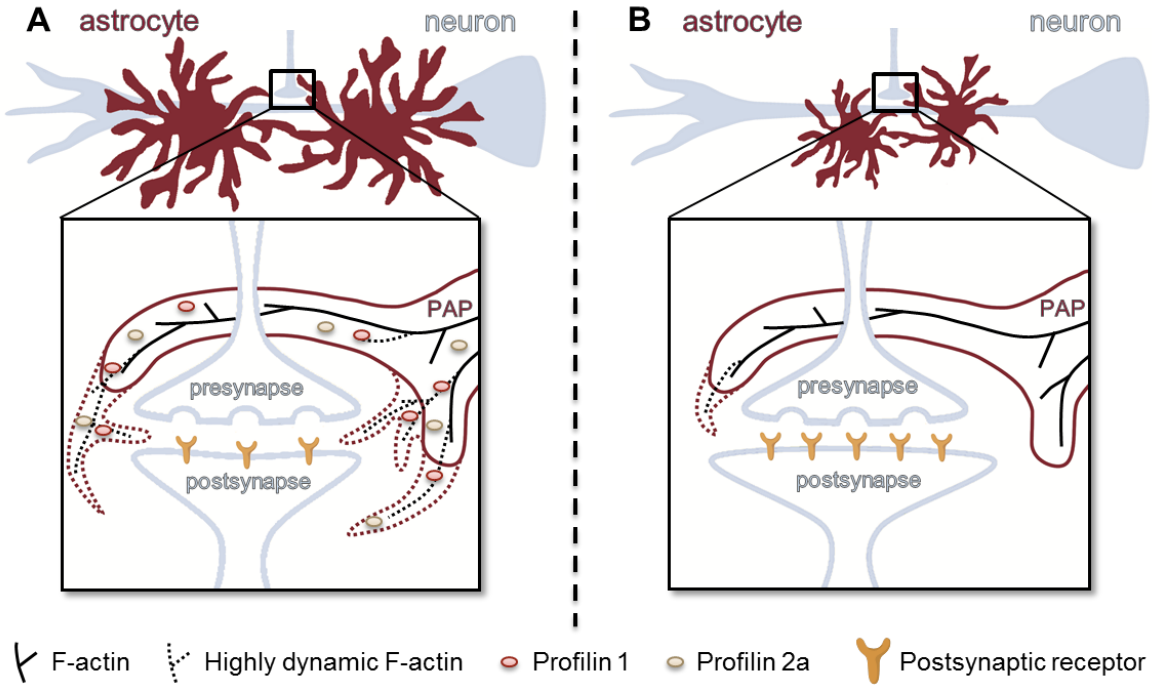

Figure 4.3 | Illustration of the proposed cellular function of profilins in glia-neuronal networks. (A) In the presence of all actin binding proteins, astrocytes are very complex and occupy large areas. Their highly motile processes (PAP) sense and modify synaptic input on the engulfed synapse. Profilins might regulate the motility of these processes either by direct binding to actin (PFN1) or by influencing its dynamics (PFN2a). **(B)** The absence of profilins results in a reduced size and complexity of astrocytes. Motility of astrocytic processes deficient of profilin isoforms is drastically reduced. This may lead to altered synaptic properties and plasticity.

4.4. Outlook

The results presented in this thesis provide starting points for the investigation of profilins and cortactin in glia-neuronal networks. Since only cultured astrocytes were analyzed in the current study, *in vivo* experiments are necessary to verify the obtained results. Moreover, the simultaneous depletion of both profilin isoforms is indispensable to confirm the cellular function of profilins in astrocytic morphology and motility.

4.4.1. Regulation of the astrocytic cytoskeleton

The expression of two profilin isoforms in astrocytes and their partly isoform-specific functions promote the further examination of the astrocytic role of PFN1 and PFN2a. Therefore, gene replacement constructs used for pyramidal neurons (Michaelsen et al., 2010) should be modified with an astrocyte-specific promoter to facilitate identification and targeted analysis of astrocytes in both dissociated cultures and slice cultures. Subsequently, rescue experiments with both profilin isoforms as well as actin-binding or PLP-binding deficient mutants would be helpful to refine and characterize the cellular functions of PFN1 and PFN2a in accordance to their interaction partners. Moreover, live imaging analysis of the motility of astrocytic processes in dependence on profilin isoforms will be mandatory. All the aforementioned experimental approaches should be repeated with a knockdown targeting both expressed profilin isoforms. This double knockdown appeared to drastically reduce the viability of the respective cells in this thesis. Consequently, an approach using mutant profilins as gene replacement could answer specific questions. The influence of profilin phosphorylation on the activity and interaction of PFN1 and PFN2a with isoform-specific ligands should be investigated. Since protein phosphorylation provides as fast time-scale modification of profilin activity, this mechanism is highly indicated in the context of plasticity in both neurons and astrocytes. Characterization of common as well as isoform-specific interaction partners of profilins in astrocytes would be crucial to gain insights into the respective signaling cascades and to further understand their cellular functions. After initial biochemical identification, the dynamics of the interaction could be monitored by FRET (**F**luorescence **R**esonance **E**nergy **T**ransfer) probes. FRET probes would also provide an interesting tool to evaluate the interaction of profilins with the cell membrane. Time lapse imaging could provide information of the temporal and stimulus dependent regulation of profilin isoforms by PIP_2. Especially for biochemical approaches, an alternative preparation of dissociated astrocytes by immunopanning closely resembling characteristics of *in vivo* astrocytes (Foo et al., 2011) would be interesting. Future structural and functional analysis should focus on astrocytes with *in vivo*-like morphology in slice cultures, since both the morphology and

the interconnection with neurons is preserved, while still permitting DNA-based modification methods.

Functional interdependence of cortactin and Cx43 in the intercellular communication of astrocytes encourages further analysis of the connection between the astrocytic cytoskeleton and gap junctions. Initially, the subcellular localization of Cx43 and Cx30 in slice cultures of cortactin knockout should be analyzed. Furthermore, alterations in the astrocytic coupling in *cttn*$^{-/-}$ astrocytes could be addressed by dual-patch-clamp (Ngezahayo et al., 2003Ngezahayo et al., 2003). Also the stability of Cx43 could be addressed using FRAP technique on GFP-labeled Cx43. Comparative fluorescence recovery analysis would indicate potential alterations in the turn-over of Cx43. Altogether, this could refine the phenotype of *cttn*$^{-/-}$ astrocytes. Using genetic calcium indicators driven by an astrocyte specific promoter and delivered by a virus, network characteristics of cortactin deficient astrocytes could be addressed in slice cultures. Thus, new insights into the molecular mechanism underlying astrocytic interconnectivity could be gained.

4.4.2. Interaction between astrocytes and neurons

Slice cultures generally provide the advantage of the concurrent analysis of interconnected astrocytes and neurons. Nevertheless, they are still an *in vitro* model, not necessarily preserving every aspect of the *in vivo* situation. Impaired motility of astrocytic processes by the downregulation of profilin isoforms suggests the investigation of the functional interdependence of profilin regulated motility and synaptic plasticity. Live imaging experiments under both basal and stimulated conditions could offer new insights into the dynamics of the tripartite synapse with focus on the actin cytoskeleton. Functional discrimination between PFN1 and PFN2a should also be targeted in the context of glia-neuronal interaction. Targeted modification of either neurons or astrocytes by the use of cell type-specific promoters offer the possibility to alter the properties of distinct parts of the tripartite synapse directly.

Slice cultures of *cttn*$^{-/-}$ animals can be used to analyze cortactin deficient neurons and astrocytes simultaneously. Rescue experiments by targeted viral delivery of recombinant cortactin in the mature circuits could elucidate the adaptation of glia-neuronal networks in dependence on cortactin. Furthermore, calcium imaging of these slices could illuminate the functional consequences of cortactin loss on the intercellular communication in an intact network of astrocytes and neurons.

To sum up, coordinated regulation of the cytoskeleton within the tripartite synapse and the organization of astrocytes to glial networks in particular still hold fascinating secrets to unravel for future research.

5. Reference List

Abe, K. and Misawa, M. (2003). Astrocyte stellation induced by Rho kinase inhibitors in culture. *Developmental Brain Research* **143**, 99-104.

Ackermann, M. and Matus, A. (2003). Activity-induced targeting of profilin and stabilization of dendritic spine morphology. *Nat Neurosci* **6**, 1194-200.

Aguilera, M. O., Beron, W. and Colombo, M. I. (2012). The actin cytoskeleton participates in the early events of autophagosome formation upon starvation induced autophagy. *Autophagy* **8**, 1590-603.

Allen, N. J. and Barres, B. A. (2009). Neuroscience: Glia - more than just brain glue. *Nature* **457**, 675-7.

Ammer, A. G. and Weed, S. A. (2008). Cortactin branches out: roles in regulating protrusive actin dynamics. *Cell Motil Cytoskeleton* **65**, 687-707.

Andre, C., Dos Santos, G. and Koulakoff, A. (1994). Muscarinic receptor profiles of mouse brain astrocytes in culture vary with their tissue of origin but differ from those of neurons. *Eur J Neurosci* **6**, 1702-9.

Andrianantoandro, E. and Pollard, T. D. (2006). Mechanism of actin filament turnover by severing and nucleation at different concentrations of ADF/cofilin. *Mol Cell* **24**, 13-23.

Andriezen, W. L. (1893). The Neuroglia Elements in the Human Brain. *Br Med J* **2**, 227-30.

Araque, A., Carmignoto, G., Haydon, P. G., Oliet, S. H., Robitaille, R. and Volterra, A. (2014). Gliotransmitters travel in time and space. *Neuron* **81**, 728-39.

Arrington, D. D. and Schnellmann, R. G. (2008). Targeting of the molecular chaperone oxygen-regulated protein 150 (ORP150) to mitochondria and its induction by cellular stress. *Am J Physiol Cell Physiol* **294**, C641-50.

Bae, Y. H., Ding, Z., Zou, L., Wells, A., Gertler, F. and Roy, P. (2009). Loss of profilin-1 expression enhances breast cancer cell motility by Ena/VASP proteins. *J Cell Physiol* **219**, 354-64.

Balendran, A., Biondi, R. M., Cheung, P. C., Casamayor, A., Deak, M. and Alessi, D. R. (2000). A 3-phosphoinositide-dependent protein kinase-1 (PDK1) docking site is required for the phosphorylation of protein kinase Czeta (PKCzeta) and PKC-related kinase 2 by PDK1. *J Biol Chem* **275**, 20806-13.

Baorto, D. M., Mellado, W. and Shelanski, M. L. (1992). Astrocyte process growth induction by actin breakdown. *J Cell Biol* **117**, 357-67.

Barry, F. A. and Gibbins, J. M. (2002). Protein kinase B is regulated in platelets by the collagen receptor glycoprotein VI. *J Biol Chem* **277**, 12874-8.

Bates, D. C., Sin, W. C., Aftab, Q. and Naus, C. C. (2007). Connexin43 enhances glioma invasion by a mechanism involving the carboxy terminus. *Glia* **55**, 1554-64.

Bennett, M. V., Contreras, J. E., Bukauskas, F. F. and Saez, J. C. (2003). New roles for astrocytes: gap junction hemichannels have something to communicate. *Trends Neurosci* **26**, 610-7.

Benziane, B., Bjornholm, M., Lantier, L., Viollet, B., Zierath, J. R. and Chibalin, A. V. (2009). AMP-activated protein kinase activator A-769662 is an inhibitor of the Na(+)-K(+)-ATPase. *Am J Physiol Cell Physiol* **297**, C1554-66.

Berthoud, V. M., Beyer, E. C. and Seul, K. H. (2000). Peptide inhibitors of intercellular communication. *Am J Physiol Lung Cell Mol Physiol* **279**, L619-22.

Bhutia, S. K., Kegelman, T. P., Das, S. K., Azab, B., Su, Z. Z., Lee, S. G., Sarkar, D. and Fisher, P. B. (2010). Astrocyte elevated gene-1 induces protective autophagy. *Proc Natl Acad Sci U S A* **107**, 22243-8.

Biosse Duplan, M., Zalli, D., Stephens, S., Zenger, S., Neff, L., Oelkers, J. M., Lai, F. P., Horne, W., Rottner, K. and Baron, R. (2014). Microtubule dynamic instability controls podosome patterning in osteoclasts through EB1, cortactin, and Src. *Mol Cell Biol* **34**, 16-29.

Boitano, S. and Evans, W. H. (2000). Connexin mimetic peptides reversibly inhibit Ca(2+) signaling through gap junctions in airway cells. *Am J Physiol Lung Cell Mol Physiol* **279**, L623-30.

Böning, A. T. (2012). Charakterisierung der Interaktion von Profilin 2a und der Proteinkinase M zeta im zellulären Kontext.

Bottcher, R. T., Wiesner, S., Braun, A., Wimmer, R., Berna, A., Elad, N., Medalia, O., Pfeifer, A., Aszodi, A., Costell, M. et al. (2009). Profilin 1 is required for abscission during late cytokinesis of chondrocytes. *EMBO J* **28**, 1157-69.

Bourguignon, L. Y., Gilad, E., Peyrollier, K., Brightman, A. and Swanson, R. A. (2007). Hyaluronan-CD44 interaction stimulates Rac1 signaling and PKN gamma kinase activation leading to cytoskeleton function and cell migration in astrocytes. *J Neurochem* **101**, 1002-17.

Bouzakri, K., Zachrisson, A., Al-Khalili, L., Zhang, B. B., Koistinen, H. A., Krook, A. and Zierath, J. R. (2006). siRNA-based gene silencing reveals specialized roles of IRS-1/Akt2 and IRS-2/Akt1 in glucose and lipid metabolism in human skeletal muscle. *Cell Metab* **4**, 89-96.

Bowden, E. T., Onikoyi, E., Slack, R., Myoui, A., Yoneda, T., Yamada, K. M. and Mueller, S. C. (2006). Co-localization of cortactin and phosphotyrosine identifies active invadopodia in human breast cancer cells. *Exp Cell Res* **312**, 1240-53.

Bowser, D. N. and Khakh, B. S. (2007). Vesicular ATP is the predominant cause of intercellular calcium waves in astrocytes. *J Gen Physiol* **129**, 485-91.

Braun, A., Aszodi, A., Hellebrand, H., Berna, A., Fassler, R. and Brandau, O. (2002). Genomic organization of profilin-III and evidence for a transcript expressed exclusively in testis. *Gene* **283**, 219-25.

Bravo-Cordero, J. J., Magalhaes, M. A., Eddy, R. J., Hodgson, L. and Condeelis, J. (2013). Functions of cofilin in cell locomotion and invasion. *Nat Rev Mol Cell Biol* **14**, 405-15.

Bryce, N. S., Clark, E. S., Leysath, J. L., Currie, J. D., Webb, D. J. and Weaver, A. M. (2005). Cortactin promotes cell motility by enhancing lamellipodial persistence. *Curr Biol* **15**, 1276-85.

Buffo, A., Rolando, C. and Ceruti, S. (2010). Astrocytes in the damaged brain: molecular and cellular insights into their reactive response and healing potential. *Biochem Pharmacol* **79**, 77-89.

Burnstock, G. and Knight, G. E. (2004). Cellular distribution and functions of P2 receptor subtypes in different systems. *Int Rev Cytol* **240**, 31-304.

Bushong, E. A., Martone, M. E., Jones, Y. Z. and Ellisman, M. H. (2002). Protoplasmic astrocytes in CA1 stratum radiatum occupy separate anatomical domains. *J Neurosci* **22**, 183-92.

Butt, A. M. (2011). ATP: a ubiquitous gliotransmitter integrating neuron-glial networks. *Semin Cell Dev Biol* **22**, 205-13.

Caglayan, E., Romeo, G. R., Kappert, K., Odenthal, M., Sudkamp, M., Body, S. C., Shernan, S. K., Hackbusch, D., Vantler, M., Kazlauskas, A. et al. (2010). Profilin-1 is expressed in human atherosclerotic plaques and induces atherogenic effects on vascular smooth muscle cells. *PLoS One* **5**, e13608.

Cahoy, J. D., Emery, B., Kaushal, A., Foo, L. C., Zamanian, J. L., Christopherson, K. S., Xing, Y., Lubischer, J. L., Krieg, P. A., Krupenko, S. A. et al. (2008). A transcriptome database for astrocytes, neurons, and oligodendrocytes: a new resource for understanding brain development and function. *J Neurosci* **28**, 264-78.

Campellone, K. G. and Welch, M. D. (2010). A nucleator arms race: cellular control of actin assembly. *Nat Rev Mol Cell Biol* **11**, 237-51.

Canman, J. C., Lewellyn, L., Laband, K., Smerdon, S. J., Desai, A., Bowerman, B. and Oegema, K. (2008). Inhibition of Rac by the GAP activity of centralspindlin is essential for cytokinesis. *Science* **322**, 1543-6.

Cao, H., Orth, J. D., Chen, J., Weller, S. G., Heuser, J. E. and McNiven, M. A. (2003). Cortactin is a component of clathrin-coated pits and participates in receptor-mediated endocytosis. *Mol Cell Biol* **23**, 2162-70.

Carlsson, L., Nystrom, L. E., Sundkvist, I., Markey, F. and Lindberg, U. (1977). Actin polymerizability is influenced by profilin, a low molecular weight protein in non-muscle cells. *J Mol Biol* **115**, 465-83.

Chaytor, A. T., Martin, P. E., Evans, W. H., Randall, M. D. and Griffith, T. M. (1999). The endothelial component of cannabinoid-induced relaxation in rabbit mesenteric artery depends on gap junctional communication. *J Physiol* **520 Pt 2**, 539-50.

Chen, Y. K. and Hsueh, Y. P. (2012). Cortactin-binding protein 2 modulates the mobility of cortactin and regulates dendritic spine formation and maintenance. *J Neurosci* **32**, 1043-55.

Cho, S. Y. and Klemke, R. L. (2002). Purification of pseudopodia from polarized cells reveals redistribution and activation of Rac through assembly of a CAS/Crk scaffold. *J Cell Biol* **156**, 725-36.

Cina, C., Maass, K., Theis, M., Willecke, K., Bechberger, J. F. and Naus, C. C. (2009). Involvement of the cytoplasmic C-terminal domain of connexin43 in neuronal migration. *J Neurosci* **29**, 2009-21.

Clarke, L. E. and Barres, B. A. (2013). Emerging roles of astrocytes in neural circuit development. *Nat Rev Neurosci* **14**, 311-21.

Cooper, J. A., Buhle, E. L., Jr., Walker, S. B., Tsong, T. Y. and Pollard, T. D. (1983). Kinetic evidence for a monomer activation step in actin polymerization. *Biochemistry* **22**, 2193-202.

Cornell-Bell, A. H., Finkbeiner, S. M., Cooper, M. S. and Smith, S. J. (1990). Glutamate induces calcium waves in cultured astrocytes: long-range glial signaling. *Science* **247**, 470-3.

Cosen-Binker, L. I. and Kapus, A. (2006). Cortactin: the gray eminence of the cytoskeleton. *Physiology (Bethesda)* **21**, 352-61.

Cotrina, M. L., Lin, J. H. and Nedergaard, M. (1998). Cytoskeletal assembly and ATP release regulate astrocytic calcium signaling. *J Neurosci* **18**, 8794-804.

Croce, C. M. (2008). Oncogenes and cancer. *N Engl J Med* **358**, 502-11.

Da Silva, J. S., Medina, M., Zuliani, C., Di Nardo, A., Witke, W. and Dotti, C. G. (2003). RhoA/ROCK regulation of neuritogenesis via profilin IIa-mediated control of actin stability. *J Cell Biol* **162**, 1267-79.

Dai, Y. P., Bongalon, S., Tian, H., Parks, S. D., Mutafova-Yambolieva, V. N. and Yamboliev, I. A. (2006). Upregulation of profilin, cofilin-2 and LIMK2 in cultured pulmonary artery smooth muscle cells and in pulmonary arteries of monocrotaline-treated rats. *Vascul Pharmacol* **44**, 275-82.

Davies, S. P., Reddy, H., Caivano, M. and Cohen, P. (2000). Specificity and mechanism of action of some commonly used protein kinase inhibitors. *Biochem J* **351**, 95-105.

Decourt, B., Bouleau, Y., Dulon, D. and Hafidi, A. (2005). Expression analysis of neuroleukin, calmodulin, cortactin, and Rho7/Rnd2 in the intact and injured mouse brain. *Brain Res Dev Brain Res* **159**, 36-54.

Del Puerto, A., Wandosell, F. and Garrido, J. J. (2013). Neuronal and glial purinergic receptors functions in neuron development and brain disease. *Front Cell Neurosci* **7**, 197.

del Río-Hortega, P. (1932). Microglia. *Cytology and Pathology of the Nervous System* **2**, 482-534.

del Río-Hortega, P. o. (1920). Estudios sobre la neuroglia. La microglía y su transformación en células en bastoncito y cuerpos gránulo-adiposos: [Madrid].

Derangeon, M., Bourmeyster, N., Plaisance, I., Pinet-Charvet, C., Chen, Q., Duthe, F., Popoff, M. R., Sarrouilhe, D. and Herve, J. C. (2008). RhoA GTPase and F-actin dynamically regulate the permeability of Cx43-made channels in rat cardiac myocytes. *J Biol Chem* **283**, 30754-65.

Dettori, R., Sonzogni, S., Meyer, L., Lopez-Garcia, L. A., Morrice, N. A., Zeuzem, S., Engel, M., Piiper, A., Neimanis, S., Frodin, M. et al. (2009). Regulation of the interaction between protein kinase C-related protein kinase 2 (PRK2) and its upstream kinase, 3-phosphoinositide-dependent protein kinase 1 (PDK1). *J Biol Chem* **284**, 30318-27.

Di Castro, M. A., Chuquet, J., Liaudet, N., Bhaukaurally, K., Santello, M., Bouvier, D., Tiret, P. and Volterra, A. (2011). Local Ca2+ detection and modulation of synaptic release by astrocytes. *Nat Neurosci* **14**, 1276-84.

Di Nardo, A., Gareus, R., Kwiatkowski, D. and Witke, W. (2000). Alternative splicing of the mouse profilin II gene generates functionally different profilin isoforms. *J Cell Sci* **113 Pt 21**, 3795-803.

Didry, D., Carlier, M. F. and Pantaloni, D. (1998). Synergy between actin depolymerizing factor/cofilin and profilin in increasing actin filament turnover. *J Biol Chem* **273**, 25602-11.

Dimitrova, D. S. (2006). Nuclear transcription is essential for specification of mammalian replication origins. *Genes Cells* **11**, 829-44.

Ding, Z., Bae, Y. H. and Roy, P. (2012). Molecular insights on context-specific role of profilin-1 in cell migration. *Cell Adh Migr* **6**, 442-9.

Ding, Z., Gau, D., Deasy, B., Wells, A. and Roy, P. (2009). Both actin and polyproline interactions of profilin-1 are required for migration, invasion and capillary morphogenesis of vascular endothelial cells. *Exp Cell Res* **315**, 2963-73.

Ding, Z., Lambrechts, A., Parepally, M. and Roy, P. (2006). Silencing profilin-1 inhibits endothelial cell proliferation, migration and cord morphogenesis. *J Cell Sci* **119**, 4127-37.

Diniz, L. P., Almeida, J. C., Tortelli, V., Vargas Lopes, C., Setti-Perdigao, P., Stipursky, J., Kahn, S. A., Romao, L. F., de Miranda, J., Alves-Leon, S. V. et al. (2012). Astrocyte-induced synaptogenesis is mediated by transforming growth factor beta signaling through modulation of D-serine levels in cerebral cortex neurons. *J Biol Chem* **287**, 41432-45.

Doyle, J. P., Dougherty, J. D., Heiman, M., Schmidt, E. F., Stevens, T. R., Ma, G., Bupp, S., Shrestha, P., Shah, R. D., Doughty, M. L. et al. (2008). Application of a translational profiling approach for the comparative analysis of CNS cell types. *Cell* **135**, 749-62.

Dupin, I. and Etienne-Manneville, S. (2011). Nuclear positioning: mechanisms and functions. *Int J Biochem Cell Biol* **43**, 1698-707.

El Sayegh, T. Y., Arora, P. D., Laschinger, C. A., Lee, W., Morrison, C., Overall, C. M., Kapus, A. and McCulloch, C. A. (2004). Cortactin associates with N-cadherin adhesions and mediates intercellular adhesion strengthening in fibroblasts. *J Cell Sci* **117**, 5117-31.

Elias, L. A., Wang, D. D. and Kriegstein, A. R. (2007). Gap junction adhesion is necessary for radial migration in the neocortex. *Nature* **448**, 901-7.

Engh, R. A., Girod, A., Kinzel, V., Huber, R. and Bossemeyer, D. (1996). Crystal structures of catalytic subunit of cAMP-dependent protein kinase in complex with isoquinolinesulfonyl protein kinase inhibitors H7, H8, and H89. Structural implications for selectivity. *J Biol Chem* **271**, 26157-64.

Epstein, D., Elias-Bishko, S. and Hershko, A. (1975). Requirement for protein synthesis in the regulation of protein breakdown in cultured hepatoma cells. *Biochemistry* **14**, 5199-204.

Eroglu, C. and Barres, B. A. (2010). Regulation of synaptic connectivity by glia. *Nature* **468**, 223-31.

Etienne-Manneville, S. (2004). Actin and microtubules in cell motility: which one is in control? *Traffic* **5**, 470-7.

Etienne-Manneville, S. (2013). Microtubules in cell migration. *Annu Rev Cell Dev Biol* **29**, 471-99.

Etienne-Manneville, S. and Hall, A. (2001). Integrin-mediated activation of Cdc42 controls cell polarity in migrating astrocytes through PKCzeta. *Cell* **106**, 489-98.

Etienne-Manneville, S. (2006). In Vitro Assay of Primary Astrocyte Migration as a Tool to Study Rho GTPase Function in Cell Polarization. **406**, 565-578.

Evans, W. H., De Vuyst, E. and Leybaert, L. (2006). The gap junction cellular internet: connexin hemichannels enter the signalling limelight. *Biochem J* **397**, 1-14.

Fan, Y., Arif, A., Gong, Y., Jia, J., Eswarappa, S. M., Willard, B., Horowitz, A., Graham, L. M., Penn, M. S. and Fox, P. L. (2012). Stimulus-dependent phosphorylation of profilin-1 in angiogenesis. *Nat Cell Biol* **14**, 1046-56.

Fededa, J. P. and Gerlich, D. W. (2012). Molecular control of animal cell cytokinesis. *Nat Cell Biol* **14**, 440-7.

Figiel, M., Allritz, C., Lehmann, C. and Engele, J. (2007). Gap junctional control of glial glutamate transporter expression. *Mol Cell Neurosci* **35**, 130-7.

Foo, L. C., Allen, N. J., Bushong, E. A., Ventura, P. B., Chung, W. S., Zhou, L., Cahoy, J. D., Daneman, R., Zong, H., Ellisman, M. H. et al. (2011). Development of a method for the purification and culture of rodent astrocytes. *Neuron* **71**, 799-811.

Fort, A. G., Murray, J. W., Dandachi, N., Davidson, M. W., Dermietzel, R., Wolkoff, A. W. and Spray, D. C. (2011). In vitro motility of liver connexin vesicles along microtubules utilizes kinesin motors. *J Biol Chem* **286**, 22875-85.

Francis, R., Xu, X., Park, H., Wei, C. J., Chang, S., Chatterjee, B. and Lo, C. (2011). Connexin43 modulates cell polarity and directional cell migration by regulating microtubule dynamics. *PLoS One* **6**, e26379.

Frisch, C., Theis, M., De Souza Silva, M. A., Dere, E., Sohl, G., Teubner, B., Namestkova, K., Willecke, K. and Huston, J. P. (2003). Mice with astrocyte-directed inactivation of connexin43 exhibit increased exploratory behaviour, impaired motor capacities, and changes in brain acetylcholine levels. *Eur J Neurosci* **18**, 2313-8.

Fujiwara, I., Takahashi, S., Tadakuma, H., Funatsu, T. and Ishiwata, S. (2002). Microscopic analysis of polymerization dynamics with individual actin filaments. *Nat Cell Biol* **4**, 666-73.

Fushiki, S., Perez Velazquez, J. L., Zhang, L., Bechberger, J. F., Carlen, P. L. and Naus, C. C. (2003). Changes in neuronal migration in neocortex of connexin43 null mutant mice. *J Neuropathol Exp Neurol* **62**, 304-14.

Gareus, R., Di Nardo, A., Rybin, V. and Witke, W. (2006). Mouse profilin 2 regulates endocytosis and competes with SH3 ligand binding to dynamin 1. *J Biol Chem* **281**, 2803-11.

Genoud, C., Quairiaux, C., Steiner, P., Hirling, H., Welker, E. and Knott, G. W. (2006). Plasticity of astrocytic coverage and glutamate transporter expression in adult mouse cortex. *PLoS Biol* **4**, e343.

Giaume, C., Fromaget, C., el Aoumari, A., Cordier, J., Glowinski, J. and Gros, D. (1991). Gap junctions in cultured astrocytes: single-channel currents and characterization of channel-forming protein. *Neuron* **6**, 133-43.

Giaume, C. and Liu, X. (2012). From a glial syncytium to a more restricted and specific glial networking. *J Physiol Paris* **106**, 34-9.

Goldman, J. E. and Abramson, B. (1990). Cyclic AMP-induced shape changes of astrocytes are accompanied by rapid depolymerization of actin. *Brain Res* **528**, 189-96.

Goley, E. D. and Welch, M. D. (2006). The ARP2/3 complex: an actin nucleator comes of age. *Nat Rev Mol Cell Biol* **7**, 713-26.

Gorlich, A., Zimmermann, A. M., Schober, D., Bottcher, R. T., Sassoe-Pognetto, M., Friauf, E., Witke, W. and Rust, M. B. (2012). Preserved morphology and physiology of excitatory synapses in profilin1-deficient mice. *PLoS One* **7**, e30068.

Gourine, A. V., Kasymov, V., Marina, N., Tang, F., Figueiredo, M. F., Lane, S., Teschemacher, A. G., Spyer, K. M., Deisseroth, K. and Kasparov, S. (2010). Astrocytes control breathing through pH-dependent release of ATP. *Science* **329**, 571-5.

Gozuacik, D. and Kimchi, A. (2004). Autophagy as a cell death and tumor suppressor mechanism. *Oncogene* **23**, 2891-906.

Grigera, P. R., Ma, L., Borgman, C. A., Pinto, A. F., Sherman, N. E., Parsons, J. T. and Fox, J. W. (2012). Mass spectrometric analysis identifies a cortactin-RCC2/TD60 interaction in mitotic cells. *J Proteomics* **75**, 2153-9.

Gronborg, M., Kristiansen, T. Z., Iwahori, A., Chang, R., Reddy, R., Sato, N., Molina, H., Jensen, O. N., Hruban, R. H., Goggins, M. G. et al. (2006). Biomarker discovery from pancreatic cancer secretome using a differential proteomic approach. *Mol Cell Proteomics* **5**, 157-71.

Haarer, B. K., Lillie, S. H., Adams, A. E., Magdolen, V., Bandlow, W. and Brown, S. S. (1990). Purification of profilin from Saccharomyces cerevisiae and analysis of profilin-deficient cells. *J Cell Biol* **110**, 105-14.

Haber, M., Zhou, L. and Murai, K. K. (2006). Cooperative astrocyte and dendritic spine dynamics at hippocampal excitatory synapses. *J Neurosci* **26**, 8881-91.

Halassa, M. M., Fellin, T., Takano, H., Dong, J. H. and Haydon, P. G. (2007). Synaptic islands defined by the territory of a single astrocyte. *J Neurosci* **27**, 6473-7.

Halassa, M. M., Florian, C., Fellin, T., Munoz, J. R., Lee, S. Y., Abel, T., Haydon, P. G. and Frank, M. G. (2009). Astrocytic modulation of sleep homeostasis and cognitive consequences of sleep loss. *Neuron* **61**, 213-9.

Hama, H., Hara, C., Yamaguchi, K. and Miyawaki, A. (2004). PKC signaling mediates global enhancement of excitatory synaptogenesis in neurons triggered by local contact with astrocytes. *Neuron* **41**, 405-15.

Hamby, M. E., Uliasz, T. F., Hewett, S. J. and Hewett, J. A. (2006). Characterization of an improved procedure for the removal of microglia from confluent monolayers of primary astrocytes. *J Neurosci Methods* **150**, 128-37.

Han, J., Kesner, P., Metna-Laurent, M., Duan, T., Xu, L., Georges, F., Koehl, M., Abrous, D. N., Mendizabal-Zubiaga, J., Grandes, P. et al. (2012). Acute cannabinoids impair working memory through astroglial CB1 receptor modulation of hippocampal LTD. *Cell* **148**, 1039-50.

Hansson, A., Skoglund, G., Lassing, I., Lindberg, U. and Ingelman-Sundberg, M. (1988). Protein kinase C-dependent phosphorylation of profilin is specifically stimulated by phosphatidylinositol bisphosphate (PIP2). *Biochem Biophys Res Commun* **150**, 526-31.

Hatten, M. E. (1985). Neuronal regulation of astroglial morphology and proliferation in vitro. *J Cell Biol* **100**, 384-96.

Haugwitz, M., Noegel, A. A., Karakesisoglou, J. and Schleicher, M. (1994). Dictyostelium amoebae that lack G-actin-sequestering profilins show defects in F-actin content, cytokinesis, and development. *Cell* **79**, 303-14.

Haydon, P. G. (2001). GLIA: listening and talking to the synapse. *Nat Rev Neurosci* **2**, 185-93.

Helwani, F. M., Kovacs, E. M., Paterson, A. D., Verma, S., Ali, R. G., Fanning, A. S., Weed, S. A. and Yap, A. S. (2004). Cortactin is necessary for E-cadherin-mediated contact formation and actin reorganization. *J Cell Biol* **164**, 899-910.

Henneberger, C., Papouin, T., Oliet, S. H. and Rusakov, D. A. (2010). Long-term potentiation depends on release of D-serine from astrocytes. *Nature* **463**, 232-6.

Hering, H. and Sheng, M. (2003). Activity-dependent redistribution and essential role of cortactin in dendritic spine morphogenesis. *J Neurosci* **23**, 11759-69.

Hershko, A. and Tomkins, G. M. (1971). Studies on the degradation of tyrosine aminotransferase in hepatoma cells in culture. Influence of the composition of the medium and adenosine triphosphate dependence. *J Biol Chem* **246**, 710-4.

Hodgkinson, C. P. and Sale, G. J. (2002). Regulation of both PDK1 and the phosphorylation of PKC-zeta and -delta by a C-terminal PRK2 fragment. *Biochemistry* **41**, 561-9.

Honore, B., Madsen, P., Andersen, A. H. and Leffers, H. (1993). Cloning and expression of a novel human profilin variant, profilin II. *FEBS Lett* **330**, 151-5.

Hotulainen, P., Llano, O., Smirnov, S., Tanhuanpaa, K., Faix, J., Rivera, C. and Lappalainen, P. (2009). Defining mechanisms of actin polymerization and depolymerization during dendritic spine morphogenesis. *J Cell Biol* **185**, 323-39.

Hotulainen, P., Paunola, E., Vartiainen, M. K. and Lappalainen, P. (2005). Actin-depolymerizing factor and cofilin-1 play overlapping roles in promoting rapid F-actin depolymerization in mammalian nonmuscle cells. *Mol Biol Cell* **16**, 649-64.

Hou, P., Estrada, L., Kinley, A. W., Parsons, J. T., Vojtek, A. B. and Gorski, J. L. (2003). Fgd1, the Cdc42 GEF responsible for Faciogenital Dysplasia, directly interacts with cortactin and mAbp1 to modulate cell shape. *Hum Mol Genet* **12**, 1981-93.

Hu, E., Chen, Z., Fredrickson, T. and Zhu, Y. (2001). Molecular cloning and characterization of profilin-3: a novel cytoskeleton-associated gene expressed in rat kidney and testes. *Exp Nephrol* **9**, 265-74.

Huang, S., McDowell, J. M., Weise, M. J. and Meagher, R. B. (1996). The Arabidopsis profilin gene family. Evidence for an ancient split between constitutive and pollen-specific profilin genes. *Plant Physiol* **111**, 115-26.

Hughes, E. G., Elmariah, S. B. and Balice-Gordon, R. J. (2010). Astrocyte secreted proteins selectively increase hippocampal GABAergic axon length, branching, and synaptogenesis. *Mol Cell Neurosci* **43**, 136-45.

Hummel, T., Leifker, K. and Klambt, C. (2000). The Drosophila HEM-2/NAP1 homolog KETTE controls axonal pathfinding and cytoskeletal organization. *Genes Dev* **14**, 863-73.

Hussey, P. J., Ketelaar, T. and Deeks, M. J. (2006). Control of the actin cytoskeleton in plant cell growth. *Annu Rev Plant Biol* **57**, 109-25.

Iguchi, H., Mitsui, T., Ishida, M., Kanba, S. and Arita, J. (2011). cAMP response element-binding protein (CREB) is required for epidermal growth factor (EGF)-induced cell proliferation and serum response element activation in neural stem cells isolated from the forebrain subventricular zone of adult mice. *Endocr J* **58**, 747-59.

Iki, J., Inoue, A., Bito, H. and Okabe, S. (2005). Bi-directional regulation of postsynaptic cortactin distribution by BDNF and NMDA receptor activity. *Eur J Neurosci* **22**, 2985-94.

Isakson, B. E., Evans, W. H. and Boitano, S. (2001). Intercellular Ca2+ signaling in alveolar epithelial cells through gap junctions and by extracellular ATP. *Am J Physiol Lung Cell Mol Physiol* **280**, L221-8.

Janke, J., Schluter, K., Jandrig, B., Theile, M., Kolble, K., Arnold, W., Grinstein, E., Schwartz, A., Estevez-Schwarz, L., Schlag, P. M. et al. (2000). Suppression of tumorigenicity in breast cancer cells by the microfilament protein profilin 1. *J Exp Med* **191**, 1675-86.

Jin, H. Y., Song, B., Oudit, G. Y., Davidge, S. T., Yu, H. M., Jiang, Y. Y., Gao, P. J., Zhu, D. L., Ning, G., Kassiri, Z. et al. (2012). ACE2 deficiency enhances angiotensin II-mediated aortic profilin-1 expression, inflammation and peroxynitrite production. *PLoS One* **7**, e38502.

Jockusch, B. M., Murk, K. and Rothkegel, M. (2007). The profile of profilins. *Rev Physiol Biochem Pharmacol* **159**, 131-49.

Kaksonen, M., Peng, H. B. and Rauvala, H. (2000). Association of cortactin with dynamic actin in lamellipodia and on endosomal vesicles. *J Cell Sci* **113 Pt 24**, 4421-6.

Kase, H., Iwahashi, K., Nakanishi, S., Matsuda, Y., Yamada, K., Takahashi, M., Murakata, C., Sato, A. and Kaneko, M. (1987). K-252 compounds, novel and potent inhibitors of protein kinase C and cyclic nucleotide-dependent protein kinases. *Biochem Biophys Res Commun* **142**, 436-40.

Keezer, S. M. and Gilbert, D. M. (2002). Sensitivity of the origin decision point to specific inhibitors of cellular signaling and metabolism. *Exp Cell Res* **273**, 54-64.

Kettenmann, H. and Verkhratsky, A. (2011). [Neuroglia--living nerve glue]. *Fortschr Neurol Psychiatr* **79**, 588-97.

Kim, I. H., Racz, B., Wang, H., Burianek, L., Weinberg, R., Yasuda, R., Wetsel, W. C. and Soderling, S. H. (2013). Disruption of Arp2/3 results in asymmetric structural plasticity of dendritic spines and progressive synaptic and behavioral abnormalities. *J Neurosci* **33**, 6081-92.

Kinnunen, T., Kaksonen, M., Saarinen, J., Kalkkinen, N., Peng, H. B. and Rauvala, H. (1998). Cortactin-Src kinase signaling pathway is involved in N-syndecan-dependent neurite outgrowth. *J Biol Chem* **273**, 10702-8.

Kitamura, Y., Kitamura, T., Sakaue, H., Maeda, T., Ueno, H., Nishio, S., Ohno, S., Osada, S., Sakaue, M., Ogawa, W. et al. (1997). Interaction of Nck-associated protein 1 with activated GTP-binding protein Rac. *Biochem J* **322 (Pt 3)**, 873-8.

Koyama, Y., Fukuda, T. and Baba, A. (1996). Inhibition of vanadate-induced astrocytic stress fiber formation by C3 ADP-ribosyltransferase. *Biochem Biophys Res Commun* **218**, 331-6.

Kuga, N., Sasaki, T., Takahara, Y., Matsuki, N. and Ikegaya, Y. (2011). Large-scale calcium waves traveling through astrocytic networks in vivo. *J Neurosci* **31**, 2607-14.

Kullmann, J. A., Neumeyer, A., Gurniak, C. B., Friauf, E., Witke, W. and Rust, M. B. (2012). Profilin1 is required for glial cell adhesion and radial migration of cerebellar granule neurons. *EMBO Rep* **13**, 75-82.

Kurklinsky, S., Chen, J. and McNiven, M. A. (2011). Growth cone morphology and spreading are regulated by a dynamin-cortactin complex at point contacts in hippocampal neurons. *J Neurochem* **117**, 48-60.

Lai, F. P., Szczodrak, M., Block, J., Faix, J., Breitsprecher, D., Mannherz, H. G., Stradal, T. E., Dunn, G. A., Small, J. V. and Rottner, K. (2008). Arp2/3 complex interactions and actin network turnover in lamellipodia. *EMBO J* **27**, 982-92.

Lai, F. P., Szczodrak, M., Oelkers, J. M., Ladwein, M., Acconcia, F., Benesch, S., Auinger, S., Faix, J., Small, J. V., Polo, S. et al. (2009). Cortactin promotes migration and platelet-derived growth factor-induced actin reorganization by signaling to Rho-GTPases. *Mol Biol Cell* **20**, 3209-23.

Lambrechts, A., Braun, A., Jonckheere, V., Aszodi, A., Lanier, L. M., Robbens, J., Van Colen, I., Vandekerckhove, J., Fassler, R. and Ampe, C. (2000). Profilin II is alternatively spliced, resulting in profilin isoforms that are differentially expressed and have distinct biochemical properties. *Mol Cell Biol* **20**, 8209-19.

Lawson, C. D. and Burridge, K. (2014). The on-off relationship of Rho and Rac during integrin-mediated adhesion and cell migration. *Small GTPases* **5**.

Lazareno, S., Popham, A. and Birdsall, N. J. (2000). Allosteric interactions of staurosporine and other indolocarbazoles with N-[methyl-(3)H]scopolamine and acetylcholine at muscarinic receptor subtypes: identification of a second allosteric site. *Mol Pharmacol* **58**, 194-207.

Le Good, J. A., Ziegler, W. H., Parekh, D. B., Alessi, D. R., Cohen, P. and Parker, P. J. (1998). Protein kinase C isotypes controlled by phosphoinositide 3-kinase through the protein kinase PDK1. *Science* **281**, 2042-5.

Lederer, M. I. (2002). Charakterisierung des Myb-Transkriptionsfaktors p42POP: Eine Verbindung des Mikrofilamentsystems zur Transkription. *Dissertation*.

Lee, S. G., Su, Z. Z., Emdad, L., Sarkar, D., Franke, T. F. and Fisher, P. B. (2008). Astrocyte elevated gene-1 activates cell survival pathways through PI3K-Akt signaling. *Oncogene* **27**, 1114-21.

Lehre, K. P. and Rusakov, D. A. (2002). Asymmetry of glia near central synapses favors presynaptically directed glutamate escape. *Biophys J* **83**, 125-34.

Levin, V. A., Panchabhai, S. C., Shen, L., Kornblau, S. M., Qiu, Y. and Baggerly, K. A. (2010). Different changes in protein and phosphoprotein levels result from serum starvation of high-grade glioma and adenocarcinoma cell lines. *J Proteome Res* **9**, 179-91.

Leybaert, L., Braet, K., Vandamme, W., Cabooter, L., Martin, P. E. and Evans, W. H. (2003). Connexin channels, connexin mimetic peptides and ATP release. *Cell Commun Adhes* **10**, 251-7.

Lim, R., Mitsunobu, K. and Li, W. K. (1973). Maturation-stimulation effect of brain extract and dibutyryl cyclic AMP on dissociated embryonic brain cells in culture. *Exp Cell Res* **79**, 243-6.

Lindahl, E., Nyman, U., Melles, E., Sigmundsson, K., Stahlberg, M., Wahren, J., Obrink, B., Shafqat, J., Joseph, B. and Jornvall, H. (2007). Cellular internalization of proinsulin C-peptide. *Cell Mol Life Sci* **64**, 479-86.

Lorente, G., Syriani, E. and Morales, M. (2014). Actin filaments at the leading edge of cancer cells are characterized by a high mobile fraction and turnover regulation by profilin I. *PLoS One* **9**, e85817.

Lovatt, D., Sonnewald, U., Waagepetersen, H. S., Schousboe, A., He, W., Lin, J. H., Han, X., Takano, T., Wang, S., Sim, F. J. et al. (2007). The transcriptome and metabolic gene signature of protoplasmic astrocytes in the adult murine cortex. *J Neurosci* **27**, 12255-66.

MacGrath, S. M. and Koleske, A. J. (2012). Cortactin in cell migration and cancer at a glance. *J Cell Sci* **125**, 1621-6.

Mathew, R., Karantza-Wadsworth, V. and White, E. (2007). Role of autophagy in cancer. *Nat Rev Cancer* **7**, 961-7.

Matyash, V. and Kettenmann, H. (2010). Heterogeneity in astrocyte morphology and physiology. *Brain Res Rev* **63**, 2-10.

Mayboroda, O., Schluter, K. and Jockusch, B. M. (1997). Differential colocalization of profilin with microfilaments in PtK2 cells. *Cell Motil Cytoskeleton* **37**, 166-77.

Michaelsen, K., Murk, K., Zagrebelsky, M., Dreznjak, A., Jockusch, B. M., Rothkegel, M. and Korte, M. (2010). Fine-tuning of neuronal architecture requires two profilin isoforms. *Proc Natl Acad Sci U S A* **107**, 15780-5.

Middeldorp, J. and Hol, E. M. (2011). GFAP in health and disease. *Prog Neurobiol* **93**, 421-43.

Min, R. and Nevian, T. (2012). Astrocyte signaling controls spike timing-dependent depression at neocortical synapses. *Nat Neurosci* **15**, 746-53.

Minichiello, L. (2009). TrkB signalling pathways in LTP and learning. *Nat Rev Neurosci* **10**, 850-60.

Mizushima, N., Levine, B., Cuervo, A. M. and Klionsky, D. J. (2008). Autophagy fights disease through cellular self-digestion. *Nature* **451**, 1069-75.

Moldovan, N. I., Milliken, E. E., Irani, K., Chen, J., Sohn, R. H., Finkel, T. and Goldschmidt-Clermont, P. J. (1997). Regulation of endothelial cell adhesion by profilin. *Curr Biol* **7**, 24-30.

Mollinari, C., Reynaud, C., Martineau-Thuillier, S., Monier, S., Kieffer, S., Garin, J., Andreassen, P. R., Boulet, A., Goud, B., Kleman, J. P. et al. (2003). The mammalian passenger protein TD-60 is an RCC1 family member with an essential role in prometaphase to metaphase progression. *Dev Cell* **5**, 295-307.

Molotkov, D., Zobova, S., Arcas, J. M. and Khiroug, L. (2013). Calcium-induced outgrowth of astrocytic peripheral processes requires actin binding by Profilin-1. *Cell Calcium* **53**, 338-48.

Murk, K. (2004). Die PKA-abhängige Phosphorylierung von Profilin, einem Regulator der Aktindynamik.

Murk, K. (2008). Analyse der funktionellen Diversität der Profilin-Isoformen 1 und 2a.

Murk, K., Blanco Suarez, E. M., Cockbill, L. M., Banks, P. and Hanley, J. G. (2013). The antagonistic modulation of Arp2/3 activity by N-WASP, WAVE2 and PICK1 defines dynamic changes in astrocyte morphology. *J Cell Sci* **126**, 3873-83.

Murk, K., Buchmeier, S., Jockusch, B. M. and Rothkegel, M. (2009). In birds, profilin-2a is ubiquitously expressed and contributes to actin-based motility. *J Cell Sci* **122**, 957-64.

Murk, K., Wittenmayer, N., Michaelsen-Preusse, K., Dresbach, T., Schoenenberger, C. A., Korte, M., Jockusch, B. M. and Rothkegel, M. (2012). Neuronal profilin isoforms are addressed by different signalling pathways. *PLoS One* **7**, e34167.

Murray, A. J. (2008). Pharmacological PKA inhibition: all may not be what it seems. *Sci Signal* **1**, re4.

Naus, C. C., Bechberger, J. F., Zhang, Y., Venance, L., Yamasaki, H., Juneja, S. C., Kidder, G. M. and Giaume, C. (1997). Altered gap junctional communication, intercellular signaling, and growth in cultured astrocytes deficient in connexin43. *J Neurosci Res* **49**, 528-40.

Navarrete, M. and Araque, A. (2011). Basal synaptic transmission: astrocytes rule! *Cell* **146**, 675-7.

Navarrete, M., Perea, G., Fernandez de Sevilla, D., Gomez-Gonzalo, M., Nunez, A., Martin, E. D. and Araque, A. (2012). Astrocytes mediate in vivo cholinergic-induced synaptic plasticity. *PLoS Biol* **10**, e1001259.

Neuhoff, H., Sassoe-Pognetto, M., Panzanelli, P., Maas, C., Witke, W. and Kneussel, M. (2005). The actin-binding protein profilin I is localized at synaptic sites in an activity-regulated manner. *Eur J Neurosci* **21**, 15-25.

Newman, E. A. and Zahs, K. R. (1998). Modulation of neuronal activity by glial cells in the retina. *J Neurosci* **18**, 4022-8.

Ngezahayo, A., Altmann, B. and Kolb, H. A. (2003). Regulation of ion fluxes, cell volume and gap junctional coupling by cGMP in GFSHR-17 granulosa cells. *J Membr Biol* **194**, 165-76.

Nolle, A., Zeug, A., van Bergeijk, J., Tonges, L., Gerhard, R., Brinkmann, H., Al Rayes, S., Hensel, N., Schill, Y., Apkhazava, D. et al. (2011). The spinal muscular atrophy disease protein SMN is linked to the Rho-kinase pathway via profilin. *Hum Mol Genet* **20**, 4865-78.

O'Brien, J. A. and Lummis, S. C. (2006). Biolistic transfection of neuronal cultures using a hand-held gene gun. *Nat Protoc* **1**, 977-81.

Obermann, H., Raabe, I., Balvers, M., Brunswig, B., Schulze, W. and Kirchhoff, C. (2005). Novel testis-expressed profilin IV associated with acrosome biogenesis and spermatid elongation. *Mol Hum Reprod* **11**, 53-64.

Oda, K., Matsuoka, Y., Funahashi, A. and Kitano, H. (2005). A comprehensive pathway map of epidermal growth factor receptor signaling. *Mol Syst Biol* **1**, 2005 0010.

Oey, J., Vogel, A. and Pollack, R. (1974). Intracellular cyclic AMP concentration responds specifically to growth regulation by serum. *Proc Natl Acad Sci U S A* **71**, 694-8.

Ogata, K. and Kosaka, T. (2002). Structural and quantitative analysis of astrocytes in the mouse hippocampus. *Neuroscience* **113**, 221-33.

Okada, S., Nakamura, M., Katoh, H., Miyao, T., Shimazaki, T., Ishii, K., Yamane, J., Yoshimura, A., Iwamoto, Y., Toyama, Y. et al. (2006). Conditional ablation of Stat3 or Socs3 discloses a dual role for reactive astrocytes after spinal cord injury. *Nat Med* **12**, 829-34.

Oliet, S. H., Piet, R. and Poulain, D. A. (2001). Control of glutamate clearance and synaptic efficacy by glial coverage of neurons. *Science* **292**, 923-6.

Olk, S., Turchinovich, A., Grzendowski, M., Stuhler, K., Meyer, H. E., Zoidl, G. and Dermietzel, R. (2010). Proteomic analysis of astroglial connexin43 silencing uncovers a cytoskeletal platform involved in process formation and migration. *Glia* **58**, 494-505.

Olsen, M. K., Reszka, A. A. and Abraham, I. (1998). KT5720 and U-98017 inhibit MAPK and alter the cytoskeleton and cell morphology. *J Cell Physiol* **176**, 525-36.

Orellana, J. A., Shoji, K. F., Abudara, V., Ezan, P., Amigou, E., Saez, P. J., Jiang, J. X., Naus, C. C., Saez, J. C. and Giaume, C. (2011). Amyloid beta-induced death in neurons involves glial and neuronal hemichannels. *J Neurosci* **31**, 4962-77.

Orellana, J. A., von Bernhardi, R., Giaume, C. and Saez, J. C. (2012). Glial hemichannels and their involvement in aging and neurodegenerative diseases. *Rev Neurosci* **23**, 163-77.

Orthmann-Murphy, J. L., Abrams, C. K. and Scherer, S. S. (2008). Gap junctions couple astrocytes and oligodendrocytes. *J Mol Neurosci* **35**, 101-16.

Oser, M. and Condeelis, J. (2009). The cofilin activity cycle in lamellipodia and invadopodia. *J Cell Biochem* **108**, 1252-62.

Osmani, N., Peglion, F., Chavrier, P. and Etienne-Manneville, S. (2010). Cdc42 localization and cell polarity depend on membrane traffic. *J Cell Biol* **191**, 1261-9.

Pak, C. W., Flynn, K. C. and Bamburg, J. R. (2008). Actin-binding proteins take the reins in growth cones. *Nat Rev Neurosci* **9**, 136-47.

Pannasch, U., Freche, D., Dallerac, G., Ghezali, G., Escartin, C., Ezan, P., Cohen-Salmon, M., Benchenane, K., Abudara, V., Dufour, A. et al. (2014). Connexin 30 sets synaptic strength by controlling astroglial synapse invasion. *Nat Neurosci* **17**, 549-58.

Pannasch, U. and Rouach, N. (2013). Emerging role for astroglial networks in information processing: from synapse to behavior. *Trends Neurosci* **36**, 405-17.

Pannasch, U., Vargova, L., Reingruber, J., Ezan, P., Holcman, D., Giaume, C., Sykova, E. and Rouach, N. (2011). Astroglial networks scale synaptic activity and plasticity. *Proc Natl Acad Sci U S A* **108**, 8467-72.

Parpura, V., Scemes, E. and Spray, D. C. (2004). Mechanisms of glutamate release from astrocytes: gap junction "hemichannels", purinergic receptors and exocytotic release. *Neurochem Int* **45**, 259-64.

Parri, H. R., Gould, T. M. and Crunelli, V. (2001). Spontaneous astrocytic Ca2+ oscillations in situ drive NMDAR-mediated neuronal excitation. *Nat Neurosci* **4**, 803-12.

Perez, V., Bouschet, T., Fernandez, C., Bockaert, J. and Journot, L. (2005). Dynamic reorganization of the astrocyte actin cytoskeleton elicited by cAMP and PACAP: a role for phosphatidylInositol 3-kinase inhibition. *Eur J Neurosci* **21**, 26-32.

Persad, S., Attwell, S., Gray, V., Mawji, N., Deng, J. T., Leung, D., Yan, J., Sanghera, J., Walsh, M. P. and Dedhar, S. (2001). Regulation of protein kinase B/Akt-serine 473 phosphorylation by integrin-linked kinase: critical roles for kinase activity and amino acids arginine 211 and serine 343. *J Biol Chem* **276**, 27462-9.

Peters, O., Schipke, C. G., Hashimoto, Y. and Kettenmann, H. (2003). Different mechanisms promote astrocyte Ca2+ waves and spreading depression in the mouse neocortex. *J Neurosci* **23**, 9888-96.

Pfrieger, F. W. and Barres, B. A. (1997). Synaptic efficacy enhanced by glial cells in vitro. *Science* **277**, 1684-7.

Pilo Boyl, P., Di Nardo, A., Mulle, C., Sassoe-Pognetto, M., Panzanelli, P., Mele, A., Kneussel, M., Costantini, V., Perlas, E., Massimi, M. et al. (2007). Profilin2 contributes to synaptic vesicle exocytosis, neuronal excitability, and novelty-seeking behavior. *EMBO J* **26**, 2991-3002.

Pinto, S. S., Gottfried, C., Mendez, A., Goncalves, D., Karl, J., Goncalves, C. A., Wofchuk, S. and Rodnight, R. (2000). Immunocontent and secretion of S100B in astrocyte cultures from different brain regions in relation to morphology. *FEBS Lett* **486**, 203-7.

Pirkmajer, S. and Chibalin, A. V. (2011). Serum starvation: caveat emptor. *Am J Physiol Cell Physiol* **301**, C272-9.

Polet, D., Lambrechts, A., Vandepoele, K., Vandekerckhove, J. and Ampe, C. (2007). On the origin and evolution of vertebrate and viral profilins. *FEBS Lett* **581**, 211-7.

Pollard, T. D. (1986). Rate constants for the reactions of ATP- and ADP-actin with the ends of actin filaments. *J Cell Biol* **103**, 2747-54.

Pollard, T. D. and Cooper, J. A. (2009). Actin, a central player in cell shape and movement. *Science* **326**, 1208-12.

Puschmann, T. B., Zanden, C., Lebkuechner, I., Philippot, C., de Pablo, Y., Liu, J. and Pekny, M. (2014). HB-EGF affects astrocyte morphology, proliferation, differentiation, and the expression of intermediate filament proteins. *J Neurochem* **128**, 878-89.

Qiu, C., Coutinho, P., Frank, S., Franke, S., Law, L. Y., Martin, P., Green, C. R. and Becker, D. L. (2003). Targeting connexin43 expression accelerates the rate of wound repair. *Curr Biol* **13**, 1697-703.

Racchetti, G., D'Alessandro, R. and Meldolesi, J. (2012). Astrocyte stellation, a process dependent on Rac1 is sustained by the regulated exocytosis of enlargeosomes. *Glia* **60**, 465-75.

Racz, B. and Weinberg, R. J. (2004). The subcellular organization of cortactin in hippocampus. *J Neurosci* **24**, 10310-7.

Ramakers, G. J. and Moolenaar, W. H. (1998). Regulation of astrocyte morphology by RhoA and lysophosphatidic acid. *Exp Cell Res* **245**, 252-62.

Ramón y Cajal, S. (1913). Contribucion al conocimiento de la neuroglia del cerebro humano. *Trab. Lab. Inuest. Biol. Uniu. Madrid* **11**, 255-315.

Rash, J. E., Yasumura, T., Dudek, F. E. and Nagy, J. I. (2001). Cell-specific expression of connexins and evidence of restricted gap junctional coupling between glial cells and between neurons. *J Neurosci* **21**, 1983-2000.

Rawe, V. Y., Payne, C. and Schatten, G. (2006). Profilin and actin-related proteins regulate microfilament dynamics during early mammalian embryogenesis. *Hum Reprod* **21**, 1143-53.

Reinhard, M., Giehl, K., Abel, K., Haffner, C., Jarchau, T., Hoppe, V., Jockusch, B. M. and Walter, U. (1995). The proline-rich focal adhesion and microfilament protein VASP is a ligand for profilins. *EMBO J* **14**, 1583-9.

Remus, A. (2012). Molecular mechanisms regulating the neuronal architecture in the mouse brain.

Rizzoli, S. O. and Betz, W. J. (2005). Synaptic vesicle pools. *Nat Rev Neurosci* **6**, 57-69.

Robel, S., Bardehle, S., Lepier, A., Brakebusch, C. and Gotz, M. (2011). Genetic deletion of cdc42 reveals a crucial role for astrocyte recruitment to the injury site in vitro and in vivo. *J Neurosci* **31**, 12471-82.

Rodnight, R. B. and Gottfried, C. (2013). Morphological plasticity of rodent astroglia. *J Neurochem* **124**, 263-75.

Rostosky, C. M. (2014). Einfluss von Cortactin auf räumliches Lernen und seine regionsspezifische Rolle im murinen Hippocampus.

Salhia, B., Rutten, F., Nakada, M., Beaudry, C., Berens, M., Kwan, A. and Rutka, J. T. (2005). Inhibition of Rho-kinase affects astrocytoma morphology, motility, and invasion through activation of Rac1. *Cancer Res* **65**, 8792-800.

Sands, W. A. and Palmer, T. M. (2008). Regulating gene transcription in response to cyclic AMP elevation. *Cell Signal* **20**, 460-6.

Sathish, K., Padma, B., Munugalavadla, V., Bhargavi, V., Radhika, K. V. N., Wasia, R., Sairam, M. and Singh, S. S. (2004). Phosphorylation of profilin regulates its interaction with actin and poly (L-proline). *Cell Signal* **16**, 589-596.

Savchenko, V. L., McKanna, J. A., Nikonenko, I. R. and Skibo, G. G. (2000). Microglia and astrocytes in the adult rat brain: comparative immunocytochemical analysis demonstrates the efficacy of lipocortin 1 immunoreactivity. *Neuroscience* **96**, 195-203.

Scemes, E. and Giaume, C. (2006). Astrocyte calcium waves: what they are and what they do. *Glia* **54**, 716-25.

Scharkowski, F. (2013). Die Rolle von Cortactin in Hippokampus-abhängiger Gedächtnisbildung und synaptischer Plastizität.

Schindelin, J., Arganda-Carreras, I., Frise, E., Kaynig, V., Longair, M., Pietzsch, T., Preibisch, S., Rueden, C., Saalfeld, S., Schmid, B. et al. (2012). Fiji: an open-source platform for biological-image analysis. *Nat Methods* **9**, 676-82.

Schleicher, M. and Jockusch, B. M. (2008). Actin: its cumbersome pilgrimage through cellular compartments. *Histochem Cell Biol* **129**, 695-704.

Schnoor, M., Lai, F. P., Zarbock, A., Klaver, R., Polaschegg, C., Schulte, D., Weich, H. A., Oelkers, J. M., Rottner, K. and Vestweber, D. (2011). Cortactin deficiency is associated with reduced neutrophil recruitment but increased vascular permeability in vivo. *J Exp Med* **208**, 1721-35.

Seese, R. R., Babayan, A. H., Katz, A. M., Cox, C. D., Lauterborn, J. C., Lynch, G. and Gall, C. M. (2012). LTP induction translocates cortactin at distant synapses in wild-type but not Fmr1 knock-out mice. *J Neurosci* **32**, 7403-13.

Selbach, M. and Backert, S. (2005). Cortactin: an Achilles' heel of the actin cytoskeleton targeted by pathogens. *Trends Microbiol* **13**, 181-9.

Shao, J. and Diamond, M. I. (2012). Protein phosphatase 1 dephosphorylates profilin-1 at Ser-137. *PLoS One* **7**, e32802.

Shao, J., Welch, W. J., Diprospero, N. A. and Diamond, M. I. (2008). Phosphorylation of profilin by ROCK1 regulates polyglutamine aggregation. *Mol Cell Biol* **28**, 5196-208.

Shapiro, D. L. (1973). Morphological and biochemical alterations in foetal rat brain cells cultured in the presence of monobutyryl cyclic AMP. *Nature* **241**, 203-4.

Shaw, R. M., Fay, A. J., Puthenveedu, M. A., von Zastrow, M., Jan, Y. N. and Jan, L. Y. (2007). Microtubule plus-end-tracking proteins target gap junctions directly from the cell interior to adherens junctions. *Cell* **128**, 547-60.

Shi, J., Wu, X., Surma, M., Vemula, S., Zhang, L., Yang, Y., Kapur, R. and Wei, L. (2013). Distinct roles for ROCK1 and ROCK2 in the regulation of cell detachment. *Cell Death Dis* **4**, e483.

Simpson, K. J., Selfors, L. M., Bui, J., Reynolds, A., Leake, D., Khvorova, A. and Brugge, J. S. (2008). Identification of genes that regulate epithelial cell migration using an siRNA screening approach. *Nat Cell Biol* **10**, 1027-38.

Skare, P., Kreivi, J. P., Bergstrom, A. and Karlsson, R. (2003). Profilin I colocalizes with speckles and Cajal bodies: a possible role in pre-mRNA splicing. *Exp Cell Res* **286**, 12-21.

Smyth, J. W., Vogan, J. M., Buch, P. J., Zhang, S. S., Fong, T. S., Hong, T. T. and Shaw, R. M. (2012). Actin cytoskeleton rest stops regulate anterograde traffic of connexin 43 vesicles to the plasma membrane. *Circ Res* **110**, 978-89.

Sofroniew, M. V. (2009). Molecular dissection of reactive astrogliosis and glial scar formation. *Trends Neurosci* **32**, 638-47.

Somjen, G. G. (1988). Nervenkitt: notes on the history of the concept of neuroglia. *Glia* **1**, 2-9.

Steffen, A., Ladwein, M., Dimchev, G. A., Hein, A., Schwenkmezger, L., Arens, S., Ladwein, K. I., Margit Holleboom, J., Schur, F., Victor Small, J. et al. (2013). Rac function is crucial for cell migration but is not required for spreading and focal adhesion formation. *J Cell Sci* **126**, 4572-88.

Steffen, A., Rottner, K., Ehinger, J., Innocenti, M., Scita, G., Wehland, J. and Stradal, T. E. (2004). Sra-1 and Nap1 link Rac to actin assembly driving lamellipodia formation. *EMBO J* **23**, 749-59.

Stoppini, L., Buchs, P. A. and Muller, D. (1991). A simple method for organotypic cultures of nervous tissue. *J Neurosci Methods* **37**, 173-82.

Stout, C. E., Costantin, J. L., Naus, C. C. and Charles, A. C. (2002). Intercellular calcium signaling in astrocytes via ATP release through connexin hemichannels. *J Biol Chem* **277**, 10482-8.

Struve, J., Maher, P. C., Li, Y. Q., Kinney, S., Fehlings, M. G., Kuntz, C. t. and Sherman, L. S. (2005). Disruption of the hyaluronan-based extracellular matrix in spinal cord promotes astrocyte proliferation. *Glia* **52**, 16-24.

Stuven, T., Hartmann, E. and Gorlich, D. (2003). Exportin 6: a novel nuclear export receptor that is specific for profilin.actin complexes. *EMBO J* **22**, 5928-40.

Suidan, H. S., Nobes, C. D., Hall, A. and Monard, D. (1997). Astrocyte spreading in response to thrombin and lysophosphatidic acid is dependent on the Rho GTPase. *Glia* **21**, 244-52.

Suraneni, P., Rubinstein, B., Unruh, J. R., Durnin, M., Hanein, D. and Li, R. (2012). The Arp2/3 complex is required for lamellipodia extension and directional fibroblast cell migration. *J Cell Biol* **197**, 239-51.

Suzuki, A., Stern, S. A., Bozdagi, O., Huntley, G. W., Walker, R. H., Magistretti, P. J. and Alberini, C. M. (2011). Astrocyte-neuron lactate transport is required for long-term memory formation. *Cell* **144**, 810-23.

Takata, N., Mishima, T., Hisatsune, C., Nagai, T., Ebisui, E., Mikoshiba, K. and Hirase, H. (2011). Astrocyte calcium signaling transforms cholinergic modulation to cortical plasticity in vivo. *J Neurosci* **31**, 18155-65.

Terra, L. F., Garay-Malpartida, M. H., Wailemann, R. A., Sogayar, M. C. and Labriola, L. (2011). Recombinant human prolactin promotes human beta cell survival via inhibition of extrinsic and intrinsic apoptosis pathways. *Diabetologia* **54**, 1388-97.

Theis, M. and Giaume, C. (2012). Connexin-based intercellular communication and astrocyte heterogeneity. *Brain Res* **1487**, 88-98.

Theis, M., Speidel, D. and Willecke, K. (2004). Astrocyte cultures from conditional connexin43-deficient mice. *Glia* **46**, 130-41.

Theiss, C. (2002). Microinjected Anti-actin Antibodies Decrease Gap Junctional Intercellular Commmunication in Cultured Astrocytes. *Exp Cell Res* **281**, 197-204.

Thomsen, R. and Lade Nielsen, A. (2011). A Boyden chamber-based method for characterization of astrocyte protrusion localized RNA and protein. *Glia* **59**, 1782-92.

Tsai, W., Morielli, A. D. and Peralta, E. G. (1997). The m1 muscarinic acetylcholine receptor transactivates the EGF receptor to modulate ion channel activity. *EMBO J* **16**, 4597-605.

Tsuji, T., Ishizaki, T., Okamoto, M., Higashida, C., Kimura, K., Furuyashiki, T., Arakawa, Y., Birge, R. B., Nakamoto, T., Hirai, H. et al. (2002). ROCK and mDia1 antagonize in Rho-dependent Rac activation in Swiss 3T3 fibroblasts. *J Cell Biol* **157**, 819-30.

Ullian, E. M., Sapperstein, S. K., Christopherson, K. S. and Barres, B. A. (2001). Control of synapse number by glia. *Science* **291**, 657-61.

Vemuri, B. and Singh, S. S. (2001). Protein kinase C isozyme-specific phosphorylation of profilin. *Cell Signal* **13**, 433-9.

Venance, L., Premont, J., Glowinski, J. and Giaume, C. (1998). Gap junctional communication and pharmacological heterogeneity in astrocytes cultured from the rat striatum. *J Physiol* **510 (Pt 2)**, 429-40.

Ventura, R. and Harris, K. M. (1999). Three-dimensional relationships between hippocampal synapses and astrocytes. *J Neurosci* **19**, 6897-906.

Vincent, S. and Settleman, J. (1997). The PRK2 kinase is a potential effector target of both Rho and Rac GTPases and regulates actin cytoskeletal organization. *Mol Cell Biol* **17**, 2247-56.

Vitale, M. L., Akpovi, C. D. and Pelletier, R. M. (2009). Cortactin/tyrosine-phosphorylated cortactin interaction with connexin 43 in mouse seminiferous tubules. *Microsc Res Tech* **72**, 856-67.

Wallraff, A., Kohling, R., Heinemann, U., Theis, M., Willecke, K. and Steinhauser, C. (2006). The impact of astrocytic gap junctional coupling on potassium buffering in the hippocampus. *J Neurosci* **26**, 5438-47.

Wang, N., De Bock, M., Antoons, G., Gadicherla, A. K., Bol, M., Decrock, E., Evans, W. H., Sipido, K. R., Bukauskas, F. F. and Leybaert, L. (2012). Connexin mimetic peptides inhibit Cx43 hemichannel opening triggered by voltage and intracellular Ca2+ elevation. *Basic Res Cardiol* **107**, 304.

Wang, X., Lou, N., Xu, Q., Tian, G. F., Peng, W. G., Han, X., Kang, J., Takano, T. and Nedergaard, M. (2006). Astrocytic Ca2+ signaling evoked by sensory stimulation in vivo. *Nat Neurosci* **9**, 816-23.

Wang, Y. and Rose, B. (1995). Clustering of Cx43 cell-to-cell channels into gap junction plaques: regulation by cAMP and microfilaments. *J Cell Sci* **108 (Pt 11)**, 3501-8.

Warner, A., Clements, D. K., Parikh, S., Evans, W. H. and DeHaan, R. L. (1995). Specific motifs in the external loops of connexin proteins can determine gap junction formation between chick heart myocytes. *J Physiol* **488 (Pt 3)**, 721-8.

Watanabe, S., Ando, Y., Yasuda, S., Hosoya, H., Watanabe, N., Ishizaki, T. and Narumiya, S. (2008). mDia2 induces the actin scaffold for the contractile ring and stabilizes its position during cytokinesis in NIH 3T3 cells. *Mol Biol Cell* **19**, 2328-38.

Wei, C. J., Francis, R., Xu, X. and Lo, C. W. (2005). Connexin43 associated with an N-cadherin-containing multiprotein complex is required for gap junction formation in NIH3T3 cells. *J Biol Chem* **280**, 19925-36.

Weller, M. M. S. (2012). Analyse der Interaktion von Proteinkinase M zeta (PKMζ) und Profilin.

Wellmann, H., Kaltschmidt, B. and Kaltschmidt, C. (1999). Optimized protocol for biolistic transfection of brain slices and dissociated cultured neurons with a hand-held gene gun. *J Neurosci Methods* **92**, 55-64.

White, E. and DiPaola, R. S. (2009). The double-edged sword of autophagy modulation in cancer. *Clin Cancer Res* **15**, 5308-16.

Witke, W. (2004). The role of profilin complexes in cell motility and other cellular processes. *Trends Cell Biol* **14**, 461-9.

Witke, W., Podtelejnikov, A. V., Di Nardo, A., Sutherland, J. D., Gurniak, C. B., Dotti, C. and Mann, M. (1998). In mouse brain profilin I and profilin II associate with regulators of the endocytic pathway and actin assembly. *EMBO J* **17**, 967-76.

Witke, W., Sutherland, J. D., Sharpe, A., Arai, M. and Kwiatkowski, D. J. (2001). Profilin I is essential for cell survival and cell division in early mouse development. *Proc Natl Acad Sci U S A* **98**, 3832-6.

Wu, C., Asokan, S. B., Berginski, M. E., Haynes, E. M., Sharpless, N. E., Griffith, J. D., Gomez, S. M. and Bear, J. E. (2012). Arp2/3 is critical for lamellipodia and response to extracellular matrix cues but is dispensable for chemotaxis. *Cell* **148**, 973-87.

Wu, H. and Parsons, J. T. (1993). Cortactin, an 80/85-kilodalton pp60src substrate, is a filamentous actin-binding protein enriched in the cell cortex. *J Cell Biol* **120**, 1417-26.

Wu, H., Reynolds, A. B., Kanner, S. B., Vines, R. R. and Parsons, J. T. (1991). Identification and characterization of a novel cytoskeleton-associated pp60src substrate. *Mol Cell Biol* **11**, 5113-24.

Wu, N., Zhang, W., Yang, Y., Liang, Y. L., Wang, L. Y., Jin, J. W., Cai, X. M. and Zha, X. L. (2006). Profilin 1 obtained by proteomic analysis in all-trans retinoic acid-treated hepatocarcinoma cell lines is involved in inhibition of cell proliferation and migration. *Proteomics* **6**, 6095-106.

Wu, X. S., Tsan, G. L. and Hammer, J. A., 3rd. (2005). Melanophilin and myosin Va track the microtubule plus end on EB1. *J Cell Biol* **171**, 201-7.

Xu, J., Xiao, N. and Xia, J. (2010). Thrombospondin 1 accelerates synaptogenesis in hippocampal neurons through neuroligin 1. *Nat Neurosci* **13**, 22-4.

Yamane, Y., Shiga, H., Asou, H. and Ito, E. (2002). GAP junctional channel inhibition alters actin organization and calcium propagation in rat cultured astrocytes. *Neuroscience* **112**, 593-603.

Yun, S. P., Ryu, J. M., Kim, M. O., Park, J. H. and Han, H. J. (2012). Rapid actions of plasma membrane estrogen receptors regulate motility of mouse embryonic stem cells through a profilin-1/cofilin-1-directed kinase signaling pathway. *Mol Endocrinol* **26**, 1291-303.

Zemljic-Harpf, A. E., Godoy, J. C., Platoshyn, O., Asfaw, E. K., Busija, A. R., Domenighetti, A. A. and Ross, R. S. (2014). Vinculin directly binds zonula occludens-1 and is essential for stabilizing connexin-43-containing gap junctions in cardiac myocytes. *J Cell Sci* **127**, 1104-16.

Zessin, S. (2010). Role of Profilin Isoforms in the Structural Plasticity of Pyramidal Neurons in the Mouse Hippocampus.

Zetterberg, A. and Larsson, O. (1985). Kinetic analysis of regulatory events in G1 leading to proliferation or quiescence of Swiss 3T3 cells. *Proc Natl Acad Sci U S A* **82**, 5365-9.

Zhao, Y., Yang, J., Liao, W., Liu, X., Zhang, H., Wang, S., Wang, D., Feng, J., Yu, L. and Zhu, W. G. (2010). Cytosolic FoxO1 is essential for the induction of autophagy and tumour suppressor activity. *Nat Cell Biol* **12**, 665-75.

Ziegenfuss, J. S., Doherty, J. and Freeman, M. R. (2012). Distinct molecular pathways mediate glial activation and engulfment of axonal debris after axotomy. *Nat Neurosci* **15**, 979-87.

Zoidakis, J., Makridakis, M., Zerefos, P. G., Bitsika, V., Esteban, S., Frantzi, M., Stravodimos, K., Anagnou, N. P., Roubelakis, M. G., Sanchez-Carbayo, M. et al. (2012). Profilin 1 is a potential biomarker for bladder cancer aggressiveness. *Mol Cell Proteomics* **11**, M111 009449.

Zou, L., Jaramillo, M., Whaley, D., Wells, A., Panchapakesa, V., Das, T. and Roy, P. (2007). Profilin-1 is a negative regulator of mammary carcinoma aggressiveness. *Br J Cancer* **97**, 1361-71.

6. List of relevant abbreviations

Acronym	Definition
ABP	Actin-binding protein
ADF	Actin depolymerzation factor
ADP	Adenosine-di-phosphate
AP	Alkaline phosphatase
ATP	Adenosine-tri-phosphate
BDNF	Brain derived neurotrophic factor
cAMP	Cyclic Adenosine-mono-phosphate
Cdc42	Cell division control protein 42 homolog
CFL	cofilin
CNS	Central nervous system
CTTN	Cortactin
Cx	Connexin
DAPI	4',6-diamidino-2-phenylindole
DIV	Days *in vitro*
DNA	Deoxyribonucleic acid
EGF	Epidermal growth factor
FCS	Fetal calf serum
FRAP	Fluorescence recovery after photobleaching
FSK	forskolin
GFAP	Glial fibrillary acidic protein
GFP	Green fluorescent protein
ICW	Intercellular calcium wave
KD	Knockdown
kDA	Kilo Dalton
LIMK	LIM domain kinase 1
mRNA	Messenger ribonucleic acid
NPF	Nucleation promoting factor
P2X	Metabotrophic purinoreceptors
P2Y	Ionotrophic purinoceptors
PAP	Peripheral astrocytic process
PDK1	phosphoinositide-dependent kinase 1
PFN	Profilin
PI3K	Phosphoinositide 3-kinase
PIP_2	phosphatidylinositol 4,5 bisphosphate
PKA	cAMP dependent protein kinase A
PKC	Protein kinase C
PKMζ	N-terminal truncated PKCζ
PLP	poly-(L)-proline
Rac1	Ras-related C3 botulinum toxin substrate 1
RhoA	Ras homolog family member A
RNAi	RNA interference
ROCK	Rho-associated coiled coil-containing protein kinase
shRNA	Small hairpin ribonucleic acid
siRNA	Small interfering ribonucleic acid
WASP	Wiskott-Aldrich syndrome protein
WAVE	WASP family Verprolin-homologous protein

Danksagung

Hiermit möchte ich allen danken, die zum Gelingen meiner Doktorarbeit beigetragen haben:

Zunächst danke ich Prof. Dr. Martin Korte für die Möglichkeit in seiner Arbeitsgruppe meine Arbeit anfertigen zu dürfen.

Prof. Dr. Reinhard Köster danke ich für die Übernahme des Korreferats und Anregungen im Seminar, sowie Prof. Dr. Andre Fleißner für die Leitung der Prüfungskommission.

Mein besonderer Dank gilt Dr. Martin Rothkegel. Für die Unterstützung, die während meiner Master- und meiner Doktorarbeit erfahren habe. Für das stundenlange Reden über mal mehr und mal weniger wissenschaftliche Probleme. Und natürlich auch für das Zuhören, wenn ich einfach nur mal meckern musste.

Tania Meßerschmidt möchte ich für die Hilfestellungen in allen nur erdenklichen methodischen Aspekten danken. Für den Eifer, mit dem sie den 2-D Gelen an den Kragen gerückt ist und es einfach nur viel besser hingekriegt hat als ich. Und für die schönen gemeinsamen Stunden im Labor.

Diane Mundil danke ich für die wunderschönen organotypischen Cortex Kulturen und die Unmengen an Cortices, die für meine Astrozytenkulturen abgefallen sind. Nicht zu vergessen, ihre permanent gute Laune.

Bei Birte Ackenhausen, Eva Saxinger, Heike Kessler und Carmen Wucherpfennig möchte ich mich für die Ausführung von diversen experimentellen Tätigkeiten bedanken, die zum Gelingen dieser Arbeit beigetragen haben.

Prof. Dr. Robert Hänsch, Prof. Dr. Anaclet Ngezahayo, Dr. Kristin Michaelsen-Preusse, Dr. Marta Zagrebelsky und Dr. Gayane Grigoryan danke ich für hilfreiche Tipps und die eine oder andere Diskussion.

Meiner Lieblings-Leidens- und Freudensgenossin Sabine Zessin kann ich gar nicht genug danken für alles, was wir gemeinsam erlebt haben während der letzten Jahre. <3

Ich danke der ganzen Doktoranden-Rasselbande, Melissa O'Brien, Yves Kellner, Ulrike Herrmann, Dr. Anita Remus, Dr. Andrea Delekate, Dr. Martin Polack, Dr. Franziska Neuser, Dr. Stella Kramer, Marianna Weller, Nina Gödecke, Franziska Scharkowski, Qin Li, Cristina Iobbi, Susann Ludewig und Jan Kleveman für die schöne gemeinsame Zeit, die vielen lustigen Stunden und natürlich auch den fachlichen Austausch.

Rika und Alice danke ich dafür, dass immer noch alles so ist wie früher, egal was passiert. Anja und Anne haben meine Zeit in Braunschweig bunter gestaltet – danke ☺

Connie hat mich durch meine ganze Doktorarbeit begleitet, mir immer Rückhalt gegeben und mich mit seiner verrückten Art aufgemuntert. Danke für einfach alles!

Der tollsten Schwester der Welt danke dafür, dass sie mich einfach versteht und ich immer mit ihr Reden kann. Natürlich auch für das stundenlange Korrekturlesen.

Zu guter Letzt möchte ich mich bei meinen Eltern für alles Bedanken, was sie für mich getan haben.